Testing of extended shear tab and coped beam-to-girder connections subject to shear loading

By

Nathan Goldstein Apt

Department of Civil Engineering and Applied Mechanics

McGill University

Montreal, Quebec, Canada

December 2015

A thesis submitted to McGill University in partial fulfillment of the requirements of the Degree of Master's of Engineering

ABSTRACT

Beam-to-girder steel connections are commonly constructed using either extended shear tabs or coped beams. The American Institute of Steel Construction has outlined a design procedure for coped beams, and as of 2011 also included guidelines for the design of extended shear tabs. On the other hand, Canadian standards do not provide professional engineers with guidelines for the design of coped beams and only address conventional shear tab connections. Therefore, a total of thirteen full-scale tests were performed in order to provide structural engineers with relevant experimental results from which to predict the behaviour of extended shear tabs of different depths and coped beams with varying reinforcements, cope details, and connectors subject to shear loading.

Four of the tests were used to investigate two specific limit states: buckling of extended full depth shear tabs and localized deformations in the supporting girder web of partial depth extended shear tabs. It was found that by reducing the slenderness of the shear tab plate, out-of-plane deformations in the plate were reduced but not avoided. In order to more accurately represent the restraints in a building, a pseudo-concrete slab was installed to prevent girder rotation; however, this did not prevent girder web deformation. As a result, a retrofit steel plate was welded, connecting the shear tab and the girder web in order to engage a larger area of the supporting member. Even though the local girder web punching was decreased with this retrofit, the web deformation was not eliminated.

In order to gain a better understanding of the behaviour of coped beams, nine full-scale tests were conducted. These specimens were divided into four categories: bolted single coped (coped compression flange), bolted double coped (coped compression and tension flanges), single and double coped welded in-shop, and single coped haunched beams. The bolted configurations were connected to the supporting girder with the use of a stiffener plate welded to the girder flanges and web. Two reinforcement schemes were also investigated; horizontal stiffeners and doubler plates were considered to assess their effectiveness in improving the strength of coped beams. The interaction between shear and flexural forces based on the Von Mises criterion, which is not part of any current design standard, consistently governed the design and could be used to accurately predict the behaviour of coped beam configurations, and as such, is proposed for inclusion in a standard design procedure.

RÉSUMÉ

Les connections poutre-poutre en acier sont souvent réalisées avec des plaques de cisaillement étendues ou avec des poutres à ailes entaillées. L'American Institue of Steel Construction (AISC) a développé une procédure de conception pour les poutres à ailes entaillées et, en 2011, a aussi inclus des instructions pour la conception des plaques de cisaillement étendues. Malheureusement, les normes canadiennes ne fournissent pas d'instructions aux ingénieurs pour la conception de poutres à ailes entaillées et traitent seulement des connections avec plaques de cisaillement conventionnelles. Par conséquent, un total de treize essais à échelle réelle ont été réalisés dans le but de fournir aux ingénieurs en structures des résultats expérimentaux pertinents permettant de prévoir le comportement des plaques de cisaillement étendues de différentes profondeurs et des poutres à ailes entaillées avec divers renforts, entailles et connecteurs sujets à des efforts de cisaillement.

Quatre des essais ont été utilisés pour comprendre deux états limites spécifiques : le flambement des plaques de cisaillement étendues à profondeur complète et les déformations locales dans l'âme de la poutre porteuse pour les plaques de cisaillement étendues à profondeur partielle. Il a été constaté que, en réduisant l'élancement de la plaque de cisaillement, les déformations hors du plan de la plaque ont été réduites sans être évitées. Afin de représenter plus précisément les contraintes dans un bâtiment, une dalle de pseudo-béton a été installée pour empêcher la rotation de la poutre. Cependant, cela n'a pas empêché la déformation de l'âme de celle-ci. Par conséquent, dans le but de solliciter une portion plus grande de la membrure porteuse, une plaque en acier a été soudée pour connecter l'âme de la poutre porteuse et le prolongement de l'âme. Même si la déformation locale de l'âme de la poutre a été diminuée avec cette modification, la déformation de l'âme n'a pu été éliminée.

Afin d'avoir une meilleure compréhension du comportement des poutres à ailes entaillées, neuf essais à échelle réelle ont été effectués. Les spécimens ont été divisés en quatre catégories : boulonné à une entaille (aile de compression entaillée), boulonné à deux entailles (ailes de compression et de tension entaillées), soudé en atelier à une et deux entailles, et gousset à une entaille. Les poutres boulonnées ont été connectées à la poutre porteuse à l'aide d'une plaque de raidissement soudée aux ailes et à l'âme de la poutre. Deux solutions de renforts ont également été étudiées ; les raidisseurs horizontaux et les plaques de renfort d'âme ont été considérés pour

déterminer leur efficacité pour améliorer la résistance des poutres entaillées. L'interaction entre les forces de flexion et de cisaillement, fondée sur le critère de Von Mises, que l'on ne trouve dans aucune norme de conception actuelle, gouverne systématiquement la conception et pourrait être utilisée pour prédire avec précision le comportement des assemblages avec des poutres entaillées. Pour cette raison, il est proposé de l'inclure dans la procédure de conception standard.

ACKNOWLEDGEMENTS

The research presented in this thesis is not only the result of a two-year graduate degree at McGill University; it is the culmination of seven years in Montreal and a lifetime of lessons and experiences that have made me the person I am today. There are many people to whom I owe a debt of gratitude and would like to thank for making this research possible and for shaping me as an individual.

My supervisors, Professor Colin Rogers and Professor Dimitrios Lignos, are two individuals I truly respect and admire. It has been an honor to learn from and work alongside them over the last few years; they trusted me during my undergraduate years and provided me with an opportunity to pursue higher learning under their tutelage. Their knowledge, guidance, and dedication have instilled in me a sense of professionalism and a strive for excellence that I will carry forward into all future endeavors.

Special thanks to the Natural Science and Engineering Research Council of Canada (NSERC) as well as ADF Group Inc. and DPHV Structural Consultants for their financial and technical support, which made this research possible. The contributions of Denis D'Aronco and Martin Frappier were invaluable during the design process; it was a pleasure to work with these two highly motivated and competent professionals.

Laboratory testing was made possible with the immeasurable support of Siriane Lawless, David Pizzuto, Milad Moradi, Mohammad Motallebi, and Keisuke Inoue. Thank you for working by my side over the summer in order to bring this research to fruition. I would also like to thank Dr. Bill Cook, John Bartczak, and Damon Kiperchuk for all the support in laboratory and for always having a solution to the many difficulties that arose during this time.

No one has influenced the person I have become more than my family. A mis padres, gracias por su apoyo y amor incondicional. Me enseñaron desde niño los valores del trabajo y la familia, sobre dedicación y bondad. Ustedes inculcaron en mí un sentido de curiosidad y perseverancia en todo emprendimiento. Mi hermana Perla, yo siempre he admirado tu habilidad para sobrellevar todo desafío que se te presente en tu camino – estoy muy orgulloso de ti. Abuela Elica, tú siempre has sido un ejemplo a seguir: fuerte, atenta y generosa. Tu compañía siempre trae sorpresas para ambos, sea un desayuno de huevos poché no esperados o una lámpara rota.

Lamentablemente no es posible agradecer a todos por nombre, pero quiero decirles gracias por siempre creer en mí y estar a mi lado a través de todos estos años.

I have been fortunate enough to meet the most inspiring and caring people, who I now have the privilege to call my friends. From "los chicos" in Bolivia to the eclectic group of people I met in Montreal, you have always been there for me, be it for a new adventure or when I needed a hug. There is no adequate way for me to express how thankful I am to have all of you in my life; may we continue to go on new adventures and come back with great stories to share.

I would be remiss if I did not mention Jesse, Bassam, and Danny; thank you for taking time from your busy schedule to help me with the preparation of this thesis.

I am especially thankful for Rolando Moreau and Alireza Mirzaei whose insight, patience, and willingness to always go above and beyond is inspiring – thank you for your mentorship and friendship.

My life over the last six months would not have been the same without the support of my colleagues. Thank you Evelina, Angela, Fred, and Zaid for your help in a professional capacity but also for the laughs and countless cups of coffee shared that have made this experience enjoyable.

I would also like to thank everyone at Equipe Tanque, in particular Eric, Thiago, and Julian for welcoming me not only as another student, but for opening your arms and taking me in as part of a family. Oss!

Special thanks to the administrative and technical staff of the Civil Engineering Department who have readily assisted me over the course of my studies at McGill. I have to thank in particular Anna Dinolfo and Sun Chee Wong who have been my guardian angels over these last seven years.

I am fortunate enough to be surrounded by exceptional individuals who continuously encourage me to strive and become a master of my craft and a better member of society. None of this could have been possible without all of these people. Thank you. Gracias.

TABLE OF CONTENTS

LIST OF FIGURES

LIST OF TABLES

CHAPTER 1

INTRODUCTION

1.1 OVERVIEW

Beam-to-girder connections are common in steel construction, principally in steel frame buildings. These configurations consist of secondary beams connected to main girders generally using simple shear connectors. When the two framing members have to be connected at the same elevation, typically these connections are detailed with either an extended shear tab or a coped beam as illustrated in Figure 1.1. Typically, connections can be considered as a "rigid" support or a "flexible" support – shear tabs and coped beams are the latter. Flexible connections do not possess the ability to develop the full moment of the supported beam; therefore it is assumed they only resist shear forces. The additional rotational flexibility the girder web provides at the beam end releases some of the moment in the connection which increases the flexibility of the beam-to-girder connection.

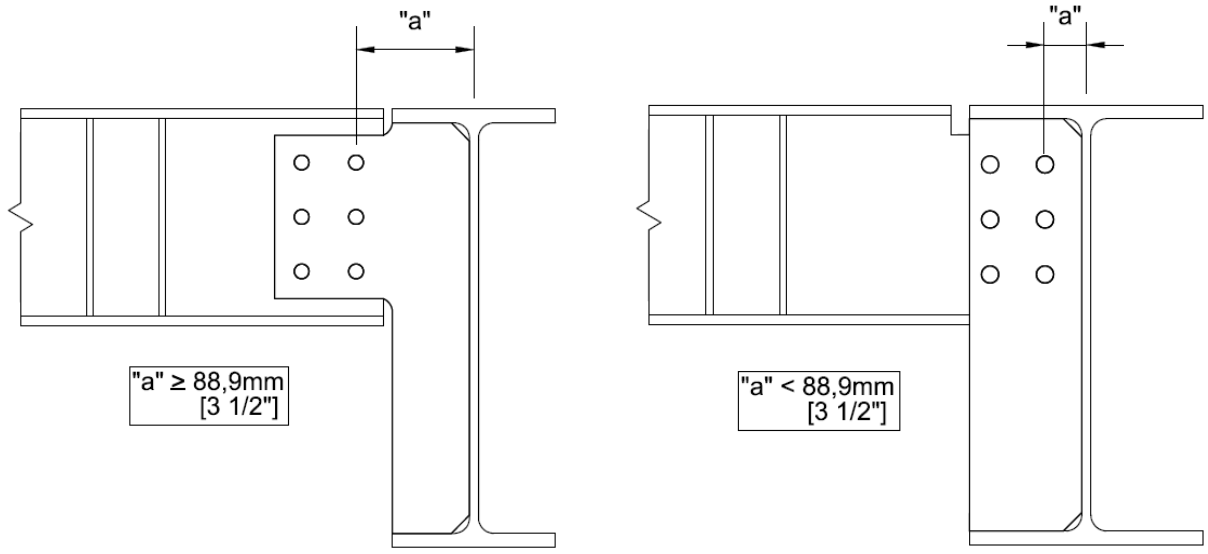

(a) (b)

Figure 1.1 – (a) Extended shear tab connection (b) coped beam connection

Shear tab connections consist of a single plate fillet welded to the supporting member, in this case the girder web, and bolted to the supported beam. The connecting plate is first drilled and then welded to the supporting girder in the fabrication shop; once the members is on site, the beam is simply lowered into position and bolted to the girder. These connections do not only offer economic advantages due to their low cost, but also provide benefits with regards to speed of fabrication and installation; as a result, engineers have increasingly preferred using this connection in their designs.

The extended shear tab connection (Figure 1.1a) is a general configuration referring to single plate shear connectors with varying distance between the weld line and bolts, thickness of plate, and number of bolts utilized. The 14th edition of the American Institute of Steel Construction (AISC) Steel Construction Manual (2011), hereafter referred to as the AISC Manual, outlines five criteria that define "conventional" single plate configurations. Amongst them, these connections only permitted a single vertical row of two to twelve bolts, and the distance from the weld line to the first row of bolts, denominated as the "*a*" distance, must be less than or equal to 89mm (3 1/2"); therefore, if either of these requirements is not met, the configuration is considered to be "extended."

Alternatively, the flange(s) of the secondary beam can be notched in order for this member to frame into the supporting girder; such a notch is denominated as a cope. When this configuration is selected, the "*a*" distance tends to be less than 89mm as illustrated in Figure 1.1b. Depending on the depth of both framing members, the beam might be coped on the top (compression flange), the bottom (tension flange), or doubly coped. Due to the reduced cross-section of the beam, it is common to reinforce the coped portion of the beam.

Two common reinforcement schemes are to install horizontal stiffeners or doubler plates (Figure 1.2). The reasoning behind the stiffeners is to replace the notched flanges and provide lateral stability to the member; the doubler plate would increase the web thickness and therefore the capacity of the section in shear as well as the local buckling resistance of the web.

Several details can be used to connect coped beams to supporting girders including welded end plates and double angles; however, the research described in this thesis will only address the performance of drilled stiffener plates welded to the supporting girder, as seen in Figure 1.1b, and the directly welded coped beams shown in Figure 1.3.

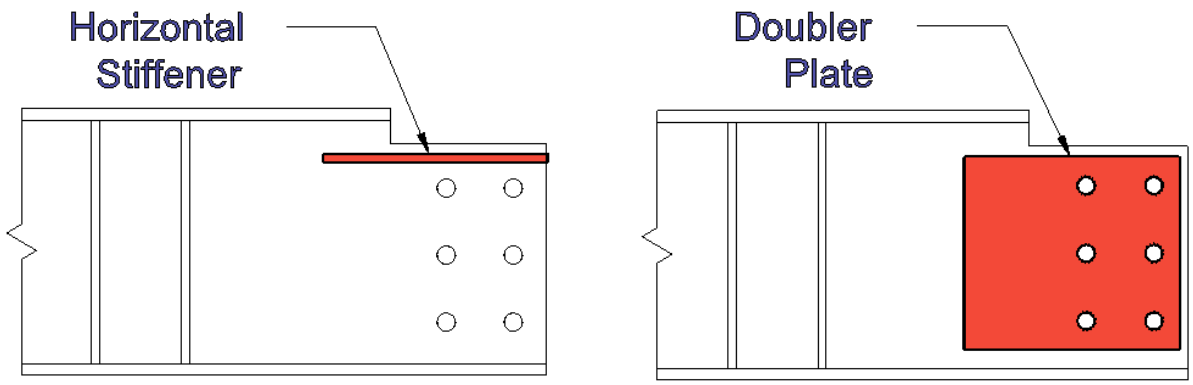

(a) (b)

Figure 1.2 – Coped beam reinforcements (a) horizontal stiffener (b) doubler plate

When designing directly welded connections, one option is for the welding procedure to take place at the fabrication shop. One benefit for engineers would be that welds that are done in-shop are of higher quality compared to connections that are welded on-site. These directly welded connections facilitate erection in the field since no additional bolting or welding is required in situ.

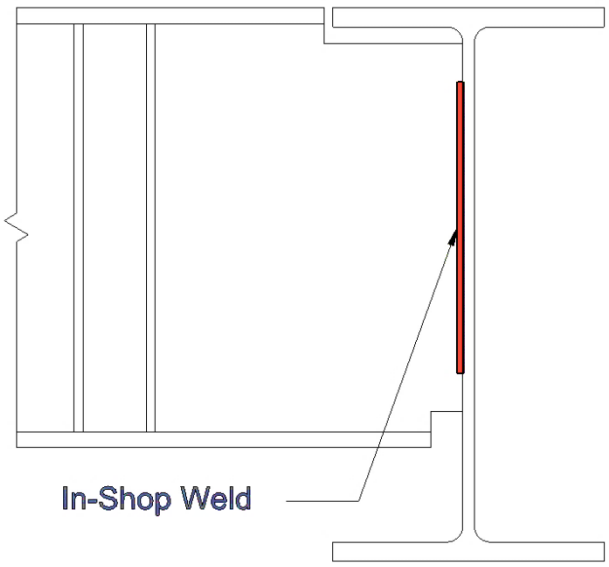

Figure 1.3 – Directly welded coped beam

Another instance in which a beam might be coped is when two components of different depths or elevations, connect to the same supporting girder. This is common when a rolled steel section and an open web steel joist (OWSJ) frame into the same girder as seen in Figure 1.4a. As a result, an additional steel plate is welded to the bottom of the beam in order to connect to the welded stiffener in the girder – this plate is denominated as a haunch plate (Figure 1.4b).

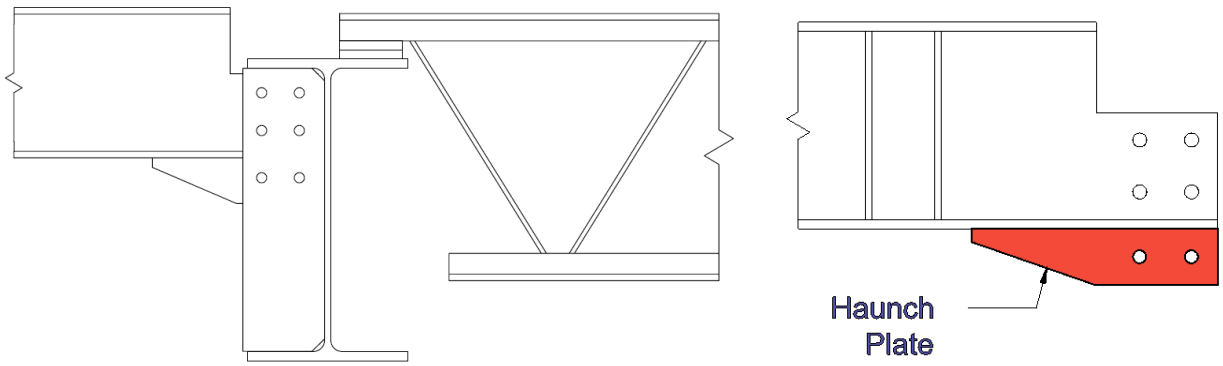

(a) (b)

Figure 1.4 – (a) Haunch beam with open web steel joist (OWSJ), (b) coped haunched beam

1.2 OBJECTIVES

The primary objective of the research program described herein was to determine the applicability and accuracy of existing design provisions for extended shear tab and coped beam-to-girder connections along with commonly used reinforcements. Both the American and Canadian engineering standards, in the form of the Canadian Standards Association (CSA) S16 Standard (2009), the 10th Edition of the CISC Handbook of Steel Construction (2010), the American National Standards Institute (ANSI) AISC 360 Specification for Structural Steel Buildings (2010), and the 14th Edition of the American Institute of Steel Construction Manual (2011) were implemented in the design and evaluation of test members. The research seeks to study the performance of flexible shear connections having multiple vertical rows of bolts as well as directly welded beam-to-girder configurations. The design and behaviour of a single coped haunched beam, the first specimen of its kind to be tested, is included in this thesis. Representative connection configurations of current North American design practice were selected with the purpose of providing professional structural engineers insight into the behaviour of commonly used connections and to assess the corresponding standard design procedures.

1.3 SCOPE

A series of thirteen full-scale beam-to-girder tests were performed at the Jamieson Structures Laboratory at McGill University in order to provide structural engineers with relevant experimental results from which to predict the behaviour of extended shear tabs of different depths and coped beams with varying reinforcements, cope details, and connectors subject to shear loading. In order to more accurately represent the boundary conditions in such

connections, a pseudo-concrete slab was installed to prevent girder rotation. During testing, a series of measurements recording strain, deflection, rotation, and strength were taken in order to observe and quantify the performance and damage progression of each configuration. Conclusions and observations regarding the behaviour of the tested connections are made; this includes comparing predicted load resistances with experimental results in order to assess current design procedures of beam-to-girder connections subject to shear loading. Additionally, based on the observed behaviour, areas of interest for future research are also suggested.

1.4 OUTLINE

In Chapter 2, a literature review is provided on the behaviour and design of beam-to-girder connections. Both extended shear tab and coped beam configurations are discussed. Different methods to connect these members are examined along with common failure modes and reinforcement details. Current North American design provisions are also summarized.

In Chapter 3, the motivation behind the selection of each test specimen and details the design of each configuration, which is representative of current professional practice, is explained. The experimental setup, instrumentation, specimen installation, and testing procedure are described in detail.

In Chapter 4, the results of the laboratory tests are examined and then compared and contrasted with the recorded data for different specimens in order to better understand the behaviour of the different configurations tested. Predicted and experimental resistances are compared to assess the accuracy and applicability of the utilized design procedure. Expected and empirical material properties are presented and discussed based on coupon testing.

In Chapter 5, a summary of the main findings of this thesis can be found along with suggestions for future research related to configurations of interest for full-scale testing as well as connections to be studied with the use of finite element models.

CHAPTER 2

LITERATURE REVIEW

2.1 OVERVIEW

This chapter contains a summary of the primary studies associated with the behaviour of extended shear tab connections as well as coped beams. The chapter is divided into two main portions; research publications and current design procedures. Within these topics, directly welded connections, various failure modes, and varied reinforcement details are covered to provide background information for the design and analysis of the aforementioned connections.

2.2 RESEARCH PUBLICATIONS

2.2.1 Girder Web Punching and Movement of Inflection Point

Shaw and Astaneh (1992) performed six full-scale tests of beam-to-girder configurations with the purpose of investigating the effects of the girder web flexibility on the strength and deformation of the connection. It must be noted that beam members were selected as to avoid lateral torsional buckling. Beams had a single cope on the top flange and were bolted to a partial depth shear plate that was welded to the girder web.

It was observed that for configurations where the girder web clear height (the "T" distance of the member) was long, flexibility of the connection was provided by the elastic bending of the shear plate, which then led to yielding. On the other hand, configurations with smaller girder web clear heights, resulting in stiffer webs, did not exhibit any bending prior to yielding. As loading continued, the stiffness of the girder web increased which resulted in a decrease in the connection rotation but an increase in tensile forces at the upper portion of the weld between the girder web and shear plate, which resulted in weld tearing. Figure 2.1 depicts the yield lines that developed on the girder web prior to weld tearing.

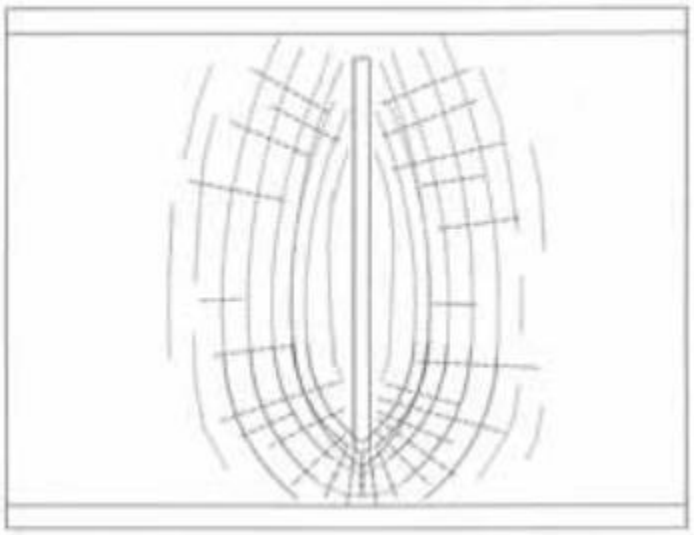

Figure 2.1 – Girder web punching (Shaw and Astaneh, 1992)

The high flexibility of the girder web along with slight eccentricity in loading resulted in large deformations in the girder web in the region where this member connects to the bottom of the shear plate (Figure 2.2); this mechanism is referred to as girder web punching. Shaw and Astaneh suggested that in order to avoid such deformation, the shear plate should be welded to the top flange of the girder.

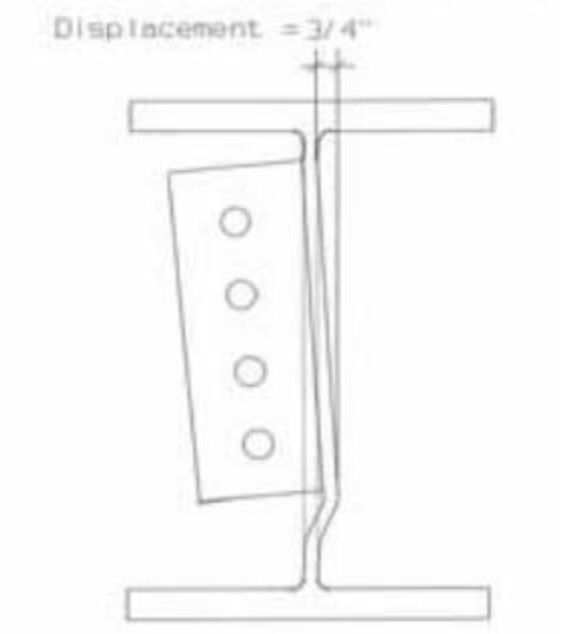

Figure 2.2 – Girder web punching
(Shaw and Astaneh, 1992)

Another phenomenon observed due to the girder web flexibility was twisting and warping of the shear plate as seen in Figure 2.3. In some specimens this twisting of the shear plate also caused the beam to twist at early stages of loading. However, Shaw and Astaneh stated that even though this failure mode was observed in the lab, it is not likely to occur in actual buildings with adequate floor bracing.

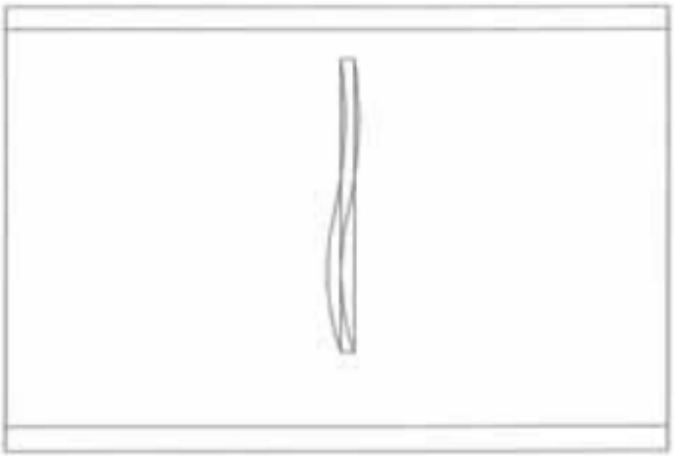

Figure 2.3 – Shear tab twisting
(Shaw and Astaneh, 1992)

Shaw and Astaneh also investigated the location of the inflection point on the beam by determining the distance from the weld line to the point of zero moment in the test specimen – this distance is referred to as the eccentricity of the connection (e_w). Unlike their previous research on beam-to-column connections (Astaneh et al. 1989), much of the movement of the inflection point was caused by bending and eventual yielding of the girder web rather than yielding in the shear plate. Shaw and Astaneh determined that the most important variables in determining the eccentricity were the shear plate length, girder web thickness, and girder clear web height. As a result, Equation (2-1) was proposed to determine the eccentricity of the connection as measured from the weld line (e_w) where h_c is the girder clear web height, t_w is the girder web thickness, and N is the number of bolts.

$$e_w = \frac{40}{(h_c/t_w)}\, x\, N \qquad \textbf{(2-1)}$$

2.2.2 Extended Shear Tab Connections

Hertz (2014) performed a laboratory test program to investigate the behaviour and performance of extended shear tab connections. Among the specimens tested were three full depth extended shear tabs and four partial depth extended shear tabs. In the case of a full depth shear tab, said component is of equal height to the interior depth of the supporting girder and is welded to the girder web and both top and bottom flanges; on the other hand, partial depth extended shear tabs are welded to the girder web and top flange only.

Three full depth extended shear plate configurations with varying number of bolts and vertical bolt rows were tested. Buckling at the neck of the shear tab was observed for all tested specimens. Figure 2.4a shows a schematic drawing of the observed phenomenon and highlights the buckled neck region of the shear tab in gray. Figure 2.4b is a section view showing the out-of-plane deformation of the shear tab. As the out-of-plane deformation continued, the rotational stiffness of the connections decreased significantly. Eventually, the connections had rotated such that the beam ends were binding with the buckled shear plates which resulted in an increase in the stiffness and strength of the connection.

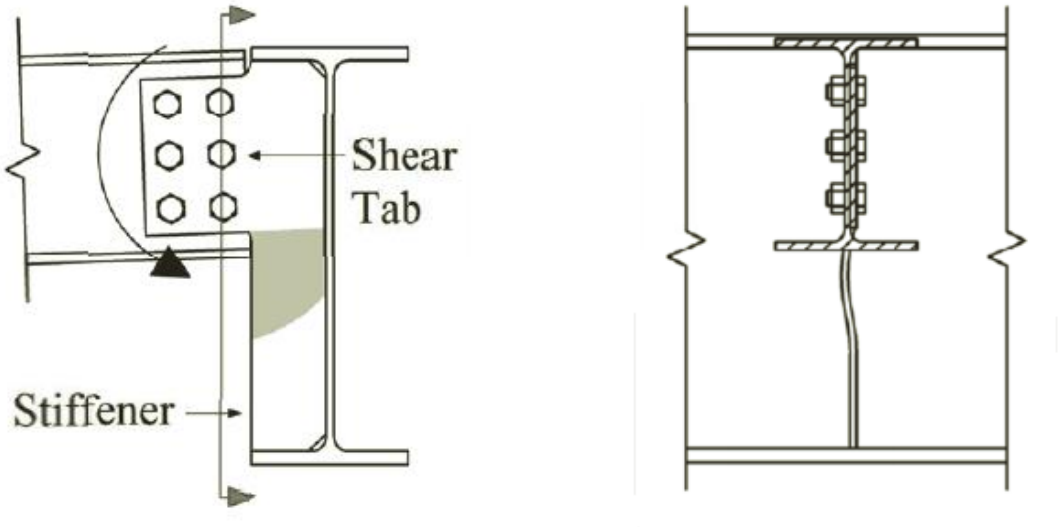

(a) **(b)**

Figure 2.4 – Buckling at neck of shear tab (a) buckling schematic (b) section view (Hertz, 2014)

It was observed that as the depth of the test beam increased, buckling of the shear tab occurred at an earlier stage of loading. Hertz (2014) explains that the buckling of the shear tab is attributed to the combination of vertical compressive stresses from transfer of shear into the supporting

girder and the horizontal compressive stresses caused from flexure in the beam. As such, a deeper beam would be subject to higher horizontal stresses, which would result in the shear tab buckling at a lower applied vertical connection load compared to a configuration with a smaller beam.

Four partial depth extended shear tabs were tested in order to investigate the effect of including an additional stiffener welded to the back of the supporting girder for configurations with two different "*a*" distances. It must be noted that the failure mode for all test specimens was large out-of-plane deformations in the web of the supporting girder, also referred to as girder web punching. Hertz (2014) states this mechanism developed due to the concentrated horizontal compressive stresses transferred to the girder web at the base of the shear tab and the vertical tension stresses on the underside of the girder top flange; as such, not only was girder web punching observed but rotation of the top flange of the girder was also recorded (Figure 2.5). Based on the recommendations presented by Shaw and Astaneh (1992), see Section 2.2.1, the test configurations were detailed such that the shear plates were welded to the top flange of the supporting girder; however, the results presented by Hertz (2014) demonstrate this did not prevent the aforementioned mechanism from developing.

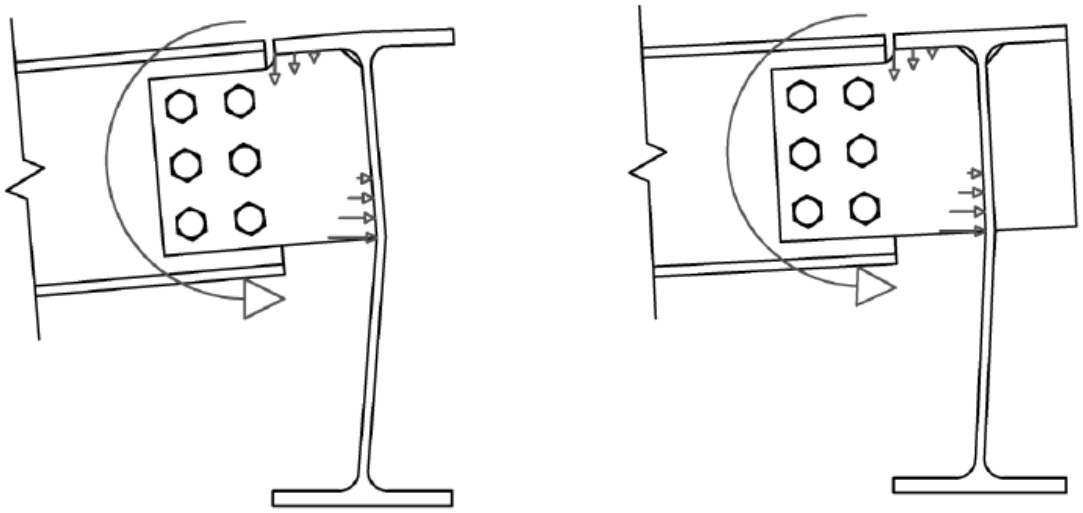

(a) **(b)**

Figure 2.5 – Girder web punching and top flange rotation (a) without stiffener (b) with stiffener (Hertz, 2014)

When comparing the effect of the additional stiffener on the two specimens with an "*a*" distance of 165.1mm (6 1/2"), it was observed that the inclusion of the reinforcing element delayed yielding in the supporting girder. Yielding on the girder web was recorded at 26kN for the unstiffened specimen whereas the girder of the reinforced connection yielded at 210kN. Similarly, the stiffened connection reached a maximum rotation fourteen times greater than the unstiffened counterpart – 0.127 radians as opposed to 0.009 radians.

The remaining two specimens were detailed with a greater "*a*" distance – 241.3mm (9 1/2"); however, unlike the previously tested configurations, no significant increase in girder yielding resistance or rotation were observed due to the addition of the reinforcing stiffener. Hertz (2014) attributes this to the increased larger girder section used for these connection; the configurations with an "*a*" distance of 165.1mm were supported by a W610x125 (W24x84) girder whereas the specimens with an "*a*" distance of 241.3mm were supported by a W760x257 (W30x173) section.

Muir and Hewitt (2009) developed a new procedure to design extended single-plate shear connections, which then became the basis of the design procedure outlined in the 14th Edition AISC Steel Construction Manual (2011). As such, the equations developed are presented in Section 3.5.4. Muir and Hewitt, based on already existing research in the field, noted that developing a simple and comprehensive design procedure for such a connection could be erroneous given that the moment distribution along the same was poorly understood; as such, they relied on the lower bound (static) theorem stating: "If an equilibrium state can be found which does not violate the yield condition, then however 'unlikely' that state may seem to be, the structure is safe. (Baker and Heyman, 1969)."

In other words, Muir and Hewitt explain that since the applied external forces are in equilibrium with the internal forces, and that the same external forces are less than or equal to the critical loads that would cause failure of the connection, then the limit states are satisfied and the connection has enough ductility to allow these forces to redistribute safely. The assumed model was a pinned-end model since that is the usual assumption taken by practicing engineers during design for such members. In order to accomplish this redistribution of forces, the authors developed an equation to determine the maximum shear plate thickness to ensure this component acted as a fuse element, for it was considered to be the most ductile element in the connection. For this portion of the analysis, the system was modeled as a fixed-end beam in which the

moment applied on the bolt group was equal to the applied shear force multiplied by the distance from the support to the center of the bolt group. This was done because as soon as the plate yields, the forces would be distributed to the beam, which would reduce the applied moment on the connection and support therefore preventing failure – and also satisfying the lower bound theorem.

Additionally, Muir and Hewitt indicated that the stability must be checked and suggested this be done with the procedure developed by Muir and Thornton (2004). Said procedure is described in further detail in Section 3.5.2 – it refers to the equation for plate buckling labeled as the Q-equation. An additional contribution of the authors was the verification of the results found by Metzger (2006) suggesting that the weld size of the shear tab to the supporting member be at least 5/8ths of the plate thickness with the purpose of preventing unzipping of the weld.

An extensive background and review of shear tab connections can be found in the theses published by Creech (2005), Marosi (2011), Mirzaei (2014), and D'Aronco (2014). Furthermore, more detailed investigation of the background of extended shear tab connection design can be found in Hertz's (2014) thesis on that subject.

2.2.3 Directly Welded Connections

Gaylord and Gaylord (1957) investigated welded beam connections and provided recommendations with regards to weld length and width. It was noted that these connections may develop a resisting moment at the beam end which is not accounted for in design. Depending on the weld size and length used, the beam-to-girder connection might become relatively rigid. As a result, the authors suggested that the weld length should be longer than one-half the beam depth but shorter than two-thirds the beam depth; similarly, the weld leg should be at least four-fifths of the beam web thickness. These recommendations would allow the welds to withstand the overstrain due to rotation and assure adequate flexibility of the connection.

Blodgett (1966) investigated directly welded web connections. He suggested that the leg size of the fillet weld must be equal to two-thirds of the beam web thickness when loaded in shear and equal to the beam web thickness when loaded in tension, this was shown by calculating the capacity of the welds in order to match the allowable shear and ultimate tensile strength of the beam respectively.

A simply supported W460x128 (18" WF 85#) beam made of ASTM A373 steel with a span of 4572mm (15') was tested under uniform loading equal to 139 kips. It was observed that the beam started yielding at the lower end of the weld once the calculated end moment reached 360 kip-in, followed by tearing at the top of the weld at 870 kip-in, which occurred at a rotation of 0.011 radians. Once the moment reached 1000 kip-in, the beam came into contact with the column, this binding action resulted in an increase in the connection stiffness; the maximum moment reached was 1918 kip-in.

Based on these observations, Blodgett deemed the directly welded connection to be "not as dependable" as a connection with a top connecting plate designed to yield at a working load (similar to a reduced beam section) or a flexible web framing angle connection, Figure 2.6 and Figure 2.7 respectively, due to the increased rotational ductility of these other connections.

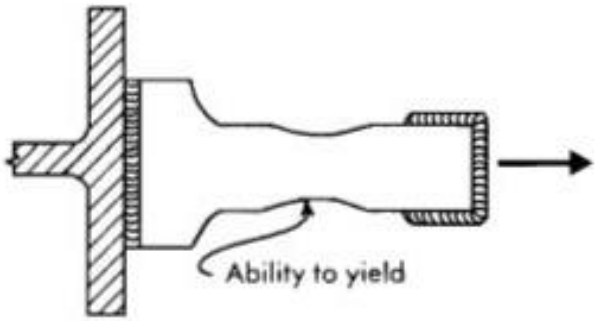

Figure 2.6 – Top connecting plate (Blodgett, 1966)

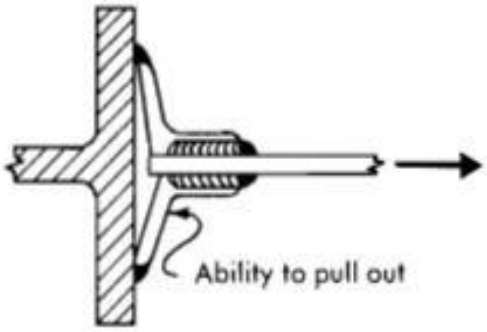

Figure 2.7 – Flexible web framing angle (Blodgett, 1966)

2.2.4 Coped Beam Failure Modes

Cheng et al. (1984) produced the seminal report on coped beams and possible reinforcement configurations. Results and observations by Cheng and Yura (1986) and Cheng et al. (1988), presented herein, were based on the experimental and analytical results by Cheng et al. (1984). The experimental portion of this research consisted of 14 rolled sections and 2 plate girders. Note that the connections for all test specimens were clip angles that were then bolted to a stub column. The researchers focused on two distinct failure modes, lateral torsional buckling and local web buckling, corresponding to Cheng and Yura (1986) and Cheng et al. (1988), respectively. It is important to note that the scope of the research only included members with a cope length (c) less than or equal to twice the nominal beam depth (d) and a cope depth (d_c) less

than or equal to half the beam depth. Included in this publication were the results of an investigation of the effects of different coping arrangements on the above mentioned failure modes; results and observations are presented below.

2.2.4.1 Lateral Torsional Buckling

The portion of the report produced by Cheng et al (1984) regarding lateral torsional buckling failure consisted of six hot-rolled steel sections, and multiple analytical models. It was concluded that when beams have a single cope on the compression flange the lateral buckling capacity of the member is determined by the interaction of the coped and uncoped section depending on the cope length. If the cope lengths were small, then the section would behave similar to an uncoped beam; however, with longer copes, the uncoped region would buckle with rigid body motion. It was also observed that a specimen with copes at both ends of an unbraced length had a lower capacity than a beam of the same length but with only one coped end. Cheng et al. (1988) developed equations for both these instances. For beams with copes on the tension flange, a reduction in the capacity of the beam of approximately 14% is observed and a simple arithmetic reduction of 10% of the buckling capacity of the uncoped beam is suggested for design. As per double coped beams, referring to beams with both the compression and tension flanges removed, these behave in a similar fashion to the compression flange coped beams, but designers must consider the reduced rectangular area of the beam in design.

Cheng et al. (1988) investigated the lateral torsional buckling behaviour of coped beams with the purpose of providing practical design recommendations. W410x39 (W16x26) sections were used because these have slender webs, and as such would provide conservative results for other rolled sections. Three variables were explored in this study: span length, cope length, and cope depth. The study looked at two different bracing scenarios; Case 1 was unbraced, therefore was coped at both ends of the unbraced length, whereas Case 2 had a lateral brace at the mid-span of the beam, resulting with only one cope at the end of the unbraced length, which also was the point of load application.

The behaviour of a short beam measuring 1524mm (5’) and a long beam 9144mm (30’) in length were compared; both had copes on the tension side at both ends of the unbraced length, these were 203.2mm (8”) long and 3.1mm (1.5”) deep. For the short beam, the coped section controlled in a buckling failure mode while the uncoped region deflected by rigid body motion

regardless of the bracing scenario. On the other hand, the long beam behaved similar to an uncoped beam with the buckling load reaching 90% of the theoretical elastic buckling capacity of the section; therefore, the buckling capacity of the long beam was controlled by the uncoped section.

When investigating the effects of cope length, 6096mm (20') long beams with cope depths equal to 38.1mm (1.5") were used; cope length varied from 0 to 812.8mm (0" to 32"). For Case 1 it was observed that lateral buckling always occurred before yielding and that the reduction in strength had a linear relationship with the cope length. For Case 2 bracing, if the cope length was less than 177.8mm (7") then the beam would yield at mid-span; however, if the length was increased, then lateral buckling would control and the relationship between the cope length and member capacity would become nonlinear. Based on the aforementioned observations, a series of design interaction equations relating buckling capacity of the uncoped and coped regions were suggested. For short beams, the capacity of the member was controlled by the coped section whereas for the long beams the member was treated as two separate buckling problems – the coped and uncoped regions.

However, in order to account for cope depth, a second set of modified design equations had to be developed; this was because most copes are of a depth less than or equal to 10% of the beam depth, but for those cases where the cope is deeper, a second set of equations accounting for cross-sectional distortion in the cope region were needed to better describe the behaviour of the members. It was observed that the top flange tends to tip over which results in decreased buckling capacity. The equations developed for Case 1 accounted for both lateral buckling at the top flange and the tipping effect whereas those for Case 2 only accounted for the tipping effect – lateral buckling at the top cope was not included. This second set of equations can be used to calculate the reduced buckling capacity of the coped beams taking into consideration the above mentioned observed phenomenon. These equations were developed by modeling the top flange of the beam as an axially loaded column restrained laterally; the restraints were modeled using spring stiffness. Using the same method, and for the same reason, equations describing the behaviour of thin web members were also suggested since it was found that the lateral buckling capacity of these members was reduced up to 65% when the cope depth was equal to half the beam depth.

Lam et al. (2000) investigated the lateral torsional buckling of coped beams with an emphasis on stockier sections, as compared to Cheng et al. (1984), as well as the effect of different loading scenarios on this failure mode. By means of analytical models it was observed that the equations proposed by Cheng et al. (1988) accurately predict the behaviour of the connection when the beams are slender and long, longer than 4000mm (13'); they render poor estimates for stocky and short coped beams. Cheng et al. (1988) state that the elastic lateral torsional buckling of short coped beams is controlled by the buckling capacity of the coped region; however, this was not what was observed in the analytical models that had been developed.

Lam et al. (2000) suggest that both the local web buckling strength and overall elastic lateral torsional buckling strength of the reduced beam region should be used with the interaction equations proposed by Cheng et al. (1988) – these equations did not consider local web buckling. It was observed through the results of the analytical models that when the cope length-to-web depth ratio is small, the local web buckling capacity of the section might control over lateral torsional buckling; therefore it was suggested that the local web buckling moment capacity be used instead of the lateral torsional buckling moment of the coped section in the design interaction equations between the coped and uncoped regions of the beam when cope length-to-web depth ratio is less than or equal to 2.5. Using the new proposed equation, the test-to-predicted ratio ranged from 0.91 to 1.16 compared to the ratio calculated for the original equations which ranged from 0.52 to 1.06.

Additionally, Lam et al. (2000) also performed a numerical parametric study to assess the validity of the original interaction equation under different types of loading, other than a single point load at mid-span. The load configuration was two symmetrically located point loads. It was found that this interaction equation did not adequately predict the behaviour for stockier sections; therefore, the authors suggested including the influence of the resulting moment distribution and the local web buckling capacity of the reduced section. The authors proposed an equation, which did include these parameters and as a result, the test-to-predicted ratios for the symmetrically loaded specimens improved from the range of 0.29 to 0.90 utilizing the original equation to a range of 0.93 to 1.19 with the proposed equation.

As stated above, the proposed changes to the interaction equation apply to members with a cope length-to-web depth ratio less than or equal to 2.5; however, the effect of changing the cope

length to achieve a higher ratio were investigated by Lam et al. (2000) by means of a parametric study through numerical analysis. It was concluded that for those instances, the lower of the overall lateral torsional buckling capacity and the local web buckling capacity of the reduced beam section should be used in the proposed interaction equation. For short beam members with small cope length-to-web depth ratios, the lower of the elastic lateral torsional buckling capacity and the shear yielding capacity of the reduced beam section should be used in the design interaction equation.

Dowswell and Whyte (2014) intended to expand the finite element model database in order to expand the applicability of the design equations originally developed by Cheng et al. (1984) for double coped beams. Additionally, by plotting the critical stress (F_{cr}) values for lateral torsional buckling and local buckling against the ratio of the reduced beam section to the beam depth (h_o/d) it was seen that these two curves trend in opposite directions (Figure 2.3). Note that the reduced beam section (h_o) is calculated by subtracting the cope depth (d_c) from the nominal beam depth (d). As the h_o/d ratio increases, the lateral torsional buckling curve increases while the local buckling curve decreases; therefore, Dowswell and Whyte set out to formulate a single continuous function that accounts for both these phenomena simultaneously. Note, these curves were plotted for a cope length- to-beam depth ratio equal to unity and a beam web thickness equal to 7.6mm (0.3”). Lateral torsional buckling was calculated using the equations developed by Cheng et al. (1984) whereas local buckling was calculated based on the equations developed by Muir and Thornton (2004) – both are included in the 14th Edition AISC Manual (2011) and are described in detail in Section 3.5.1.

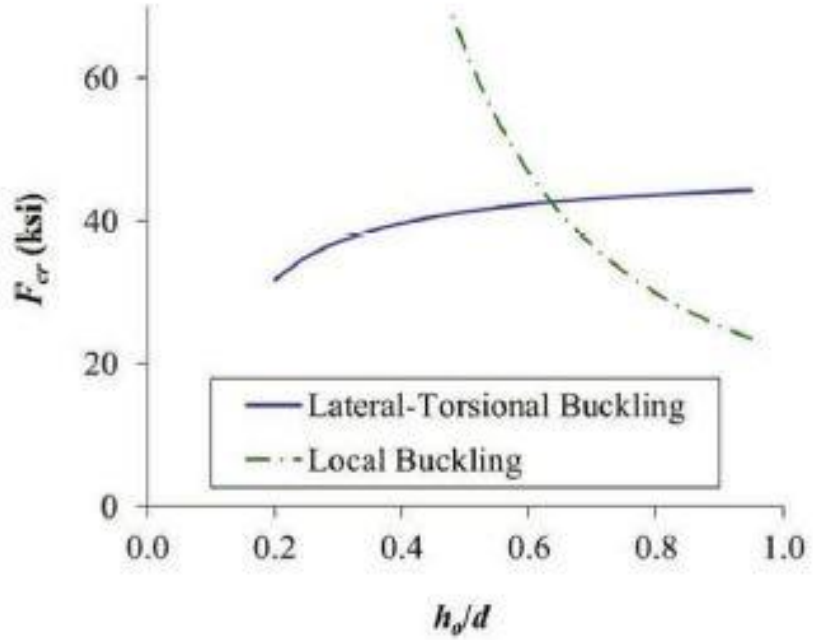

Figure 2.8 – Lateral torsional buckling and local web buckling trending lines (Dowswell and Whyte, 2014)

The study by Dowswell and Whyte consisted of 54 elastic finite element models used to address three issues: cope depths greater than 20%, unequal cope depth at the top and bottom, and unequal cope length at the top and bottom of the beam. The results of these models show that the tension edge of the beam at the reduced section displaces laterally while the compression edge buckled; this phenomenon partially extended to the gross beam section therefore confirming the results of Cheng et al. (1984). Then, in order to develop a design model, the buckling modes had to be identified; it was observed that specimens with short cope lengths were controlled by shear buckling while those with long cope lengths were controlled by lateral torsional buckling. However, since the observed buckled shapes of all configurations most closely resemble lateral torsional buckling, the proposed deign models were based on the corresponding equation suggested by Cheng et al. (1984) and part of Section F11 of the AISC Manual (2011).

Dowswell and Whyte used a design procedure based on plastic flexural strength, which is different than the procedure used in the AISC Manual (2011), which incorporates beam theory based on flexural stresses. In the latter, the maximum normal and shear stresses occur at different locations whereas in the former they occur in the same location on the cross-section;

this results in the need to combine these effects, which reduces the flexural capacity of the section. Therefore, the proposed design equations also suggest reducing the moment capacity of the members based on the available shear stress of the section.

Based on the results of these models, a new set of equations to calculate the lateral torsional buckling modification factor (C_b) were suggested in order to more accurately calculate the inelastic lateral-torsional buckling capacity of members. Due to the fact that these equations were also developed using a finite element model, they also have certain application limits based on the models investigated: the cope lengths should be less than or equal to twice the beam depth, also the top cope depth should be less than or equal to 40% of the beam depth – effectively expanding the applicability of the design procedure. However, it was found that the geometry of the tension flange cope was not significant; therefore, no limitations were set on the bottom cope depth or length. Finally, it was found that if the ratio of the top cope depth to the beam depth was less than 0.5, the proposed equations produced unreasonably low values for C_b; therefore a limit of 1.84 was set on this parameter. It was found that when applying these equations to calculate the capacity of the members, the proposed equations had an average finite element-to-calculated load ratio of 1.01 with a standard deviation of 0.0535 compared to the current design procedure, which has an average finite element-to-calculated load ratio of 1.54 with a standard deviation of 0.496.

2.2.4.2 Local Web Buckling

Cheng et al. (1984) investigated local web buckling through the completion of ten full-scale test specimens and the development of a series of numerical models. It was found that the local web buckling failure mechanism is only present in specimens where there compression flange is coped or both top and bottom flanges are coped. Cheng et al. (1984) developed a series of equations to better predict the behaviour of these members, which are explained by Cheng and Yura (1986). It was determined that as the cope length increases, the stress concentrations at the cope decrease, this phenomenon is represented in the calculation of the stress concentration factor which is utilized in the equations.

Cheng and Yura (1986) conducted a parametric study through numerical analysis to establish the effects of stress concentration, shear stress, cope length, and cope depth on local web buckling strength. At the time of this research, the design procedure for local web buckling was governed

by the 8th edition of the AISC Manual of Steel Construction (1980) and detailing examples were provided in the AISC Manual for Structural Steel Detailing (1971). The latter suggested that yielding due to bending moment be checked using the reduced cross-sectional area properties; this in turn would neglect stress concentrations occurring at the cope. Similarly, neither of the two provisions addressed cope length and depth, which both could decrease the lateral stability of the member. At the time, the plate buckling coefficient (*k*) used in design for the critical bending stress of coped beams was based on the assumption of an infinitely long plate; however, if the cope length were longer than the beam depth this value could be significantly increased. Based on ten full-scale tests performed by Cheng and Yura, as well as four additional tests taken from another project, the researchers suggested a new design model.

In order to better represent the buckling behaviour of coped beams, Cheng and Yura obtained values for the plate buckling coefficient from the Japanese Column Research Council Handbook (1971). Using the computer program BASP, originally written by H. U. Akay and C. P. Johnson at The University of Texas, further research was done to determine the elastic web buckling loads, and using curve fitting techniques Equations (2-2) and (2-3) were suggested to determine this coefficient based on the ratio between cope length and reduced beam depth.

$$k = 2.2\left(\frac{h_o}{c}\right)^{1.65} \quad when \ \frac{c}{h_o} \leq 1.0 \qquad \textbf{(2-2)}$$

$$k = \frac{2.2h_o}{c} \quad when \ \frac{c}{h_o} > 1.0 \qquad \textbf{(2-3)}$$

As can be seen, these equations only consider cope length (*c*) and reduced beam depth (d_c); stress concentration, shear stress, cope depth, or moment variation in the region between the beam end and the cope end are not considered. However, after a parametric study was performed by Cheng and Yura (1986), it was determined that a single adjustment factor could be used to address the effect of these variables. This adjustment factor (*f*) was defined by Equation (2-4) and (2-5):

$$f = \frac{2c}{d} \quad when \ \frac{d}{c} \leq 1.0 \qquad \textbf{(2-4)}$$

$$f = 1 + \frac{c}{d} \; when \; \frac{d}{c} > 1.0 \qquad \textbf{(2-5)}$$

Therefore, Equation (2-6) was proposed to determine the critical bending stress (F_{cr}) in a coped beam. During design, the maximum M_c/I stress at the coped region must be less than the value obtained from Equation (2-6); naturally, the M_c/I and $V/h_o t_w$ stresses must also be compared to the yield stress. Where M_c = bending moment; I = moment of inertia; V = shear force; and t_w = beam web thickness.

$$F_{cr} = \frac{\pi^2 E}{12(1-\nu)^2}\left(\frac{t_w}{h_1}\right)^2 fk \qquad \textbf{(2-6)}$$

where E = modulus of elasticity, ν = Poisson's ratio; and h_1 = effective reduced depth.

Equations (2-2) through (2-6) were adopted by the 1983 edition of the AISC Detailing Manual (1983), and are still used to design coped beams as described in the 14th Edition AISC Manual (2011).

Yam et al. (2003) investigated local web buckling of coped beams by means of four full-scale tests and a series of numerical studies; the result was a modified plate buckling formula. A single end plate was welded perpendicular to the bema web to be connected to the reaction wall. The test specimens failed due to local web buckling in the cope region. It was observed that by increasing the cope-to-depth ratio, the capacity of the connections decreased. The authors also plotted the load versus in-plane deflection curves for each of the specimens and observed a linear load-deflection behaviour. This lead to the conclusion that none of the four test specimens experienced significant yielding prior to the local web buckling failure mode. It was also noted that specimens with small cope depths experienced higher bending stresses whereas specimens with large cope depths underwent relatively smaller stresses in the coped region. This observation also implies that the stress concentration at the cope corner, the location with the highest stress in all specimens, are not as significant for specimens with large cope depths as compared to those with small cope depths.

Both the full-scale tests and the numerical models showed a buckling line oriented at an angle of 45° from a vertical line for specimens with short cope lengths, when the cope length-to-reduced beam depth ratio was less than 1.5. This indicated that shear stresses dominated the buckling

behaviour for these specimens. In the proposed equation, bending stresses are neglected for that reason – finite element studies were performed by Yam et al. (2003) to substantiate this assumption. The proposed equation introduced a shear buckling coefficient (k_s) based on the cope length-to-reduced beam depth for different values of the cope depth-to-beam depth ratio to replace both the plate buckling coefficient (k) and the adjustment factor (f). In order to calculate this coefficient, the authors propose a series of equations; these express a relationship in which the shear buckling coefficient decreases as the cope length-to-reduced beam depth increases, but the coefficient decreases as the cope depth-to-beam depth ratio increases for a constant value of the cope length-to-reduced beam depth ratio.

The modified plate buckling equation was compared to that developed by Cheng et al. (1984). The latter was found to be conservative with test-to-predicted ratios ranging from 1.10 to 1.39, while the modified equation had test-to-predicted ranging from 0.92 to 1.06.

2.2.4.3 Block Shear

Franchuk et al. (2003) conducted 17 full-scale tests on coped wide-flange beams with an emphasis on block shear failure. Bolted double-angle header connections were used for these tests. The authors point out that at the time, design equations for this failure mode were largely based on testing performed on gusset plates; however, end rotation and asymmetric stress distribution on the block that are present in beams, but not gusset plates, has significant impact on the resistance of these members. The test beams were connected using double-angles to the face of a column. The load was applied close to the connection in order to ensure block shear failure occurred. The test specimens were laterally supported at the load point and the reaction end to avoid lateral torsional buckling, and local web buckling was also prevented with appropriate restraints. All but one of the specimens, a double coped beam, failed in block shear; the entire block (classical tear-out) was observed for most cases, but for three specimens only partial tear-out occurred. Figure 2.9 and Figure 2.10 are used to illustrate the difference between the two failure modes. It is also important to note that the researchers found that the moment that developed at the connection, calculated using statics, was approximately 0.5 – 5% of the yielding moment.

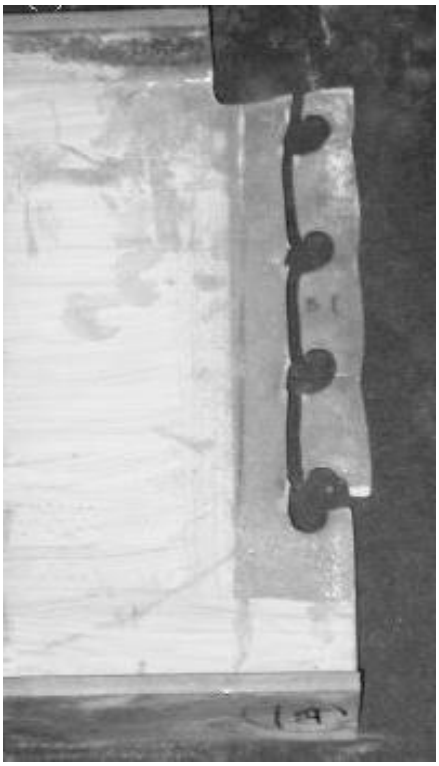

Figure 2.9 – Classical tear-out (Franchuk et al. 2003)

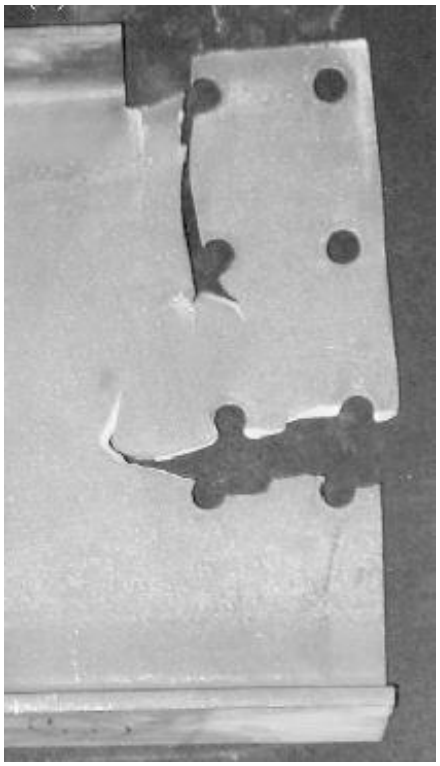

Figure 2.10 – Partial tear-out (Franchuk et al. 2003)

In order to investigate the effect of end rotation on coped beams, three different rotation levels were applied on three different connections. In general, the ultimate capacity of the sections was reached regardless of the connection configuration tested; therefore, it was concluded by the researchers that end rotation has negligible effect on the ductility of a connection.

The effect of the gross shear area was investigated by testing two specimens with equal net tension areas and net shear areas but different gross shear areas. It was observed that the connection with the greater gross shear area, 10% greater, exhibited a higher capacity by 18%; however, it was also observed that the fracture surface slightly intersected the bolt holes as seen in Figure 2.9. As a result, the authors concluded that the governing shear area is somewhere between the gross and net areas tending closer to the gross area.

Several other parameters were investigated yet deemed to have negligible effect on the capacity of these sections. Edge and end distances of connections were also inspected, and even though an increase in these distances did yield higher capacity, this increase was simply attributed to the increase in tension and shear areas. Similarly, increasing bolt diameter from a 3/4" Ø (19.1mm)

bolt to a 1" Ø (25.4mm) bolt lead to a capacity increase of 11%; however, this too was attributed to the 13% increase in the edge distance required by design provisions and 3% increase in gross shear area due to the larger bolt hole spacing required. An increase in the beam section depth, from a W310x60 (W12x40) to W410x46 (W16x31) did result in a 16% higher capacity, but this increase was associated with a 13% difference in the web thickness of the two specimens. Considering different bolt hole spacing, and therefore different connection depths, lead to similar results; the specimen with larger spacing had a capacity that was 19% higher which resulted mostly from the 24% increase in gross shear area – therefore deemed to have a negligible effect on the connection. Increasing the number of bolt rows lead to similar conclusions about this variable; testing specimens with three and four bolt rows it was concluded that the latter had a 32% higher capacity but this was associated to a 30% higher gross shear area.

Two variables were tested which the authors were not able to make any comments on with regards to the ductility of the connection; number of bolt lines and the effect of a double cope. For the former, by increasing the number of bolt lines from one to two there was an increase in capacity of 34%; however, the failure mode changed from classical tear-out to partial tear-out, which makes the assessment of the effect on ductility difficult. For the latter, the researchers had some problems measuring deflections and therefore were not able to discuss the effect of double copes on connection ductility. Based on these observations, the authors concluded that only the tension and shear areas had significant impact on the capacity of these connections with regards to block shear failure.

Franchuk et al. (2004) performed a reliability analysis on coped wide-flange beams in order to assess the level of safety provided by concurrent design standards in Canada, United States, Europe, and Japan. The authors found that these design standards were inconsistent in predicting block shear failure and grossly over-predicted the capacity of connections with two vertical rows of bolts.

The Canadian standard at the time, CSA S16 (2001), provided two equations to calculate block shear failure. The theory behind these equations was that when the capacity of the connection was reached, the net tension area had a nonuniform stress distribution. These equations were found to be conservative with average test-to-predicted ratio of 1.20 and a coefficient of variability of 0.12.

The American design provisions, AISC (1999), also contained two equations. One of them combined yielding on the gross tension area with rupture on the net shear area while the other combined rupture on the net tension area with yielding on the gross shear area. This design method had a test-to-predicted ratio of 1.00 with a coefficient of variation of 0.19, which show relatively low precision. Even more so, when observing tests with two vertical rows of bolts, the test-to-predicted ratio drops to 0.76 indicating the design method under predicts the actual capacity of the member.

The Eurocode 3 *ENV* 1993-1-1 (ECS 1992) set forth an equation that combined shear yielding on the gross shear area with a reduced normal stress over the tension area of the connection. This design provision produced conservative results, with a test-to-predicted ratio of 1.20 and a coefficient of variation of only 0.11. This design standard was the most consistent amongst the standards compared; also, the results between specimens with one and two vertical rows of bolts were similar.

The design provisions outlined in The Standard for Limit States Design of Structures of the Architectural Institute of Japan (AIJ 1990) are theoretically the most conservative of the ones investigated. This is because it is assumed that stresses always act over the net area of the connection. Franchuk et al. (2004) noted that not only did this design standard have a test-to-predicted ratio of 1.29 with a coefficient of variation of 0.23, the highest amongst all the tests, but the method outlined was not representative of the actual failure mechanisms for block shear in coped beams.

The safety factor of each of the investigated provisions was calculated. It is important to note that members such as beams are designed to have a safety index of 3.0 while connections are assigned a value of 4.5. Franchuk et al. (2004) found that on average the safety factor for connection with one vertical row of bolts ranged from 4.1 to 4.7 while that for connections with two vertical rows of bolts ranged from 1.9 to 3.1; evidently, the concurrent design provisions were inadequate for beam connections with two vertical rows of bolts.

Franchuk et al. (2004) propose a single equation to design for block shear failure; this is possible due to the fact that the observed failure mode is consistent – rupture on the tension face after yielding has occurred on the shear face, but prior to shear rupture. Equation (2-7) was proposed, which is also the basis of the current provision outlined in the Canadian Standard, S16 (2009).

This equation had a test-to-predicted ratio of 1.01 and a coefficient of variation of only 0.12; important to note is the fact that for connections with one vertical row of bolts the values attained are a ratio of 0.98 with a coefficient of 0.09, and for connections with two vertical rows of bolts the ratio is 1.07 with a variation of 0.15. Out of all the design provisions investigated, the proposed equation is the most accurate and consistent.

$$V_{BS} = R_t A_{nt} F_u + A_{gv}\left(\frac{F_y + F_u}{2\sqrt{3}}\right) \qquad \textbf{(2-7)}$$

where R_t = tension face stress connections (set to 0.9 for connections with one row of bolts and 0.3 for connections with two rows of bolts; A_{nt} = net tension area; A_{gv} = gross shear area; F_y = yield strength; and F_u = tensile strength.

2.2.5 Coped Beam Reinforcements

While investigating the lateral torsional buckling and local web buckling on coped beams, Cheng et al. (1984) also inspected the effect of different cope reinforcements on these failure modes. With regards to lateral torsional buckling, two reinforcement configurations were investigated: a single horizontal stiffener and the combination of a horizontal and vertical stiffener. It was found that the latter configuration is more effective and therefore the authors suggested that it should be used for beams that are doubly coped or when only the compression flange is removed. It was observed that web crippling occurred at the end of the horizontal stiffener; as such, it was suggested that the extension of the reinforcement past the cope should be at least one-third of the cope length in order to distribute the concentrated load along the stiffener length. If these guidelines are followed, then no reduction in the lateral buckling capacity of the section is required in design. For specimens that only have the tension flange removed, the recommended stiffener extension length is equivalent to the cope depth.

Cheng et al. (1984) provided similar recommendations in order to avoid local buckling with the use of reinforcement. For this particular failure mode, three different reinforcement configurations were investigated: a horizontal stiffener, combined horizontal and vertical stiffeners, and a doubler plate. For rolled sections it was suggested to use either a horizontal stiffener with an extension length greater than or equal to the cope depth or a doubler plate with the same extension and of a thickness similar to that of the beam web. For the latter configuration, it should be verified that the new thickness of the beam web is sufficient to reach

the predicted critical buckling load. For thin web members, those with a depth-to-thickness ratio greater than 60, the authors suggest using the combined horizontal and vertical stiffeners with an extension length greater than or equal to a third of the cope length. If these suggestions were followed it was found that no reduction has to be made in design with regards to the capacity of the members; however, it is still necessary to check the yielding and buckling capacity of the sections.

Yam et al. (2011) investigated the behaviour of reinforced coped beams building on the recommendations of Cheng et al. (1984). The same connection as Yam et al. (2003), welded end plate to the beam web and bolted to the stub column, was used for this experimental program. The detailing suggestions provided by Cheng et al. (1984) were developed mainly based on finite element models; Yam et al. (2011) intended to provide experimental evidence for these reinforcement details. Figure 2.11 shows the detailing suggested by Cheng et al. (1984), which are the current details specified in the 14th Edition AISC Manual (2011); Figure 2.12 shows the three different reinforcement configurations tested in the 2011 study. The configuration with longitudinal stiffeners was used to assess the effectiveness of the same in increasing the strength of the coped section; on the other hand, the specimens with transverse stiffeners (both single and double) were used to assess the capability of these configurations in preventing the failure mode of rigid body moment of the longitudinal stiffeners.

Ten full-scale tests using 3400mm long W360x6 (UB356x127x33) Grade S355 steel (i.e., $f_{y,\text{nominal}}$ = 345MPa) were conducted by Yam et al. to investigate the effects of longitudinal stiffeners (L_x), length of transverse stiffeners (L_y), combined longitudinal and transverse stiffeners, double transverse stiffeners, cope depth (d_c), and cope length (c). The specimens were divided into two series; Series A specimens in general had a cope depth approximately equal to 60mm, whereas Series B specimens had a cope depth equal to 105mm. The cope length was between 265mm and 315mm for both series. The length of the longitudinal stiffeners varied from 265mm to 412mm with the purpose of detailing the extension equal to the cope depth; this was the case for all specimens except for one that had an extension length equal to twice the cope depth (this specimen had a cope depth of 105mm and cope length of 315.2mm). The length of the transverse stiffeners was detailed to be twice the cope depth. It is also important to note that the test setup used was designed to allow for moderate rotation at the end of the beam.

The failure mode observed for the two control (unstiffened) coped beams consisted of local web buckling at the cope. For the specimens with longitudinal stiffeners with an extension length equal to the cope depth, flexural yielding of the full beam section was observed first followed by lateral movement of the stiffeners due to web crippling. These specimens were able to develop the full plastic moment capacity of the section; however, once the maximum applied moment was reached, the moment-deflection curves of these decreased abruptly due to web crippling. For the specimen with a longer extension length, lateral rigid body movement of the stiffener was observed without any significant yielding in the full beam section; also, as opposed to the other specimens, this beam exhibited a more gradual loss in stiffness after the maximum moment was reached.

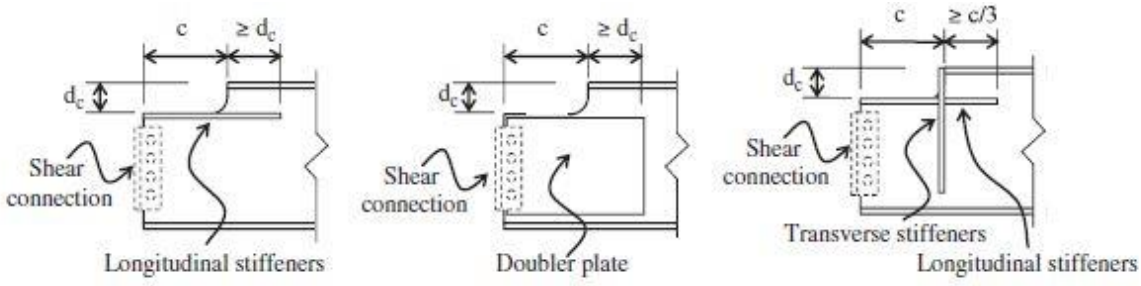

Figure 2.11 – Reinforcement configurations tested by Cheng et al. (1984) (Yam et al. 2011)

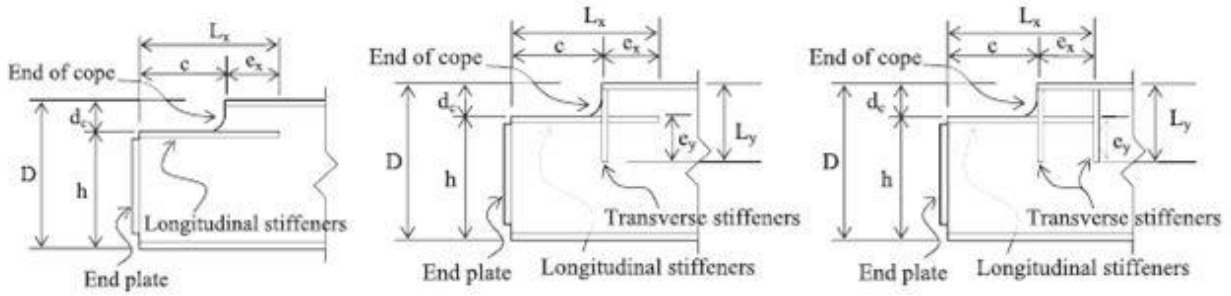

Figure 2.12 – Reinforcement configurations tested by Yam et al. (2011)

The specimens with combined longitudinal and transverse stiffeners first underwent flexural yielding of the full beam section followed by buckling of the flange near the loading position. Little to no lateral movement of the longitudinal stiffeners was recorded especially in the case of the specimens with double transverse stiffeners. These specimens were able to withstand larger deflections at the ultimate load levels compared to the other reinforced specimens; this was true with the exception of the specimen with a longer extension.

As expected, it was observed that if the cope depth of an unreinforced member increased then the web buckling capacity of the member decreased. However, since the reinforcing stiffeners prevented web crippling from happening and allowed for the beam to develop the full plastic capacity, the cope depth did not affect the capacity of the reinforced members. When observing the effect of cope length, by increasing the length by 52% the capacity of the section decreased 18%; hence, an increased cope length has an adverse effect on coped beam capacity. This study validates the detailing proposed by Cheng et al. (1984) but suggests that the horizontal stiffener length be at least twice the cope depth rather than greater than or equal to the cope depth.

Additionally, Yam et al. (2011) observed that that the ultimate end moments of the specimens were only 1.7% to 8.8% of the maximum bending moment of the section. The authors suggested that even if there was no end moment developed in the connection, this assumes a "perfect" pinned connection, the ultimate reaction at this location would only slightly decrease. Since the ratio of the maximum bending moment to the corresponding plastic moment capacity ranged from 1.08 to 1.20 it can be stated that in the case that the connection was a perfect pin, the section would still be able to develop the full plastic moment capacity.

Yam and Chung (2013) conducted a finite element validation study based on the ten full-scale specimens tested by Yam et al. (2011) using ABAQUS (Abaqus, 2013). Based on a parametric study the effects of the length of longitudinal stiffeners, combined longitudinal and transverse stiffeners, cope length, and cope depth on the strength and behaviour of reinforced coped beams were examined. The coped beams were modeled using four-node, reduced integration, and finite strain shell elements. Spring elements were used to simulate the washers used between the end plate and the support column flange as well as bolt shanks on the bolt holes. In order to allow for local web buckling in the model, an initial imperfection was introduced based on the buckled shape of the web from an elastic analysis, and a scale factor of 0.05 was used in ABAQUS to adjust the magnitude of the imperfection.

The finite element model results compared well with those of the experimental studies. The observed failure modes included web buckling in the coped region, rigid body movement of the longitudinal stiffeners due to web crippling, flexural yielding of the gross section at the location of loading followed by rigid body movement of the longitudinal stiffeners, and flexural yielding of the gross section followed by local buckling of the flange at the loading position. By

observing the load deflection curves produced from the finite element models and comparing them to the experimental results it can be seen that the model captures the deflection, including local web buckling, accurately. From these curves it was also observed that specimens with combined longitudinal and transverse stiffeners and double transverse stiffeners have a more stable inelastic load deflection behaviour than specimens with horizontal stiffeners only. By observing the strain distribution data, it was also observed that longitudinal stiffeners having a shorter extension length (extension equal to the cope depth rather than twice the cope depth), the neutral axis of the specimen shifts slightly downwards away from the stiffener demonstrating that the gross beam section has a higher influence on the specimen with the short extension.

The parametric study consisted of 66 models using the same reinforcement configurations as those that were tested and three different beam sections – W460x74 (UB 457x191x75), W360x33 (UB 356x127x33), and W410x39 (UB 406x140x39) – representing a spectrum of web depth-to-thickness ratios. None of the models analyzed experienced flexural failure at the coped section; however, flexural failure in the gross region did take place. Most of the W460 and W360 specimens were able to reach their full moment capacity in the gross region of the beam or shear yielding capacity in the coped region; however, the W410 sections exhibited web crippling before reaching their corresponding flexural or shear capacities. It was also noted that by increasing the cope depth, rigid body movement of the longitudinal stiffeners due to web crippling was observed which resulted in a decreased resistance of the specimens. With regards to cope length, it was observed that for specimens that experienced rigid body movement of the longitudinal stiffeners due to web crippling, an increase in cope length resulted in in a decrease in capacity. On the other hand, for specimens that exhibited local buckling in the flange close to the loading point, change in cope length resulted in negligible change in beam capacity.

For the most part, the specimens reinforced by only longitudinal stiffeners with extension length equal to the cope depth failed due to rigid body movement of the stiffeners due to web crippling (referred to in the study as failure mode “R”) or due to yielding of the gross beam section with subsequent rigid body movement of the stiffeners due to web crippling (YR). The specimens with an extension equal to twice the cope depth and those with combined longitudinal and transverse stiffeners failed due to yielding of the gross beam section with subsequent flange buckling near the loading position (YF) or failure mode R.

In all cases, the specimens reinforced with longitudinal and transverse stiffeners had a larger ultimate moment and shear capacity, and in most cases these were greater than the predicted plastic moment and shear yielding capacities respectively. For the W460 section, most of the specimens that were reinforced only with longitudinal stiffeners were not able to develop the full plastic moment capacity but did develop their full shear yielding capacity. All but two of the W360 sections, regardless of reinforcement, were able to develop the full moment capacity but none developed the full yielding capacity. For the W410 specimens, only the sections with a cope length-to-beam depth ratio of 0.3 were able to develop both the moment and shear capacities; therefore the configuration with longitudinal and double transverse stiffeners was analyzed and results showed that this reinforcement configuration did allow for the specimen to develop both capacities.

The proposed coped beam reinforcement details after the numerical study remain essentially the same as those proposed by Yam et al. (2011) with only slight variations on the limits of applicability of these proposed equations. These limits are based on the web depth-to-thickness ratio, cope depth-to-beam depth ratio, and cope length-to-beam depth ratio. Recommendations are made for specimens with longitudinal stiffeners (there are to have an extension of twice the cope depth) and specimens with combined longitudinal and double transverse stiffeners (the extensions of these are to be equal to the cope depth). These two reinforcement configurations are suggested in order to cover as many specimens and failure modes as possible.

2.3 CURRENT DESIGN PROCEDURES

Current design procedures for both extended shear tabs and coped beams used in North America are outlined in this section. For the experimental program and results contained herein, guidelines presented in the Canadian Standards Association (CSA) S16 Standard (2009), the 10th Edition of the CISC Handbook of Steel Construction (2010), the American National Standards Institute (ANSI) AISC 360 Specification for Structural Steel Buildings (2010), and the 14th Edition of the American Institute of Steel Construction Manual (2011) were followed. These procedures are outlined in this section and further detail is provided in Section 3.5 where the design of the test specimens is described.

2.3.1 Shear Tab Connections

2.3.1.1 United States of America – American Institute of Steel Construction

Based on the research of Muir and Thornton (2004) and Muir and Hewitt (2009) a design procedure for conventional and extended shear tabs has been developed, and included in the 14th Edition of the AISC Manual (2011).

In order for a shear plate to be categorized as a conventional configuration it must satisfy five different criteria:

1) Only a single vertical row of bolts ranging between 2 and 12 bolts
2) The distance from the bolt line to the weld line, the "*a*" distance, must be less than or equal to 88.9mm (3 1/2")
3) Standard holes or short-slotted holes transverse to the direction of the supported member reaction are permitted
4) Vertical and horizontal edge distances must satisfy the outlined requirements
5) Either the plate thickness or the beam web thickness must satisfy the maximum thickness requirement outlines in the design manual

For conventional configurations, the shear capacity of the bolt and plate must be checked, and the guidelines state that plate buckling will not occur.

Extended configurations are those that do not satisfy the criteria of conventional configurations. The design standard outlines six design checks that must be performed for such configurations:

1) Design bolt group for bolt shear and bolt bearing
2) Determine the maximum plate thickness in order to ensure the connection has enough ductility yet does not exceed the capacity of the bolt group
3) Verify the shear yielding, shear rupture, and block shear rupture capacity of the shear plate
4) Verify the shear yielding and combined yielding due to flexure and shear of the plate using the Von Mises criteria
5) Verify the buckling capacity of the shear plate
6) Ensure sufficient lateral support to prevent lateral torsional buckling

2.3.1.2 Canada – Canadian Institute of Steel Construction

It must be noted that the Canadian design standard does not provide a detailed design procedure for extended shear tabs, only guidelines for conventional shear tab connections are provided in the Handbook of Steel Construction (CISC, 2010). These connections have an "*a*" distance of 89mm (3.5"), a single vertical row of bolts ranging from two to seven bolt holes, and also distinguish between rigid and flexible supports. The CISC Handbook provides engineers with tables based on these parameters to determine shear plate thickness and required weld size. The design methodology outlined in the Canadian standard is based on the design method established by Astaneh et al. (1989). In this publication, the researchers outline the design procedure of shear plates in five steps:

1) Calculate the number of bolts required to resist the both the applied shear and moment – equations were developed to determine the effective bolt eccentricity based on end support conditions
2) Calculate required gross area of plate
3) Check effective net section strength
4) Calculate actual allowable shear yield strength of the selected shear plate
5) Check bearing capacity of bolt group

The developed design procedure had certain limitations, including but not limited to bolt spacing equal to 76.2mm (3"), the thickness of the shear plate had to be less than equal to half of the bolt diameter plus 1.6mm (1/16").

2.3.2 Coped Beams

2.3.2.1 United States of America – American Institute of Steel Construction

The design procedure outlined by the American Manual of Steel Construction is based on the research performed by Cheng et al. (1984). The following checks are outlined:

- Flexural rupture strength for top or double coped beams
- Flexural local buckling strength for top or double coped beams

It is important to note that two formulations are provided for the local buckling strength of coped beams. When the cope depth is less than or equal to 20% of the beam depth, the lateral torsional buckling model developed by Cheng et al. (1984) and Cheng and Yura (1986) is presented;

however, when the cope depth is larger than that, the classical plate buckling may be used conservatively.

This Manual also provides engineers with guidelines for reinforcing coped beams. These are the same procedures developed by Cheng et al. (1984).

2.3.2.2 Canada – Canadian Institute of Steel Construction

Neither the current edition of the CSA S16 Standard (2009) nor the Handbook of Steel Construction (CISC 2010) provide engineers with guidelines to design coped beams with the exception of guidelines for block shear rupture. An equation to predict this failure mode, based on the findings of Franchuk et al. (2004), is presented along with a design aid table with coefficients allowing engineers to easily calculate the block shear resistance of a given connection based on the same equation.

2.4 SUMMARY AND CONCLUSIONS

Extensive research has been performed on shear tab connections, which have led to the current design recommendations included in the AISC 14th Edition Manual of Steel Construction (2011). Until the newest edition of this document became available, design guidelines were only available for conventional connection configurations limiting the applicability of these methods to shear plates with only a single row of bolts and with an eccentricity ("*a*" distance) of no more than 88.9mm (3 1/2") inches.

The seminal work and subsequent recommendations developed by Cheng et al. (1984) for coped beams have been proven by multiple researchers to be applicable yet conservative in most design situations. These researchers outlined the two most prevalent failure modes observed in coped beam – lateral torsional buckling and local web buckling and provided a set of equations to design for both.

The equations developed to design for lateral torsional buckling are based on the interaction of the coped and uncoped regions of the beam. Variables such as span length, cope length (c), and cope depth (d_c) were investigated. Different sets of equations were developed for specimens with copes at both ends of the unbraced length and for specimens with a single cope at the end of the unbraced length. Subsequent research by Yam et al. (2000) suggest changes to these interaction equations in order to account for the fact that local web buckling might occur prior to

lateral torsional buckling when the cope length-to-web depth ratio is less than or equal to 2.5. Similarly, Dowswell and Whyte (2014) also noted that local bucking may occur prior to lateral torsional buckling; therefore, they proposed a modified design procedure to account for this phenomenon based on reduced plastic moment strength for the coped beam.

With regards to local web buckling, the equation developed by Cheng et al. (1984) has been shown to still be appropriate for design and is currently part of the AISC 14th Edition Manual (2011). This equation is based on two factors, a plate buckling factor (k) and a single adjustment factor (f) accounting for cope length-to-reduced beam depth. Yam et al. (2003) suggest a factor, a shear buckling factor (k_s) based on analytical testing indicating that shear stresses dominate the buckling behaviour. According to this study, the modified equation provides engineers with more accurate predictions.

Another failure mode was investigated by Franchuk et al. (2003) and (2004) – block shear failure. These investigations targeted block shear failure in coped beams and compared measured results with design provisions around the world (United States, Canada, Europe, and Japan). The researchers found that the concurrent design provisions were inconsistent in predicting this failure mode and also grossly over-predicted the capacity of two-lines connections compared to single line connections. It was observed that the development of block shear in the test specimens consisted of rupture on the tension face after yielding had occurred shear face, but prior to shear rupture. Based on these observations, a single equation predicting block shear, and accounting for one and two lines of bolts, was proposed and is the current design equation outlined in the Canadian S16 Standard (2009).

Cheng et al. (1984) also investigated reinforcement configurations to prevent lateral torsional buckling and local web buckling. The recommendations set forth are characterized by the appropriate extension length of the stiffener or double plate past the cope; three reinforcement configurations are outlined in this research: horizontal stiffener, combined horizontal and longitudinal stiffener, and doubler plate. Yam and Chung (2013) investigated the effectiveness of the two stiffener configurations mentioned above and a third configuration, which was a horizontal stiffener with two longitudinal stiffeners. This experimental program validated the results presented by Cheng et al. (1984), but suggest doubling the extension length of horizontal stiffeners (making the extension length twice the cope depth) when using the single horizontal

stiffener configuration; also, the authors suggest utilizing the configuration with two longitudinal stiffeners in order to avoid web crippling at the end of the horizontal stiffener.

Despite the fact that research has covered both rigid and flexible supports, it is important to highlight that no design guidelines exist for the girder webs to avoid a punching mechanism when beam-to-girder flexible connections are designed. The importance of developing such provisions is highlighted by the fact that said failure mode has been observed by multiple researchers and no guidelines have been suggested that effectively prevent this limit state.

Research on directly welded connections has shown that such connections are less desirable due to limited ductility; however, more research is required in this field before ruling out the implementation of this connection. The benefits involved with designing directly welded beam-to-girder connections warrant further research into the capacity and ductility of the same.

Based on the reviewed literature, the behaviour of coped beams is complex; so much so, that currently there are no design provisions in Canada for these members. Additional research into the performance of these members along and varying reinforcement details is required.

CHAPTER 3

DESIGN OF TEST SPECIMENS AND DESCRIPTION OF TESTING APPARATUS

3.1 OVERVIEW

Thirteen full-scale tests were performed at McGill's Jamieson Structures Laboratory in order to investigate the behaviour of beam-to-girder extended shear tab and coped beam connections subject to shear. The design of these specimens was done in accordance with Canadian and American Standards: the Canadian Standards Association (CSA) S16 Standard (2009), the 10th Edition of the CISC Handbook of Steel Construction (2010), the American National Standards Institute (ANSI) AISC 360 Specification for Structural Steel Buildings (2010), and the 14th Edition of the American Institute of Steel Construction Manual (2011). Our industry partners provided feedback into selecting specimens that represent the current state of practice in North America.

The test setup used for these experiments was, in general, conceived following the setup designed by Marosi (2011), and furthermore was similar to the beam-to-girder reaction frame used by Hertz (2014). Hertz's configuration for the beam-to-girder reaction frame was modified in order to simulate the presence of a concrete slab in an actual connection. This restraint is shown in subsequent figures as an HSS member resting on the test girder.

3.2 SPECIMEN SELECTION

Thirteen specimens were selected with the purpose of investigating common practice in the professional field. These specimens can be separated into six distinct categories: extended partial depth shear tabs, extended full depth shear tabs, double coped beams, single coped beams, coped beams welded in-shop, and single cope haunched beams. It is important to note that for all the configurations with the exception of the haunched specimen, the pitch and gauge of the bolt holes was equal to 76.2mm (3"). The steel used for all hot-rolled sections was A992 Grade

50 (i.e., $f_{y,\text{nominal}}$ = 345MPa) (CISC, 2010) while the steel used for all other components (shear plates, supporting stiffeners, reinforcing components, retrofit plate, and haunch plate) was ASTM A572 Grade 50 (i.e., $f_{y,\text{nominal}}$ = 345MPa) (CISC, 2010) steel.

For the bolted connections, A325 bolts (i.e., $F_{u,nominal}$ = 825MPa) (CISC, 2010) were used snug tight in standard holes, and were detailed such that the threads were not in the shear plane. The supporting stiffener or extended shear plates for all these specimens were welded on three sides to the supporting stiffener using 7.9mm (5/16") fillet welds. The exception to this were the two partial depth extended shear tabs, for these two specimens, 6.4mm (1/4") fillet welds were used on two sides of the shear plate.

In Section 3.2, a description of the specimen configurations is provided; the explanation of the design of the test specimens can be found in Section 3.3.

3.2.1 Single Coped Beams

Three single coped beam specimens were tested. The three specimens consisted of a W310x60 (W12x40) beam connected to a W760x257 (W30x173) girder with a 19.1mm (3/4") thick supporting stiffener and six 3/4" Ø (19.1mm) bolts. The top flange was coped with a cope length of 177.8mm (7") and a depth of 39.7mm (1 9/16").

The first specimen was unreinforced (Figure 3.1a) and served as a benchmark for the other two specimens that were reinforced. The second specimen was reinforced with a 266.7mm (10 1/2") long horizontal stiffener at the cope (Figure 3.1b); therefore, the extension length of the stiffener past the cope was 88.9mm (3 1/2"), which is greater than twice the cope depth – the suggested length provided by Yam et al. (2011). The third specimen was reinforced with a welded doubler plate (Figure 3.1c) that extended 66.7mm (2 5/8") past the cope, a distance greater than the cope depth, which is suggested by Cheng et al. (1984).

It is important to note that the coping details as well as the reinforcements were selected based on the recommendations suggested by Cheng et al. (1984) and substantiated by subsequent research as presented in Chapter 2.

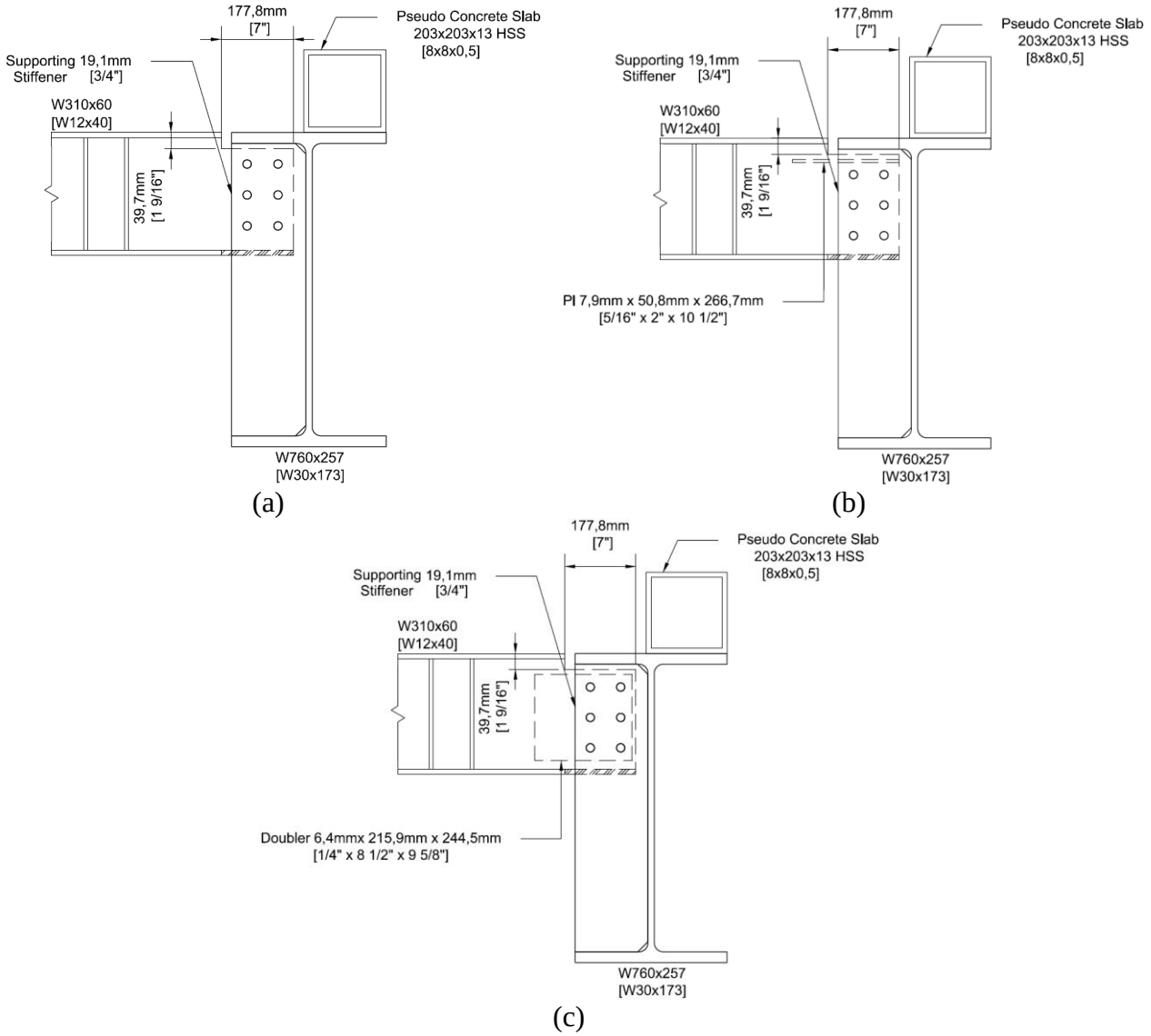

Figure 3.1 – Single coped beams: (a) Specimen 1, (b) Specimen 2, (c) Specimen 3

3.2.2 Double Coped Beams

Similarly, three double coped beam specimens were tested. The first specimen was unreinforced (Figure 3.2a), the second had horizontal stiffeners on both top and bottom copes (Figure 3.2b) that extended 114.3mm (4 1/2”), which was greater than twice the cope depth. The third configuration had a doubler plate (Figure 3.2c), which was also designed with adequate extension length based on the suggestions of Cheng et al. (1984).

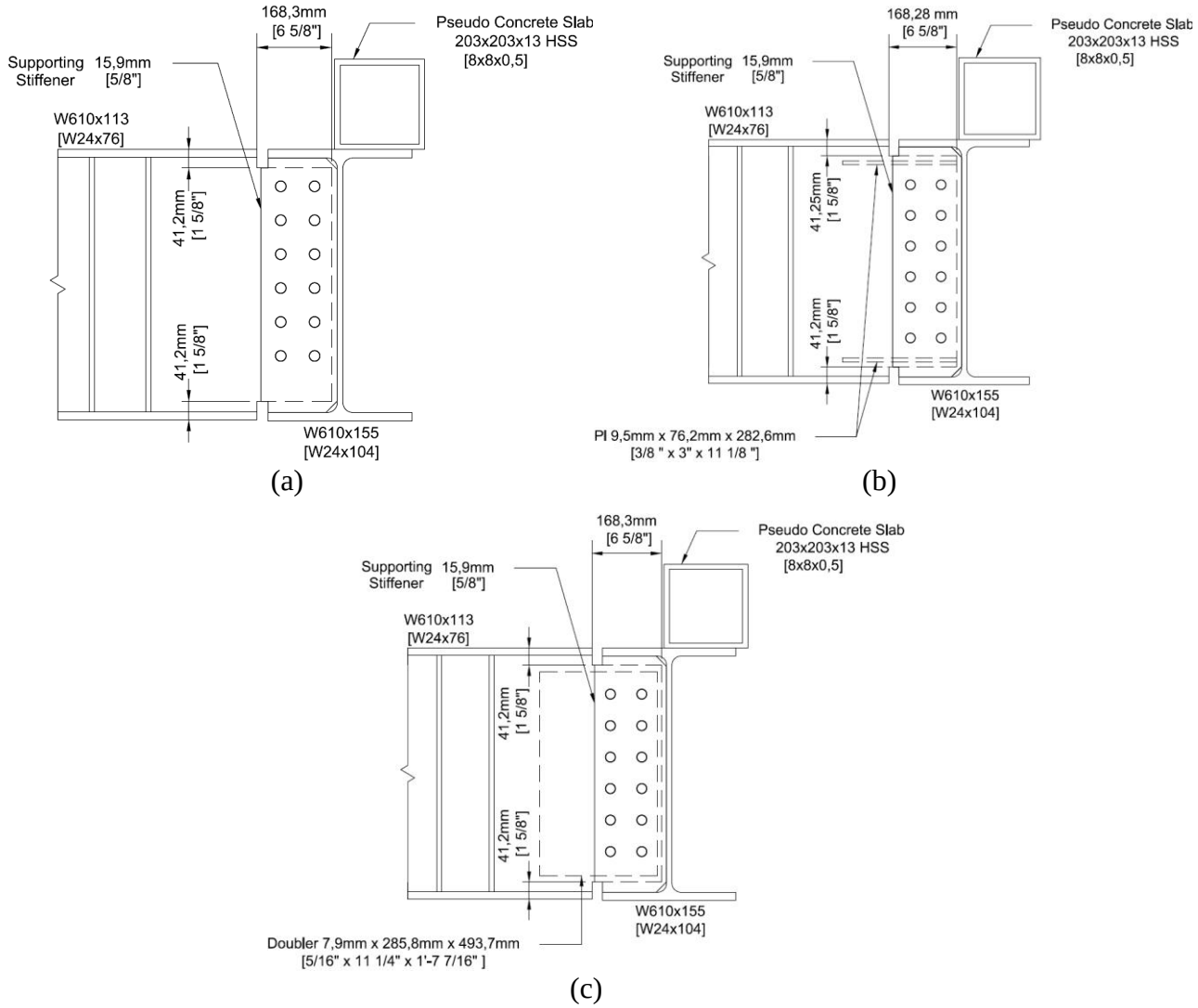

Figure 3.2 – Double coped beams: (a) Specimen 4, (b) Specimen 5, (c) Specimen 6

All three configurations were composed of a W610x113 (W24x76) beam, a W610x155 (W24x104) girder and a 15.9mm (5/8") supporting stiffener with two rows of six 7/8" Ø (22.2mm) bolts. For these specimens both the top and bottom flanges were coped; the detailing of the two copes was nominally identical, 168.3mm (6 5/8") long and 41.2mm (1 5/8") deep.

3.2.3 Coped Beams Welded In-Shop

Two specimens that were coped and welded in-shop were also tested. In the first configuration, the beam, W310x74 (W12x50), and the girder, W310x143 (W12x96), were of approximately the same depth (Figure 3.3a); therefore, both the top and bottom flanges were coped. The cope length was 161.0mm (6 3/8") long, the top cope was 47.6mm (1 7/8") deep and the bottom cope was 38.1mm (1 1/2") deep. The reduced beam web was welded on both sides with 7.9mm

(5/16") fillet welds that were 203.2mm (8") long. In the case of the second specimen, a W610x140 (W24x94) beam framed into a W760x257 (W30x170) girder (Figure 3.3b) connected by 11.1mm (7/16") fillet welds over a length of 406.4mm (16") on both sides of the reduced beam. The top flange of the beam had a cope that was 195.4mm (7 11/16") long and 50.8mm (2") deep.

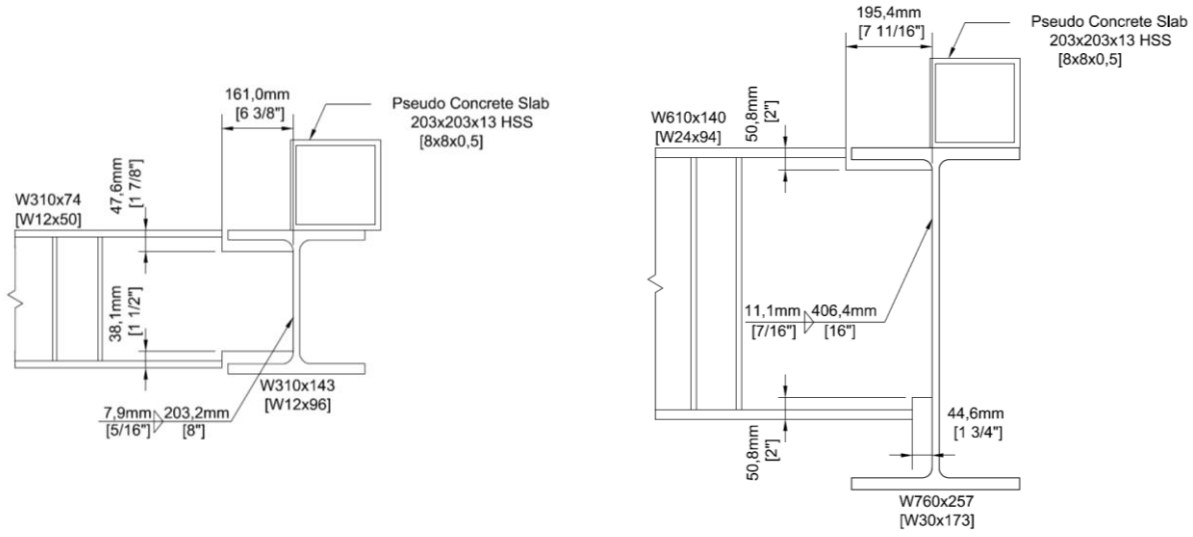

(a) (b)

Figure 3.3 – Coped beams welded in shop: (a) Specimen 8, (b) Specimen 10

As shown in Figure 3.3b, a small portion of the bottom flange was also removed; however, this is not considered to be a cope. This portion of the beam was removed in order to avoid binding between the beam and girder during testing at relatively small connection rotations and to facilitate the welding procedure in the fabrication shop. Therefore, the first specimen is detailed as a double coped beam whereas the second specimen is detailed as a single coped beam. The purpose of these specimens was to test the performance of connections that are welded in-shop and therefore have higher quality welds compared to connections that are welded on-site; it is important to note that these configurations may also facilitate erection during construction. It is important to note that both weld size and length were determined following the findings presented in Section 2.2.2.

3.2.4 Single Coped Haunched Beam

Haunched beams are commonly used in structures when two components of different depths, or with different elevations, connect to the same girder. The haunch beam allows for the top of

steel of the two components, such as a beam and an open web steel joist, to be the same resulting in a level plane, as was shown in Figure 1.4a. One haunched beam with a single cope was also tested (Figure 3.4).

This is the first specimen of its kind to ever be tested and therefore would provide engineers with valuable information for a configuration that is used in practice. Figure 3.4 shows how the beam, W310x60 (W12x40), connects to the girder, W610x155 (W24x104), through a supporting stiffener with a thickness of 15.9mm (5/8") and six 3/4" Ø (19.1mm) bolts. The 7.9mm (5/16") thick haunched plate was welded to the bottom of the beam using a combination of a 6.4mm (1/4") fillet weld on one side of the plate and a partial penetration weld on the other. The cope length selected was 177.8mm (7") while the cope depth was 133.4mm (5 1/4").

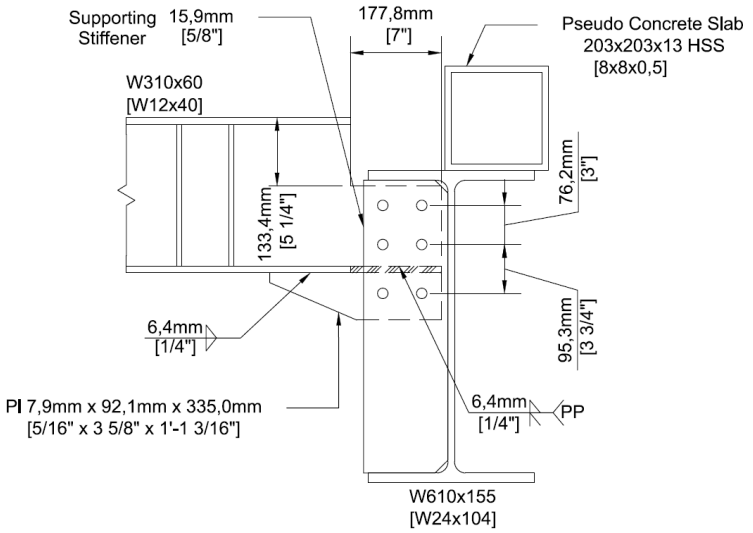

Figure 3.4 – Single coped haunched beam

3.2.5 Partial Depth Extended Shear Tabs

Two partial depth extended shear tabs were tested; these configurations were nominally identical to the configurations tested by Hertz (2014). The purpose for testing these configurations a second time was to investigate if by including a pseudo concrete slab, the mechanism of girder web punching and top flange rotation observed by Hertz would be prevented.

The first of these specimens, Configuration 6J (Figure 3.5a), consisted of a W310x60 (W12x40) beam connected to a W610x125 (W24x84) girder by means of a 9.5 mm (3/8") shear plate and six 3/4" Ø (19.1mm) bolts. This connection was designed with an "*a*" distance of 165.1mm (6 1/2"). After this specimen was tested, it became evident that the additional restraint, although

did aid in reducing the plastic deformation in the girder, was not enough to prevent it altogether; as a result, the second partial depth extended shear tab specimen, Configuration 9J (Figure 3.5b), was retrofitted before testing. The idea behind this retrofit was to engage a larger area of the girder web in resisting the applied load by welding a steel plate between the shear tab and the girder web. This configuration, which also used a W310x60 (W12x40) beam, was connected to a W760x257 (W30x173) girder with a 9.5mm (3/8") shear plate and six 3/4" Ø (19.1mm) bolts; the "*a*" distance used for this specimen was originally 241.3mm (9 1/2"); however, once the retrofit plate was installed it was concluded that the "*a*" distance was reduced to 81.0mm (3 3/16"). This occurred because by adding the steel plate, a "beam-like" component was created using the shear plate as a web and the girder top flange and retrofit steel plate as flanges; the new "*a*" distance was taken as the distance between the first row of bolts and the edge of the retrofit plate. The retrofit plate was dimensioned 19.1mm x 177.8mm x 228.6mm (3/4" x 7" x 9"), and was connected to the bottom of the shear plate and the girder web with 6.4mm (1/4") fillet welds using an E4918 electrode.

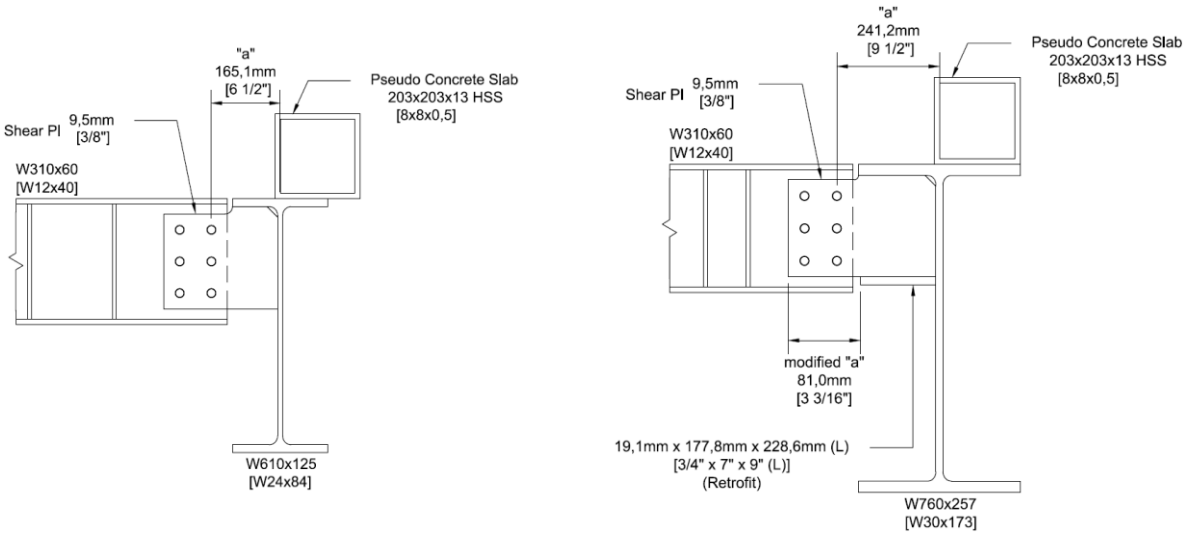

(a) (b)

Figure 3.5 – Extended shear tab partial depth (a) Specimen 6J, (b) Specimen 9J

3.2.6 Full Depth Extended Shear Tabs

Two full depth extended shear tabs were tested that also corresponded to a configuration tested by Hertz (2014). The intent behind these specimens was to explore the impact of the additional restraint and increased plate thickness on the observed buckling in the shear tab. The test performed by Hertz underwent buckling at the neck of the shear tab; therefore the intent was to

decrease the *b/t* ratio of this component by increasing the thickness of the same. In this instance, the *b* distance is defined as the maximum width of the shear tab as shown in Figure 3.6; *t* is the thickness of the respective shear tab. The specimen tested by Hertz (2014) had a plate thickness equal to 9.5 mm (3/8") while the ones tested in this experimental program were 12.7 mm (1/2") thick; therefore, the *b/t* ratio of the shear tab would decrease from 28.7 to 21.5. The two tested specimens were nominally identical with W310x60 (W12x40) beams and W760x257 (W30x173) girders, but one of them was tested with the designed restraining system (Figure 3.6a) while the other was tested without the restraint (Figure 3.6b).

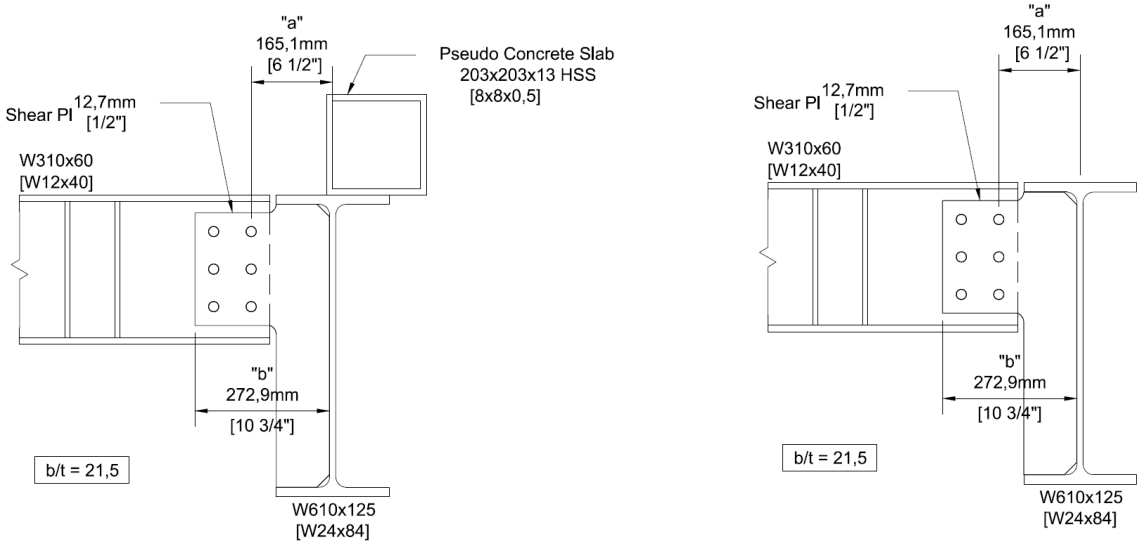

Figure 3.6 – Extended shear tab full depth (a) Specimen A1, (b) Specimen A2

3.3 DESIGN OF TEST SPECIMENS

All thirteen specimens were designed in accordance with CSA S16 (2009) Design of Steel Structures Standard, and the CISC (10th Edition, 2010) Handbook of Steel Construction, AISC 360 Specification for Structural Steel Buildings (2010), and the AISC (14th Edition, 2011) Manual of Steel Construction. Table 3.1 summarizes the key design parameters of all thirteen tested specimens as discussed throughout Section 3.2.

In line with the objectives of this research, the Canadian standards were used whenever possible, but as outlined in Section 2.3, there is a lack of guidance for the design of extended shear tabs and coped beams in these documents; therefore, the AISC Manual of Steel Construction was used to supplement the design as described herein.

Table 3.1 – Specimen summary

Category	Specimen	Beam Size	Girder Size	Shear Plate / Supporting Stiffener		Connection			Cope Details		"a" Distance	Steel Reinforcement, Retrofit, and Haunch	Notes
				Thickness	Weld Size	Bolts (# - size)	Weld Size	Weld Length	Cope length (c)	Cope depth (d)			
Partial Depth Extended Shear Tab	Specimen 6J	W310x60 (W12x40)	W610x125 (W24x84)	9.5mm (3/8")	6.4mm (1/4")	6 - M20 (6 - 3/4" Ø)	-	-	-	-	165.1mm (6 1/2)	-	Based on Hertz (2014)
	Specimen 9J	W310x60 (W12x40)	W760x257 (W30x173)	9.5mm (1/8")	6.4mm (1/4")	6 - M20 (6 - 3/4" Ø)	-	-	241.3mm (9 1/2)	-		Retrofit 19.1mmx 177.8mm x 228.6mm (3/4" x 7" x 9")	Based on Hertz (2014) Retrofit steel plate
Full Depth Extended Shear Tab	Specimen A1	W310x60 (W12x40)	W610x125 (W24x84)	12.7mm (1/2")	7.9mm (5/16")	6 - M20 (6 - 3/4" Ø)	-	-	165.1mm (6 1/2)	-		-	Based on Hertz (2014)
	Specimen A2	W310x60 (W12x40)	W610x125 (W24x84)	12.7mm (1/2")	7.9mm (5/16")	6 - M20 (6 - 3/4" Ø)	-	-	165.1mm (6 1/2)	-		-	Based on Hertz (2014) No restraint
Single Coped	Specimen 1	W310x60 (W12x40)	W760x257 (W30x173)	19.1mm (3/4")	7.9mm (5/16")	6 - M20 (6 - 3/4" Ø)	-	-	177.8mm (7")	39.7mm (1 9/16")		-	Unreinforced
	Specimen 2	W310x60 (W12x40)	W760x257 (W30x173)	19.1mm (3/4")	7.9mm (5/16")	6 - M20 (6 - 3/4" Ø)	-	-	177.8mm (7")	39.7mm (1 9/16")		Horizontal Stiffener 7.9mm x 50.8mm x 266.7mm (5/16" x2" 10 1/2")	Horizontal Stiffener
	Specimen 3	W310x60 (W12x40)	W760x257 (W30x173)	19.1mm (3/4")	7.9mm (5/16")	6 - M20 (6 - 3/4" Ø)	-	-	177.8mm (7")	39.7mm (1 9/16")		Doubler Plate 6.4mm x 215.9mm 244.5mm (1/4" x 8 1/2" x 9 5/8")	Doubler Plate
Double Coped	Specimen 4	W610x113 (W24x76)	W610x155 (W24x104)	15.9mm (5/8")	7.9mm (5/16")	12 - M22 (12 - 7/8" Ø)	-	-	168.3mm (6 5/8")	41.2mm (1 5/8")		-	Unreinforced
	Specimen 5	W610x113 (W24x76)	W610x155 (W24x104)	15.9mm (5/8")	7.9mm (5/16")	12 - M22 (12 - 7/8" Ø)	-	-	168.3mm (6 5/8")	41.2mm (1 5/8")		Horizontal Stiffener 9.5mm x 76.2mm x 282.6mm (3/8" x 3" x 11 1/8")	Horizontal Stiffeners
	Specimen 6	W610x113 (W24x76)	W610x155 (W24x104)	15.9mm (5/8")	7.9mm (5/16")	12 - M22 (12 - 7/8" Ø)	-	-	168.3mm (6 5/8")	41.2mm (1 5/8")		Doubler Plate 7.9mm x 285.8mm x 493.7mm (5/16" x 11 1/4" x 1' 7 7/16")	Doubler Plate
Single Coped and Haunched	Specimen 7	W310x60 (W12x40)	W610x155 (W24x104)	15.9mm (5/8")	7.9mm (5/16")	6 - M20 (6 - 3/4" Ø)	-	-	177.8mm (7")	133.4mm (5 1/4")	Top 47.6mm (1 7/8") Bottom 38.1mm (1 1/2")	Haunch Plate 7.9mm x 92.1mm x 335.0mm (5/16" x 3 5/8" x 1' 1 3/16")	Haunch Plate
Welded In-Shop	Specimen 8	W310x74 (W12x50)	W310x143 (W12x96)	-	-	-	7.9mm (5/16")	203.2mm (8")	161.0mm (6 3/8")			-	Welded In-Shop Double Cope
	Specimen 10	W610x140 (W24x94)	W760x257 (W30x173)	-	-	-	11.1mm (7/16")	406.4mm (16")	194.5mm (7 11/16")	50.8mm (2")		-	Welded In-Shop Single Cope

During design, factored resistances were calculated using the applicable resistance factors and nominal material properties corresponding to the Canadian provisions. Also in accordance with CSA S16, the probable resistances were calculated by omitting the resistance factors and taking the yield stress as R_yF_y where $R_y = 1.1$; note that for ultimate resistances the same R_y factor was used. Detailed calculations of all the test specimens can be found in Appendix A.

3.3.1 Design of Coped Beam Specimens

Bolt shear resistance was calculated in accordance with Clause 13.12.1.2c of CSA S16 (2009). It is important to note that the bolt group was loaded eccentrically; as a result, the shear resistance of a single bolt was calculated and then multiplied by the coefficient "C" obtained by applying the Instantaneous Center of Rotation (ICR) method provided in the CISC Handbook (2010) in order to obtain the resistance of the complete connection based on the shear failure of the bolts. It is important to note that bolt lengths were selected such that the bolt threads did not intercept any shearing planes. Bearing resistance was calculated for both the beam web and the shear tabs based on Clause 13.12.1.2a of CSA S16 (2009) and Equation J3-6b of the AISC Specification (2010). The latter equation is a local check for tear-out rupture of a single bolt when deformation due to service loads is not a design consideration. Also, the block shear capacity of the beams was calculated according to Clause 13.11of CSA S16 (2009).

Shear yielding for the supporting stiffeners as well as the test beams was calculated in accordance with Clause 13.4.1.1 of CSA S16 (2009). It is important to note that the calculated gross shear area of the beams did not include the remaining flange for the single coped specimens nor the horizontal stiffeners for either specimen detailed with this particular reinforcement (Specimen 2 and Specimen 5); however, the doubler plate (Specimen 3 and Specimen 6) was included as part of the shear area. In a similar fashion to the shear yielding capacity of the section, the net shear rupture resistance was also calculated. The local stability of the supporting stiffener was also calculated according to Table 1 of CSA S16 (2009) to ensure the *b/t* ratio limit was met; it was assumed that this component can be treated as the stem of a WT shape – this was a conservative assumption.

The flexural yielding capacity at the cope section was determined based on the gross reduced area of the beam. Reduced area indicates that the cope depth was subtracted from the nominal beam depth. It is important to note that when calculating the section modulus of the section, the remaining flange area (in the case of single coped beams) was included as well as any

reinforcing components (stiffeners or doubler plates). The eccentricity considered for this design check was the distance from the centroid of the girder web to the end of the cope on the beam.

The same engineering principles used to calculate flexural yielding were used to calculate the flexural rupture resistance of the section. However, the area considered was the net reduced area at the last line of bolts; as a result, the area corresponding to the bolt holes was subtracted from the reduced gross area used in the previous calculation. Also, the eccentricity taken into consideration was the distance from the centroid of the girder to the last line of bolts on the beam.

Due to the lack of design provisions in CSA S16 (2009) to design for flexural buckling of coped beams, the procedure outlined in Part 9 of the 14th Edition AISC (2011) Manual was followed for both single and double coped beams. As shown in Sections 3.2.1 and 3.2.2, selected specimens had cope lengths less than or equal to twice the beam depth ($c \leq 2d$) and cope depths less than half the beam depth ($d_c \leq d/2$). The eccentricity used for these calculations was the distance from the centroid of the girder to the end of the cope. Also, the gross reduced area was used to calculate the section modulus as was the case for the flexural yielding at the cope.

The interaction between shear and axial forces based on the Von Mises criteria was performed based on the suggestions of the industrial sponsors. This design check for beams is not part of either the Canadian or the American design standards but has been requested by professional structural designers and was therefore included in the design of the laboratory specimens for this experimental program. Equation (3-1) is the interaction equation for shear and bending forces following the Von Mises criteria from which one can solve for the Von Mises shear force shown in Equation (3-2).

$$\left(\frac{V_{SY}}{V_{VM}}\right)^2 + \left(\frac{M_{FY}}{M_{VM}}\right)^2 \leq 1.0 \qquad \textbf{(3-1)}$$

$$V_{VM} = \frac{\phi_s F_y S_x'}{\sqrt{\left(\frac{S_x'}{0.66A_{gv}}\right)^2 + e^2}} \qquad \textbf{(3-2)}$$

where ϕ_s = resistance factor for structural steel; F_y = yield stress (nominal and probable); V_{SY} = shear yielding resistance; V_{VM} = shear Von Mises resistance; M_{FY} = flexural yielding resistance

at the cope; M_{VM} = flexural Von Mises resistance; S_x' = section modulus of the gross reduced beam section; e = eccentricity (taken as the distance from the centroid of the girder to the end of the cope); and A_{gv} = gross shear area (excludes remaining flange but includes any reinforcement).

The welds along the supporting web and flanges of the girder were sized the same based on the resistance of the former. The length of the weld was taken as the "*T*" distance of the supporting girder and the weld resistance was calculated based on Clause 13.13.2.2 of CSA S16 (2009).

Part 9 of the 14th Edition AISC Manual (2011) was used to design the horizontal stiffeners used as reinforcement for the coped beams. One of the checks is to ensure that the extension length of the stiffener past the cope is greater than the cope depth; however, based on the research by Yam et al. (2011) it was decided that the extension past the cope was to be at least twice the cope depth. The slenderness of the stiffener must also be checked in order to avoid buckling. Both the Canadian and American design standards were checked to determine the critical slenderness limit. With regards to CSA S16 (2009), Table 1 is used considering the stiffener to be the flange of either an I or T-section. The AISC 360 Specification (2010) treats the stiffener as a flange of the reduced beam which in turn is considered a welded shape due to the connectivity between the reinforcement and the beam; therefore, the corresponding check is done based on Table B4.1a of the AISC 360 Specification (2010). Also, the welds connecting the horizontal stiffener and the beam web were designed to resist axial stresses due to bending; for this check, the length of weld considered to resist this stress was only the length of weld past the cope. It must also be verified that the beam web will not yield in shear along the welded region; the resisting shear area considered in this instance was only the section of the beam web connected to the stiffener past the cope.

Similar to horizontal stiffeners, the only guideline provided by the AISC Manual (2011) regarding doubler plate reinforcement is the length past the cope the plate must extend. The slenderness of the doubler plate is not something that was checked during design. This is due to the fact that the doubler plate was welded on three sides and any risk of possible out-of-plane buckling is prevented due to these welds as well as the bolted connection between the beam and the supporting stiffener. As a result, the thickness of the doubler plate was selected such that it was of similar thickness to the beam web without exceeding it.

The design of the welds between the doubler plate and supporting beam is based on the research performed by Blodgett (1966). It is important to note that similar to the design of horizontal stiffeners, the welds past the cope are design to resist the flexural strength of the doubler which is determined by the following equation:

$$M_{DP} = \phi_s S_{DP} F_y \quad \textbf{(3-3)}$$

where M_{DP} = flexural resistance of the doubler plate; and S_{DP} = section modulus of the doubler plate.

The C-shape weld shall resist a torque equivalent to M_{DP}; therefore, the vertical and horizontal allowable loads have to be determined as suggested by Blodgett (1966):

$$f_x = \frac{M_{DP} e_x}{J_w} \quad \textbf{(3-4)}$$

$$f_y = \frac{M_{DP} e_y}{J_w} \quad \textbf{(3-5)}$$

where

$$J_w = \frac{(2b + d)^3}{12} - \frac{b^2 (b + d)^2}{(2b + d)} \quad \textbf{(3-6)}$$

where f_x = force on the weld per linear inch in the horizontal direction; f_y = force on the weld per linear inch in the vertical direction; e_x = horizontal distance from the end of the leg of the C-shape weld to the centroid of the weld; e_y = vertical distance from the bottom of the C-shape weld to the centroid of the weld group; J_w = polar moment of inertia; b = horizontal width of weld group (length of C-shape leg); and d = vertical depth of weld group (height of C-shape weld).

The resulting allowable force is determined by calculating the root of the sum of the squares of the two forces as seen in Equation (3-7). Then, the required weld size is determined according to Equation (3-8).

$$f_w = \sqrt{f_x^2 + f_y^2} \quad \textbf{(3-7)}$$

$$D_w \geq \frac{f_w}{V_w} \quad \textbf{(3-8)}$$

where f_w = total force on weld group per unit length; D_w = weld size; and V_w = shear resistance of fillet weld.

With the size of the weld selected, it is important to ensure the resistance of the base metal along the welds is greater than weld metal resistance; this check is performed according to Table 3-21 of the CISC Handbook of Steel Construction (2010).

3.3.2 Design of Welded In-Shop Specimens

The design of the specimens that were welded in-shop required only five checks: shear yielding, flexural yielding at the cope, flexural buckling at the cope, Von Mises resistance, and weld resistance – all which are explained in Section 3.2.1. However, it is important to note one distinction in the design of the two specimens that were welded in-shop. Specimen 10 is considered a single coped beam that satisfies the criteria that the cope depth is less than or equal to half the beam depth ($d_c \leq d/2$); on the other hand, Specimen 8 is detailed as a double coped beam, that when considering d_c to be the sum of both the top and bottom copes, does not satisfy this condition. As a result, the 14th Edition AISC Manual (2011) suggests a conservative procedure to design for flexural buckling when a beam is coped at both flanges and $d_c > 0.2d$ based on classical plate buckling rather than using the equations developed by Cheng et al. (1984).

3.3.3 Design of Single Coped Haunched Beam

For the design of the single coped haunched specimen, the checks for bolt shear, bearing resistance of the beam and supporting stiffener, shear yielding resistance of the beam and supporting stiffener, supporting stiffener stability, shear rupture of the beam, flexural yielding at the cope, flexural buckling at the cope and Von Mises resistance were performed as described in Section 3.2.1. However, it is important to note that since the pitch between bolt rows was not the same, as seen in Figure 3.4; the average of the two corresponding "*C*" coefficient terms defined by the ICR method was calculated. Similar to Specimen 8, since the cope depth was greater than 20% of the beam depth ($d_c < 0.2d$), the equations developed by Cheng et al. (1984) do not apply and classical plate buckling was used instead to design for flexural buckling resistance at the cope as indicated in Part 9 of the AISC Manual (2011).

In order to calculate the capacity of the haunch plate, the force which it must resist (V_{BSH}) was first determined. Since two of the six bolts are located in the plate it was assumed that one-third of the beam reaction was transferred to the plate. Once the force was determined it was divided into two components, tensile stresses (F_T) and bending stresses (F_b) according to the Equation (3-9) and Equation (3-10) respectively. The total stress applied (F_{TOT}) was calculated as the arithmetic sum of the tensile and bending stresses and then compared to the yielding capacity of the plate.

$$F_T = \frac{V_{BSH}}{t_H L_H} \quad \textbf{(3-9)}$$

$$F_b = \frac{V_{BSH} L_{H-CI}}{\left(\frac{t_H L_H^2}{6}\right)} \quad \textbf{(3-10)}$$

$$F_{TOT} = F_T + F_b \quad \textbf{(3-11)}$$

where t_H = thickness of haunch plate; L_H = length of haunch plate; and L_{H-CI} = distance from the centroid of supporting girder to the interface point between the haunch and the beam flange (Figure 3.7).

In order to check the local web crippling capacity of the beam, Clause 14.3.2a.i of CSA S16 (2009) was applied. First, the applied force on the beam web had to be determined; therefore, based on the profiles of the tensile and bending stresses, the bearing length (N) was calculated as seen in Equation (3-12). After calculating the bearing length, the corresponding tensile (P_T) and bending (P_b) forces were calculated using Equation (3-13) and Equation (3-14) respectively; the total force applied (P_{TOT}) is the arithmetic sum of both these forces as seen in Equation (3-15). Then, in order to avoid local web crippling, it was important to ensure that the local bearing resistance of the beam (B_{r-crip}), as calculated by Equation (3-16), was greater than the total applied force. It is assumed that the concentrated load is applied at the center of the bearing length (N); therefore, because the depth of the supported member is considered to be the reduced beam depth due to the cope plus the depth of the haunch plate, then it can be observed that the concentrated load is applied at a distance from the end of the beam greater than the beam depth. As such, the formation for the bearing resistance of an interior load, Equation (3-16), is implemented in the design.

$$N = \frac{2}{3}\left(\frac{L_H}{2}\right) \quad \textbf{(3-12)}$$

$$P_T = F_T t_H N \quad \textbf{(3-13)}$$

$$P_b = \frac{F_b\left(\frac{L_H}{2}\right)}{2} t_H \quad \textbf{(3-14)}$$

$$P_{TOT} = P_T + P_b \quad \textbf{(3-15)}$$

$$B_{r-crip} = \phi_{bi} t_w \left(N + 10t_f\right) F_y \quad \textbf{(3-16)}$$

where L_H = length of haunch plate; ϕ_{bi} = resistance factor for interior beam web bearing; t_w = web thickness; t_f = flange thickness

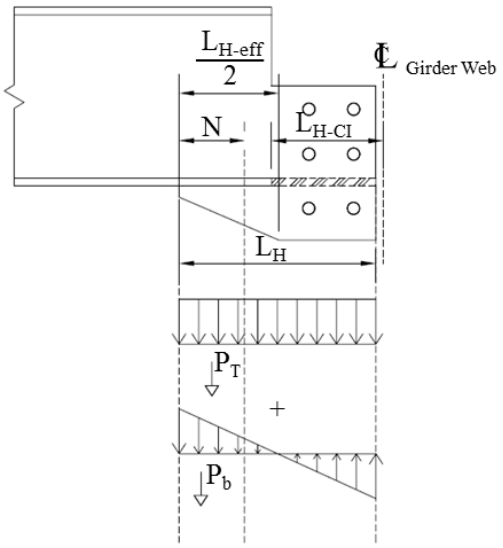

Figure 3.7 – Hunched beam extension plate design diagram

Based on the total tensile and bending stresses, Equation (3-17) and Equation (3-18) are used to calculate the tensile (f_{Tw}) and bending (f_{bw}) forces applied per unit length on the welds connecting the haunch plate to the beam and then summed together (f_{wTOT}) to find the total applied force as shown by Equation (3-19). This value was then divided by the calculated weld resistance per weld area in order to appropriately size the weld between these two components as shown by Equation (3-20).

$$f_{Tw} = \frac{F_T t_H}{2} \quad \textbf{(3-17)}$$

$$f_{bw} = \frac{F_b t_H}{2} \quad \textbf{(3-18)}$$

$$f_{wTOT} = F_{Tw} + F_{bw} \quad \textbf{(3-19)}$$

$$D_w \geq \frac{f_{wTOT}}{V_w} \quad \textbf{(3-20)}$$

3.3.4 Design of Extended Shear Plate Specimens

Part 10 of the 14th Edition AISC Manual (2011) outlines the procedure for the design of extended shear plates which applies to both partial depth and full depth shear tabs. The checks for bolt shear, bearing, shear yielding, shear rupture, and block shear rupture are the same as the ones described in Section 3.2.1. Unlike the specimens tested by Hertz (2014), the detailing of the bolts was such that the threads did not intercept the shear plain; therefore, there was no 70% reduction in the bolt shear capacity. The procedure in the AISC Manual (2011) also outlines design checks for plate ductility combined shear and flexural yielding, and plate buckling.

It is important to note that, unlike the Von Mises resistance check outlined in Section 3.2.1 for the design of beams, which was suggested by the industry sponsor, the design check for the interaction between shear and flexural forces utilized for extended shear plates is for the connecting component itself and is found in the design procedure provided in the AISC Manual (2011). It must be noted that the former utilized the plastic section modulus to calculate the flexural capacity of the shear plate as per the procedure outlined in the AISC Manual (2011) while the latter utilized the elastic section modulus for the flexural capacity of the coped beam as per the suggestion of the industry sponsors.

When designing for buckling, the extended shear tab was treated as a doubly coped beam; as a result, the procedure outlined in Section 0 was used to check the flexural buckling resistance of the shear tab. For comparison, two methods were used to calculated the buckling capacity of the shear plate, one using the equation developed by Cheng et al. (1984) and another using the classical plate buckling formulation – both outlined in Part 9 of the AISC Manual (2011). It is important to note that for the former, the length of the cope was taken as the "*a*" distance to be conservative; similarly, the shear plate depth was taken as the reduced beam depth.

Table 3.2 summarizes the predicted failure modes for all specimens based on factored and predicted material properties.

Table 3.2 – Predicted specimen resistances

Category	Specimen	Predicted Failure Mode	Factored Resistance (kN)	Probable Resistance (kN)
Partial Depth Extended Shear Tab	Configuration 6J	Plate Buckling (Q-Equation)	156	190
	Configuration 9J	Von Mises - Plate	326	378
Full Depth Extended Shear Tab	Specimen A1	Plate Buckling (Q-Equation)	208	254
	Specimen A2	Plate Buckling (Q-Equation)	208	254
Single Coped	Specimen 1	Von Mises - Beam	169	206
	Specimen 2	Von Mises - Beam	237	288
	Specimen 3	Von Mises - Beam	262	319
Double Coped	Specimen 4	Von Mises - Beam	692	846
	Specimen 5	Von Mises - Beam	914	1116
	Specimen 6	Von Mises - Beam	1108	1354
Single Coped and Haunched	Specimen 7	Von Mises - Beam	125	152
Welded In-Shop	Specimen 8	Von Mises - Beam	138	169
	Specimen 10	Von Mises - Beam	871	1064

3.4 DESCRIPTION OF TESTING APPARATUS

3.4.1 Overview

The laboratory setup used was based on the testing frame designed by Marosi (2011) and the modifications done by Hertz (2014) in order to test steel beam-to-girder connections. The system consists of four components which are described in detail herein: reaction frame and stub columns, restraining system emulating a concrete slab, lateral bracing system, and hydraulic actuators.

Figure 3.8 and Figure 3.9 respectively show a plan and elevation view of the test setup highlighting its main components. For further illustration, Figure 3.10 is a 3D rendering of the test setup including the actuators and anchor rods used; the beam and girder test specimen (cyan), the reaction frame (green), the pseudo concrete slab restraining system (magenta), and the lateral bracing frames along with the frame supporting one of the hydraulic actuators (brown). Figure 3.11 is a panoramic photograph of the setup in the laboratory.

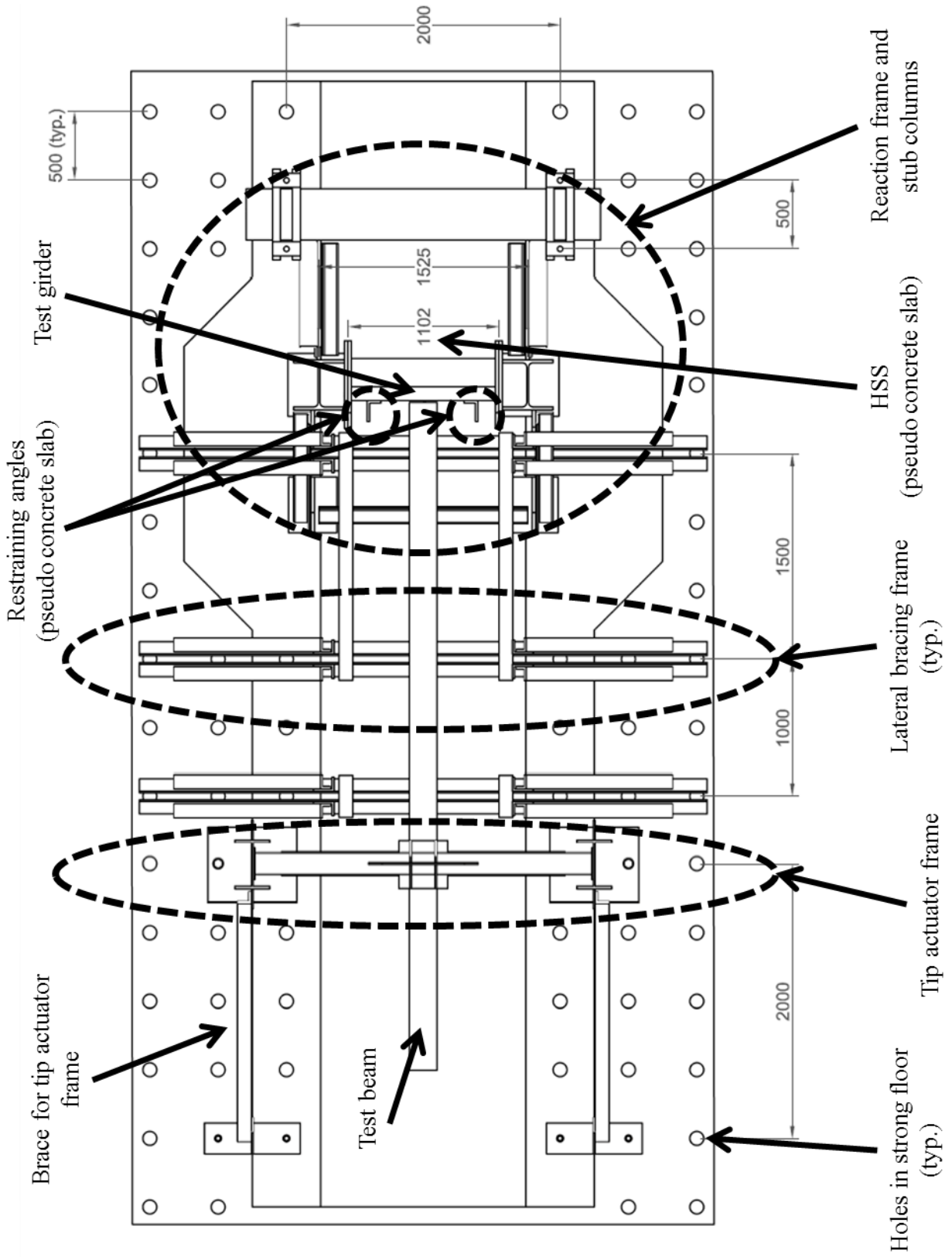

Figure 3.8 – Plan view of test setup

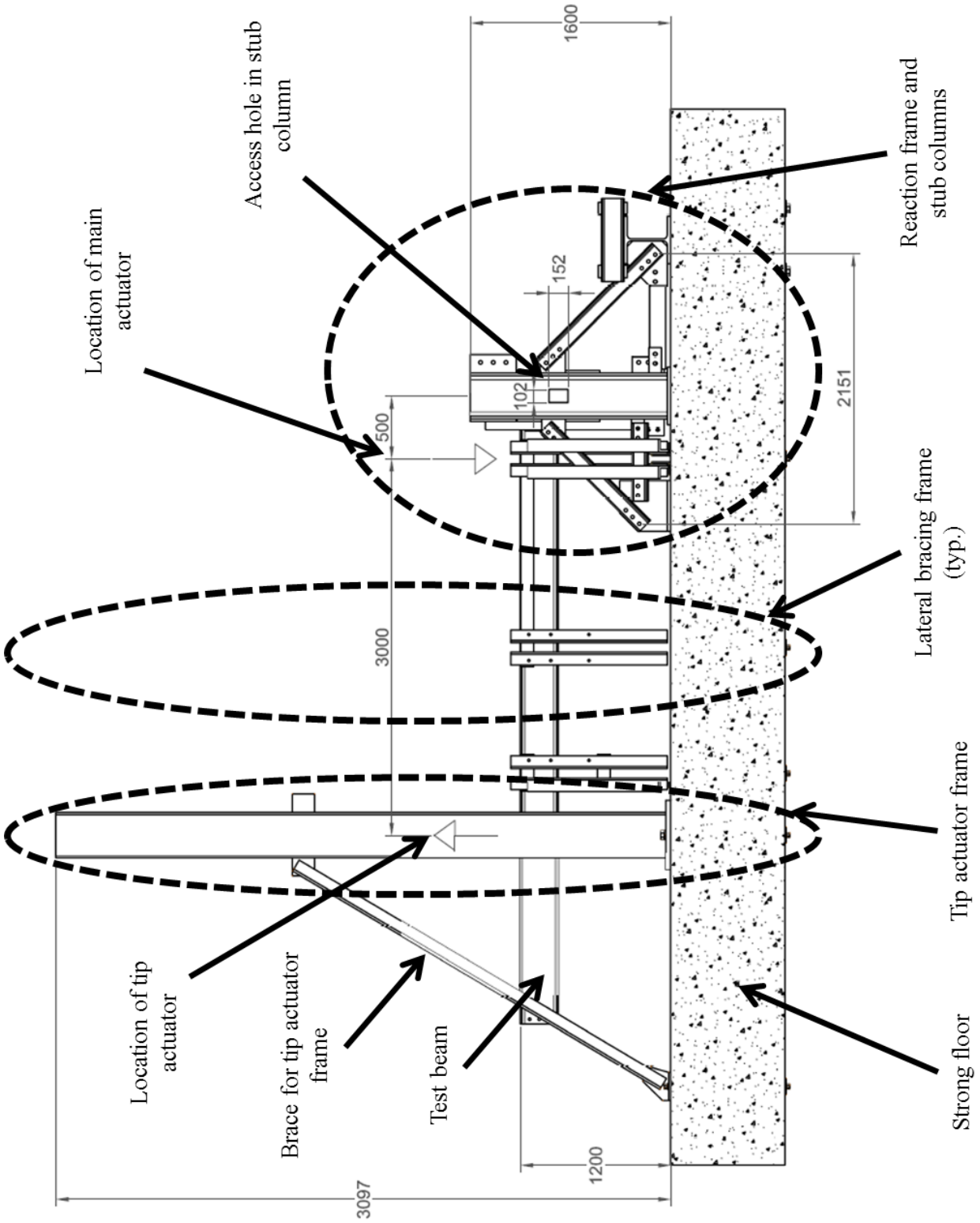

Figure 3.9 – Elevation view of test setup

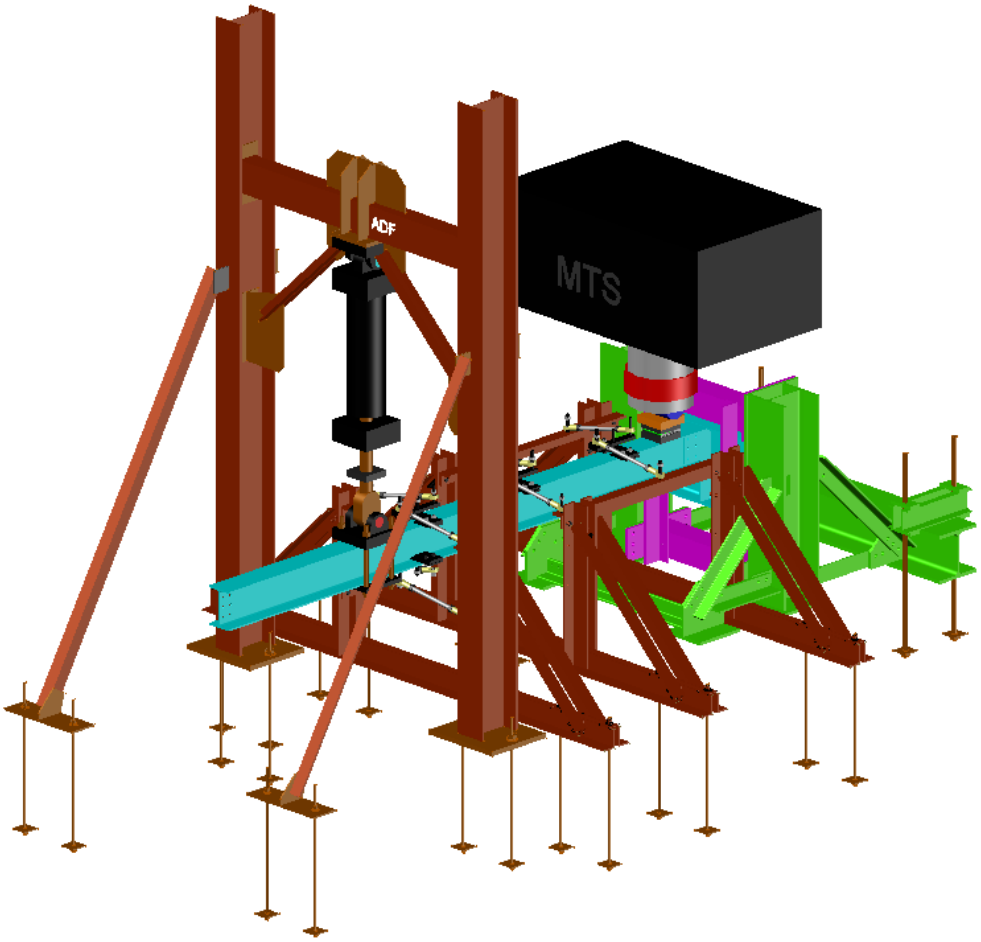

Figure 3.10 – 3D rendering of test setup

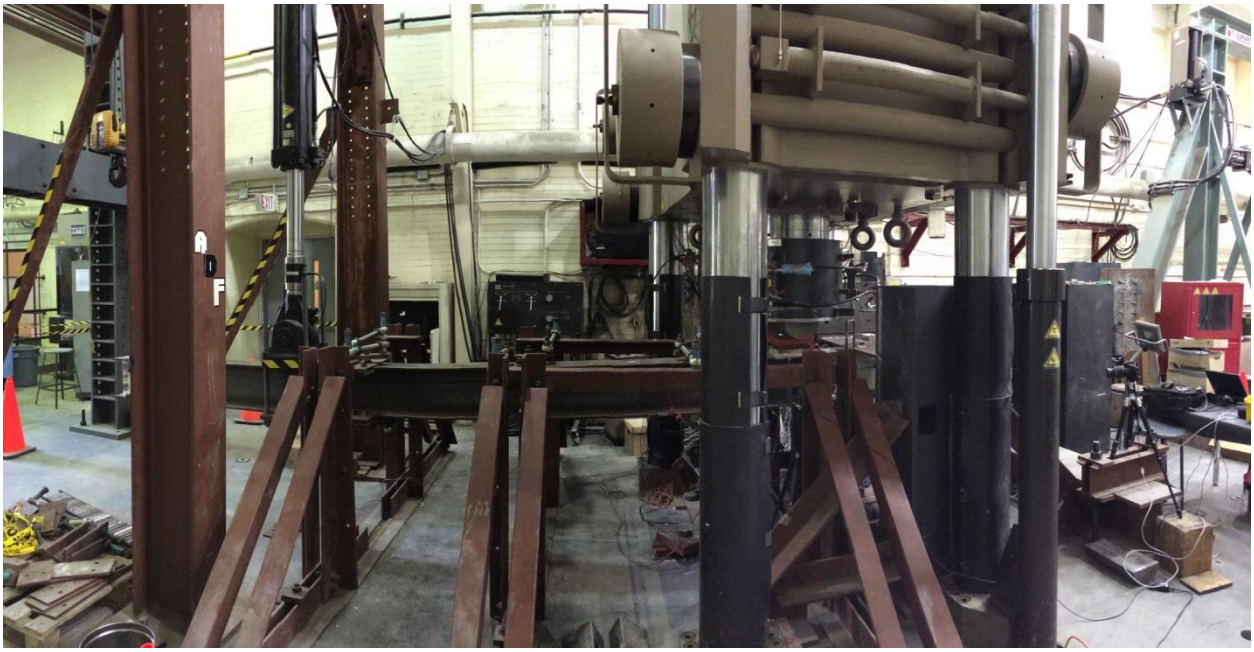

Figure 3.11 – Panoramic photograph of test setup

3.4.2 Reaction Frame and Stub Columns

The reaction frame (Figure 3.12) consisted of two W360x162 (W14x109) columns with welded 25.4mm (1") base plates that were placed 1525mm (60") centre-to-center. These columns were used to support the test girder and the two HSS members that were part of the pseudo concrete slab restraining system (see Section 3.4.3). In order for these three elements to connect to the supporting stub columns, 25.4mm (1") side plates with 30.2mm (1 3/16"Ø) holes for 1 1/8"Ø (28.6mm) bolts were welded on the inside of the column flanges. In order to facilitate the bolting of these components, a 152mm x 102mm (6" x 4") access hole was detailed in the flange of both stub columns. Detailed fabrication drawings of the stub columns can be found in Appendix B.

In order to restrain the deflection and rotation of the columns during testing bracing was provided for both tension and compression. This bracing system was constructed using L127x127x19 (L5x5x3/4) angles. The tension braces (located behind the girder, away from the test beam) were connected to a W360x196 (W14x132) beam that was in turn anchored to the strong floor using 38mm (1 1/2" Ø) pre-tensioned rods at 21MPa (3000psi). The compression braces (located on the same side as the test beam) were connected to two base plates, which in turn were connected to each other by another L127x127x19 angle in order to avoid any sliding of the base plates during testing. The framing elements were bolted together with 1" Ø (25.4mm) bolts with the use of an electric torque wrench to avoid any slipping.

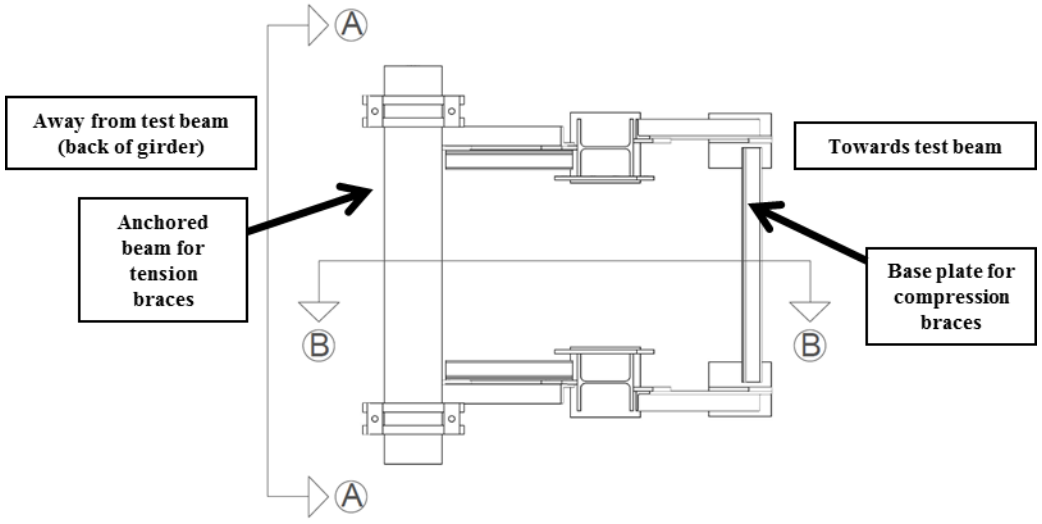

(a)

Figure 3.12 – Reaction frame: (a) plan view; (b) elevation A-A; (c) elevation B-B

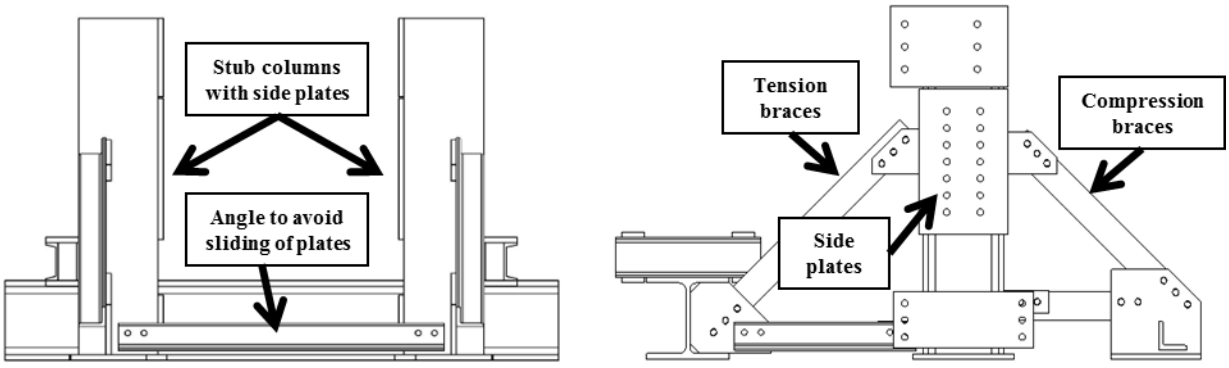

(b) (c)

Figure 3.12 (continued) – Reaction frame: (a) plan view; (b) elevation A-A; (c) elevation B-B

3.4.3 Restraining System – Pseudo Concrete Slab

Hertz (2014) suggested that preventing the rotation of the girder top flange could preclude girder web punching. Inspired by the experimental setup used by Creech (2005), it was decided to use steel elements to simulate a concrete slab placed over the girder as this would be less time consuming than pouring a concrete slab in the laboratory – the steel elements would act as a pseudo concrete slab. Creech (2005) used a welded steel tie plate for this purpose; however, it was decided this was not adequate as it would increase the rotational stiffness of the connection. The chosen alternative was to design a 203x203x13 (8x8x1/2) HSS member to rest on the top flange of the girder to prevent any rotation. The components of the pseudo concrete slab restraint system were designed through the use of a finite element model developed in ABAQUS (Abaqus, 2013).

Creech (2005) also utilized two channel members with Teflon strips to restrain the horizontal movement of the top flange of the girder while still allowing vertical deflection. These channels were attached to a strong wall using threaded rods; however, due to the lack of a strong wall at the McGill laboratory, a second 203x203x13 HSS member was installed underneath the test girder. Both HSS members were detailed with holes to allow 25.4mm (1" Ø) steel rods to pass through them; these rods would be used to tighten two L152x102x19 (L6x4x3/4) steel angles in front of the girder. As with the setup used by Creech, these angles would prevent the horizontal displacement of the girder while still allowing any vertical displacement with the help of Teflon strips installed between the contact surfaces of the angles and the girder flanges. In order to prevent any bending in the walls of the HSS members once the rods were tightened, a 25.4mm (1") plate was placed between the HSS and the nut in the rod. Figure 3.13 is a diagram of the

final design from the front and Figure 3.14 is a photograph from the back to illustrate the test setup in the laboratory.

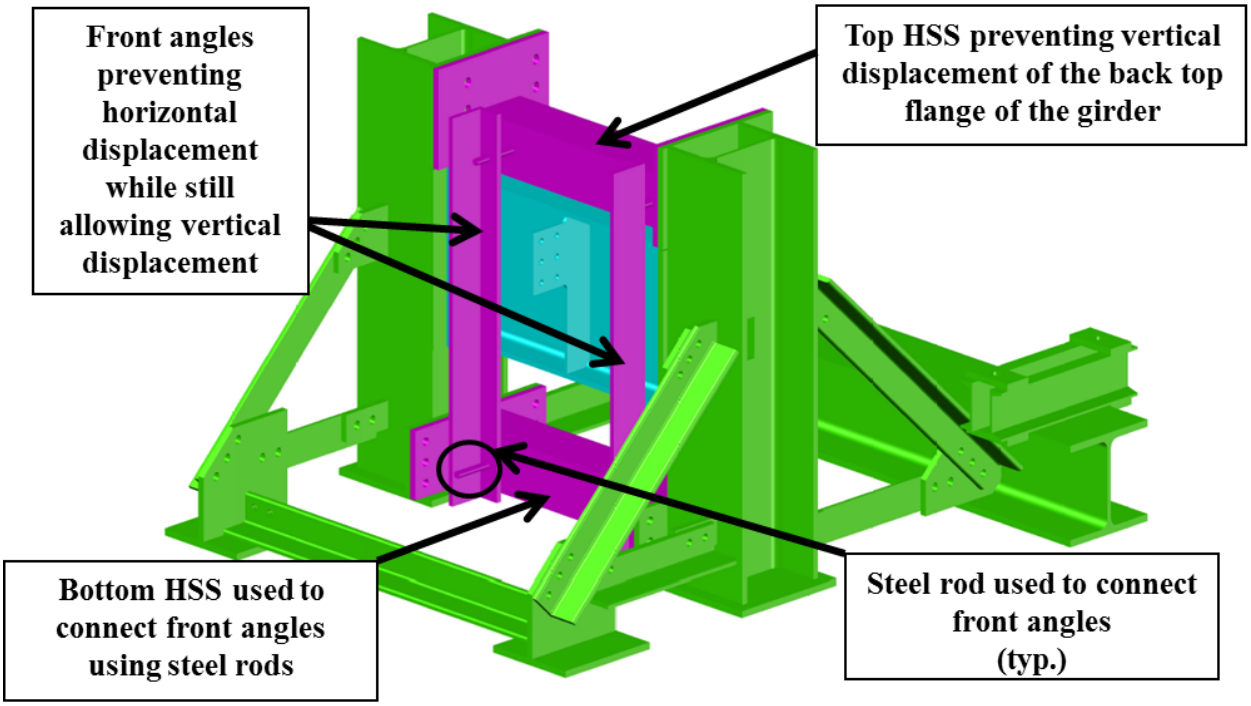

Figure 3.13 – Pseudo slab restraint diagram (front view)

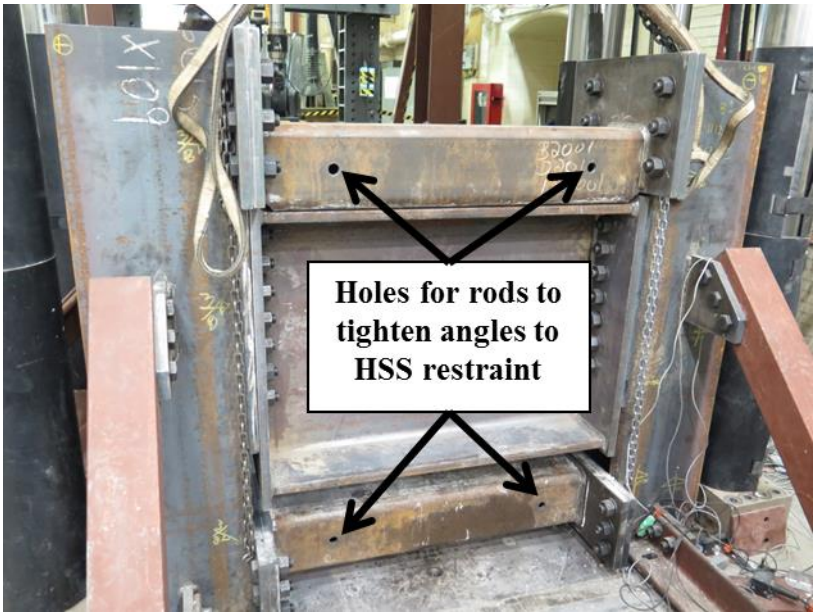

Figure 3.14 – Pseudo slab restraint in lab (back view)

3.4.4 Lateral Bracing System

The lateral bracing system was used to provide lateral stability to the test beams; lateral braces were placed along the beams' compression flange at a distance smaller than the maximum unbraced length that could be critical for lateral torsional buckling, L_u. At the end of the beam away from the connection, both the top and bottom flanges of the beam were braced.

These braces consisted of threaded rods with ball sockets at both ends therefore allowing the test beams to rotate freely in the vertical direction while preventing lateral displacements. On one end, the braces were attached to a set of clamped plates located on the beam flange, and on the other end, the braces were attached to a supporting frame that was anchored to the strong floor. Figure 3.15a shows the lateral bracing system and Figure 3.15b points more closely at the braces themselves and how they were clamped onto the test beam.

Figure 3.15 – Lateral bracing system: (a) global view; (b) local view

3.4.5 Hydraulic Actuators and Load Application

The test specimens were placed under the main hydraulic actuator, which had a nominal capacity of 12MN; this actuator was responsible for applying the shearing force. At the beam tip, a 650kN hydraulic actuator was attached to the beam. This actuator was used to control the rotation of the test specimens. Note that the tip actuator was installed on a steel frame that was connected to the concrete strong floor using pre-tensioned rods. Figure 3.16 shows the main and tip actuators attached to one of the tested specimens.

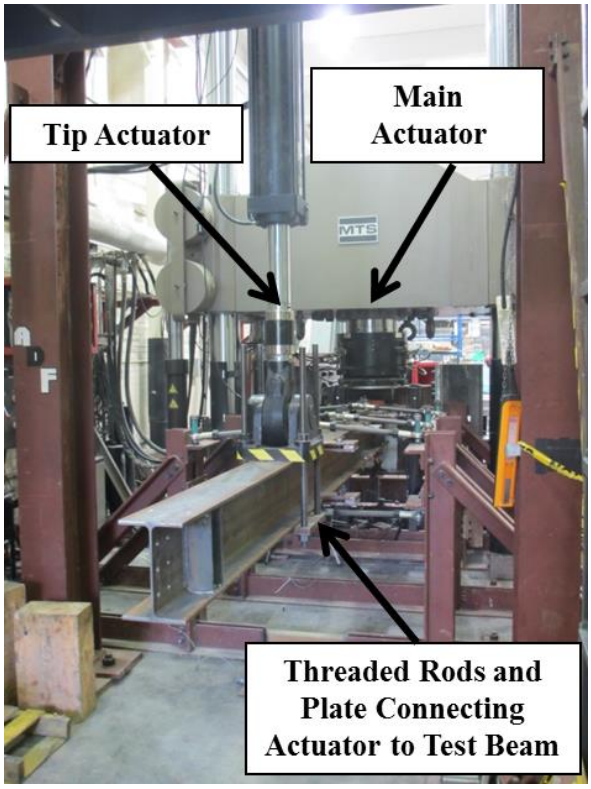

Figure 3.16 – Main and tip actuators

In order to ensure that the applied shear force remained vertical to the test beam even as it rotated, a system comprised of a half steel cylinder, set of steel plates, and a set of rollers were used. As seen in Figure 3.17, these were placed between the top flange of the beam and the main hydraulic actuator. In order to ensure the steel plates were level, an UltraCal 30 (gypsum cement) paste was placed between the bottom steel plate and the beam top flange.

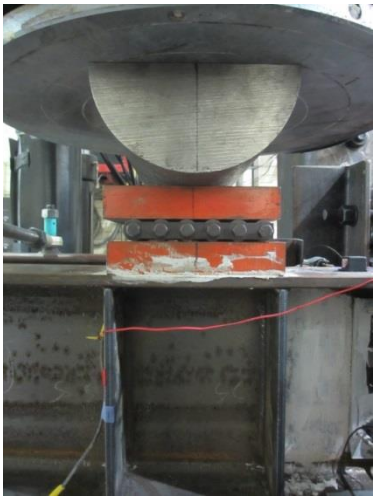

Figure 3.17 – Half cylinder and roller loading system

3.5 SPECIMEN INSTALLATION

In order to install a test specimen, the first step was to connect the test beam to the girder on the ground without fully tightening the bolts. The connected ensemble was then lifted using a set of two cranes in the laboratory and placed on two rolling tanks, which rested on two channels. With the use of the cranes and the tanks, the specimen was moved along the length of the channels and positioned between the two stub columns. Then, with the use of two car jacks placed below the test girder and the set of two cranes, which were still attached to the beam, the specimen was lifted such that the holes on the girder end plates were in line with the holes on the side plates of the stub columns. At this point, the tanks, channels, and car jacks were removed. It is important to note that the beam and girder had to be assembled and then repositioned because the head of the main actuator did not allow the cranes to directly position the girder in the reaction frame.

With the girder in place between the two stub columns, these two components were bolted together using 1 1/8" Ø (28.6mm) bolts and an electric torque wrench. In order to facilitate installation, access holes were detailed on the flanges of the stub columns as described in Section 3.4.2. Then, the tip actuator was attached to the test beam with the use of four threaded rods and a supporting plate; this can be seen in Figure 3.16. With the girder connected to the stub columns and the beam to the tip actuator, the cranes were detached from the latter and the test specimen was then levelled horizontally by displacing the tip actuator appropriately. Once the beam was leveled, the bolts in test connections (connecting the beam to the girder) were bolted snug tight.

With the test specimen in place, the top restraining HSS was lowered using chain blocks that were attached to the head of the main actuator; this component was then also bolted to the stub column using 1 1/8" bolts. In order to ensure contact between the HSS and the girder, an UltraCal 30 paste was placed between the two. At this stage, whitewash was applied on the shear tab or supporting stiffener, the beam, and girder webs before the front restraining angles were connected to the top and bottom HSS restraints using threaded rods. It is important to note that these restraining rods had two pieces of Teflon each at the locations where the angles came into contact with the girder top and bottom flanges in order to allow for vertical displacement while restraining any horizontal movement or the support. Then it was possible to install the remaining instruments (see Section 3.6.2) to the test specimen; the stands holding the

instruments were bolted to the ground. Note that in order to facilitate the installation of the strain gauges, these were connected to each specimen before the installation process mentioned.

With all the instruments in place, the half cylinder, steel plates, and rolling system were placed on the top flange of the beam underneath the main actuator. The main actuator was lowered until it came into contact with the half cylinder; it was important to ensure that these two surfaces were flat and in full contact in order not to introduce any additional eccentricity when loading the specimen. Finally, before testing, all instruments were checked to ensure that they were working properly.

3.6 TESTING PROCEDURE

3.6.1 Loading Protocol

The loading protocol was originally developed by Astaneh et al. (1989) and modified by Marosi (2011). This loading protocol requires that a connection rotation be selected, which is used as a target for a load level equal to the calculated design level resistance. Therefore, by controlling the displacement of both the main and tip actuators, a rotation of 0.02 radians was targeted for the predicted probable resistance load. The reason for selecting this rotation target was to assess the accuracy of the design method used for design level events. Once the target load and rotation level were reached, it was not possible to continue to target a predicted rotation due to the changing rotational stiffness of the connection caused by yielding of the steel; therefore, the ratio between the two actuator displacement rates was kept constant after this point. Figure 3.18 illustrates the loading protocol used.

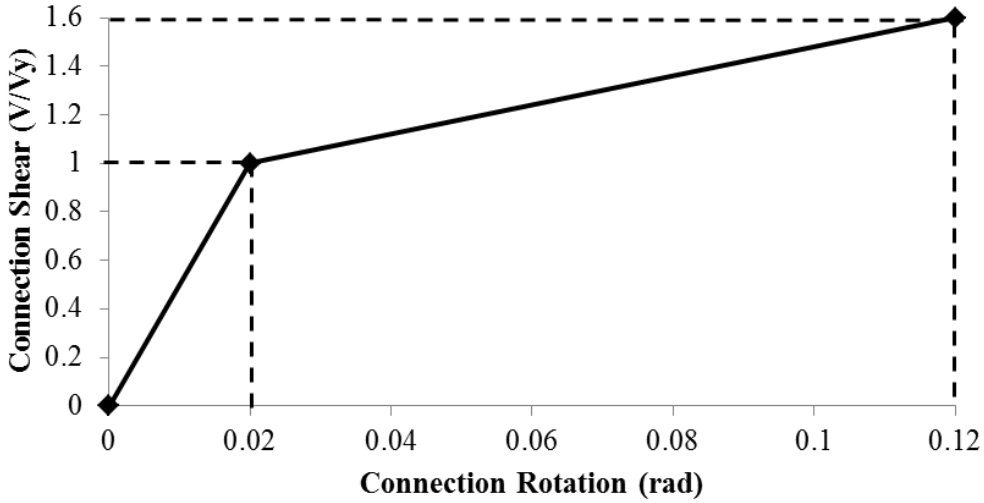

Figure 3.18 – Loading protocol

3.6.2 Instrumentation

As Figure 3.20 illustrates, a series of instruments were used to record the experimental data: string potentiometers (SP), linear variable differential transformer (LVDT or LV), inclinometers (INCL), and strain gauges (SG) – each of these instruments is explained in detail herein. It is also important to note that both actuators were equipped with built-in load cells and LVDTs that recorded loads and displacements, respectively. Instrumentation layouts similar to Figure 3.20 were produced for every tested specimen (Appendix C).

The string potentiometers were used to measure the vertical displacement of the beam, girder, and shear tab or supporting stiffener. Two string potentiometers were installed on the beam, one at the end underneath the tip actuator and another closer to the connection. These were connected to metal shelves that were themselves attached to the specimen using an epoxy adhesive; the same method was used for the string potentiometer secured to the bottom flange of the girder. For the string potentiometer measuring the vertical displacement of the shear tabs or supporting stiffener, a small hole was drilled on the plate in order to attach a 6.4mm (1/4") threaded rod to serve as a support for the instrument. Figure 3.19a shows both the string potentiometers attached with epoxy and Figure 3.19b shows the steel rod attachment.

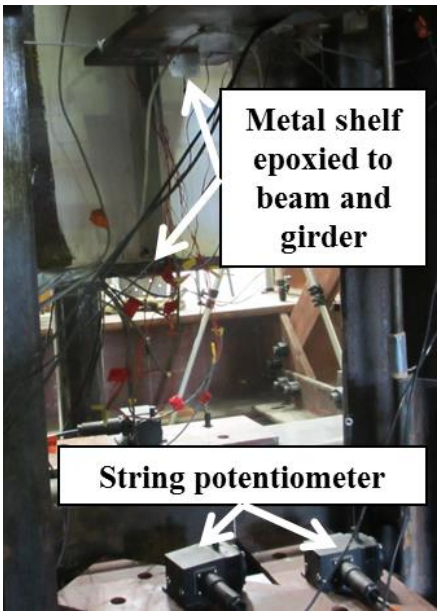

(a)

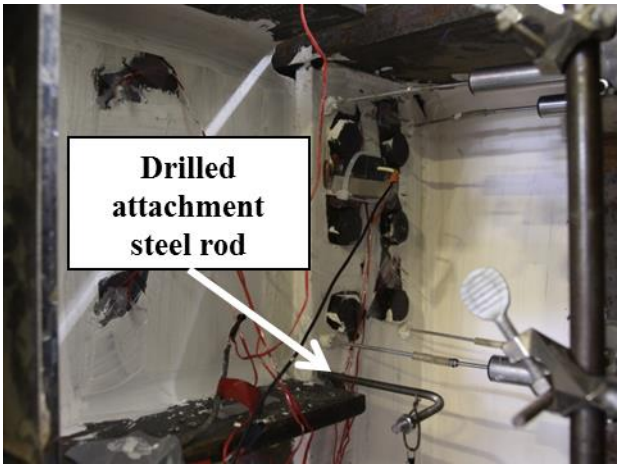

(b)

Figure 3.19 – String potentiometer attachments: (a) epoxy shelf; (b) attachment steel rod

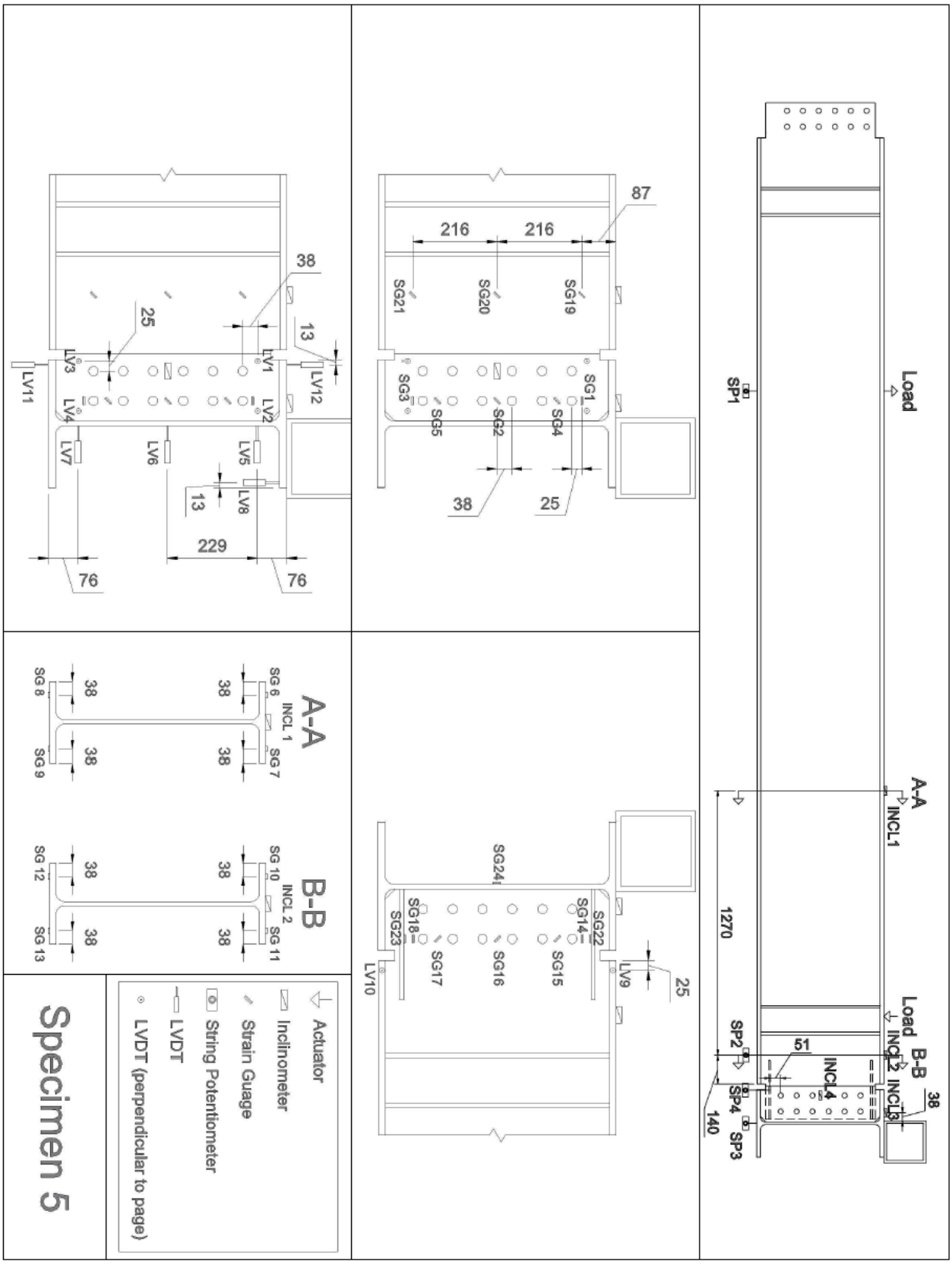

Figure 3.20 – Instrumentation layout (Specimen 5)

Linear variable differential transformers (LVDT) were used to measure smaller displacements closer to the respective connection. Four LVDTs were installed with the purpose of measuring the out-of-plane displacement of the shear tab. Extension steel rods with a flexible joint were connected to the LVDT on one end and attached to the beam using silicone on the other in order to continue recording any displacements as the beam rotated (Figure 3.21a). Two LVDTs were installed on the top and bottom flange of the beam in order to measure any out-of-plane rotation; these too had the extension rod attachments. In order to record any out-of-plane displacement in the girder web, three LVDTs were installed at the top, middle, and bottom of this component. Additionally, three LVDTs measured the vertical displacement of the girder flanges; one at the back of the top flange, one at the front of the top flange, and one at the front of the bottom flange. Once again, all the LVDTs used to measure displacements in the girder web were attached to a steel stand that was bolted to the strong floor (Figure 3.21b).

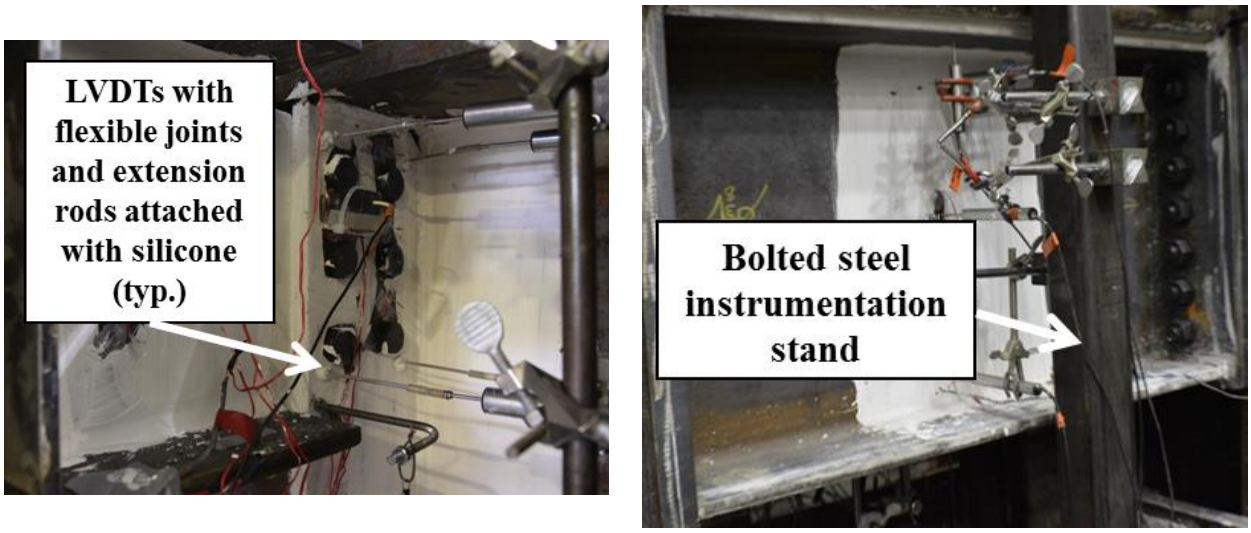

Figure 3.21 – LVDTs: (a) with extension rod; (b) bolted stand on the back of girder web

Two inclinometers were used to measure the rotation of the beam at two different locations, one close to the point of load application of the main actuator and the other further along the length of the member. Another inclinometer was placed on the top flange of the girder to measure the rotation of this component; the last inclinometer was placed on the shear tab or supporting stiffener, using a steel shelf attached to the tab using epoxy adhesive, this last one recorded both in-plane and out-of-plane rotation. All these inclinometers were secured in place using double-sided tape.

Strain gauges, 10 mm gauge length with a resistance of 120 Ω, were placed on all shear tabs or supporting stiffeners to measure both flexural and shear strain along the height of the component; also, in the coped beam specimens, strain gauges were placed on the gross and net sections of the beam to measure strains in the regions close to the cope. In the specimens that had a doubler plate as a reinforcement, these strain gauges were installed directly onto the plate. Whenever horizontal stiffeners were used as reinforcement, an additional strain gauge was installed on said reinforcement. At the same time, strain gauges were installed on both the top and bottom flanges of the beam at two different locations along the length of the member in order to calculate the moment at these locations. The last strain gauge was installed on the back of the girder web; the location of this strain gauge varied slightly from one specimen to the next depending on the location where the maximum strain was predicted. It is also important to note that whitewash (calcium hydroxide) was applied on the specimens in order to trace yielding. Figure 3.22 shows the placement of strain gauges (represented as orange rectangles) on both the supporting stiffener and the gross area of the beam past the cope; the strain gauges that are rotated 45° measure shear strains while the ones placed at 90° measure flexural strains. Also note in the image the whitewash used and the inclinometer.

The measurement instruments were connected to Vishay Model 5100B scanners that were used to record data using the Vishay System 5000 StrainSmart software. During testing, the data recorded by all the instruments was displayed and monitored. In order to follow the established loading protocol, the applied shear force and relative rotation of the connection were calculated by the data acquisition program. The first was the arithmetic difference between the compression and tension actuator while the latter was the arithmetic difference between the measured rotation of the inclinometer closer to the connection and the one installed on the girder.

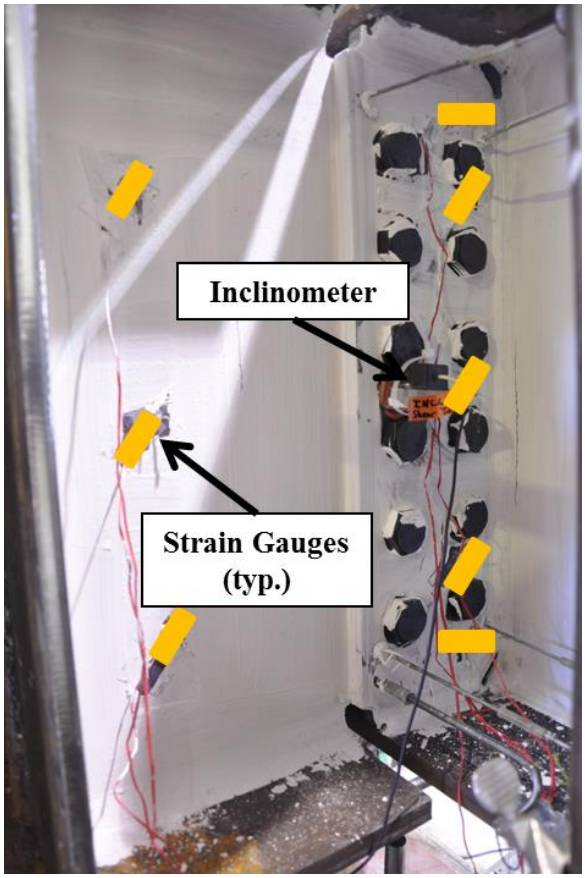

Figure 3.22 – Strain gauges and inclinometer on test specimen

3.7 SUMMARY

Thirteen full-scale tests were performed in order to observe and characterize the behaviour of beam-to-girder connections that are commonly used in the engineering practice in North America. Four of these were extended shear plates (full and partial depth), three were single coped bolted specimens (with varying reinforcement), three were double coped bolted specimens (with varying reinforcement), two were welded in-shop (single and double coped), and one was a single cope haunched specimen. These specimens were designed using the provisions outlined in CSA S16 (2009) and CISC Handbook (2010) whenever possible and supplemented with guidelines in the AISC 360 Specification for Structural Steel Buildings (2010) and the 14th Edition AISC (2011) Manual.

The test setup used was based on the original design by Marosi (2011) and modifications by Hertz (2014). An additional component to simulate a concrete slab was inspired by the setup used by Creech (2005), and designed by means of a finite element analysis in order to better represent the in situ conditions of these connections.

CHAPTER 4

EXPERIMENTAL RESULTS AND EVALUATION

4.1 OVERVIEW

The results of the thirteen full-scale beam-to-girder connection tests are presented herein. The shear-rotation relations for each of the six different types of specimens are included in order to compare and contrast their behaviour under shear loading. The extended shear tab specimens are compared against previously tested specimens in order to further understand and explain specific failure mechanisms that have been observed. The measured resistances and observed damage progression are compared with the current design provisions as outlined by the Canadian Standards Association (CSA) S16 Standard (2009), the 10th Edition of the CISC Handbook of Steel Construction (2010), the American National Standards Institute (ANSI) AISC 360 Specification for Structural Steel Buildings (2010), and the 14th Edition of the American Institute of Steel Construction Manual (2011). Material coupon testing was also performed to determine actual material properties, these were then compared with theoretical values to further understand the validity of the design provisions used.

The main objectives of the testing program were to: (a) assess the effectiveness of pseudo-concrete slab in preventing the girder web punching mechanism in partial depth extended shear tab connections; (b) to explore the effect of shear tab thickness in order to prevent bending in full depth extended shear tab connections; (c) to validate current design provisions of coped beam configurations as outlined by American and Canadian standards by observing the behaviour and damage progression tested configurations; and (d) to compare and contrast configurations in order to assess the effectiveness of different reinforcement details investigated for coped beams.

4.2 COUPON TESTING

4.2.1 Test Methodology

In order to measure the material properties of the tested specimens, uniaxial tensile testing was performed in accordance with the ASTM A370 Standard (ASTM, 2014). Coupons were cut

from both the shear tabs and the tested beams. The geometric dimensions of these samples were then measured using a digital caliper before being tested.

Six coupons were extracted from the parent plates used to fabricate the shear tabs and supporting stiffeners. Three of these were oriented with the grain (long grain) of the steel and the remaining three were oriented against the grain (short grain). In order to determine the strength of the shear plate, the arithmetic average of these six coupons was calculated.

To determine the yield and ultimate stress of the beams, a total of seven coupons were extracted from each parent beam. Figure 4.1 illustrates the location of these coupons; as it can be seen; coupons were extracted from both the top and bottom flanges as well as the web of the beam. The material properties of the beam were determined by calculating the arithmetic average of all these coupons.

Therefore, coupons were extracted from a total of five different places: beam top flange, beam bottom flange, beam web, plate with the grain, and plate against the grain. For each of these categories there were between two and three coupons, depending on the location, in order to obtain representative material properties.

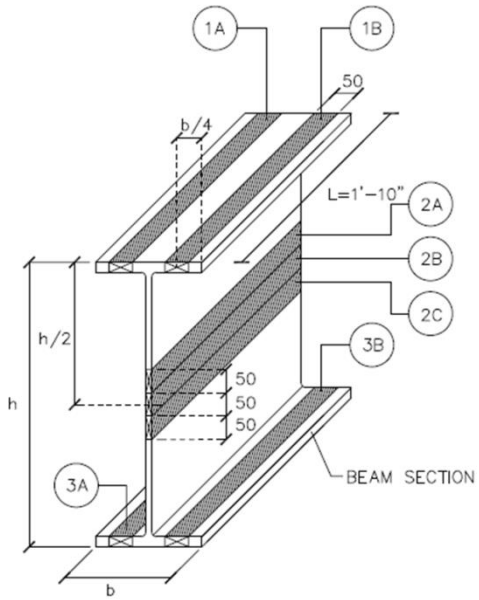

Figure 4.1 – Coupon extraction location for beams (courtesy of DPHV Structural Consultants)

Coupon testing also took place at McGill's Jamieson Structures Laboratory using the MTS main actuator (12MN capacity) equipped with a 1000kN load cell and hydraulic grips – one attached to the actuator head and another to the concrete strong floor. Once in place, a 199mm gauge extensometer was attached along the gauge length of the coupon in order to accurately calculate elastic and post yielding strains. In addition to the extensometer, one coupon from each of the five categories for any parent beam or plate, had two 120Ω resistance strain gauges installed (one on each side at the center of the gauge length) for additional precision. Therefore, the engineering strain was measured using the installed strain gauges in the elastic range and using the extensometer for the plastic range, force was measured through the integrated load cell of the MTS actuator, and displacements were measured using both the inbuilt LVDT in the actuator and the attached extensometer – Figure 4.2 shows a coupon being tested. During testing, the extensometer had to be readjusted once it reached its stroke limit of 25mm, and it was usually removed once the coupon displayed approximately a 10% loss in strength in order to capture the post ultimate behaviour yet avoid any damage to the instrument.

While testing, three different displacements rates were used for the actuator cross-head. During the elastic portion of the loading curve the displacement was set at 0.01mm/s; once the coupon yielded and reached a plastic plateau, the rate was increased to 0.02mm/s. Finally, once strain hardening was evident, the rate was increased to 0.05mm/s until the coupon ruptured.

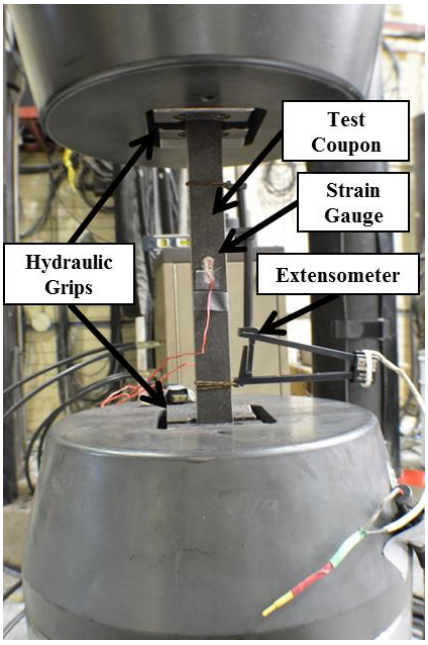

Figure 4.2 – Tensile coupon material testing

4.2.2 Test Results

Once all the data was collected, material properties were calculated for all 66 coupons. Table 4.1 and Table 4.2 summarize the material properties for each of the different regions from which coupons were tested. With the processed data it was then possible to plot the engineering stress-strain curves for each one of the coupons; Figure 4.3 and Figure 4.4 are two of such curves for a beam (bottom flange) and a shear tab (with grain) respectively. It is important to note that the yield strain (ε_y) and yield stress (F_y) were defined using the 0.2% offset method. Section 4.2.3 contains a comparison of the measured and probable material properties (R_yF_y) outlined in CSA S16 (2009).

Table 4.1 – Summary of beam tensile coupon tests

Section	Specimens	Region	E (GPa)	ε_y	F_y (MPa)	ε_u	F_u (MPa)
W310x60 (W12x40)	6J 9J A1 A2	Top Flange	201	0.0025	399	0.1720	495
		Web	193	0.0012	432	0.1587	512
		Bottom Flange	187	0.0020	404	0.1489	504
W310x60 (W12x40)	1 2	Top Flange	199	0.0019	331	0.1458	436
		Web	199	0.0019	396	0.1816	489
		Bottom Flange	198	0.0017	361	0.1840	478
W310x60 (W12x40)	3 7	Top Flange	209	0.0015	367	0.1579	494
		Web	209	0.0018	403	0.2123	498
		Bottom Flange	212	0.0015	376	0.1579	500
W610x113 (W24x76)	4 5 6	Top Flange	203	0.0018	364	0.1621	465
		Web	207	0.0021	435	0.1437	500
		Bottom Flange	201	0.0018	358	0.1724	460
W310x74 (W12x50)	8	Top Flange	205	0.0018	370	0.1740	490
		Web	208	0.0018	384	0.1812	496
		Bottom Flange	210	0.0018	368	0.1683	490
W610x140 (W24x94)	10	Top Flange	195	0.0019	362	0.1673	500
		Web	206	0.0019	405	0.1816	506
		Bottom Flange	199	0.0019	363	0.1690	496

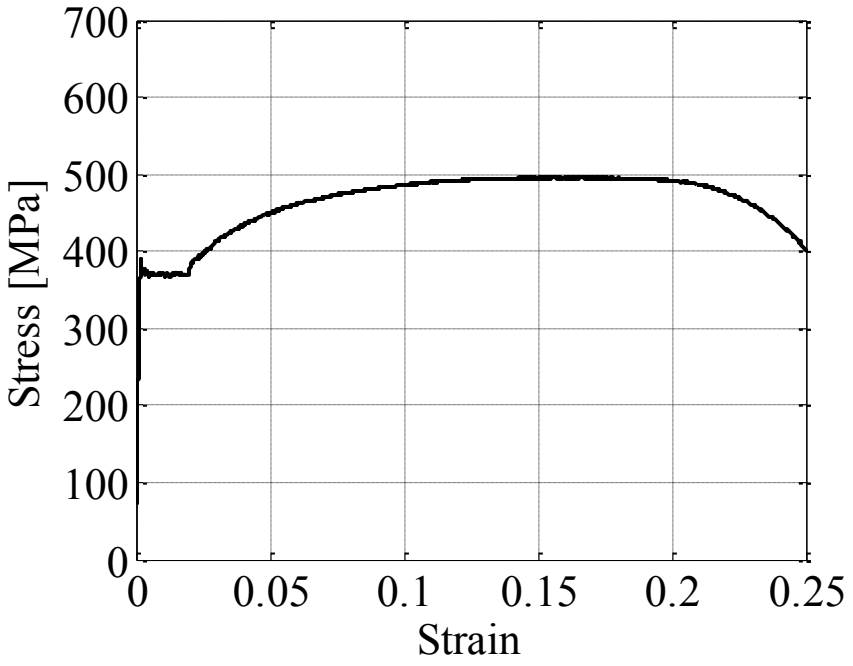

Figure 4.3 – Engineering stress vs strain (Specimens 3 and 7 beam – bottom flange)

Table 4.2 – Summary of shear tab and supporting stiffener tensile coupon tests

Section	Specimens	Region	E (GPa)	ε_y	F_y (MPa)	ε_u	F_u (MPa)
PL 12.7 (PL 1/2)	A1 A2	With Grain	161	0.0029	424	0.1146	517
		Against Grain	200	0.0022	460	0.0876	536
PL 9.5 (PL 3/8)	6J 9J	With Grain	199	0.0024	449	0.1244	561
		Against Grain	199	0.0023	449	0.1190	525
PL 19 (PL 3/4)	1 2 3	With Grain	186	0.0025	398	0.1102	547
		Against Grain	171	0.0020	354	0.1420	552
PL 15.9 (PL 5/8)	4 5 6 7	With Grain	210	0.0020	401	0.1472	561
		Against Grain	211	0.0018	393	0.1633	551

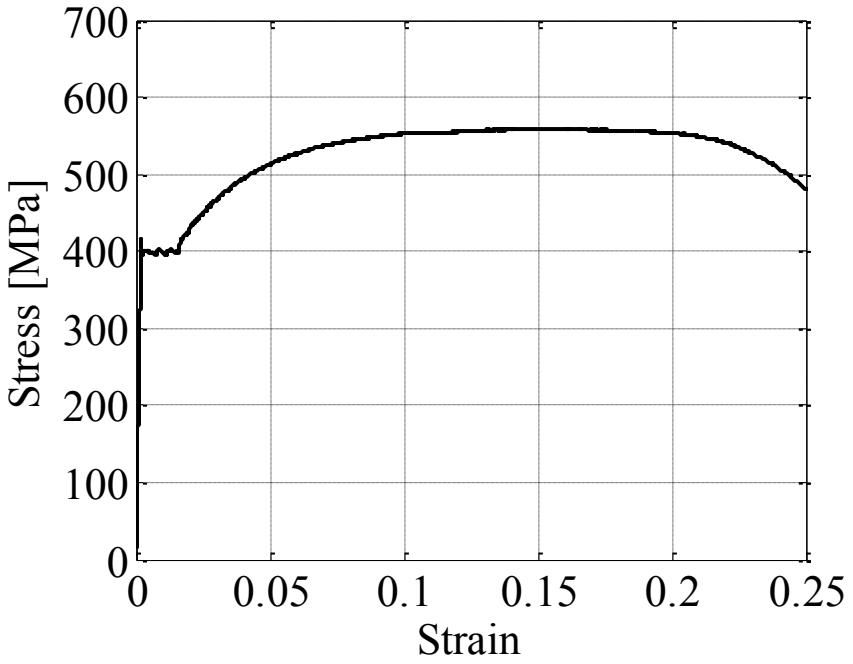

Figure 4.4 – Engineering stress vs strain (Specimens 4,5,6, and 7 stiffener plate and shear tab – Long Grain)

4.2.3 Remarks on Material Properties

In order to compare the nominal and predicted material properties with the measured tensile properties of the steel, the results presented in Table 4.1 and Table 4.2 were averaged for each steel member and presented in Table 4.3 and Table 4.4. These tables do not only present the arithmetic mean of the calculated values but also shown are the ratios between measured yield and ultimate stresses (indicated by the subscript "E") and nominal and predicted yield and ultimate stress (indicated by the subscripts "N" and "P" respectively).

As indicated in Section 3.3, the factor used to estimate the probable yield stress, R_y, used to calculate the predicted values for design was set to 1.1. Observing Table 4.3 and Table 4.4 it is evident that this assumption is in agreement with the experimental results for both yield and ultimate stresses. For the beam material properties, the experimental yield stress values are within 8% of the predicted values used for design whereas the ultimate stress values are within 6%. As for the steel used for the shear tabs and stiffener plates, the differences are slightly larger, 16% for yield stress and 12% for ultimate stress. The higher margin can be explained by the fact that the average values calculated from the tensile tests are for coupons oriented with and against the grain.

Table 4.3 – Processed beam tensile coupon tests

Section	Specimens	Avg E (GPa)	Avg $\varepsilon_{y\text{-}E}$ (MPa)	Avg $F_{y\text{-}E}$ (MPa)	Avg $F_{u\text{-}E}$ (MPa)	$F_{y\text{-}E}/F_{y\text{-}N}$	$F_{y\text{-}E}/F_{y\text{-}P}$	$F_{u\text{-}E}/F_{u\text{-}N}$	$F_{u\text{-}E}/F_{u\text{-}P}$
W310x60 (W12x40)	6J 9J A1 A2	194	0.0019	412	504	1.19	1.08	1.12	1.02
W310x60 (W12x40)	1 2	199	0.0018	363	468	1.05	0.96	1.04	0.94
W310x60 (W12x40)	3 7	210	0.0016	382	497	1.11	1.01	1.11	1.00
W610x113 (W24x76)	4 5 6	204	0.0019	386	475	1.12	1.02	1.06	0.96
W310x74 (W12x50)	8	208	0.0018	374	492	1.08	0.99	1.09	0.99
W610x140 (W24x94)	10	200	0.0019	377	501	1.09	0.99	1.11	1.01

Table 4.4 – Processed shear tab and supporting stiffener tensile coupon tests

Section	Specimens	Avg E (GPa)	Avg ε_y (MPa)	Avg F_y (MPa)	Avg F_u (MPa)	$F_y/F_{y\text{-}N}$	$F_y/F_{y\text{-}P}$	$F_u/F_{u\text{-}N}$	$F_u/F_{u\text{-}P}$
PL 12.7 (PL 1/2)	A1 A2	181	0.0026	442	527	1.28	1.16	1.17	1.06
PL 9.5 (PL 3/8)	6J 9J	199	0.0024	449	543	1.30	1.18	1.21	1.10
PL 19 (PL 3/4)	1 2 3	179	0.0023	376	550	1.09	0.99	1.22	1.11
PL 15.9 (PL 5/8)	4 5 6 7	211	0.0019	397	556	1.15	1.05	1.24	1.12

4.3 TEST RESULTS AND OBESERVATIONS

The results presented herein are divided into the six categories outlined in Section 3.2 in order to compare and contrast the capacity of each of the specimens and the effectiveness of the different configurations tested. Note that in all shear-rotation relations, the dashed portion of the curves represents the time during testing in which the target connection stiffness was sought by means of adjusting the displacement rates of the actuators as outlined in Section 3.6.1. When strain gauge yielding data is plotted, a plus sign (+) indicates tensile strain while a minus sign (-) represents compressive strain. The plotted shear was calculated by taking the sum of forces applied by the main and tip actuators (see Section 3.4.5). The plotted rotation is the relative rotation of the connection; this is calculated by subtracting the rotation recorded by the inclinometer on the beam top flange from the rotation recorded by the inclinometer on the girder flange (refer to Section 3.6.2 and Appendix C for detailed instrumentation layouts). The graphs presented herein also label the predicted design load based on the calculated probable resistance of the specimen and corresponding failure mode illustrated by horizontal dashed lines.

4.3.1 Extended Shear Tab – Partial Depth Configuration

Two partial depth extended shear tabs based on the specimens designed by Hertz (2014) were tested; the first had an eccentricity ("*a*" distance) of 165.1mm (6 1/2") while the other had an eccentricity of 241.3mm (9 1/2"). As discussed in Section 3.2.5, the purpose for testing these specimens was to observe if by adding a pseudo-concrete slab restraint, girder web punching could be avoided. After testing the first of these two specimens (Specimen 6J), it was determined that the additional restraint did reduce girder punching but did not prevent it; therefore, before testing the second specimen (Specimen 9J), the connection was retrofitted with a horizontal steel plate below the shear tab – once again, girder web punching was reduced but not prevented. It is important to note that the tests performed by Hertz (2014) will be referred to herein as Configuration 6 and Configuration 9, to avoid confusion with Specimen 6J and Specimen 9J.

Figure 4.5 shows the connection shear-rotation relation comparing Configuration 6, tested by Hertz (2014), and Specimen 6J. Configuration 6 was originally stopped due to equipment malfunction; on the other hand, Specimen 6J was stopped once it was evident that all the damage was occurring in the girder web. When testing Specimen 6J, once the load of 140kN was reached at 0.01 radians rotation, strain gauge data indicated that all the damage was occurring in

the girder; the strain gauge on the back of the girder web had yielded when the load reached 27kN while all the strain gauges on the shear tab remained elastic. Therefore, it was decided to stop the displacement of the tip actuator and continue loading only using the main actuator in order to increase the shear force at the shear tab – this portion of loading is not shown in Figure 4.5. The experiment was continued in this fashion until it was clear that the damage was still occurring in the girder web; the maximum load reached was 357kN without any recorded yielding in the shear tab. The design failure mode for both connections was calculated to be plate buckling based on the Q-Equation once the load reached 190kN; this phenomenon was not observed in either of the two tests hence no horizontal line is plotted indicating this load level. Therefore, it can be seen that the capacity of these specimens was below those calculated by the design method outlined in Section 3.3.4. The observed limit state is not accounted for in current design provisions; therefore, there is a discrepancy between the predicted and observed behaviour of these connections.

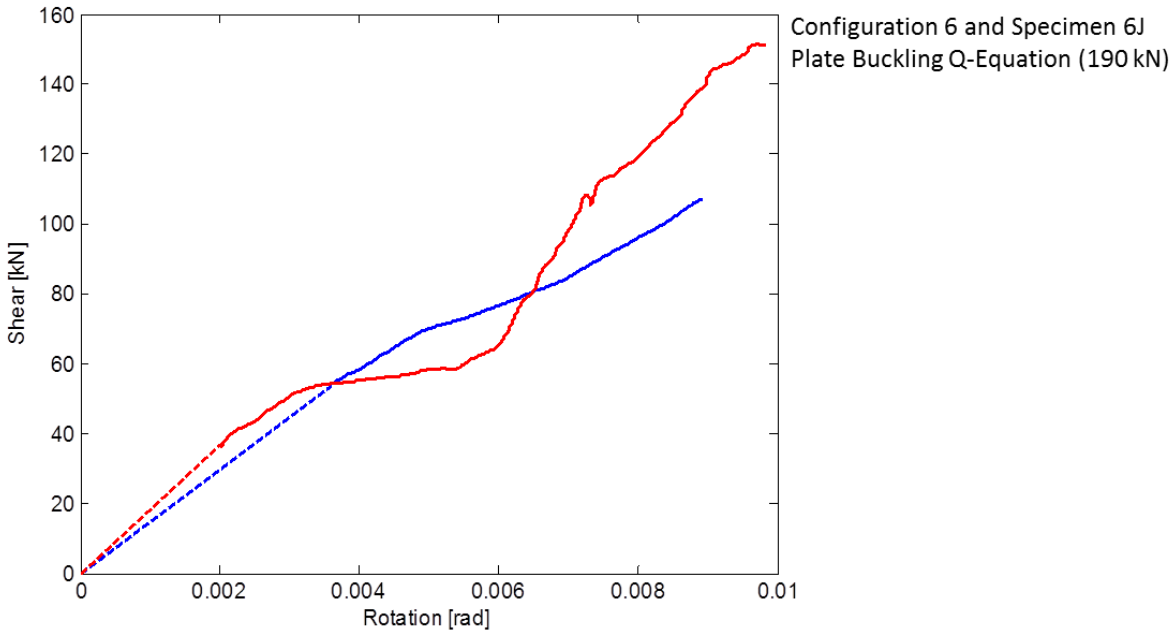

Figure 4.5 – Shear-rotation and predicted failure mode for Specimens 6J and Configuration 6

By observing the recorded data from the LVDTs on the back of the girder web, the extent of the damage in that region becomes evident. The LVDT at the top of the girder web measured almost 5mm displacement toward the connection while the LVDT located at the height of the bottom

region of the shear tab recorded deflections up to 12mm. Figure 4.6 shows the deformation in the region, a framing square was used to highlight the amount of deformation in the girder web.

Figure 4.6 – Damage in girder web (girder web punching) in Specimen 6J

In order to avoid girder web punching in the second extended shear tab with partial depth connection (Specimen 9J), the idea was to engage more area of the girder web, this was to be attained by retrofitting the connection with a horizontal steel plate welded to girder web and the bottom of the shear tab. Once the retrofit was made, it became evident that by adding the steel plate not only was more of the girder web engaged, but the eccentricity of the connection ("*a*" distance) was reduced from 241.3mm (9 1/2") to 81.0mm (3 3/16"). This occurred because by adding the steel plate, a "beam-like" component was created using the shear plate as a web and the girder top flange and retrofit steel plate as flanges; therefore, the new eccentricity was taken as the distance between the first row of bolts and the edge of the retrofit plate.

Figure 4.7 illustrates the connection shear-rotation relation comparing Configuration 9, tested by Hertz (2014), and Specimen 9J. It must be noted that Configuration 9J was tested over two days; the reason being that during the first day, testing had to be stopped due to safety concerns regarding observed bolt slip in the interface between the test girder and the supporting stub columns. As a result of the observed slippage, thin steel plates were placed at the interface between these two members to eliminate any gaps and testing was resumed the following day. In order to continue testing from the same position on the shear-rotation curve on the second day, the total applied load as well as the displacement at the tip of the beam was matched with the point at which testing stopped on the first day and testing proceeded from that point. Note that on the first day the maximum load reached was 225kN.

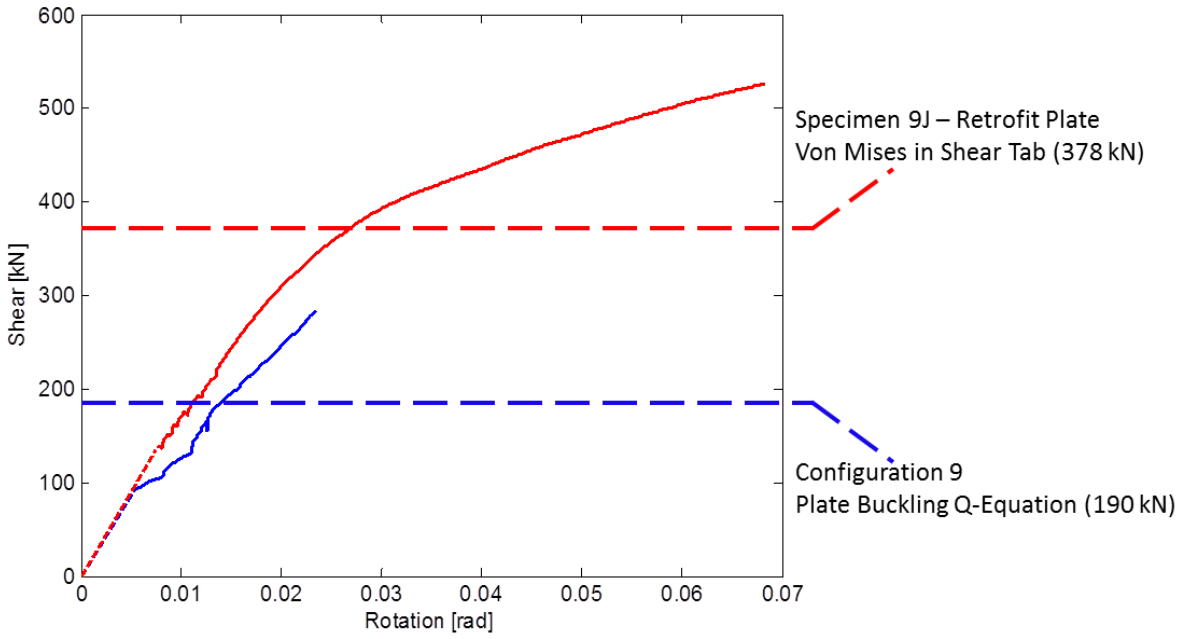

Figure 4.7 – Shear-rotation and predicted failure mode for Specimens 9J and Configuration 9

As seen by Figure 4.7, the original predicted failure mode was plate buckling based on the Q-Equation once the load reached 190kN; however, no buckling was evident in either test specimen. This indicates that the plate buckling equation outlined in Part 9 of the AISC Manual (2011) should be revisited. Once the retrofit plate was installed, the adjusted eccentricity changed the predicted failure mode to Von Mises in the shear tab at a load of 378kN. Strain

gauge data was only collected on the first day; based on the available data, no shear yielding was recorded but the top of the shear tab yielded in flexure when the load reached 100kN.

Figure 4.8 shows how by installing the retrofit steel plate more of the girder flange was engaged. Yielding of the girder web was recorded once the load reached 224kN; it is not possible to make a comparison with Configuration 9 due to the fact that the strain gauges seemed to have not worked properly during testing of Configuration 9. However, it is possible to comment on the extent of girder web punching between the two connections. During testing, the girder in both connections deformed by 15mm at the point of maximum shear, but note how the rotation of Specimen 9J is almost three times that of Configuration 9. Therefore, it can be stated that the retrofit plate did effectively improve the performance of this particular extended partial depth connection. However, the test indicated that a designer should consider the girder yielding in addition to the design of the partial depth shear tab connection.

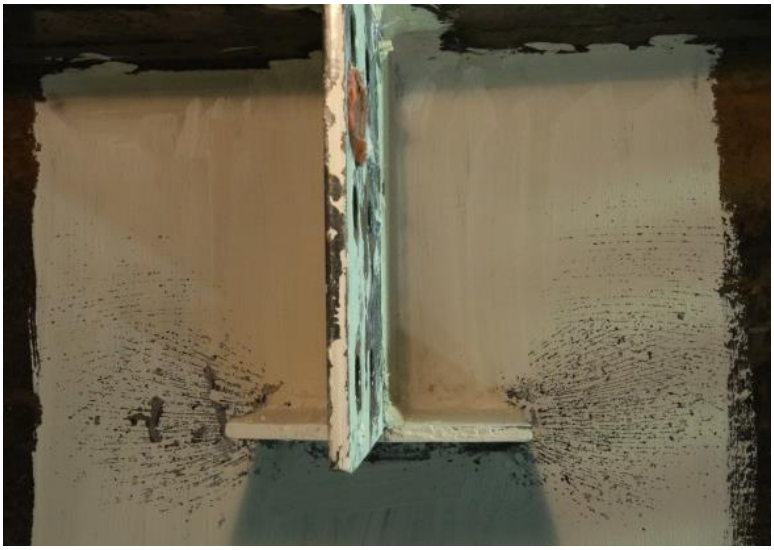

Figure 4.8 – Engagement of girder web due to retrofit plate in Specimen 9J

4.3.2 Extended Shear Tab – Full Depth

Two nominally identical full depth extend shear tab configurations were tested (i.e., Specimens A1 and A2), the only difference between the two was that Specimen A2 did not have the pseudo-concrete slab connection while Specimen A1 did. These connections were designed based on the specimen (Configuration 5) tested by Hertz (2014) with the only difference being the thickness of the shear plate; the plate thickness was increased from 9.5mm (3/8”) to 12.7mm (1/2”) in

order to reduce the slenderness of the plate stiffener (*b/t* ratio) from 28.7 to 21.5 as outlined in Section 3.2.6. Figure 4.9 illustrates the connection shear-rotation relation comparing the three connections mentioned. Testing of Configuration 5 was stopped due to binding between the beam and shear tab, this explains the slight increase in capacity at 260kN; testing of both Specimen A1 and A2 was stopped due to limitations in the test setup.

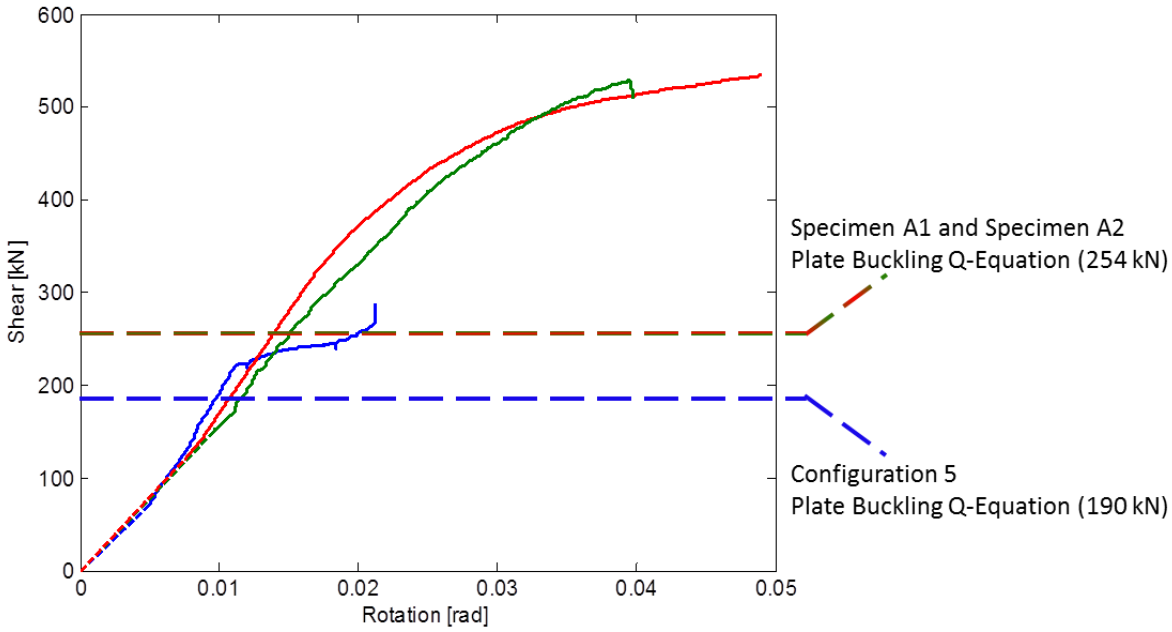

Figure 4.9 – Shear-rotation and predicted failure mode for Specimens A1 and A2 and Configuration 5

From Figure 4.9 it is evident that by increasing the thickness of the shear tab, the performance of the connection is greatly enhanced – the shear capacity is almost doubled. It is also important to note that the predicted failure mode of plate buckling for Configuration 5 occurs when the connection rotation is only 0.01 radians and has significant loss in stiffness from that point; this would lead to an underperforming connection. On the other hand, when observing the behaviour of both Specimens A1 and A2, the predicted failure mode, also plate buckling, occurred at 0.015 radians that is also below the design level of 0.02 radians; however, both connections maintained their shear strength at 0.02 radians. From these comparisons, the predicted failure mode underestimates the actual connection performance under shear.

All three specimens underwent buckling at the neck of the shear tab; it is difficult to determine when this phenomenon was initiated, but it is possible to comment on the magnitude of the out-

of-plane deformation that resulted. Figure 4.10 shows the observed deformation in this region for Configuration 5, Specimen A1, and Specimen A2. The LVDT in the deformed region for Configuration 5 recorded a maximum deformation of 2.7mm which is the most out of these three connections; Specimen A1 had a maximum deformation of 2.5mm and Specimen A2 deformed outwards 2mm.

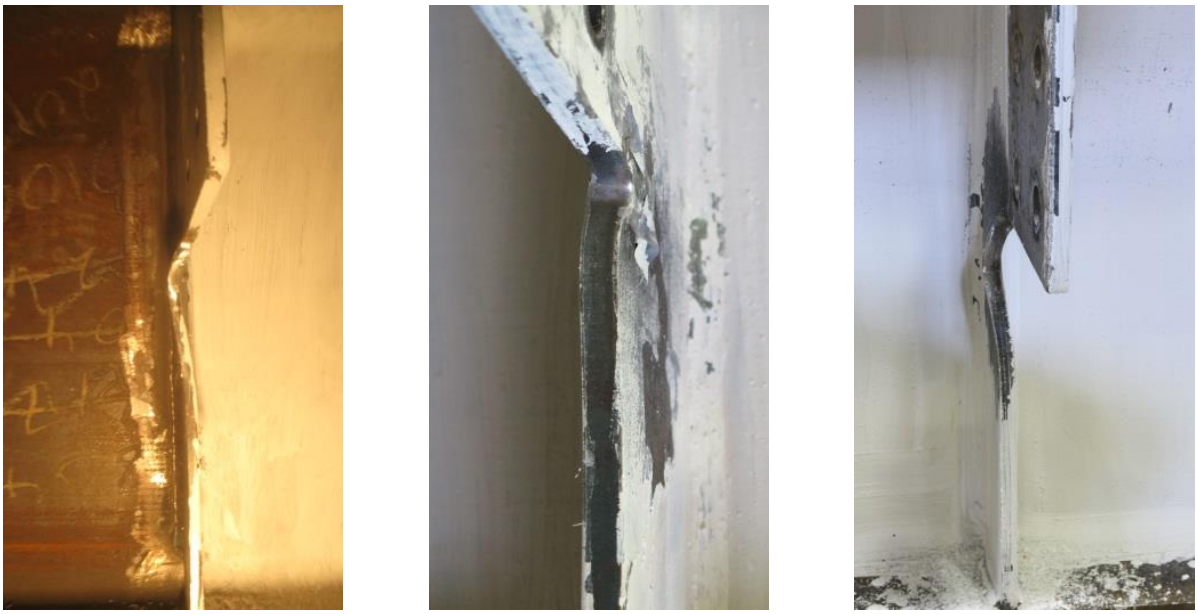

(a) (b) (c)

Figure 4.10 – Out-of-plane deformation in shear tab (a) Configuration 5; (b) Specimen A1; (c) Specimen A2

The fact that Specimen A1 had a greater deformation than Specimen A2 is a result of the pseudo-concrete restraining system. In order to properly understand the effect of the restraint it is important to also observe the deformation that occurred in the girder web. The former connection exhibited a maximum girder web punching of 9mm and this member yielded once the load reached 246kN, whereas the latter recorded deformation up to 19mm and yielding at 273kN. These measurements indicate that by including the restraining system, plastic deformation occurred in the shear tab (Specimen A1) which is a favourable failure mode, while when the girder is left unrestrained (Specimen A2), the plastic deformation was observed in the girder web. The girder web for Configuration 5 also had a maximum deformation of only 9mm; however, this occurred at a significantly lower load, once again demonstrating that the increased plate thickness and pseudo-concrete restraint did in fact improve the performance of the extended full depth shear tabs connections.

4.3.3 Single Coped Beams

Three single coped connections were tested; one of them unreinforced (Specimen 1), one with a single horizontal stiffener at the location of the cope (Specimen 2), and one with a doubler plate (Specimen 3). As can be seen in Figure 4.11, the predicted design failure mode (i.e., Von Mises in the beam in all cases) occurred in the acceptable region, 2% rotation, for design purposes. This means that at the predicted load level, the connection's stiffness remains constant (in the linear portion of the graph) and has rotated 0.02 radians or less. For Specimens 2 and 3 the tests ended once bolt rupture occurred (represented by the crosses in Figure 4.11); for Specimen 1 the test ended once the beam started binding with the supporting stiffener, this explains the strengthening of the connection around 13% rotation. Evidently, the Von Mises criterion accurately predicts the expected design performance of all three single coped bolted connections tested. In other words, the calculated probable resistance of the specimen is similar to the measured load corresponding to a 0.02 radian rotation. Note that the supporting stiffener remained elastic during loading for all three specimens.

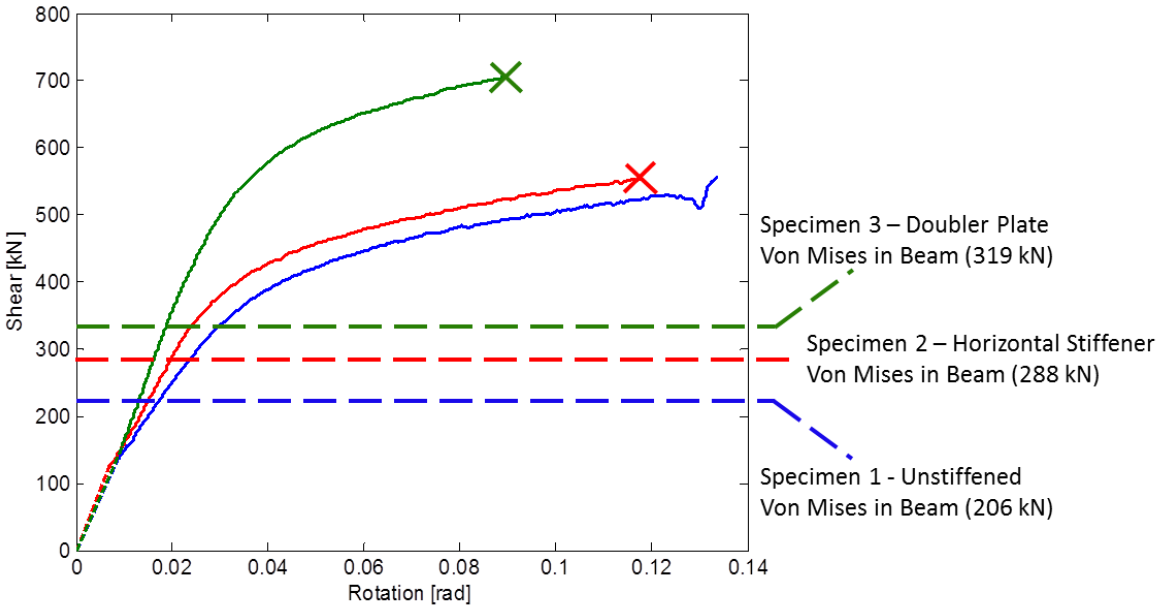

Figure 4.11 – Connection shear-rotation for Specimens 1, 2, and 3

The behaviour of the unreinforced connection (Specimen 1) is accurately predicted by the design equations as outlined in Section 3.3.1. Yielding progressed from the reduced area of the cope downwards through the beam section and gradually towards the gross section of the beam past

the cope. Figure 4.12 illustrates the progression of yielding of Specimen 1 for various levels of connection shear and Figure 4.13 shows the corresponding yielding data.

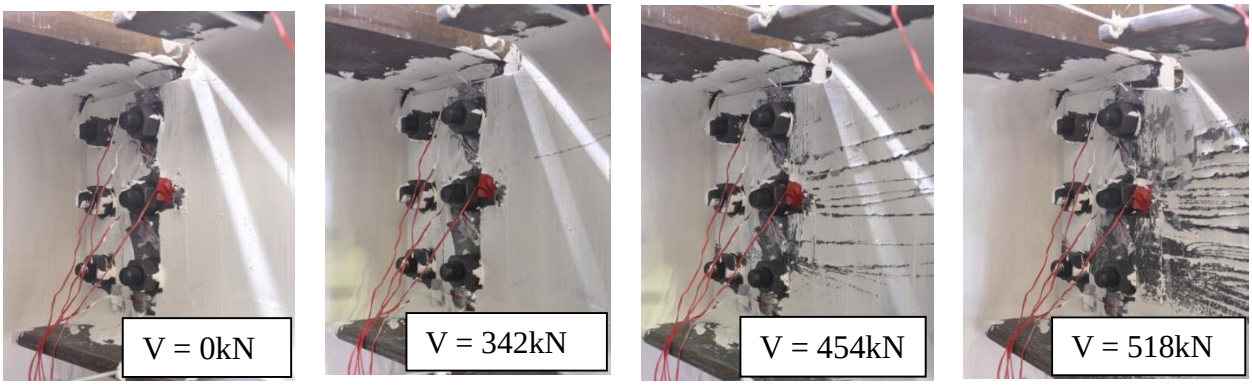

Figure 4.12 – Yield progression for Specimen 1 under various levels of shear

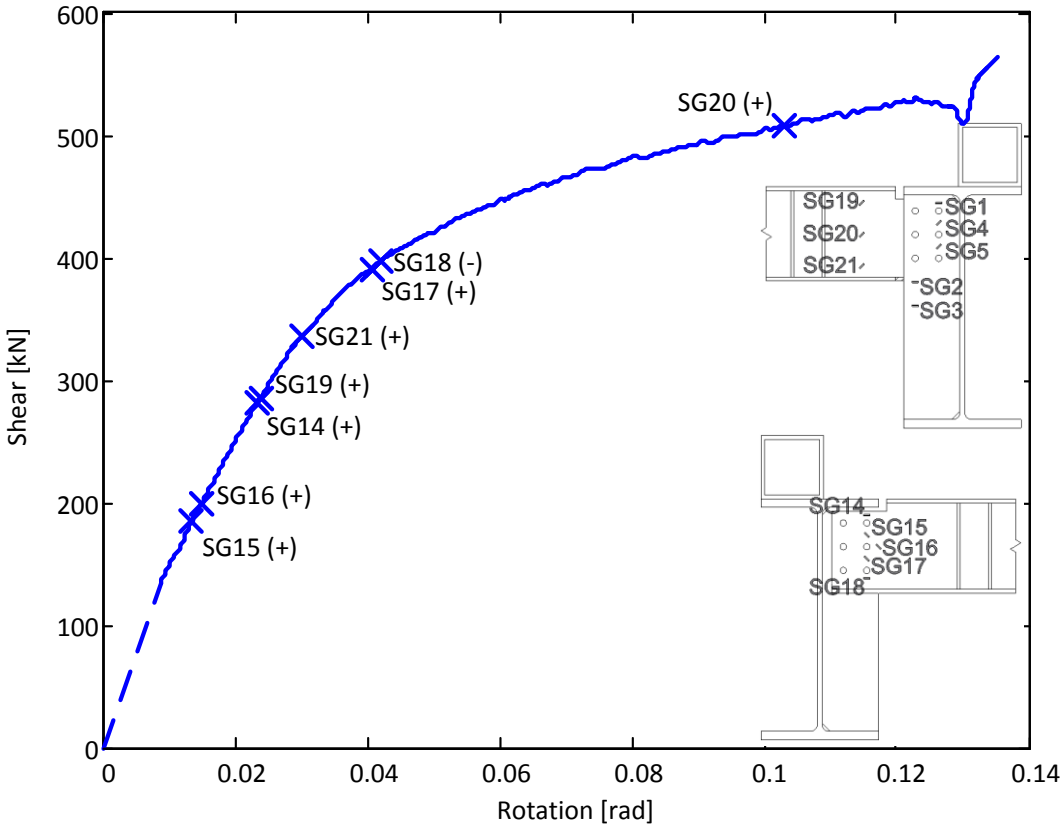

Figure 4.13 – Shear-rotation with strain gauge yielding for Specimen 1

According to the design equations per the AISC Manual (2011), flexural yielding at the cope was predicted at 227kN and actually occurred approximately at 250kN; similarly, the bearing strength of the beam was predicted at 443kN and Figure 4.11 shows a decrease in strength

slightly above 500kN. It is also important to note that a crack, approximately 36mm in length, developed on the beam in the region near the top bolt hole furthest from the connection as can be seen in Figure 4.14; the predicted load for net shear rupture was 477kN, which seems to be consistent with the crack initiation. Neither the girder web nor the supporting stiffener yielded for Specimen 1, the plastic deformation was mostly concentrated in the coped beam.

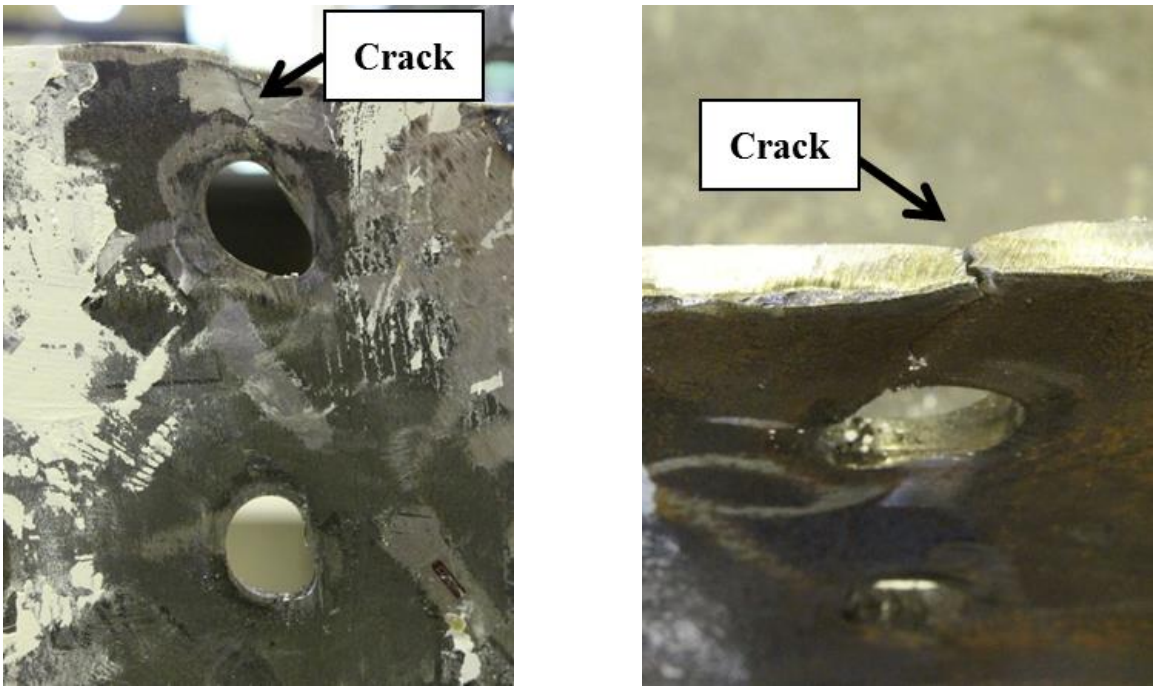

(a) **(b)**

Figure 4.14 – Crack at top bolt hole in beam for Specimen 1 (unreinforced) (a) side view; (b) top view

The purpose of the horizontal stiffener was to add lateral stability to the beam due to the removal of the top flange; however, negligible out-of-plane deformation occurred in Specimen 1 and as a result no comment can be made as to effectiveness of this reinforcement for this purpose from the performed tests. Figure 4.15 shows the web of Specimens 1, 2, and 3 after they have been tested in order to illustrate how only slight amounts of out-of-plane deformation occurred in the beam; Specimen 3 with the increased web area due to the doubler plate reinforcement, exhibited no deformation in the beam web as recorded by the LVDT data and seen in Figure 4.15.

(a) **(b)** **(c)**

Figure 4.15 – Out-of-plane deformation in beam (a) Specimen 1 (unreinforced); (b) Specimen 2 (horizontal stiffeners); (c) Specimen 3 (doubler plate)

It is important to note that the horizontal stiffener did affect the progression of yielding in the beam. The area underneath the reinforcement started yielding in shear first, at approximately 250kN and it was only when the load reached 420kN that the region close to the cope, and the cope itself, yielded in flexure. The increased stiffness did attract higher forces to that region, which lead to bolt rupture at 572kN. It is important to emphasize the fact that even though bolt rupture (a brittle failure mode) was observed, this occurred at almost 12% rotation – well past design level rotations of 2%. Figure 4.16 illustrates the progression of yielding of Specimen 2, and Figure 4.17 the corresponding strain gauge data.

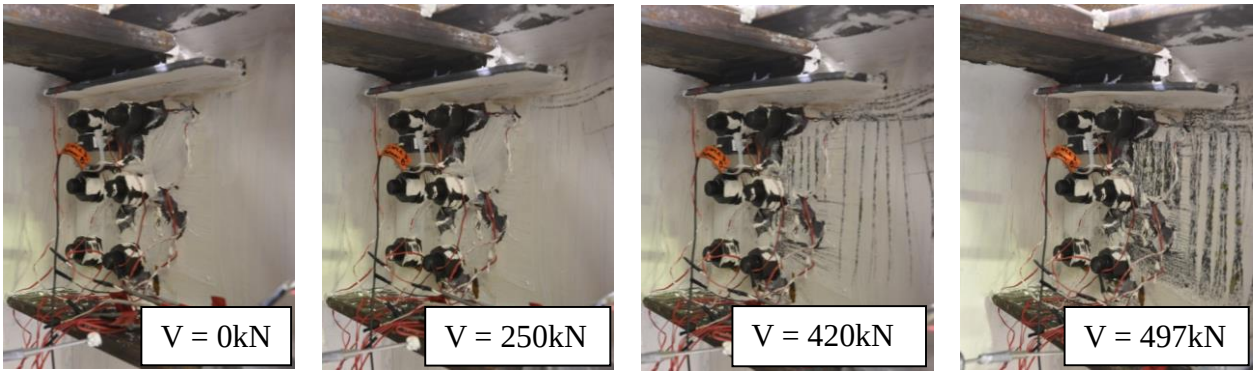

Figure 4.16 – Yield progression for Specimen 2 under various levels of shear

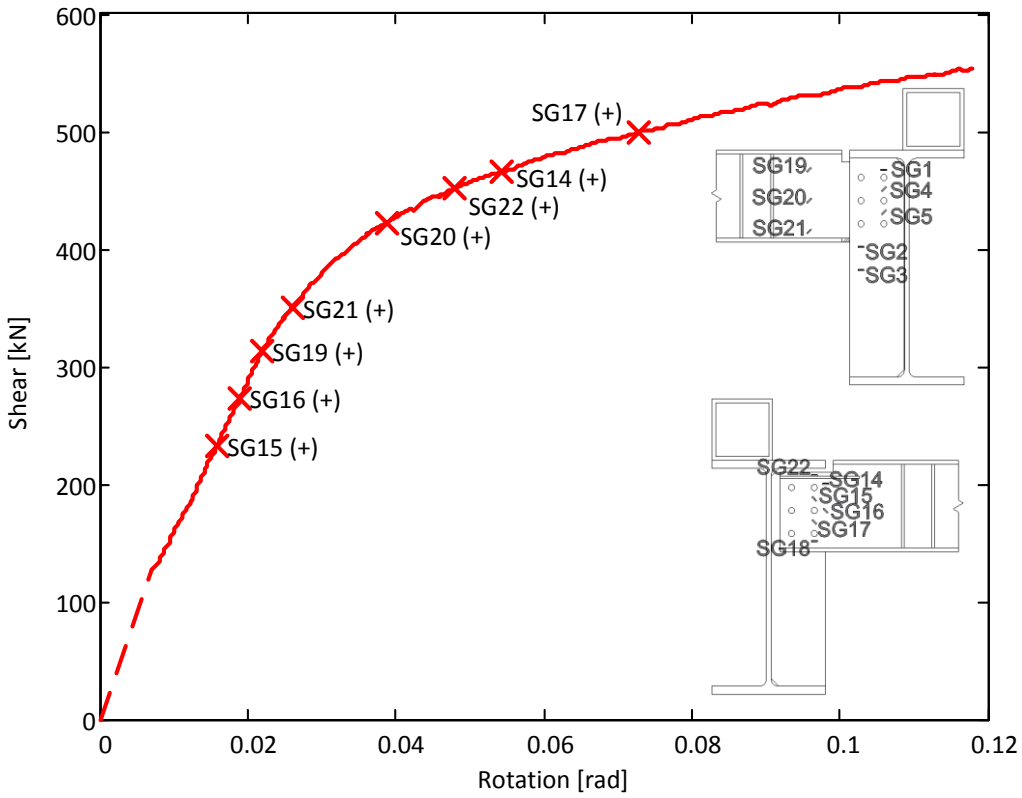

Figure 4.17 – Shear-rotation with strain gauge yielding for Specimen 2

The doubler plate of Specimen 3 did not only increase the ultimate capacity of the connection by 25%, as evidenced in Figure 4.11, but also altered the yielding pattern as compared to the previous two specimens. Shear yielding first occurred in the unreinforced gross section of the beam past the cope at approximately 200kN. Shear yielding continued in this region; it was not until the applied load reached 350kN that shear yielding was recorded on the top portion of the doubler plate coinciding with the reduced area of the beam. As the load increased, the yielding front continued to move downwards. Figure 4.18 illustrates the progression of yielding of Specimen 3 and Figure 4.19 the corresponding strain gauge data.

The increased shear stiffness of the beam web due to the reinforcing doubler plate decreased the deformation in this region of the specimen. As a result, the applied forces were dissipated by deformations in the connection bolts which ultimately lead to bolt shear rupture. The top bolt furthest from the connection was the first to rupture (Figure 4.20), at which time the test was stopped.

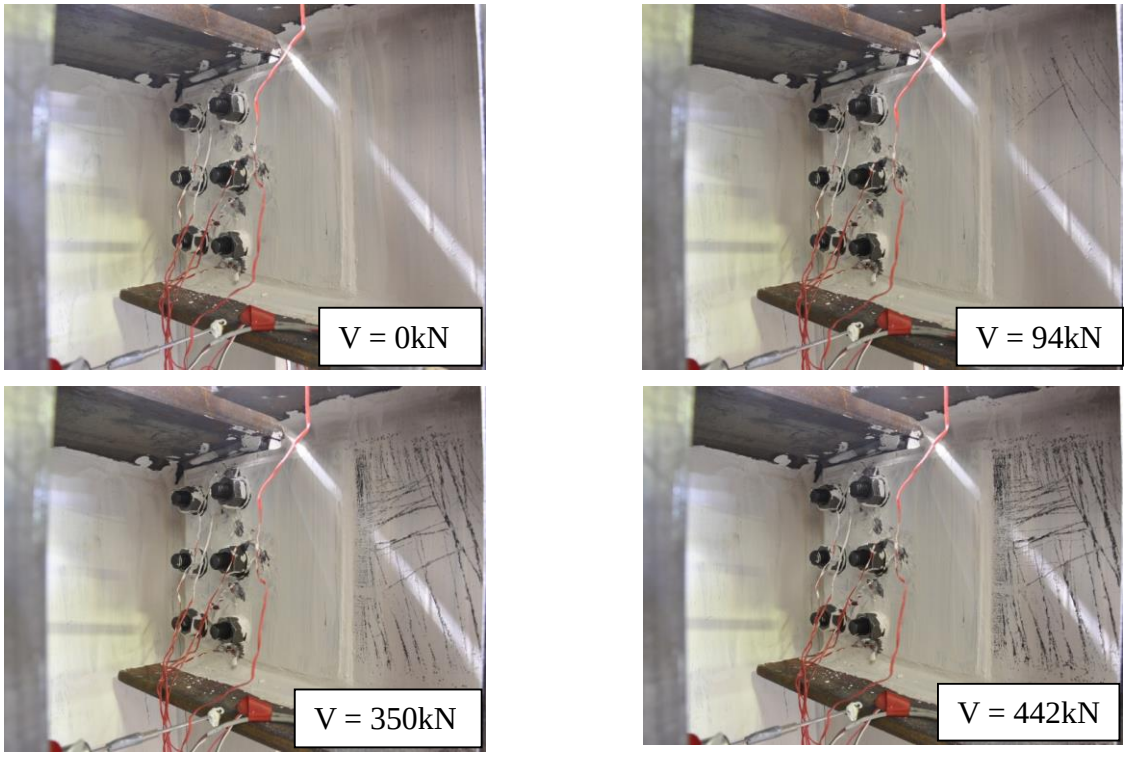

Figure 4.18 – Yield progression for Specimen 3 under various levels of shear

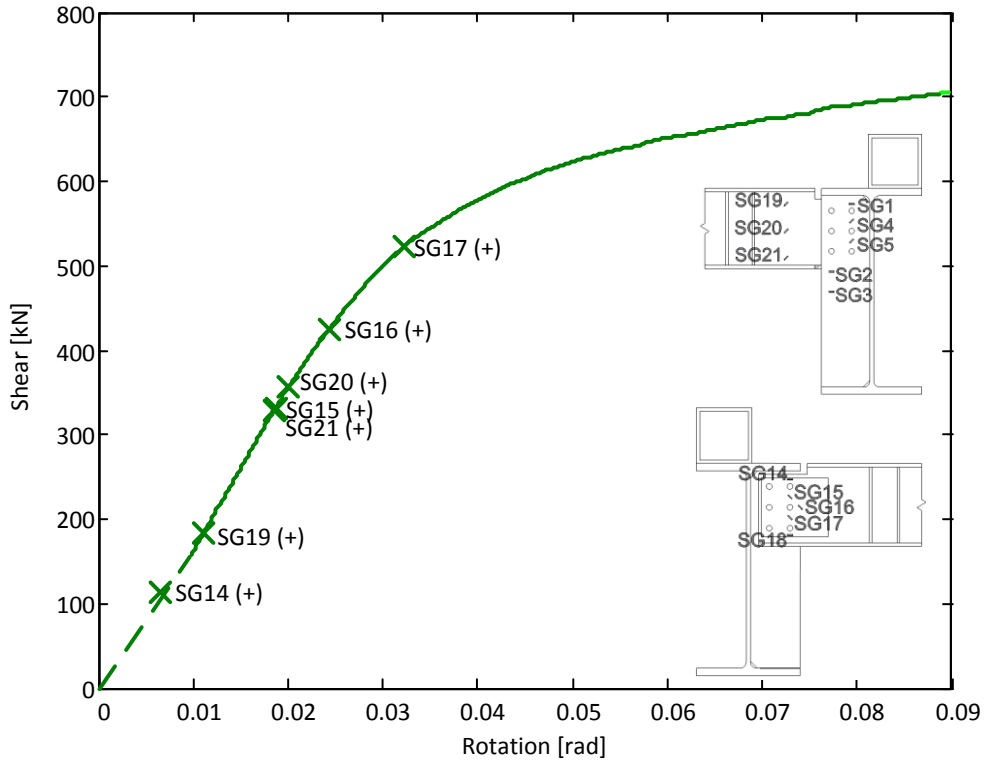

Figure 4.19 – Shear-rotation with strain gauge yielding for Specimen 3

Figure 4.20 – Rupture due to bolt shear (Specimen 3)

4.3.4 Double Coped Beams

Three double coped connections were tested; one of them unreinforced (Specimen 4), one with horizontal stiffeners at the locations of the copes (Specimen 5), and one with a doubler plate (Specimen 6). As can be seen in Figure 4.21, the expected design failure mode (Von Mises for all specimens) adequately predicts the point where Specimen 4 and Specimen 6 undergo a decrease in rotational stiffness. This occurs past the expected design level rotation of 0.02 radians which is within the acceptable region for design purposes. However, this calculated limit state slightly over predicts the capacity of Specimen 5 according to this criterion, meaning this configuration undergoes a decrease in rotational stiffness prior to the calculated load level. Testing of both reinforced specimens was stopped once bolt rupture occurred (represented by the crosses in Figure 4.21); testing of the unreinforced specimen was stopped when thinning of the beam web was observed near the top cope.

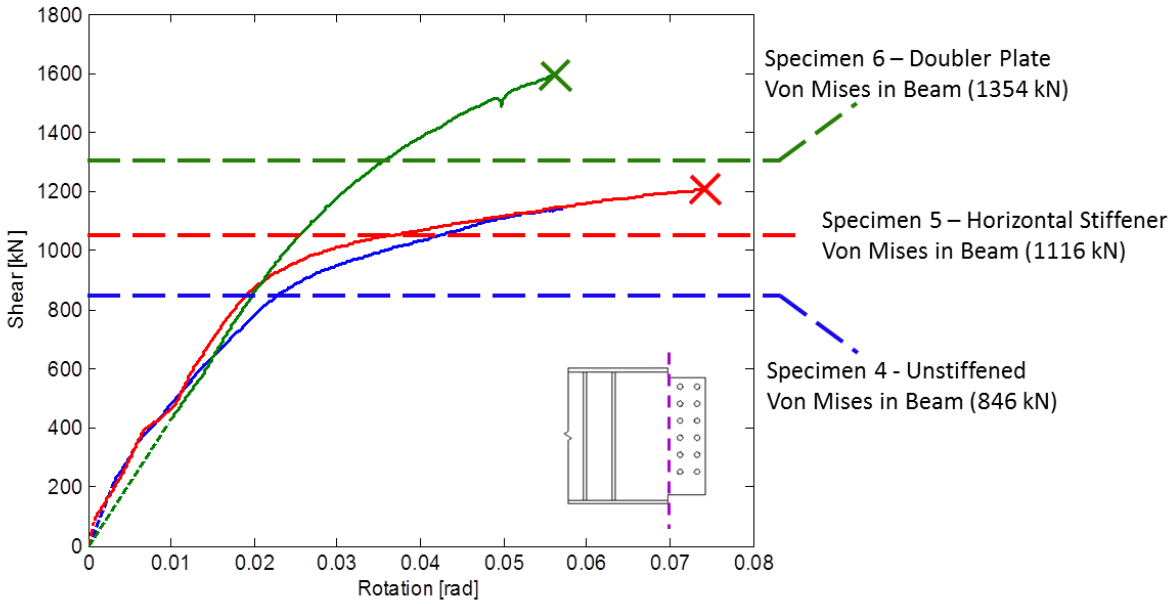

Figure 4.21 – Connection shear-rotation for Specimen 4, 5, and 6 (gross reduced area)

Yielding of the unreinforced specimen first occurred in shear at mid-height of the coped beam when the load reached 580kN and was then followed by flexural yielding at both the top and bottom regions of the beam web closest to the copes when the load reached 600kN. Similar to the single coped specimen, yielding started at the reduced section and moved away from the connection towards the gross area of beam as seen in Figure 4.22 and the corresponding strain gauge data in Figure 4.23. Yielding of the supporting girder web was measured once the load reached approximately 919kN. As the load continued to increase, shear yielding was recorded at the top portion of the supporting stiffener, this occurred once the applied shear reached 970kN. It is at this load level that a decrease in rotational stiffness of the connection is observed. However, it is important to point out that despite the fact that the girder web did yield, LVDT readings on the girder web show that this component rotated about its centroid therefore preventing any web punching.

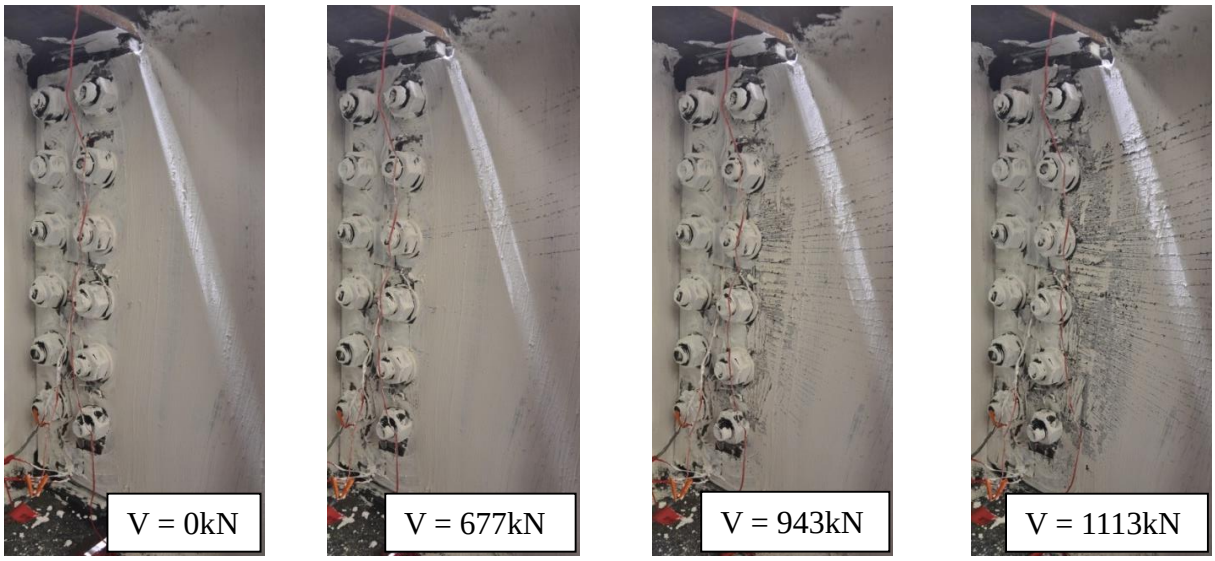

Figure 4.22 – Yield progression for Specimen 4 under various levels of shear

Unlike the single coped unreinforced specimen, Specimen 4 did undergo some bending in the lower portion of the beam web. Therefore, in this scenario it is possible to assess the effectiveness of the horizontal stiffeners in Specimen 5 to prevent this phenomenon. Figure 4.24 shows the three double coped specimens; it can be seen that the presence of both the horizontal stiffeners and the doubler plate effectively provided the reduced beam sections with additional stiffness and stability in order to avoid bending of the coped member.

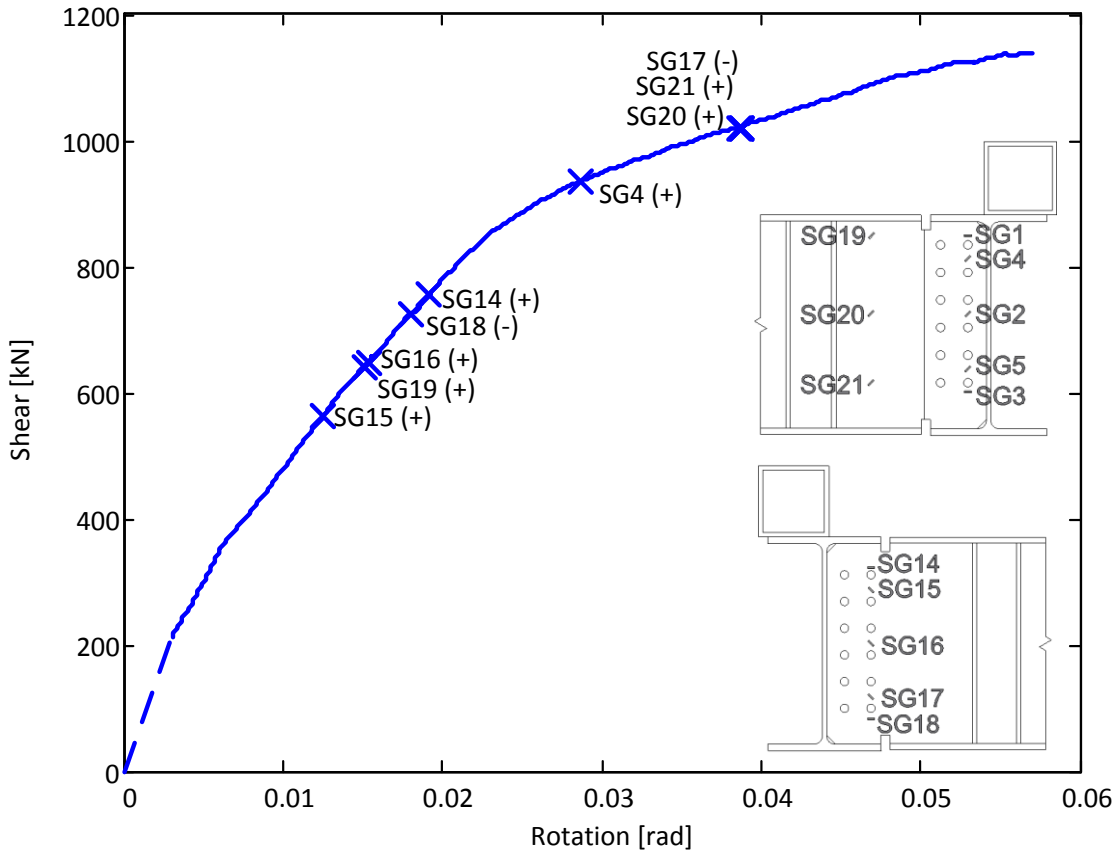

Figure 4.23 – Shear-rotation with strain gauge yielding for Specimen 4

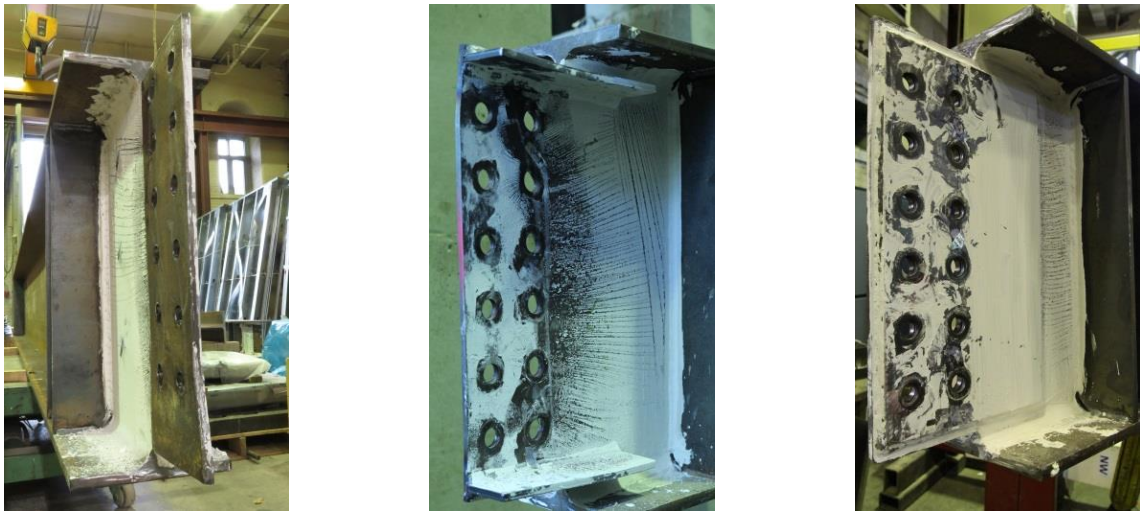

(a) **(b)** **(c)**

Figure 4.24 - Out-of-plane deformation in beam (a) Specimen 4 (unreinforced); (b) Specimen 5 (horizontal stiffeners); (c) Specimen 6 (doubler plate)

Thinning of the beam web was observed in the unreinforced specimen. This behaviour was accompanied by large bearing deformations in the bolt holes along the height of the beam; Figure 4.25 shows these phenomena.

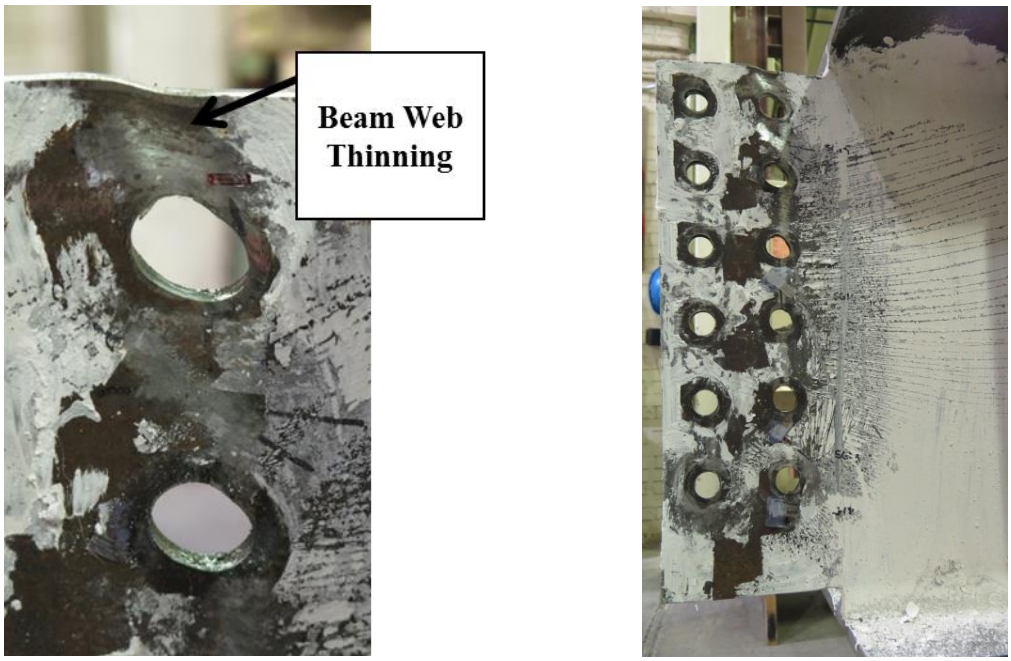

(a) **(b)**

Figure 4.25 – Beam web of Specimen 4 (unreinforced) (a) web thinning; (b) holt bearing

Shear yielding for the specimen with horizontal stiffeners, Specimen 5, was first recorded at the mid-height of the beam when the load reached 700kN. Yielding progressed radially towards the gross area and region near the copes when shear yielding was recorded at 800kN and flexural yielding was recorded at 830kN respectively. Figure 4.26 shows the progression of yielding in Specimen 5 and Figure 4.27 illustrates the corresponding strain gauge data.

When the load reached 1000kN, the bottom of the supporting stiffener started to yield in flexure. At this point, LVDT readings in the lower portion of the girder web show that the beam started to push into the girder. This is in part attributed to redistribution of forces due to the squashing of material in the beam web. However, it must be highlighted that the girder web did not yield during testing. Yielding of the top reinforcing stiffener was recorded once the load reached 1100kN; the bottom horizontal stiffener yielded just before the test was stopped at approximately 1200kN. Testing for Specimen 5 was stopped due to rupture of the top bolt furthest from the connection.

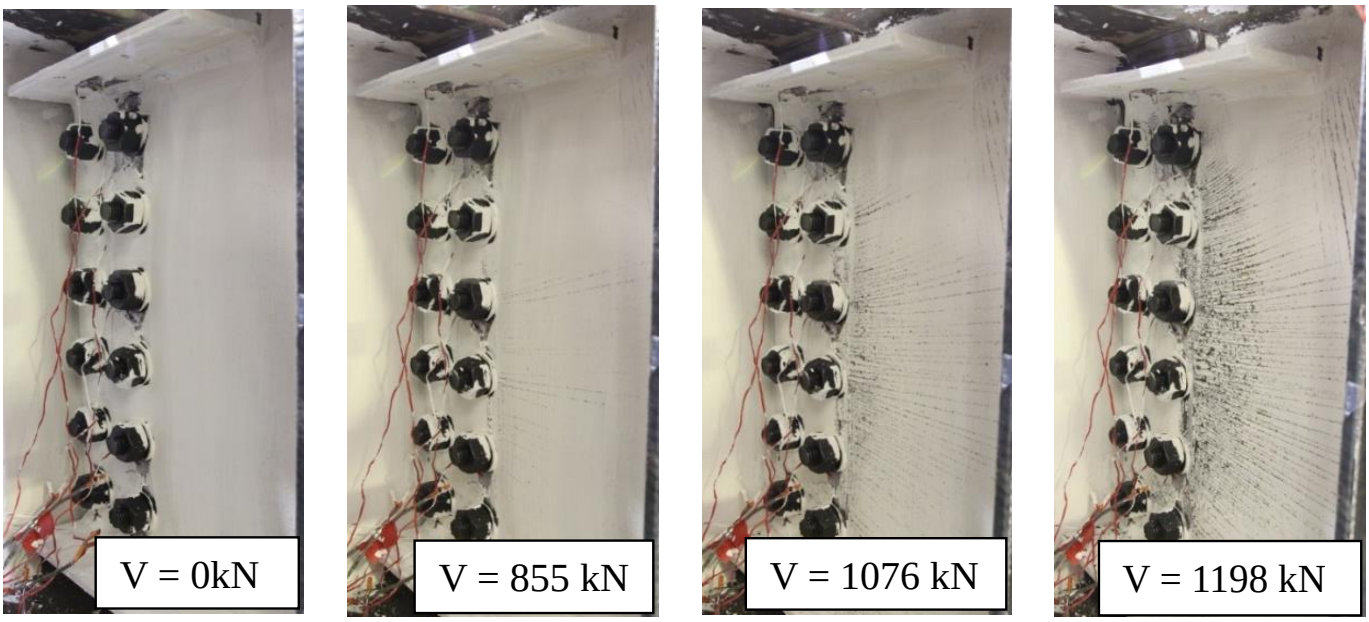

Figure 4.26 – Yield progression for Specimen 5 under various levels of shear

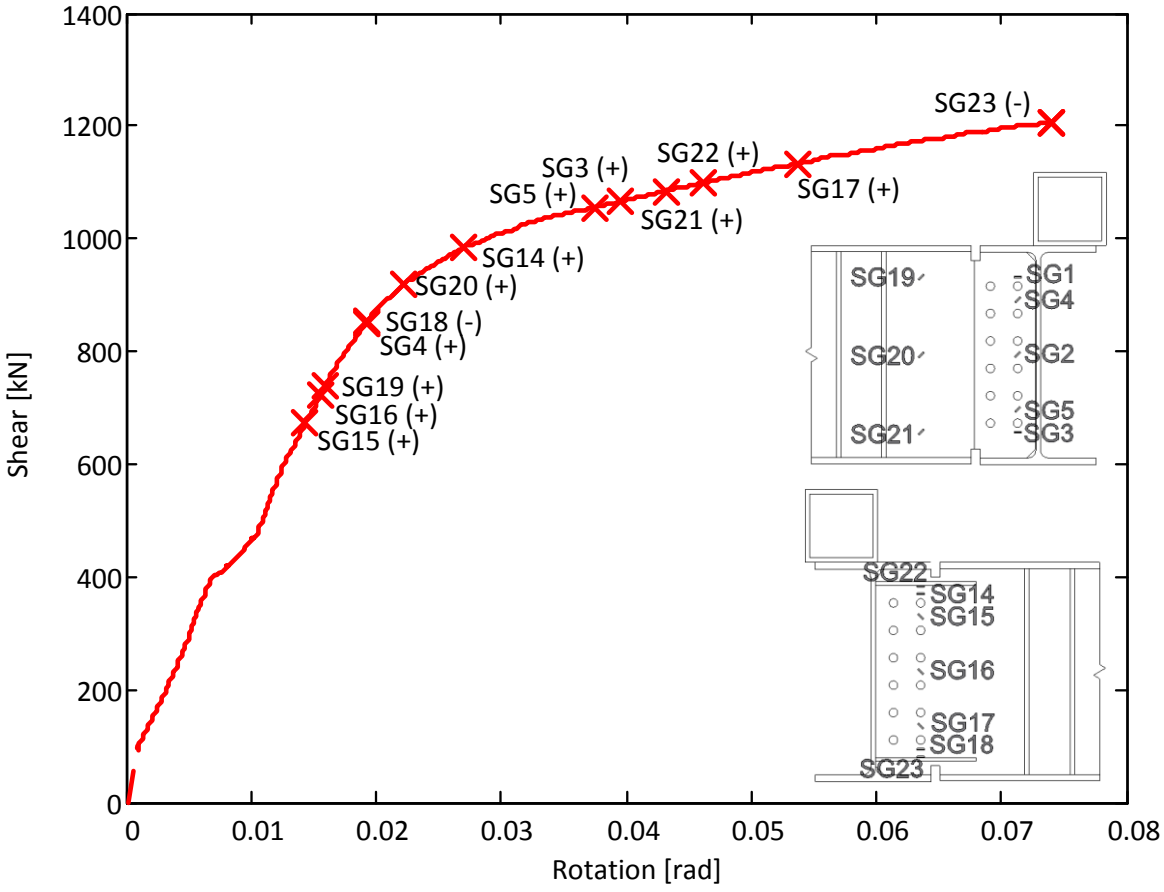

Figure 4.27 – Shear-rotation with strain gauge yielding for Specimen 5

In the case of the specimen with the doubler plate, Specimen 6, shear yielding was first recorded in the unreinforced gross area of the beam at a load of 620kN and in the lower region of the supporting stiffener at a load of 1275kN. Flexural yielding occurred in the lower region of the beam at 1300kN while it was recorded at 1000kN at the top region of the supporting stiffener. Figure 4.28 illustrates the progression of yielding seen from the side of the shear tab and Figure 4.29 illustrated the corresponding strain gauge data.

Yielding in the top region of the connection inevitably lead to the rupture of the top bolt furthest from the connection at a load of 1607kN; it is important to note that testing was stopped once a single bolt ruptured (Figure 4.30a), but by observing the extreme bolts (those at the top and bottom of the connection) after testing, it was evident that rupture was imminent in all these bolts as illustrated in Figure 4.30b. The predicted load for bolt shear rupture was 1760kN; therefore, the calculated values were 9% larger than the observed behaviour of the configuration with regards to this limit state of the connection. Based on LVDT data it can be seen that the supporting girder did rotate about a point below mid-height; this rotation did not seem to affect the rotational stiffness of the connection, and it must be noted that the supporting girder did not yield during testing.

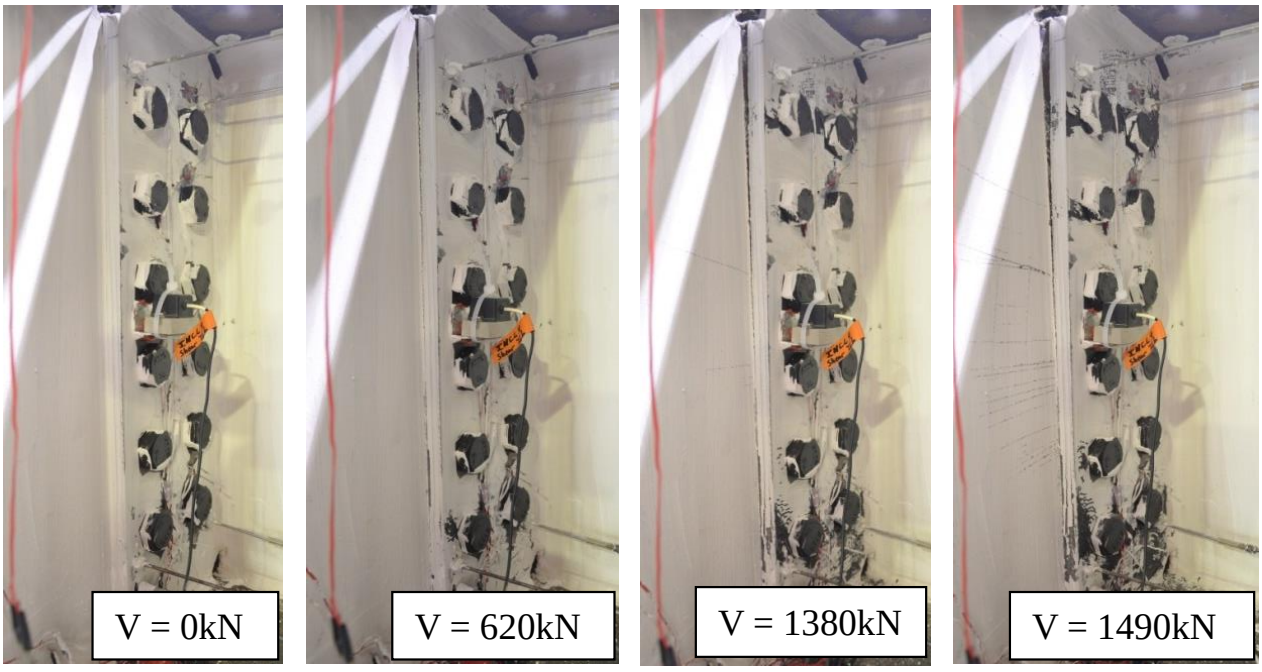

Figure 4.28 – Yield progression for Specimen 6 under various levels of shear

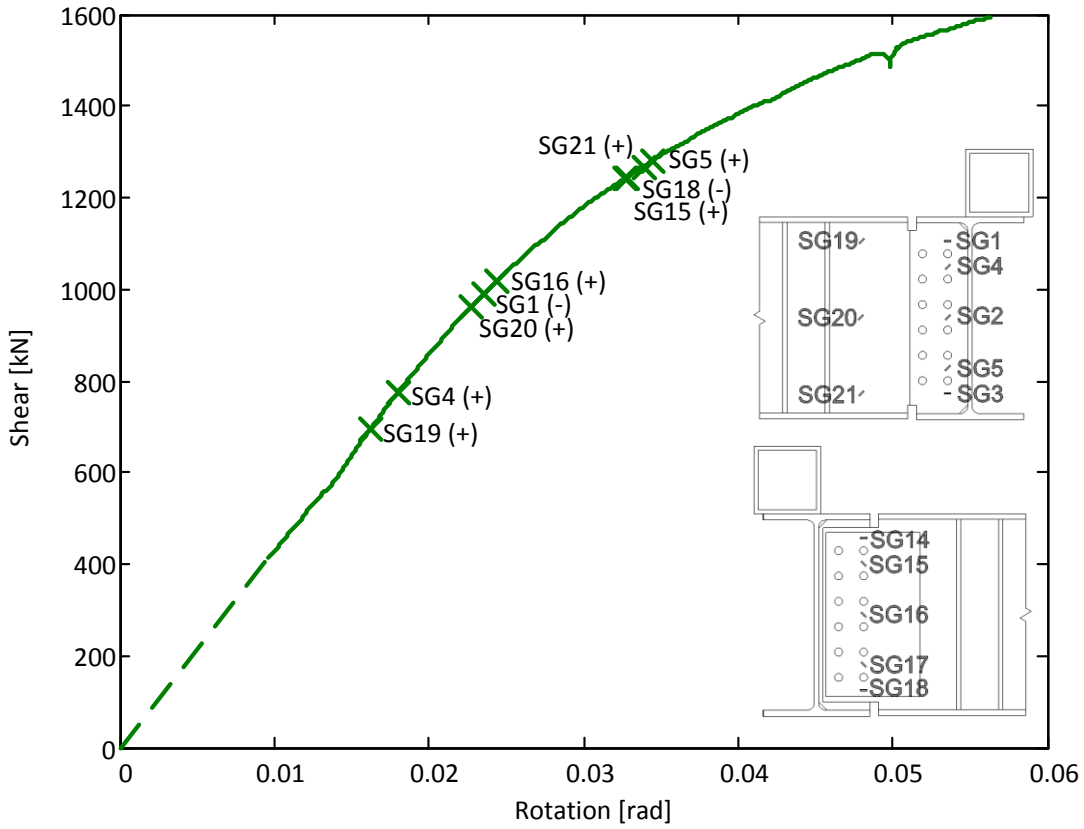

Figure 4.29 – Shear-rotation with strain gauge yielding for Specimen 6

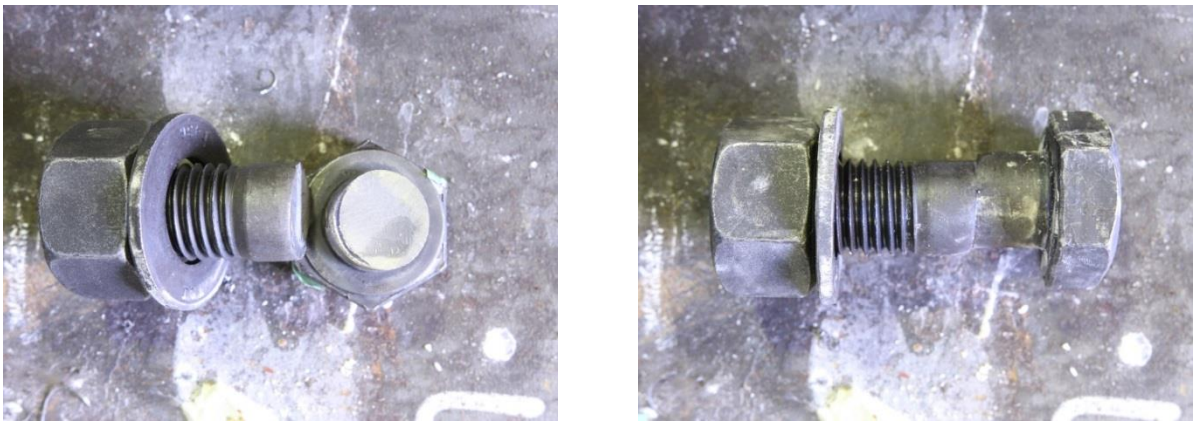

(a) **(b)**

Figure 4.30 – Bolt in Specimen 6 (doubler plate) (a) ruptured bolt; (b) imminent rupture of extreme bolt

By observing the damage progression in all three double coped specimens, it is evident that the critical region for the design of these configurations is the reduced net section furthest away from the girder. Therefore, it would be more accurate to calculate the resistance of the specimen using

the Von Mises criterion at that location rather than at the location of the cope. As seen in Table 4.5, that would decrease the design load for each of the configurations. The decrease in load resistance is due to the reduction in steel area caused by the bolt holes, and the reduction in the eccentricity considered. At these new load levels, the values calculated using the Von Mises criterion would more closely approximate the point at which the rotational stiffness of the connections decreases; however, it is important to note that for doubler plate specimen, the predicted load level still occurs past the design rotation of 0.02 radians. Figure 4.31 shows the shear-rotation curves for the three double coped specimens with the horizontal lines showing the predicted capacity of the connection based on the Von Mises criterion calculated on the net reduced section.

Table 4.5 – Double coped Von Mises resistance location comparison

Specimen	Resistance at cope (gross reduced area)	Resistance at last line of bolts (net reduced area)
Specimen 4 (unreinforced)	846 kN	742 kN
Specimen 5 (horizontal stiffeners)	1116 kN	929 kN
Specimen 6 (doubler plate)	1354 kN	1278 kN

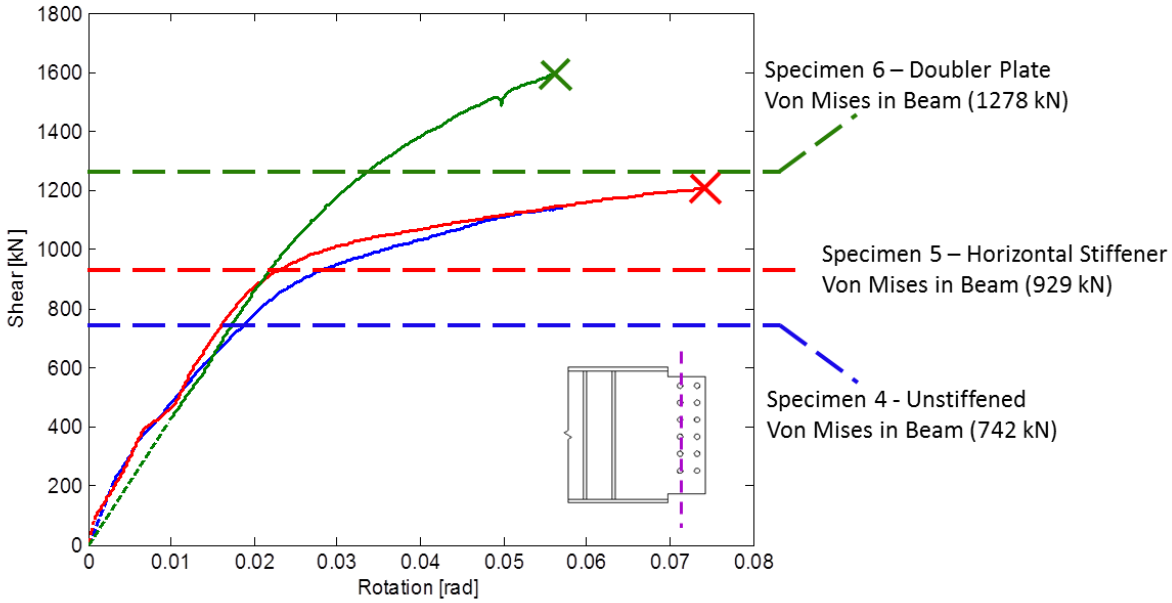

Figure 4.31 - Connection shear-rotation for Specimen 4, 5, and 6 (net reduced area)

4.3.5 Welded In-Shop Coped Beams

The welded in-shop specimens provide engineers the ability to have better control over the quality of welds when compared to those performed on site. Two welded in-shop specimens were tested, a double coped beam with a supporting girder of equal depth (Specimen 8) and a single coped beam where the girder was 152.4mm (6") deeper than the beam (Specimen 10). In both cases, the predicted design failure mode was Von Mises stresses in the beam, which accurately predicted the behaviour of the connections. It is important to note, that in both specimens, the Von Mises criterion accurately predicts the load level at which the desired 0.02 radian rotation occurs which also corresponds to a load level lower than the point at which the rotational stiffness of the connections decreases.

Due to detailing errors, the front angles restraining the horizontal displacement of the girder flanges could not be used when testing Specimen 8. An LVDT was placed on the back of the top flange to measure any horizontal displacements due to this – a maximum displacement of 2mm was recorded at this location. Figure 4.32 shows the global behaviour of Specimen 8. It can be seen that the Von Mises design check accurately predicted the load level, 169kN, at which the connection reached the 0.02 radian design level rotation; however, the rotational stiffness of the connection did not start decreasing until a load of 300kN was attained – a load level 78% higher than predicted. Therefore, this design check is accurate yet conservative in the design of this connection.

This decrease in load carrying capacity of the connection is attributed to a tear that developed at the top of the weld (Figure 4.33). Once the weld tear started to propagate, LVDT recordings placed on the beam web show lateral movement of the beam of a magnitude of 5mm; it would seem that the weld tearing lead to a noticeable loss of lateral stability in the beam.

Shear yielding was first recorded at the top of the gross section when the load was 200kN, and when the load reached 275kN the reduced section started to yield in shear as well. It was not until the load reached 350kN that flexural yielding was recorded, this occurred simultaneously at the top and bottom of the reduced beam section. The design equations outlined in Section 3.3.2 overestimated shear yielding, predicting it would occur at 527kN while under-predicting flexural yielding at a value of 178kN. Figure 4.34 shows the progression of yielding in Specimen 8 and Figure 4.35 shows the corresponding strain gauge data.

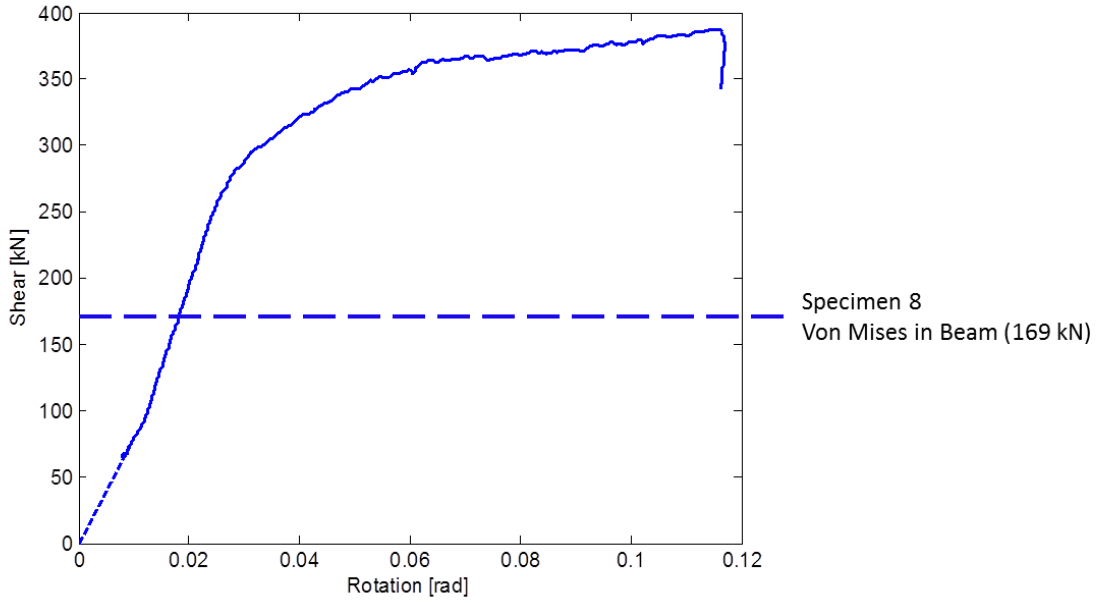

Figure 4.32 – Shear-rotation and predicted failure mode for Specimen 8

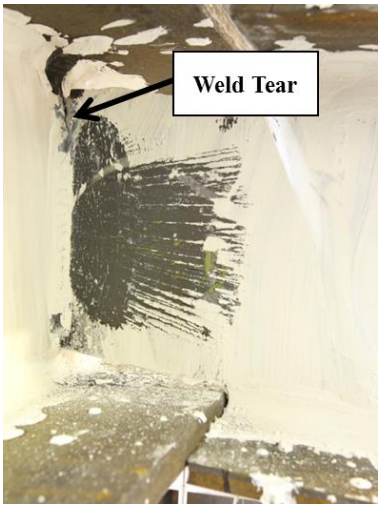

Figure 4.33 – Weld tear in Specimen 8

Based on what was observed with the double coped beam specimens (Section 4.3.4), when the beam and girder are of the same depth, yielding of the girder did not occur until the applied loads were 8% higher than the predicted failure mode if at all (out of the three double coped specimens, only one exhibited yielding in the girder web); therefore, a similar behaviour was expected for the welded specimen. However, the data from the strain gauge placed on the girder web for the welded specimen indicates that the girder yielded at an early stage – when the load

was only 62kN, but it can be seen that the yielding of this component did not govern the behaviour of the configuration.

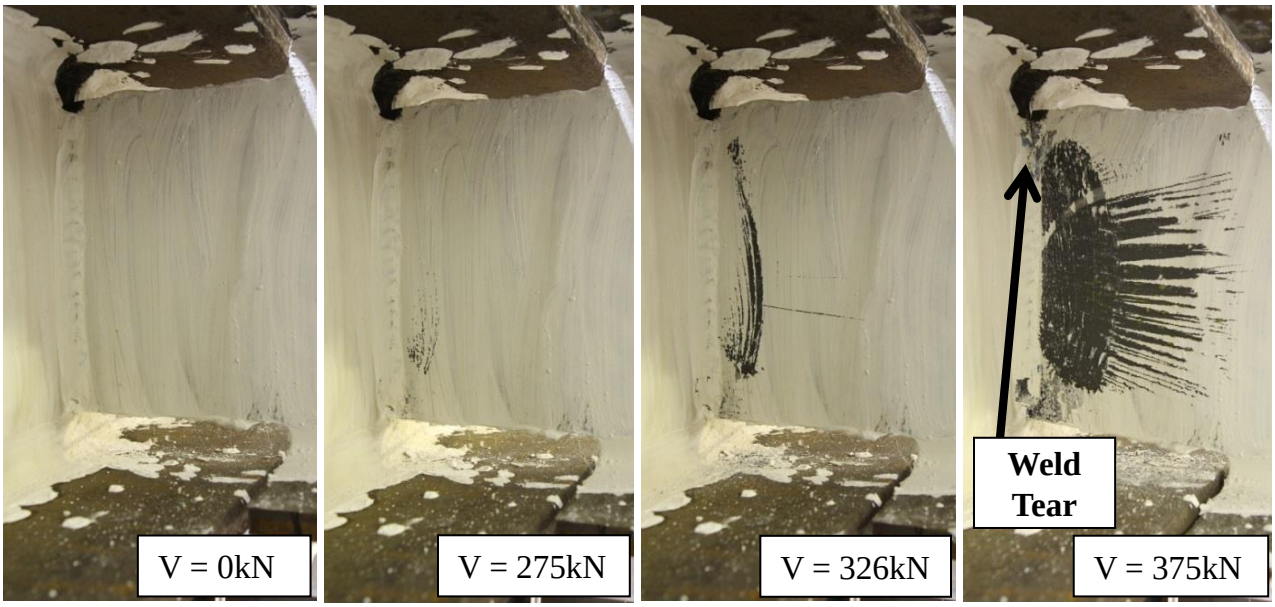

Figure 4.34 – Yield progression for Specimen 8 under various levels of shear

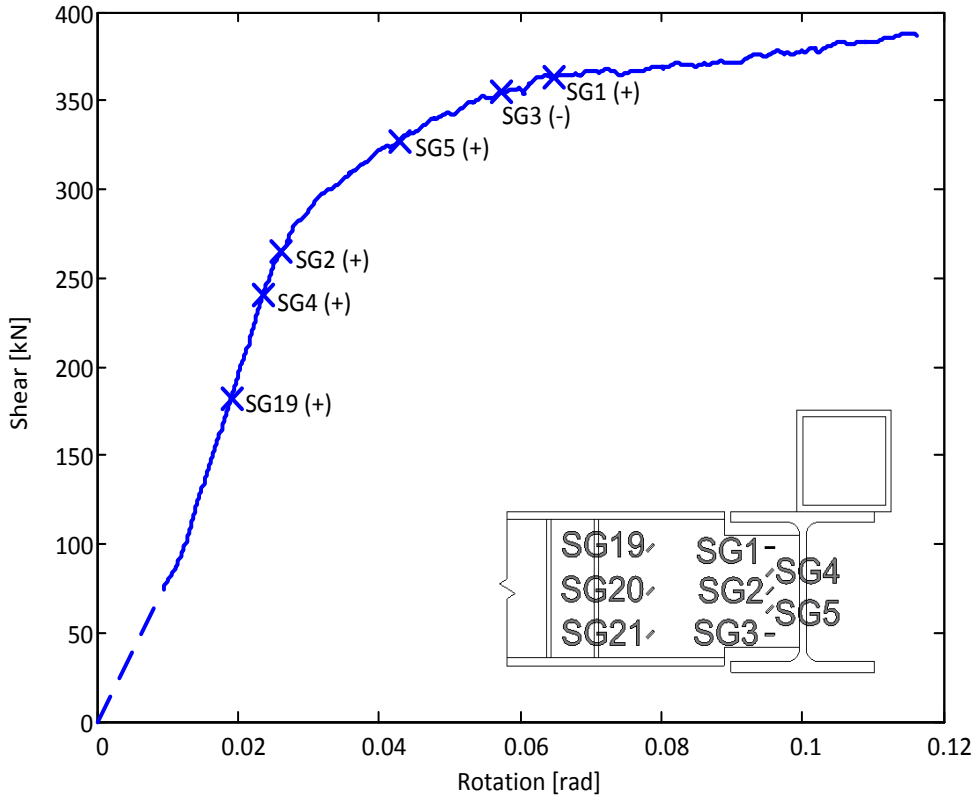

Figure 4.35 – Shear-rotation with strain gauge yielding for Specimen 8

Specimen 10 behaved in a more predictable manner based on the design equations outlined in Section 3.3.2 and observations from previous tests. Figure 4.36 shows the connection shear-rotation curve for this experiment. Similar to Specimen 8, the predicted design failure mode was Von Mises interaction of the beam, this was expected at a load of 1064kN; once again, this occurred at the target design rotation of 0.02 radians. However, unlike Specimen 8, the load level at which the load carrying capacity started decreasing was only 32% higher than the predicted value. Testing was stopped once the tip of the test beam had deflected such that it was coming into contact with the strong floor; however, as is evident from the Figure 4.36, the connection had not reached its maximum capacity even at a connection rotation larger than 10% radians.

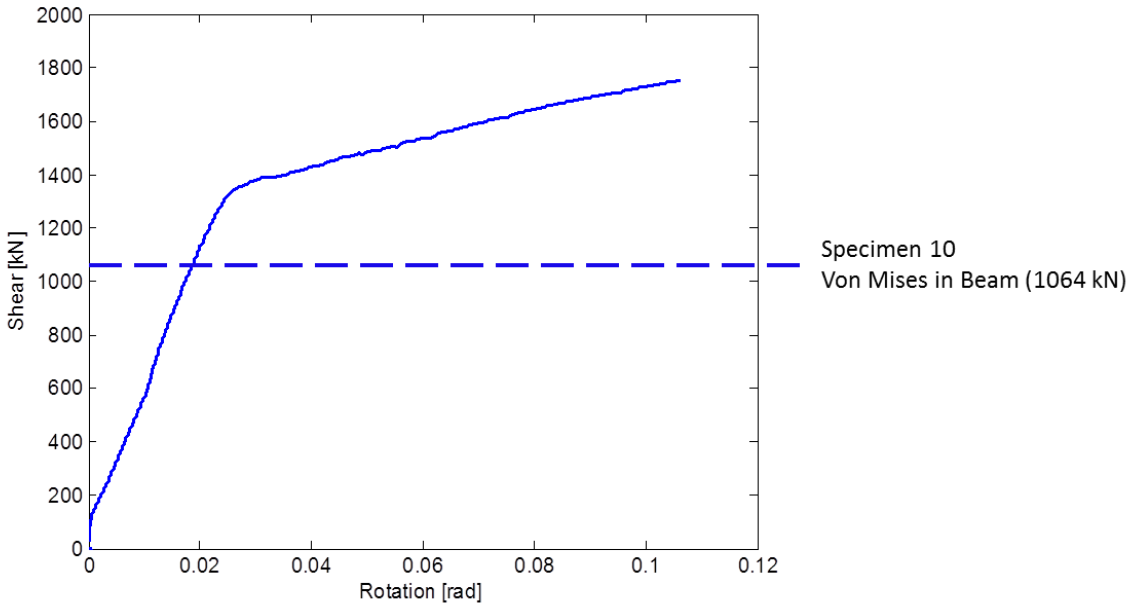

Figure 4.36 – Connection shear-rotation for Specimen 10

Shear yielding was first recorded at the bottom of the reduced section when the load reached 800kN and started moving upwards where yielding was recorded at 1210kN. Flexural yielding was then recorded, again simultaneously at the top and bottom of the beam web, when the load reached 1400kN; approximately at the same load level, the gross section of the beam also started to yield in shear. The design equations predicted flexural yielding accurately at a load of 1301kN; however, shear yielding was predicted to occur at 1851kN. Figure 4.37 depicts the progression of yielding in Specimen 10 and Figure 4.38 shows the corresponding strain gauge data.

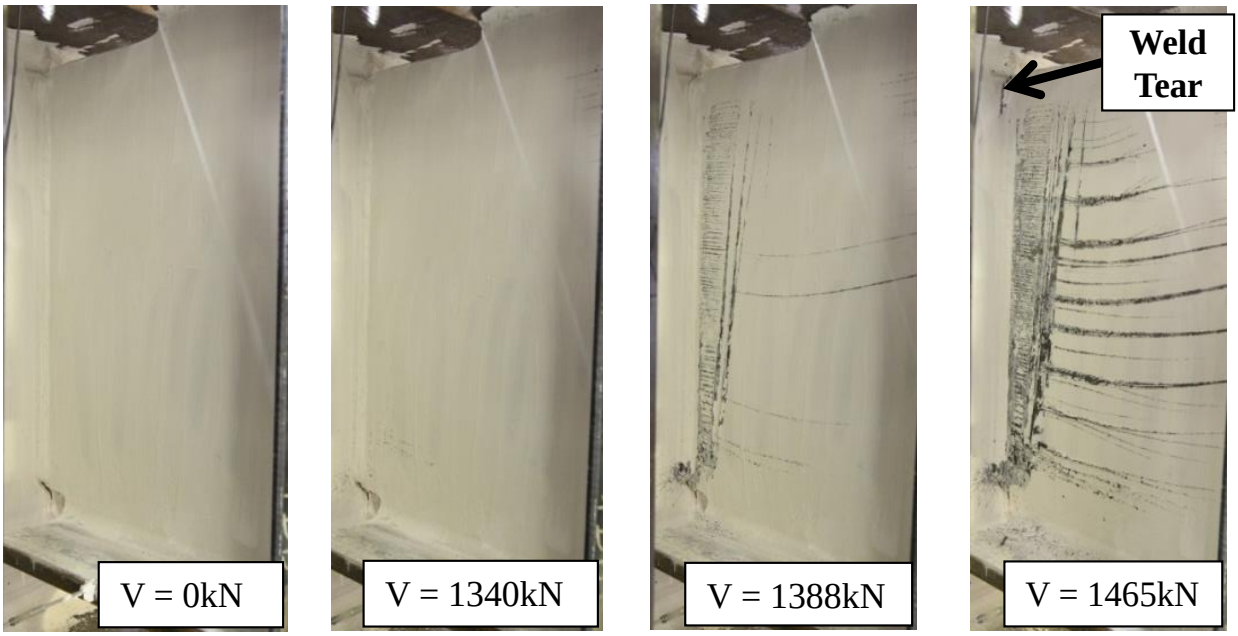

Figure 4.37 – Yield progression for Specimen 10 under various levels of shear

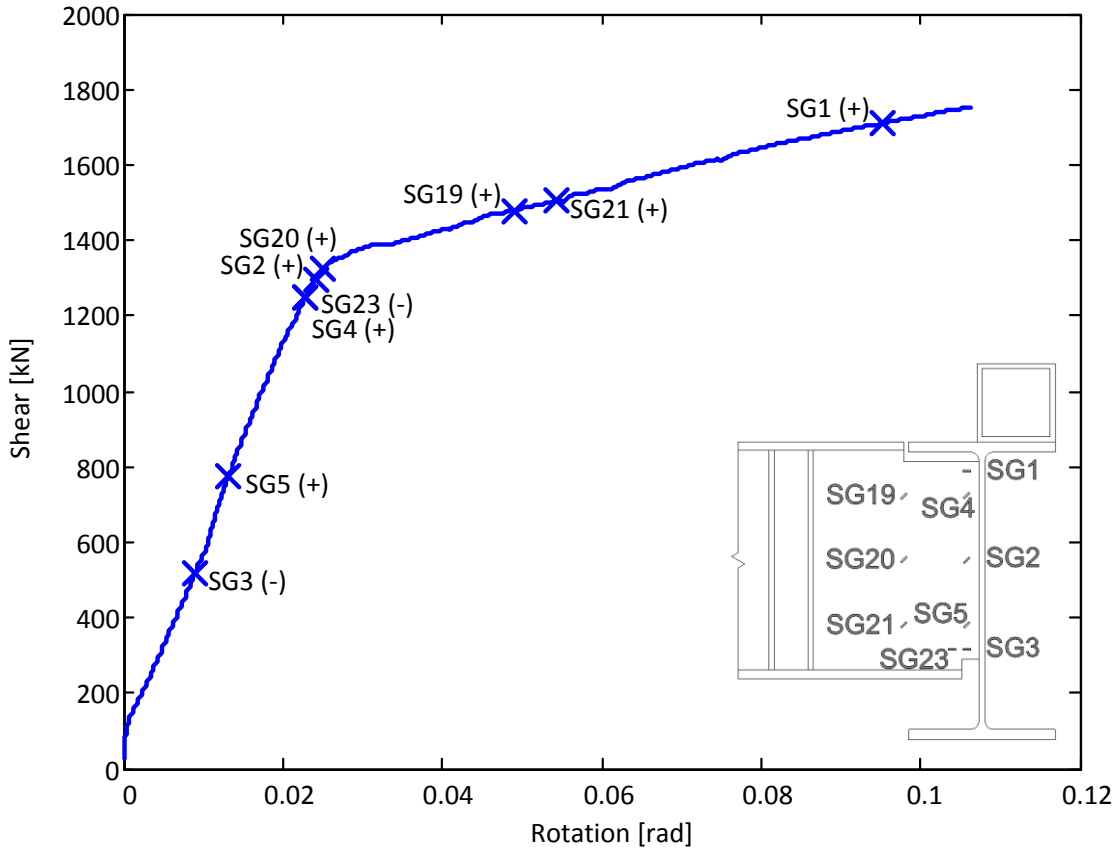

Figure 4.38 – Shear-rotation with strain gauge yielding for Specimen 10

Weld tearing (Figure 4.39) occurred soon after flexural yielding; this was identified as the main reason for the loss of shear strength in the connection at 1400kN. Displacement measured at the back of the girder web validate that welding tearing occurred at this load level, at 1400kN the top of the girder web was 'pulled' in the direction of the beam. In similar fashion to Specimen 8, once the tear started to propagate, LVDT data from the beam web show a loss of lateral stability with deformations close to 8mm.

Even though there was a 152.4mm (6") difference between the beam and girder depths, the girder yielded at much higher load compared to Specimen 8 – yielding of the supporting girder was recorded at 1400kN, 32% higher than the predicted failure mode. Due to the 152.4mm difference between the two components of this configuration, girder web punching was also evident in this specimen. The LVDT located on the back of the girder web at the point where the bottom portion of the beam connects to the supporting member recorded deformations up to 12mm. Figure 4.40a shows the connection between the beam and the girder web at the end of testing; it is evident that punching occurred where the bottom of the beam connects with the girder web. Figure 4.40b shows the girder from the back to further illustrate the extent of the deformation.

It is important to note that the maximum rotation of both welded in-shop specimens was similar to the bolted configurations. Similarly, the contribution of the supporting girder to the connection rotation was also comparable between these two sets of specimens.

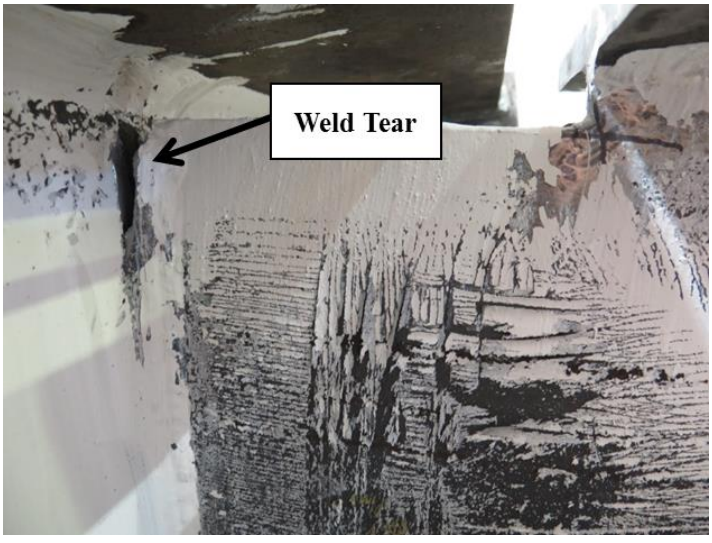

Figure 4.39 – Weld tear in Specimen 10

(a) **(b)**

Figure 4.40 – Punching damage in Specimen 10 (a) bottom of beam connecting into girder; (b) back of girder web

4.3.6 Single Coped Beam Haunched

Specimen 7, a single coped beam with a haunch plate was the first of its kind to be tested. The predicted failure mode based on the design equations per Section 3.3.3 was Von Mises stresses in the beam at a load level of 152kN. As can be seen in Figure 4.41, this load corresponds to a rotation of 0.018 radians. This means that the predicted rotation is acceptable for design level purposes; however, as the curve illustrates, the connection does not decrease rotational stiffness until the load reached approximately 375kN, a load level 2.5 times higher than the predicted design load. Therefore, it is evident that the implemented design methodology is conservative for this type of configuration.

Yielding was first recorded in flexure in the region close to the cope once the load reached 125kN which is slightly less than the predicted value of 160kN; on the other hand, the bottom portion of the connection did not yield in flexure until the load reached 380kN. Shear yielding was first recorded at the top of the gross beam section and the middle of the reduced section simultaneously when the load reached 225kN; however, the design equations used predicted shear yielding to occur at 499kN. Once this region yielded, the section immediately past the cope started to yield in shear; it was not until the load reached 400kN that the haunch plate started yield both in shear and flexure.

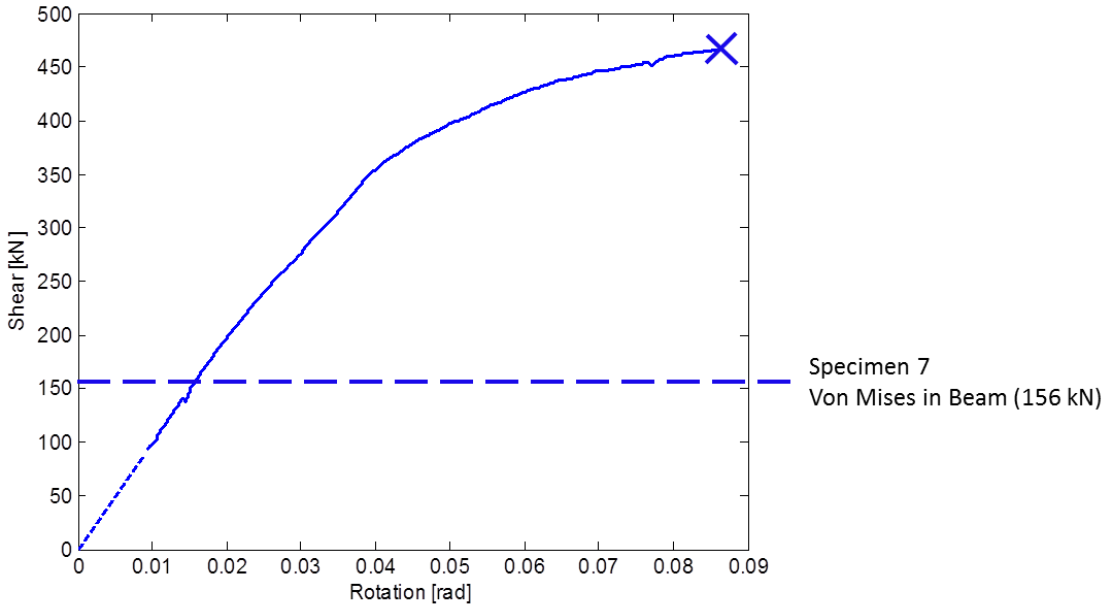

Figure 4.41 – Shear-rotation and predicted failure mode for Specimen 7

Figure 4.42 illustrates the yield progression for Specimen 7 Figure 4.43 shows the corresponding strain gauge data. Based on the observed yielding progression, the interaction of shear and flexural forces control the behaviour of the specimen, this indicates that the Von Mises criterion used is adequate for design despite the conservative predicted resistance. It must be noted that both the girder and supporting stiffener remained elastic during testing. This indicates that all the plastic deformations occurred in the coped beam and haunch plate.

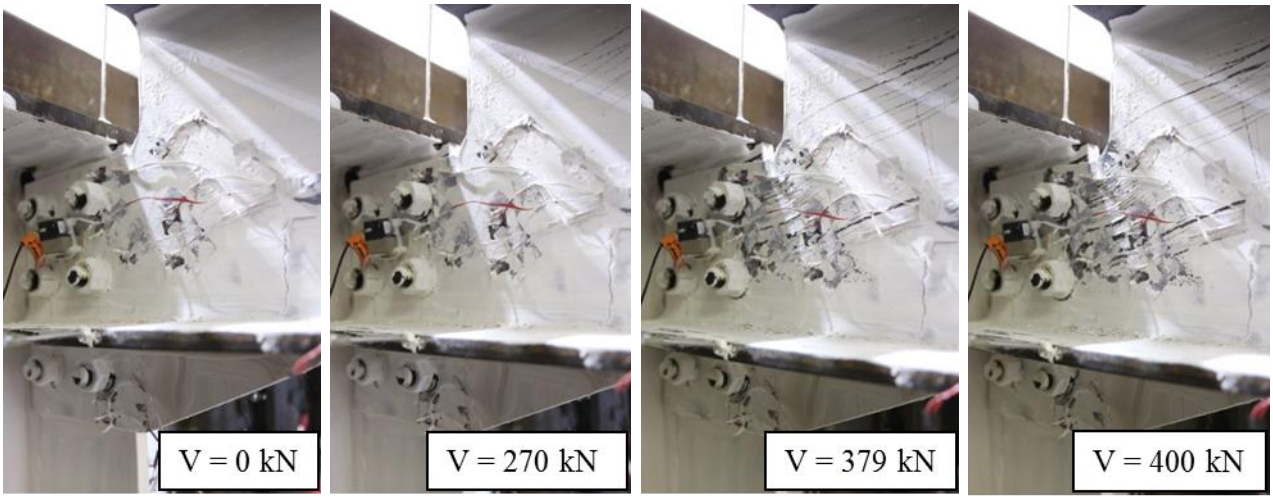

Figure 4.42 – Yield progression for Specimen 7 under various levels of shear

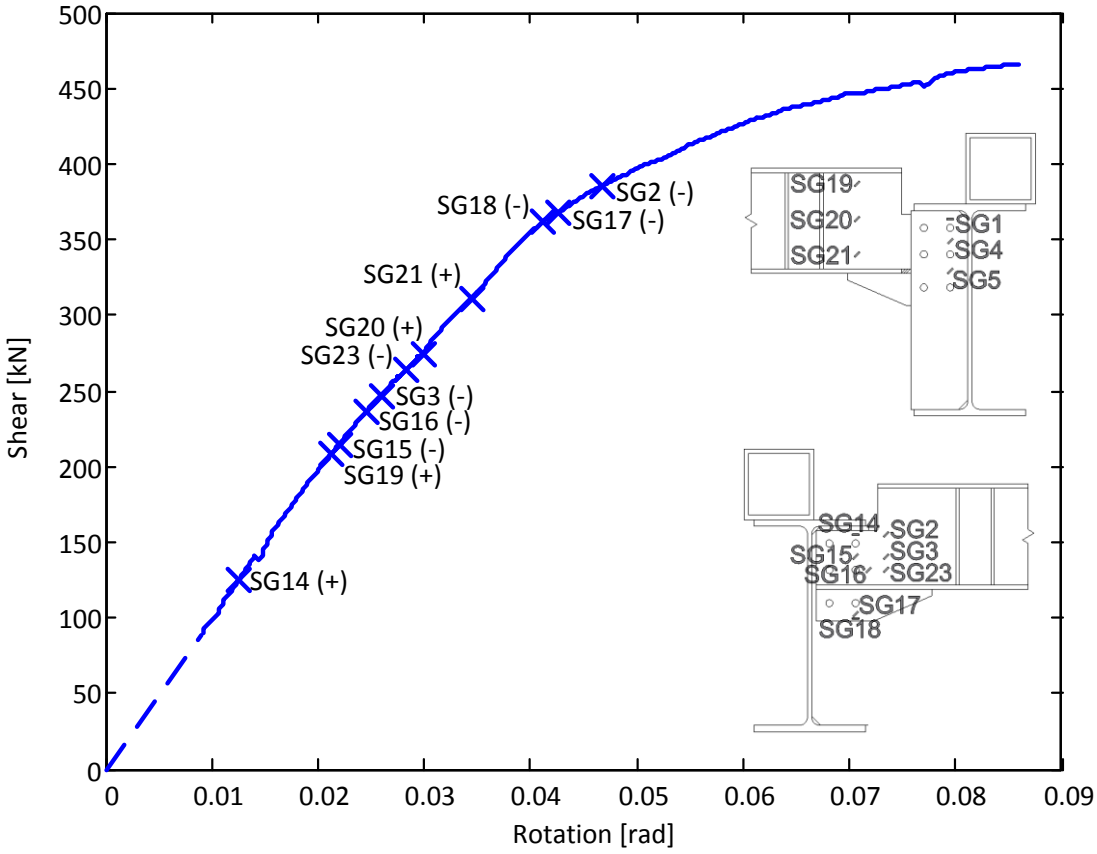

Figure 4.43 – Shear-rotation with strain gauge yielding for Specimen 7

Due to the large cope depth, the deformation in the cope region as the load increased was easily visible; Figure 4.44a shows the deformation in that region. LVDT data measuring the out-of-plane movement of the beam shows that the haunch plate and supporting stiffener remained stationary while the beam twisted approximately 5mm. Figure 4.44b shows the out-of-plane deformation of the beam; note the difference between the beam section and the haunch plate. It is important to highlight that according to the design equations used, flexural buckling was predicted to occur once the load reached 155kN, which is close to the critical Von Mises load of 152kN; however, this phenomenon was not present during testing.

Figure 4.44 also shows significant bolt bearing deformation. This illustrates that energy was dissipated by the beam web. From the same figure it is also evident that the bearing damage in the holes located on the beam web and those on the haunch plate are not the same. This might indicate that the force distribution along the member was not proportional to the number of bolts in each of these elements – therefore, the original assumption taken during design was not valid.

The design equations used predicted bearing strength of the beam at 535kN and bolt rupture at 507kN (Figure 4.40); both these values are above the ultimate capacity of the tested specimen. Testing was stopped once the top bolt furthest from the connection ruptured.

(a) **(b)**

Figure 4.44 – Deformation in Specimen 7 (haunch) (a) cope damage and bolt hole bearing; (b) out-of-plane deflection of beam

4.4 MOVEMENT OF INFLECTION POINT

The movement of the inflection point of each specimen was calculated using statics at various loading levels. The inflection point was defined as the distance from the centroid of the supporting girder to the point of zero moment in the test configuration. Eight different levels of shear were selected: 1) $0.25V_{Design}$, 2) $0.5V_{Design}$, 3) $0.75V_{Design}$, 4) V_{Design}, 5) $0.25(V_{Max} - V_{Design})$, 6) $0.5(V_{Max} - V_{Design})$, 7) $0.75(V_{Max} - V_{Design})$, and 8) V_{Max}; where V_{Design} is the corresponding probable design shear as calculated according to Section 3.3 and V_{Max} is the maximum shear load attained by any given specimen. Figure 4.45 illustrates the inflection point at these different levels for Specimen 5; the negative value indicates the distance away from the centroid of the supporting girder. Appendix D includes the corresponding inflection point graphs for all other specimens.

Shaw and Astaneh (1992) stated that that the inflection point of a single plate beam-to-girder connection moves closer to the supporting member as the shear load and rotation increase and

that the eccentricity tends to increase as the stiffness of the connection increases. It was observed this was not the case for all specimens tested as part of this experimental program.

Since the shear tabs in Configuration 6 and Specimen 6J did not yield, no conclusions can be made regarding the movement of the inflection point in these specimens. However, for the other two partial depth extended shear plate specimens, Configuration 9 and Specimen 9J, it was observed that the inflection point in the former member had a tendency to move away from the connection while the inflection point in the latter member moved towards the connection. This contradicts the observations made by Shaw and Astaneh (1992) that stiffer connections tend to exhibit inflection points further from the connection since Specimen 9J has a higher flexural stiffness when compared to Configuration 9 due to the higher rotational stiffness provided by the retrofit plate and the pseudo-concrete slab restraint.

In the case of both single and double coped specimens, the unreinforced specimens (Specimen 1 and Specimen 4) had the most variable inflection points across the different loading levels, meaning this point moved in both directions at different loading stages. The inflection point for both reinforced specimens with horizontal stiffeners (Specimen 2 and Specimen 5) moved away from the connection; the opposite was the case for both specimens reinforced with doubler plates (Specimen 3 and Specimen 6). Once again, it appears that the inflection points of configurations with higher flexural and shear stiffness tend to move towards the connection, which is contrary to what Shaw and Astaneh (1992) suggested.

Once again, in the case of the two specimens that were welded in-shop (Specimen 8 and Specimen 10), the inflection point of both configurations moved away from the connection. The same occurred for the single coped haunched specimen (Specimen 7).

The inconsistency between the tested configurations and the results presented by Shaw and Astaneh (1992) can be explained by the fact that even though the observations made by the latter were for beam-to-girder connections, the configurations considered were all unreinforced single coped beams with only a single row of bolts whereas the former experimental program consisted of more complex extended shear tab and coped beam connections.

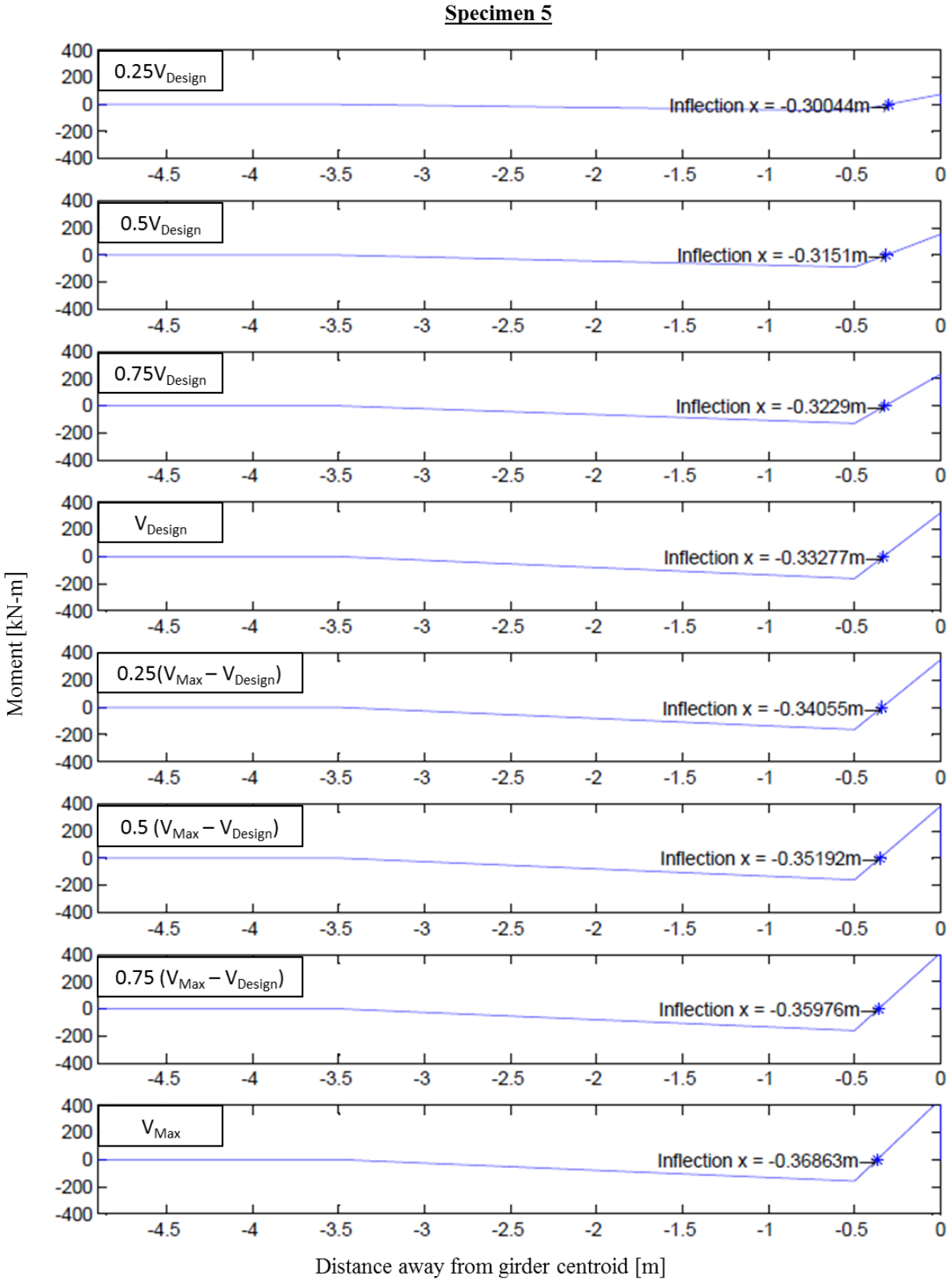

Figure 4.45 – Inflection point diagram for Specimen 5

4.5 SUMMARY

Thirteen full-scale beam-to-girder connection tests were performed, which can be divided into six categories: partial depth extended shear tabs, full depth extended shear tabs, single coped beams, double coped beams, welded in-shop coped beams, and single coped haunched beam. Experimental results were compared with the design provisions outlined in the Canadian Standards Association (CSA) S16 Standard (2009), the 10th Edition of the CISC Handbook of Steel Construction (2010), the American National Standards Institute (ANSI) AISC 360 Specification for Structural Steel Buildings (2010), and the 14th Edition of the American Institute of Steel Construction Manual (2011). Material tests were performed on coupons to obtain the measured material properties of the steel members.

When testing the partial depth extended shear tab configurations it was hypothesized that by including a restraint on the top of the supporting girder, representing the concrete slab that would commonly be present in buildings, the girder web punching mechanism could be prevented. Experimental findings demonstrated that this additional element reduced the magnitude of this phenomenon yet did not eliminate it altogether. In an attempt to engage a larger area of the girder web, a steel plate retrofit was installed between the bottom of the shear tab and the girder web. This retrofit did improve the performance of the connection, but once again, was not able to prevent girder web punching.

Previously tested configurations showed that when a full depth extended shear tab is used, bending occurred at the neck of the component. This research program tested two such specimens to assess the impact of the pseudo-concrete slab and an increased plate thickness in reducing this phenomenon. Measured data showed that the increased thickness did in fact reduce the bending of the shear tab and improve the performance of the connection; the inclusion of the girder restraint allowed for more plastic damage to occur in the shear tab rather than in the girder web. However, the girder out-of-plane deformation was not completely precluded.

Three single coped beam specimens were tested in order to assess the validity of design equations and compare two different reinforcement configurations: horizontal stiffeners and doubler plates. Test results show that the current design equations could be improved and that the design check based on the Von Mises criterion more accurately predicts the load reached by these connections at the specified design rotation of 2%. The unreinforced specimen did not

undergo any lateral deformation therefore the purpose of the horizontal stiffeners in adding lateral stability to the member cannot be assessed; however, the inclusion of the same did marginally increase the capacity of the connection. On the other hand, by including the doubler plate, the capacity of the connection increased by 25%. It is important to note that in the case of both reinforced configurations, bolt rupture, and undesirable brittle failure mode, did occur but at rotations far larger than expected in design.

Similar to the single coped beams, three double coped beams were tested with the same two reinforcement configurations. The design equations accurately describe the damage progression for these specimens. In this set of tests, the unreinforced specimen did in fact exhibit lateral deformation, which was prevented with the inclusion of both the horizontal stiffeners and the doubler plate. The former arrangement increased the connection capacity marginally while the latter exhibited an increase in capacity of 38%. Both reinforced configurations resulted in bolt rupture, but these occurred at rotations greater than 5%. The Von Mises criterion was more accurate than the design provisions included in North American design standards in predicting the load level at which the unreinforced and the specimen reinforced with a doubler plate underwent a loss in structural stiffness; however, this design check slightly over predicts the capacity of the specimen reinforced with horizontal stiffeners for design levels corresponding to 2% rotation. By observing the damage progression in these three specimens, it became evident that it would be more appropriate to use the Von Mises criterion to calculate the resistance of the configurations at the last line of bolts using the reduced net section of the beam. This would result in lower resistances compared to the ones calculated at the location of the cope leading to more accurate predictions of the load level at which the rotational stiffness of the connection decreased.

Two specimens that were welded in-shop were tested – both single and double coped configurations were investigated. In both cases, design provisions were conservative in predicting the capacity of the connection, but were accurate in determining the load level at which the expected design level rotation of 0.02 radians was reached. It must be noted that in the single coped specimen, the girder yielded earlier than expected but no punching was observed. On the other hand, the double coped specimen exhibited large deformations in the girder web, but these were expected due to the difference in depth of the two components of the connection. Both specimens exhibited tearing at the top of the connecting welds, which lead to significant

loss in the rotational stiffness of the connection. It was also observed that the welded in-shop specimens reached similar rotations as the bolted connections, and that the rotation of the supporting girder was also comparable.

The haunched beam was the first configuration of its kind to be examined in a laboratory setting. Design equations underestimated the capacity of the connection. Lateral deformation of the beam and greater bearing damage in this region when compared to bearing damage in the haunch plate indicate that the design assumption that the forces applied distribute across the connection proportionally to the number of bolts in these two elements is inaccurate. Ultimately the connection failed due to bolt shear but at a rotation of 9%, almost five times larger than the design level rotation.

When analyzing the movement of the inflection point for each specimen at different levels of loading, it was observed that the observations made by Shaw and Astaneh (1992) were not consistent with the behaviour of the tested specimens. In part, this may be attributed to the fact that Shaw and Astaneh (1992) only investigated unreinforced specimens which had a single vertical row of bolts.

CHAPTER 5

SUMMARY AND CONCLUSIONS

5.1 OBSERVATIONS AND CONCLUSIONS

Beam-to-girder steel connections are commonly constructed using either extended shear tabs or coped beams. These configurations are regularly designed and detailed by professional engineers despite the lack of design guidance in engineering standards. It was not until the latest edition of the AISC Manual of Steel Construction (2011) that a procedure for extended shear tab connections was included despite regular use in practice by engineers. In Canada, neither the CSA S16 Standard (2009) nor the CISC Handbook of Steel Construction (2010) provides professionals with guidance to design either of these commonly used beam-to-girder connections.

Thirteen full-scale tests representing beam-to-girder connections commonly used in the engineering practice in North America were performed in order to determine the applicability and accuracy of existing design provisions per the Canadian Standards Association (CSA) S16 Standard (2009), the 10th Edition of the CISC Handbook of Steel Construction (2010), the American National Standards Institute (ANSI) AISC 360 Specification for Structural Steel Buildings (2010), and the 14th Edition of the American Institute of Steel Construction Manual (2011). This was done by comparing measured shear resistances and observed damage progression with expected calculated design capacities.

Two partial depth extended shear tab connections were investigated, which have been shown to develop a girder web mechanism as a primary failure mode. In an effort to prevent this limit state, a pseudo-concrete slab was installed to minimize girder rotation. This restraint, which more accurately represented the boundary conditions of such connections did reduce out-of-plane deformations, and as such was utilized in all subsequent tests, but did not prevent the girder web mechanism from developing. It was then hypothesized that by engaging a larger area of the girder web, girder web punching would be prevented; as such, a retrofit steel plate was

welded between the shear tab and the girder web. It was observed that the out-of-plane deformation of the supporting member was in fact reduced, but not prevented. It is important to note, that in the case of the specimen that was not retrofit, the observed girder web mechanism, which is not accounted for in current design provisions, occurred prior to the connection reaching the predicted design load; therefore, there is a discrepancy between the observed and predicted behaviour of these connections.

Two specimens were tested to investigate full depth extended shear tabs. Previous studies indicated that the limit state that characterized these connections was localized inelastic buckling at the neck of the shear tab. It was suggested that by reducing the slenderness of the shear plate and including the pseudo-concrete slab restraint, these out-of-plane deformations would be avoided. Measurements recorded during testing showed that these deformations were in fact reduced but not avoided. As such, even though a full depth extended shear tab is used, it is important to consider the slenderness of the plate during design.

Three single coped bolted configurations were tested with two different reinforcement details; a) horizontal stiffeners and b) a web doubler plate. It was observed that reinforcing the specimens in this fashion did increase the capacity of the connection; however, at large rotations (i.e., larger than 0.08 radians) the observed limit state was bolt shear rupture, which is a brittle failure mode. During design, it is important to note that in addition to following the guidelines outlined in Part 9 of the AISC Manual (2011), the interaction between shear and flexural force based on the Von Mises criterion was used as a design check. The Von Mises check governed the design of all three specimens, and test results show that evidently, this criterion accurately predicted the behaviour of these configurations. This is demonstrated by the fact that the calculated predicted load matches with the behaviour of the connections at the specified design rotation of 0.02 radians. Therefore, it is recommended that the Von Mises criterion be part of the standard design procedure for these connections.

Similarly, three double coped bolted connections were also tested. As was the case for the single coped specimens, the inclusion of reinforcing elements (horizontal stiffeners and doubler plate) did increase the capacity of the connection, but resulted in bolt shear rupture at large rotations. The Von Mises criterion, which governed the design of all three connections, adequately predicted the point at which the unreinforced connection and the specimen with a doubler plate

started to experience a decrease in rotational stiffness. However, the capacity of the specimen with horizontal stiffeners is slightly over predicted, which means the connection underwent a loss in rotational stiffness prior to the load level calculated with the Von Mises criterion. Observing the damage progression in all three of these specimens, it is evident that the location near the last line of bolts away from the girder is more critical rather than at the cope; therefore, the Von Mises criterion should be used to calculate the resistance of these members in that region. This would result in a load level that more accurately predicts the point at which the connections undergo a decrease in rotational stiffness; however, the calculated load level still under predicts the target rotation of 0.02 radians for the reinforced specimen with a doubler plate.

Two beam-to-girder specimens were welded in-shop, a single coped and a double coped configuration for which the beam's web was directly attached to the girder's web. Both configurations exhibited a loss of rotational stiffness when weld tearing started at the top of the connection. During loading, the girder web of both specimens did yield, but this did not affect the ultimate load of the connection; however, it is important to highlight that the single coped configuration did also develop a punching girder web mechanism. The Von Mises criterion underestimated the performance of both welded in-shop connections. It is important to note that these load and rotation levels reached by both these specimens was comparable to the bolted connections; in other words, the welded in-shop configurations reached rotations greater than the target design rotation of 0.02 radians and this occurred at similar load levels than the bolted connections. Similarly, the contribution of the supporting girder to the global connection rotation between the bolted and welded connections was also comparable.

By comparing the expected calculated resistance of the single cope haunch plate with the observed behaviour it was evident that current design provisions underestimated the capacity of the connection. It is important to note that during design, it was assumed that the force distribution between the beam and the haunch plate is proportional to the number of bolts in each component; however, bearing damage in the bolt holes indicates this assumption was flawed and requires further investigation.

Past research states that the inflection point of a given configuration moves towards the connection as the shear load increases, and that stiffer connections tend to exhibit inflection

points further away from the support; however, by investigating the movement of the inflection point during various stages of loading, it becomes evident that this assertion is not always the case. When testing partial depth shear plates it was observed that the inflection point of the retrofit configuration, which possesses a higher flexural stiffness, moved towards the connection; this was also observed for the reinforced single and double coped beam configurations.

5.2 RECOMMENDATIONS FOR FUTURE RESEARCH

Current design procedures do not consider the resistance of the supporting girder to weak axis bending when detailing beam-to-girder connections. Results from the test program suggest that incorporating the girder as a component to be analyzed when detailing a connection is imperative. The design of the supporting member could be performed using yield line analysis; in order to develop a design methodology that incorporates the girder to prevent web punching; numerical models and a corresponding parametric study should be employed to compliment this analysis method such that the design space can be expanded.

For all thirteen full-scale tests there was only a single beam framing into the supporting girder; however, it is also common for two beams to connect into the same girder, one on each side of the web. As such, it is suggested that a full-scale test of such a layout be tested; there are no recorded tests on extended shear tabs or coped beams utilizing this layout. Additionally, if a second beam frames into the back of the supporting girder, girder web punching would be most likely prevented; therefore, such a test might provide solutions to some of the limit states observed as part of this research program.

Single coped haunched beams are commonly used in professional practice despite the fact that this is the first time such a connection was tested. Therefore, it is now possible to develop and validate a finite element model. It is evident that the current design provisions underestimate the performance of this connection; as such, with the use of a parametric study, the behaviour of haunched configurations can be further investigated, and design provisions can be improved.

REFERENCES

Abaqus (2013). *Abaqus/CAE 6.13-3.* Dessault Systemes Simulia Corp: Providence, RI, USA.

AISC (2010). *Specifications for Structural Steel Buildings, ANSI/AISC 360-10.* American Institute of Steel Construction: Chicago, IL, USA.

AISC (2011). *Steel Construction Manual, 14th Edition.* American Institute of Steel Construction: Chicago, IL, USA.

Architectural Institute of Japan (AIJ). (1990). *Standard for Limit States Design of Steel Structures:* Tokyo, Japan.

Astaneh, A., Call, S.M., McMullin, K.M. (1989). *Design of Single Plate Shear Connections.* AISC Engineering Journal, American Institute of Steel Construction, First Quarter, Volume 26, 21-32.

ASTM (2013). *ASTM 370 – 13 Standard Test Methods and Definitions for Mechanical Testing of Steel Products.* American Society for Testing and Materials: Philadelphia, PA, USA.

Blodgett, O. W. (1966). *Design of Welded Structures.* James F. Lincoln: ISBN: 978-9998474925, 5.4-10 – 5.4-13 and 7.4-6 – 7.4-10.

Cheng, J. J., Yura. J. A., and Johnson, C.P. (1984). *Design and Behavior of Coped Beams.* Ferguson Structural Engineering Laboratory Report No. 84-1. Dept. of Civil Engineering, University of Texas at Austin: Austin, TX, USA.

Cheng, J. J. R. and Yura, J. A. (1986). *Local Web Buckling of Coped Beams.* American Society of Civil Engineers – Journal of Structural Engineering, Volume 112, 2314-2331.

Cheng, J. J. R., Yura, J. A., and Johnson, C. P. (1988). *Lateral Buckling of Coped Steel Beams.* American Society of Civil Engineers – Journal of Structural Engineering, Volume 114, 1-15.

CISC (2010). *Handbook of Steel Construction, 10th Edition.* Canadian Institute of Steel Construction: Markham, ON, Canada.

Creech, D.D. (2005). *Behaviour of Single Plate Shear Connections with Rigid and Flexible Supports.* MSc Thesis, North Carolina State University: Raleigh, NC, USA.

CSA (2009). *S16-09 Design of Steel Structures*. Canadian Standards Association: Mississauga, ON, Canada.

D'Aronco, M. (2014). *Behaviour of Double and Triple Vertical Rows of Bolts Shear Tab Connections and Weld Retrofits.* MAsc Thesis, Dept. of Civil Engineering, Ecole Polytechnique: Montreal, QC, Canada.

Dowswell, B. and Whyte, R. (2014). *Local Stability of Double-Coped Beams.* American Institute of Steel Construction – Engineering Journal, 1st Quarter, 43-51.

European Committee for Standardization. (ECS). (1992). *Eurocode 3: Design of Steel Structures.* ENV 1993-1-1: Brussels, Belgium.

Franchuk, C. R., Driver, R. G., and Grondln, G. Y. (2003). *Experimental investigation of block shear failure in coped steel beams.* Canadian Journal of Civil Engineering, Volume 30, 871-881.

Franchuk, C. R., Driver, R. G., and Grondln, G. Y. (2004). *Reliability Analysis of Block Shear Capacity of Coped Steel Beams.* American Society of Civil Engineers – Journal of Structural Engineering, Volume 130, 1904-1913.

Gaylord, E. H., and Gaylord C. N. (1957). *Design of Steel Structures.* McGraw-Hill Ryerson: ISBN: 978-0070231092, 282-287.

Hertz, J. (2014). *Testing of Extended Shear Tab Configurations Subjected to Shear.* MEng Thesis, Dept. of Civil Engineering and Applied Mechanics, McGill University: Montreal, QC, Canada.

Lam, C. C., Yam, M. C. H., Iu, V. P., Cheng, J. J. R. (2000). *Design for lateral torsional buckling of coped I-beams.* American Society of Civil Engineers – Journal of Constructional Steel Research, Volume 54, 423-443.

Marosi, M. (2011). *Behaviour of Single and Double Row Bolted Shear Tab Connections and Weld Retrofits.* MEng Thesis, Dept. of Civil Engineering and Applied Mechanics, McGill University: Montreal, QC, Canada.

Metzger, K. A. B., (2006). *Experimental Verification of a New Single Plate Shear Connection Design Model.* MSc Thesis, Dept. of Civil and Environmental Engineering, Virginia Polytechnic Institute: Blacksburg, VA, USA.

Mirzaei, A. (2014). *Steel Shear Tab Connections Subjects to Combined Shear and Axial Forces.* PhD Thesis, Dept. of Civil Engineering and Applied Mechanics, McGill University: Montreal, QC, Canada.

Muir, L. S. and Thornton W. A. (2004). *A Technical Note: A Direct Method for Obtaining the Plate Buckling Coefficient for Double Coped Beams.* American Institute of Steel Construction – Engineering Journal, 3rd Quarter, 133-134.

Muir, L. S. and Hewitt, C. M. (2009). *Design of Unstiffened Extended Single-Plate Shear Connections.* American Institute of Steel Construction – Engineering Journal, 2nd Quarter, 67-79.

Shaw, A.L. and Astaneh, A. (1992). *Experimental Study of Single-Plate Steel Beam-to-Girder Connections.* Report, Dept. of Civil Engineering, University of California: Berkeley, CA, USA.

Yam, M. C. H., Lam, A. C. C, Iu, V. P., and Cheng, J. J. R. (2003). *Local Web Buckling Strength of Coped I Beams.* American Society of Civil Engineers – Journal of Structural Engineering, Volume 129, 3-11.

Yam, M. C. H. and Chung, K. F. (2013). *A numerical study of the strength and behaviour of reinforced coped beams.* American Society of Civil Engineers – Journal of Constructional Steel Research, Volume 80, 224-234.

Yam, M. C. H., Ma, H., Lam, A. C. C., and Chung, K. F. (2011). *Experimental study of the strength and behaviour of reinforced coped beams.* American Society of Civil Engineers – Journal of Constructional Steel Research, Volume 67, 1749-1759.

APPENDIX A

DESIGN CALCULATIONS

Specimen A1 and A2 - Full Depth Extended Shear Tab

Configuration Parameters

Girder		W610x125	(W24x84)	
Beam		W310x60	(W12x40)	
Plate Thickness, t_p	=	12.7 mm	1/2 in	
Offset of Bolt Group, a	=	165 mm	6 1/2 in	
Bolt Diameter, d_b	=	19.1 mm	3/4 in	
Number of Bolt Lines, m	=	2	2	
Number of Bolts Rows, n	=	3	3	
Bolt Gauge Distance, D	=	76.2 mm	3 in	
Bolt Pitch Distance, b	=	76.2 mm	3 in	
Plate Depth, d	=	229 mm	9 in	
Plate Depth in Girder, d_g	=	573 mm	22.6 in	

1) Bolt Shear & Bearing

*AISC Manual 2011 Extended Config Design Check 1 (10-5)

Compute ICR Coefficient, C

*CISC Handbook 2009 Table 3-15

Number of Bolt Lines, m	=	2	2	
Moment Arm, L	=	203.20 mm	8 in	
gage, D	=	76.2 mm	3 in	
Pitch, b	=	76.2 mm	3 in	
Number of Bolt Rows, n	=	3	3	
L1	=	200 mm		
C1	=	1.91		Linear Interpolation
L2	=	225 mm		
C2	=	1.73		
Eccentric Loading Coefficient, C	=	1.89	1.89	

Bearing

$$B_r = min\begin{cases}3\phi_b d_b (t_p F_u)_{plate} C \\ 3\phi_b d_b (t_w F_u)_{beam} C\end{cases}$$

*S16-09 Cl. 13.12.1.2a

Modification factor, $Ø_{br}$	=	0.8	0.8	
Plate Thickness, t_p	=	12.7 mm	1/2 in	
Beam Web Thickness, t_w	=	7.50 mm	0.295 in	
Bolt Diameter, d_b	=	19.1 in	3/4 in	
Tensile Strength of Plate, $F_{u,plate}$	=	450 MPa	65 ksi	
Tensile Strength of Beam $F_{u,beam}$	=	450 MPa	65 ksi	
Factored Bearing Resistance, B_r	=	291 kN	65 kip	
Probable Plate Strength, $R_Y F_{U,plate}$	=	495 MPa	72 ksi	
Probable Beam Strength, $R_Y F_{U,beam}$	=	495 MPa	72 ksi	
Probable Bearing Resistance, B_r	=	364 kN	81 kip	

Bolt Shear

$$V_{Bolt} = 0.6\phi_b n m A_b F_u C$$

*S16-09 Cl. 13.12.1.2c

Modification factor, $Ø_b$	=	0.8	0.8	
Number of Bolts, n	=	1	1	
Number of Shear Planes, m	=	1	1	
Bolt Area, A_b	=	285 mm^2	0.442 in^2	
Ultimate Strength of Bolts, F_u	=	825 MPa	120 ksi	
Factored Bolt Shear Resistance, V_{Bolt}	=	213 kN	48 kip	
Probable Bolt Shear Resistance, V_{Bolt}	=	266 kN	60 kip	

2) Plate Ductility

*AISC Manual 2011 Extended Config Design Check 2 (10-5)

$$t_{pmax} = \frac{6M_{max}}{F_y d^2}$$

$$M_{max} = \frac{F_{nv}}{0.9}(A_b C')$$

Bolt Shear Strength, F_{nV}	=	415 MPa	60 ksi	*AISC Specification 2010 Table J3.2
Bolt Area, A_b	=	285 mm^2	0.442 in^2	

Compute ICR Coefficient, C', for Moment Only Case

Number of Bolt Lines, m	=	2	2	

Column Spacing	=	76.2 mm	3 in	
Bolt Gauge Distance, D	=	76.2 mm	3 in	
Number of Bolts Rows, n	=	3	3	
ICR Coefficient, C'	=	401.32 mm	15.8 in	*AISC Manual 2011 Table 7-8
M_{max}	=	53 kN-m	465 kip-in	
Yield Stress of Plate, F_Y	=	345 MPa	50 ksi	
Probable Plate Strength, R_YF_U	=	495 MPa	72 ksi	
Plate Depth, d	=	228.6 mm	9.0 in	
Factored Maximum Plate Thickness, t_{pmax}	=	17.5 mm	0.689 in	
Probable Maximum Plate Thickness, t_{pmax}	=	12.2 mm	0.482 in	
Check Plate Thickness Based on Factored Loads? ($t_p < t_{pmax}$)		OK		
Check Plate Thickness Based on Probable Loads? ($t_p < t_{pmax}$)		OK		

3) Shear Yielding, Shear Rupture and Block Shear Rupture

*AISC Manual 2011 Extended Config Design Check 3 (10-5)

Shear Yielding

$$V_{SY} = 0.66\phi_s F_y A_w$$

*S16-09 Cl. 13.4.1.1

Resistance Factor, $Ø_s$	=	0.9	0.9	
Yield Stress of Plate, F_Y	=	345 MPa	50 ksi	
$A_g = t_p d_p$				
Plate Thickness, t_p	=	12.7 mm	1/2 in	
Plate Depth, d_p	=	228.6 mm	9 in	
Gross Plate Area, A_g	=	2903 mm^2	4.5 in^2	
Factored Shear Yielding Resistance in Beam, V_{SY}	=	541 kN	134 kip	
Probable Yield Stress, R_YF_Y	=	380 MPa	55 ksi	
Probable Shear Yielding Resistance in Beam, V_{SY}	=	661 kN	163 kip	

Shear Rupture

$$V_{SR} = 0.66\phi_u F_u A_{nv}$$

*S16-09 Cl. 13.4.1.1

Resistance Factor, $Ø_u$	=	0.75	0.75	
Tensile Strength of Plate, F_U	=	450 MPa	65 ksi	
$A_{NV} = t_p d_{pN}$				
Plate Thickness, t_p	=	12.7 mm	1/2 in	
Net Depth, d_{pN}	=	161.9 mm	6.38 in	
Net Plate Area, A_{NV}	=	2056 mm^2	3.188 in^2	
Factored Shear Rupture Resistance in Shear Plate, V_{SR}	=	416 kN	93 kip	
Probable Tensile Strength, R_YF_U	=	495 MPa	72 ksi	
Probable Shear Rupture Resistance in Shear Plate, V_{SR}	=	611 kN	137 kip	

Block Shear Rupture

$$V_{BS} = \phi_u \left[U_t A_n F_u + 0.6 A_{gv} \frac{F_y + F_u}{2} \right]$$

*S16-09 Cl. 13.11

Resistance Factor, $Ø_u$	=	0.75	0.75	
Efficiency Factor, U_t	=	0.3	0.3	
Net Area, A_n	=	1028 mm^2	1.594 in^2	
Tensile Strength of Plate, F_U	=	450 MPa	65 ksi	
Gross Area in Shear, A_{gV}	=	2419 mm^2	3.750 in^2	
Yield Stress of Plate, F_Y	=	345 MPa	50 ksi	
Factored Block Shear Failure in Beam, V_{BS}	=	537 kN	120 kip	
Probable Tensile Strength, R_YF_U	=	495 MPa	72 ksi	
Probable Yield Stress, R_YF_Y	=	380 MPa	55 ksi	
Probable Block Shear Failure in Beam, V_{BS}	=	787 kN	176 kip	

4) Flexural Shear Yielding, Shear Buckling, and Yielding (Von Mises)

*AISC Manual 2011 Extended Config Design Check 4 (10-5)
*AISC Manual 2011 Eqn 10-5, modified

$$\left(\frac{V_r}{V_c}\right)^2 + \left(\frac{M_r}{M_c}\right)^2 \leq 1.0$$

therefore

$$V_r = \sqrt{\frac{1}{V_c^2} + \left(\frac{e}{M_c}\right)^2}$$

$V_c = Ø_v V_n$

Resistance Factor, $Ø_v$	=	0.9	0.9	*use 0.9 as in S16-09 instead of 1.0
$V_n = 0.66F_Y A_g$				
Yield Stress of Plate, F_Y	=	345 MPa	50 ksi	
Gross Area of Plate, A_g	=	2903 mm^2	4.5 in^2	
Nominal Shear Capacity, V_n	=	661 kN	149 kips	
Factored Shear Capacity, V_c	=	595 kN	134 kips	
Eccentricity to first bolt column, e	=	165 mm	6 1/2 in	
$M_c = Ø_b M_n$				
Resistance Factor, $Ø_b$	=	0.9	0.9	
$M_n = F_y Z_{pl}$				
Plastic Section Modulus, Z_{pl}	=	166 x$10^3$$mm^3$	10.1 in^3	
Nominal Moment Capacity, M_n	=	57 kN-m	506 kip-in	
Factored Moment Capacity, M_c	=	52 kN-m	456 kip-in	
Factored Shear and Flexural Yielding Resistance, V_r	=	276 kN	62 kips	
Probable Yield Stress, R_YF_Y	=	380 MPa	55 ksi	
Probable Shear and Flexural Yielding Resistance, V_r	=	330 kN	74 kips	

5) Plate Buckling

*AISC Manual 2011 Extended Config Design Check 5 (10-5)

$$V_{FB} = \frac{M_{FB}}{e}$$

Resistance Factor, $Ø_s$	=	0.9	0.9	
Elastic Section Modulus of Gross Reduced Area, S_x'	=	111 x$10^3$$mm^3$	6.75 in^3	
Cope Depth at Compression Flange, d_c	=	41 mm	1.6 in	
Beam Depth, d	=	310 mm	12.2 in	
Eccentricity to first bolt column, e	=	165.1 mm	6 1/2 in	
Unsupported Length of Plate, c	=	165.1 mm	6 1/2 in	*conservative, take to first row of bolts*

fd equation (Cheng et al. 1984)

*AISC Manual 2011 Part 9

$$F_{cr} = 0.62\pi E \frac{(t_p)^2}{ch_o} f_d$$

Modulus of Elasticity, E	=	200000 MPa	29000 ksi	
Thickness of Plate, t_p	=	12.7 mm	1/2 in	
Reduced Beam Depth, h_o	=	228.6 mm	9 in	
Adjustment Factor, $f_d = 3.5 - 7.5\left(\frac{d_c}{d}\right)$	=	2.5 MPa	2.5 ksi	
Critical Stress, F_{cr}	=	4185 MPa	607.2 ksi	
Moment Buckling Resistance at Cope, $M_{FB} = \phi_s F_{cr} S_x'$				
Factored Moment Buckling Resistance at Cope, M_{FB}	=	416.8 kN-m	3688.6 kips-in	
Probable Moment Buckling Resistance at Cope, M_{FB}	=	463.1 kN-m	4098.5 kips-in	
Factored Flexural Buckling at Cope, V_{FB}	=	2520 kN	567 kip	
Probable Flexural Buckling at Cope, V_{FB}	=	2800 kN	631 kip	

Q equation (classical plate buckling)

*AISC Manual 2011 Part 9

$$F_{cr} = F_y Q$$

Resistance Factor, $Ø_s$	=	0.9	0.9	
Thickness of Plate, t_p	=	12.7 mm	1/2 in	
Reduced Beam Height, h_o	=	228.6 mm	9 in	
Unsupported Length of Plate, c	=	165.1 mm	6 1/2 in	
Eccentricity to Cope, e	=	165.10 mm	6 1/2 in	
Elastic Section Modulus of Gross Reduced Area, S_x'	=	110612.7 mm^3	6.75 in^3	
Yield Strength of Beam, F_y	=	345 MPa	50 ksi	
Probable Yield Strength of Beam, R_yF_y	=	380 MPa	55 ksi	

$$Q = \begin{cases} 1 \; for \; \lambda \le 0.7 \\ (1.34 - 0.486\lambda) \; for \; 0.7 < \lambda \le 1.41 \\ (1.30 / \lambda^2) \; for \; \lambda > 1.41 \end{cases}$$

Factored Q	=	1	1
Probable Q	=	1	1

where

$$\lambda = \frac{h_o\sqrt{F_y}}{10t_p\sqrt{475 + 280\left(\frac{h_o}{c}\right)^2}}$$

Factored λ	=	0.40	0.40

Probable λ	=	0.42	0.42
Factored Critical Buckling Stress, F_{cr}	=	349.0 MPa	50.0 ksi
Probable Critical Buckling Stress, F_{cr}	=	383.9 MPa	55.0 ksi
Moment Buckling Resistance at Cope, $M_{FB} = \phi_s F_{cr} S_x'$			
Factored Moment Buckling Resistance at Cope, M_{FB}	=	34.3 kN-m	303.8 kips-in
Probable Moment Buckling Resistance at Cope, M_{FB}	=	42.0 kN-m	371.3 kips-in
Factored Flexural Buckling at Cope, V_{FB}	=	207.5 kN	46.7 kips
Probable Flexural Buckling at Cope, V_{FB}	=	253.6 kN	57.1 kips

6) Weld to Supporting Element

*AISC Manual 2011 Extended Config Design Check 5 (10-6)
*S16-09 Cl. 13.13.2.2

$V_W = 0.67\phi_w n_w X_u A_w$

Resistance Factor, $Ø_w$	=	0.67	0.67
Number of Welds, n_w	=	2	2
Ultimate Strength of Electrode, X_u	=	490 MPa	70 ksi
Welded Area, A_w	=	2958.2 mm^2	4.59 in^2
Length of Weld (T distance of Girder), L_w	=	527.1 mm	20 3/4 in
Weld Size, t_w	=	7.9 mm	5/16 in
Factored Weld Resistance, V_w	=	1279.4 kN	288.2 kips
Probable Weld Resistance, V_w	=	1909.6 kN	430.1 kips

Specimen 6J - Partial Depth Extended Shear Tab

Configuration Parameters

Girder		W610x125	(W24x84)	
Beam		W310x60	(W12x40)	
Plate Thickness, t_p	=	9.5 mm	3/8 in	
Offset of Bolt Group, a	=	165 mm	6 1/2 in	
Bolt Diameter, d_b	=	19.1 mm	3/4 in	
Number of Bolt Lines, m	=	2	2	
Number of Bolts Rows, n	=	3	3	
Bolt Gauge Distance, D	=	76.2 mm	3 in	
Bolt Pitch Distance, b	=	76.2 mm	3 in	
Plate Depth, d	=	229 mm	9 in	
Plate Depth in Girder, d_g	=	573 mm	9 in	

1) Bolt Shear & Bearing

*AISC Manual 2011 Extended Config Design Check 1 (10-5)

Compute ICR Coefficient, C

*CISC Handbook 2009 Table 3-15

Number of Bolt Lines, m	=	2	2	
Moment Arm, L	=	203.20 mm	8 in	
gage, D	=	76.2 mm	3 in	
Pitch, b	=	76.2 mm	3 in	
Number of Bolt Rows, n	=	3	3	
L1	=	200 mm		
C1	=	1.91		Linear Interpolation
L2	=	225 mm		
C2	=	1.73		
Eccentric Loading Coefficient, C	=	1.89	1.89	

Bearing

$$B_r = min \begin{cases} 3\phi_b d_b (t_p F_u)_{plate} C \\ 3\phi_b d_b (t_w F_u)_{beam} C \end{cases}$$

*S16-09 Cl. 13.12.1.2a

Modification factor, $Ø_{br}$	=	0.8	0.8	
Plate Thickness, t_p	=	9.53 mm	3/8 in	
Beam Web Thickness, t_w	=	7.50 mm	0.295 in	
Bolt Diameter, d_b	=	19.05 in	3/4 in	
Tensile Strength of Plate, $F_{u,plate}$	=	450 MPa	65 ksi	
Tensile Strength of Beam $F_{u,beam}$	=	450 MPa	65 ksi	
Factored Bearing Resistance, B_r	=	291 kN	65 kips	
Probable Plate Strength, $R_Y F_{U,plate}$	=	495 MPa	71.5 ksi	
Probable Beam Strength, $R_Y F_{U,beam}$	=	495 MPa	71.5 ksi	
Probable Bearing Resistance, B_r	=	364 kN	81 kips	

Bolt Shear

$$V_{Bolt} = 0.6\phi_b n m A_b F_u C$$

*S16-09 Cl. 13.12.1.2c

Modification factor, $Ø_b$	=	0.8	0.8	
Number of Bolts, n	=	1	1	
Number of Shear Planes, m	=	1	1	
Bolt Area, A_b	=	285 mm^2	0.442 in^2	
Ultimate Strength of Bolts, F_U	=	825 MPa	120 ksi	
Factored Bolt Shear Resistance, V_{Bolt}	=	213 kN	48 kips	
Probable Bolt Shear Resistance, V_{Bolt}	=	266 kN	60 kips	

2) Plate Ductility

*AISC Manual 2011 Extended Config Design Check 2 (10-5)

$$t_{pmax} = \frac{6M_{max}}{F_y d^2}$$

$$M_{max} = \frac{F_{nv}}{0.9}(A_b C')$$

Bolt Shear Strength, F_{nV}	=	415 MPa	60 ksi	*AISC Specification 2010 Table J3.2
Bolt Area, A_b	=	285 mm^2	0.442 in^2	

Compute ICR Coefficient, C', for Moment Only Case

Number of Bolt Lines, m	=	2	2	
Column Spacing	=	76.2 mm	3 in	

Bolt Gauge Distance, D	=	76.2 mm	3 in	
Number of Bolts Rows, n	=	3	3	
ICR Coefficient, C'	=	401.32 mm	15.8 in	*AISC Manual 2011 Table 7-8
M_{max}	=	53 kN-m	465 kip-in	
Yield Stress of Plate, F_Y	=	345 MPa	50 ksi	
Probable Plate Strength, R_YF_U	=	495 MPa	72 ksi	
Plate Depth, d	=	228.6 mm	9.0 in	
Factored Maximum Plate Thickness, t_{pmax}	=	17.5 mm	0.689 in	
Probable Maximum Plate Thickness, t_{pmax}	=	12.2 mm	0.482 in	
Check Plate Thickness Based on Factored Loads? ($t_p < t_{pmax}$)		OK		
Check Plate Thickness Based on Probable Loads? ($t_p < t_{pmax}$)		OK		

3) Shear Yielding, Shear Rupture and Block Shear Rupture

*AISC Manual 2011 Extended Config Design Check 3 (10-5)

Shear Yielding

$$V_{SY} = 0.66\phi_s F_y A_w$$

*S16-09 Cl. 13.4.1.1

Resistance Factor, $Ø_s$	=	0.9	0.9	
Yield Stress of Plate, F_Y	=	345 MPa	50 ksi	
$A_g = t_p d_p$				
Plate Thickness, t_p	=	9.53 mm	3/8 in	
Plate Depth, d_p	=	228.6 mm	9 in	
Gross Plate Area, A_g	=	2177 mm^2	3.375 in^2	
Factored Shear Yielding Resistance in Beam, V_{SY}	=	446 kN	100 kips	
Probable Yield Stress, R_YF_Y	=	380 MPa	55 ksi	
Probable Shear Yielding Resistance in Beam, V_{SY}	=	545 kN	123 kips	

Shear Rupture

$$V_{SR} = 0.66\phi_u F_u A_{nv}$$

*S16-09 Cl. 13.4.1.1

Resistance Factor, $Ø_u$	=	0.75	0.75	
Tensile Strength of Plate, F_U	=	450 MPa	65 ksi	
$A_{NV} = t_p d_{pN}$				
Plate Thickness, t_p	=	9.53 mm	3/8 in	
Net Depth, d_{pN}	=	161.9 mm	6.38 in	
Net Plate Area, A_{NV}	=	1542 mm^2	2.391 in^2	
Factored Shear Rupture Resistance in Shear Plate, V_{SR}	=	344 kN	77 kips	
Probable Tensile Strength, R_YF_U	=	495 MPa	71.5 ksi	
Probable Shear Rupture Resistance in Shear Plate, V_{SR}	=	504 kN	113 kips	

Block Shear Rupture

$$V_{BS} = \phi_u \left[U_t A_n F_u + 0.6 A_{gv} \frac{F_y + F_u}{2} \right]$$

*S16-09 Cl. 13.11

Resistance Factor, $Ø_u$	=	0.75	0.75	
Efficiency Factor, U_t	=	0.3	0.3	
Net Area, A_n	=	771 mm^2	1.195 in^2	
Tensile Strength of Plate, F_U	=	450 MPa	65 ksi	
Gross Area in Shear, A_{gV}	=	1815 mm^2	2.813 in^2	
Yield Stress of Plate, F_Y	=	345 MPa	50 ksi	
Factored Block Shear Failure in Beam, V_{BS}	=	403 kN	90 kips	
Probable Tensile Strength, R_YF_U	=	495 MPa	71.5 ksi	
Probable Yield Stress, R_YF_Y	=	380 MPa	55 ksi	
Probable Block Shear Failure in Beam, V_{BS}	=	591 kN	132 kips	

4) Flexural Shear Yielding, Shear Buckling, and Yielding (Von Mises)

*AISC Manual 2011 Extended Config Design Check 4 (10-5)

*AISC Manual 2011 Eqn 10-5, modified

$$\left(\frac{V_r}{V_c}\right)^2 + \left(\frac{M_r}{M_c}\right)^2 \leq 1.0$$

therefore

$$V_r = \sqrt{\frac{1}{V_c^2} + \left(\frac{e}{M_c}\right)^2}$$

$V_c = Ø_v V_n$

Resistance Factor, $Ø_v$	=	0.9	0.9	*use 0.9 as in S16-09 instead of 1.0

$V_n = 0.66F_Y A_g$

Yield Stress of Plate, F_Y	=	345 MPa	50 ksi
Gross Area of Plate, A_g	=	2177 mm^2	3.375 in^2
Nominal Shear Capacity, V_n	=	496 kN	111 kips
Factored Shear Capacity, V_c	=	446 kN	100 kips
Eccentricity to first bolt column, e	=	165 mm	6 1/2 in

$M_c = Ø_b M_n$

Resistance Factor, $Ø_b$	=	0.9	0.9

$M_n = F_y Z_{pl}$

Plastic Section Modulus, Z_{pl}	=	124 x$10^3$$mm^3$	7.594 in^3
Nominal Moment Capacity, M_n	=	43 kN-m	380 kip-in
Factored Moment Capacity, M_c	=	39 kN-m	342 kip-in
Factored Shear and Flexural Yielding Resistance, V_r	=	207 kN	47 kips
Probable Yield Stress, $R_Y F_Y$	=	380 MPa	55 ksi
Probable Shear and Flexural Yielding Resistance, V_r	=	248 kN	56 kips

5) Plate Buckling

*AISC Manual 2011 Extended Config Design Check 5 (10-5)

$$V_{FB} = \frac{M_{FB}}{e}$$

Resistance Factor, $Ø_s$	=	0.9	0.9
Elastic Section Modulus of Gross Reduced Area, S_x'	=	82960 x$10^3$$mm^3$	5.06 in^3
Cope Depth at Compression Flange, d_c	=	41 mm	1.6 in
Beam Depth, d	=	310 mm	12.2 in
Eccentricity to first bolt column, e	=	165.1 mm	6 1/2 in
Unsupported Length of Plate, c	=	165.1 mm	6 1/2 in

fd equation (Cheng et al. 1984)

*AISC Manual 2011 Part 9

$$F_{cr} = 0.62\pi E \frac{(t_p)^2}{c h_o} f_d$$

Modulus of Elasticity, E	=	200000 MPa	29000 ksi
Thickness of Plate, t_p	=	9.5 mm	3/8 in
Reduced Beam Depth, h_o	=	228.6 mm	9 in
Adjustment Factor, $f_d = 3.5 - 7.5\left(\frac{d_c}{d}\right)$	=	2.5 MPa	2.5 ksi
Critical Stress, F_{cr}	=	2354 MPa	341.5 ksi

Moment Buckling Resistance at Cope, $M_{FB} = \phi_s F_{cr} S_x'$

Factored Moment Buckling Resistance at Cope, M_{FB}	=	175.8 kN-m	1556.1 kips-in
Probable Moment Buckling Resistance at Cope, M_{FB}	=	195.4 kN-m	1729.0 kips-in
Factored Flexural Buckling at Cope, V_{FB}	=	1063 kN	239 kips
Probable Flexural Buckling at Cope, V_{FB}	=	1181 kN	266 kips

Q equation (classical plate buckling)

*AISC Manual 2011 Part 9

$$F_{cr} = F_y Q$$

Resistance Factor, $Ø_s$	=	0.9	0.9
Thickness of Plate, t_p	=	9.525 mm	3/8 in
Reduced Beam Height, h_o	=	228.6 mm	9 in
Unsupported Length of Plate, c	=	165.1 mm	6 1/2 in
Eccentricity to Cope, e	=	165.10 mm	6 1/2 in
Elastic Section Modulus of Gross Reduced Area, S_x'	=	82959.5 mm^3	5.06 in^3
Yield Strength of Beam, F_y	=	345 MPa	50 ksi
Probable Yield Strength of Beam, $R_y F_y$	=	380 MPa	55 ksi

$$Q = \begin{cases} 1 \; for \; \lambda \le 0.7 \\ (1.34 - 0.486\lambda) \; for \; 0.7 < \lambda \le 1.41 \\ (1.30 / \lambda^2) \; for \; \lambda > 1.41 \end{cases}$$

Factored Q	=	1	1
Probable Q	=	1	1

where

$$\lambda = \frac{h_o \sqrt{F_y}}{10 t_p \sqrt{475 + 280\left(\frac{h_o}{c}\right)^2}}$$

Factored λ	=	0.53	0.53

Probable λ	=	0.56	0.56
Factored Critical Buckling Stress, F_{cr}	=	349.0 MPa	50.0 ksi
Probable Critical Buckling Stress, F_{cr}	=	383.9 MPa	55.0 ksi
Moment Buckling Resistance at Cope, $M_{FB} = \phi_s F_{cr} S_x'$			
Factored Moment Buckling Resistance at Cope, M_{FB}	=	25.7 kN-m	227.8 kips-in
Probable Moment Buckling Resistance at Cope, M_{FB}	=	31.5 kN-m	278.4 kips-in
Factored Flexural Buckling at Cope, V_{FB}	=	155.6 kN	35.0 kips
Probable Flexural Buckling at Cope, V_{FB}	=	190.2 kN	42.8 kips

6) Weld to Supporting Element

*AISC Manual 2011 Extended Config Design Check 5 (10-6)
*S16-09 Cl. 13.13.2.2

$V_W = 0.67\phi_w n_w X_u A_w$

Resistance Factor, $Ø_w$	=	0.67	0.67
Number of Welds, n_w	=	2	2
Ultimate Strength of Electrode, X_u	=	490 MPa	70 ksi
Welded Area, A_w	=	997.9 mm^2	1.55 in^2
Length of Weld, L_w	=	222.3 mm	8 3/4 in
Weld Size, t_w	=	6.4 mm	1/4 in
Factored Weld Resistance, V_w	=	431.6 kN	97.2 kips
Probable Weld Resistance, V_w	=	644.2 kN	145.1 kips

Specimen 9J - Partial Depth Extended Shear Tab, Retrofit

Configuration Parameters

Girder		W610x125	(W24x84)	
Beam		W310x60	(W12x40)	
Plate Thickness, t_p	=	9.5 mm	3/8 in	
Offset of Bolt Group, a	=	81 mm	3 3/16 in	*Note: "a" distance was reduced from 9 1/2 due to retrofit
Bolt Diameter, d_b	=	19.1 mm	3/4 in	
Number of Bolt Lines, m	=	2	2	
Number of Bolts Rows, n	=	3	3	
Bolt Gauge Distance, D	=	76.2 mm	3 in	
Bolt Pitch Distance, b	=	76.2 mm	3 in	
Plate Depth, d	=	229 mm	9 in	
Plate Depth in Girder, d_g	=	229 mm	9 in	

1) Bolt Shear & Bearing

*AISC Manual 2011 Extended Config Design Check 1 (10-5)

Compute ICR Coefficient, C

*CISC Handbook 2009 Table 3-15

Number of Bolt Lines, m	=	2	2	
Moment Arm, L	=	119.06 mm	4.6875 in	
gage, D	=	76.2 mm	3 in	
Pitch, b	=	76.2 mm	3 in	
Number of Bolt Rows, n	=	3	3	
L1	=	100 mm		
C1	=	3.25		Linear Interpolation
L2	=	125 mm		
C2	=	2.77		
Eccentric Loading Coefficient, C	=	2.88	2.88	

Bearing

$$B_r = min \begin{cases} 3\phi_b d_b (t_p F_u)_{plate} C \\ 3\phi_b d_b (t_w F_u)_{beam} C \end{cases}$$

Modification factor, $Ø_{br}$	=	0.8	0.8	
Plate Thickness, t_p	=	9.53 mm	3/8 in	
Beam Web Thickness, t_w	=	7.50 mm	0.295 in	
Bolt Diameter, d_b	=	19.05 in	3/4 in	
Tensile Strength of Plate, $F_{u,plate}$	=	450 MPa	65 ksi	
Tensile Strength of Beam $F_{u,beam}$	=	450 MPa	65 ksi	
Factored Bearing Resistance, B_r	=	445 kN	100 kips	
Probable Plate Strength, $R_Y F_{U,plate}$	=	495 MPa	71.5 ksi	
Probable Beam Strength, $R_Y F_{U,beam}$	=	495 MPa	71.5 ksi	
Probable Bearing Resistance, B_r	=	556 kN	125 kips	

Bolt Shear

$$V_{Bolt} = 0.6\phi_b n m A_b F_u C$$

*S16-09 Cl. 13.12.1.2c

Modification factor, $Ø_b$	=	0.8	0.8	
Number of Bolts, n	=	1	1	
Number of Shear Planes, m	=	1	1	
Bolt Area, A_b	=	285 mm^2	0.442 in^2	
Ultimate Strength of Bolts, F_U	=	825 MPa	120 ksi	
Factored Bolt Shear Resistance, V_{Bolt}	=	325 kN	73 kips	
Probable Bolt Shear Resistance, V_{Bolt}	=	407 kN	92 kips	

2) Plate Ductility

*AISC Manual 2011 Extended Config Design Check 2 (10-5)

$$t_{pmax} = \frac{6M_{max}}{F_y d^2}$$

$$M_{max} = \frac{F_{nv}}{0.9}(A_b C')$$

Bolt Shear Strength, F_{nV}	=	415 MPa	60 ksi	*AISC Specification 2010 Table J3.2
Bolt Area, A_b	=	285 mm^2	0.442 in^2	

Compute ICR Coefficient, C', for Moment Only Case

Number of Bolt Lines, m	=	2	2	
Column Spacing	=	76.2 mm	3 in	
Bolt Gauge Distance, D	=	76.2 mm	3 in	

Number of Bolts Rows, n	=	3	3	
ICR Coefficient, C'	=	401.32 mm	15.8 in	*AISC Manual 2011 Table 7-8
M_{max}	=	53 kN-m	465 kip-in	
Yield Stress of Plate, F_Y	=	345 MPa	50 ksi	
Probable Plate Strength, R_YF_U	=	495 MPa	72 ksi	
Plate Depth, d	=	228.6 mm	9.0 in	
Factored Maximum Plate Thickness, t_{pmax}	=	17.5 mm	0.689 in	
Probable Maximum Plate Thickness, t_{pmax}	=	12.2 mm	0.482 in	
Check Plate Thickness Based on Factored Loads? ($t_p < t_{pmax}$)		OK		
Check Plate Thickness Based on Probable Loads? ($t_p < t_{pmax}$)		OK		

3) Shear Yielding, Shear Rupture and Block Shear Rupture

*AISC Manual 2011 Extended Config Design Check 3 (10-5)

Shear Yielding

$$V_{SY} = 0.66\phi_s F_y A_w$$

*S16-09 Cl. 13.4.1.1

Resistance Factor, $Ø_s$	=	0.9	0.9	
Yield Stress of Plate, F_Y	=	345 Mpa	50 ksi	
$A_g = t_p d_p$				
Plate Thickness, t_p	=	9.53 mm	3/8 in	
Plate Depth, d_p	=	228.6 mm	9 in	
Gross Plate Area, A_g	=	2177 mm^2	3.375 in^2	
Factored Shear Yielding Resistance in Beam, V_{SY}	=	446 kN	100 kips	
Probable Yield Stress, R_YF_Y	=	380 MPa	55 ksi	
Probable Shear Yielding Resistance in Beam, V_{SY}	=	545 kN	123 kips	

Shear Rupture

$$V_{SR} = 0.66\phi_u F_u A_{nv}$$

*S16-09 Cl. 13.4.1.1

Resistance Factor, $Ø_u$	=	0.75	0.75	
Tensile Strength of Plate, F_U	=	450 MPa	65 ksi	
$A_{NV} = t_p d_{pN}$				
Plate Thickness, t_p	=	9.53 mm	3/8 in	
Net Depth, d_{pN}	=	161.9 mm	6.38 in	
Net Plate Area, A_{NV}	=	1542 mm^2	2.391 in^2	
Factored Shear Rupture Resistance in Shear Plate, V_{SR}	=	344 kN	77 kips	
Probable Tensile Strength, R_YF_U	=	495 MPa	71.5 ksi	
Probable Shear Rupture Resistance in Shear Plate, V_{SR}	=	504 kN	113 kips	

Block Shear Rupture

$$V_{BS} = \phi_u \left[U_t A_n F_u + 0.6 A_{gv} \frac{F_y + F_u}{2} \right]$$

*S16-09 Cl. 13.11

Resistance Factor, $Ø_u$	=	0.75	0.75	
Efficiency Factor, U_t	=	0.3	0.3	
Net Area, A_n	=	771 mm^2	1.195 in^2	
Tensile Strength of Plate, F_U	=	450 MPa	65 ksi	
Gross Area in Shear, A_{gV}	=	1815 mm^2	2.813 in^2	
Yield Stress of Plate, F_Y	=	345 Mpa	50 ksi	
Factored Block Shear Failure in Beam, V_{BS}	=	403 kN	90 kips	
Probable Tensile Strength, R_YF_U	=	495 MPa	71.5 ksi	
Probable Yield Stress, R_YF_Y	=	380 Mpa	55 ksi	
Probable Block Shear Failure in Beam, V_{BS}	=	591 kN	132 kips	

4) Flexural Shear Yielding, Shear Buckling, and Yielding (Von Mises)

*AISC Manual 2011 Extended Config Design Check 4 (10-5)

*AISC Manual 2011 Eqn 10-5, modified

$$\left(\frac{V_r}{V_c}\right)^2 + \left(\frac{M_r}{M_c}\right)^2 \leq 1.0$$

therefore

$$V_r = \sqrt{\frac{1}{V_c^2} + \left(\frac{e}{M_c}\right)^2}$$

$V_c = Ø_v V_n$

Resistance Factor, $Ø_v$	=	0.9	0.9	*use 0.9 as in S16-09 instead of 1.0

$V_n = 0.66F_Y A_g$

Yield Stress of Plate, F_Y	=	345 MPa	50 ksi
Gross Area of Plate, A_g	=	2177 mm^2	3.375 in^2
Nominal Shear Capacity, V_n	=	496 kN	111 kips
Factored Shear Capacity, V_c	=	446 kN	100 kips
Eccentricity to first bolt column, e	=	81 mm	3 3/16 in

$M_c = Ø_b M_n$

Resistance Factor, $Ø_b$	=	0.9	0.9

$M_n = F_y Z_{pl}$

Plastic Section Modulus, Z_{pl}	=	124 x$10^3$$mm^3$	7.594 in^3
Nominal Moment Capacity, M_n	=	43 kN-m	380 kip-in
Factored Moment Capacity, M_c	=	39 kN-m	342 kip-in
Factored Shear and Flexural Yielding Resistance, V_r	=	326 kN	73 kips
Probable Yield Stress, R_YF_Y	=	380 MPa	55 ksi
Probable Shear and Flexural Yielding Resistance, V_r	=	378 kN	85 kips

5) Plate Buckling

*AISC Manual 2011 Extended Config Design Check 5 (10-5)

$$V_{FB} = \frac{M_{FB}}{e}$$

Resistance Factor, $Ø_s$	=	0.9	0.9
Elastic Section Modulus of Gross Reduced Area, S_x'	=	82960 x$10^3$$mm^3$	5.06 in^3
Cope Depth at Compression Flange, d_c	=	41 mm	1.6 in
Beam Depth, d	=	310 mm	12.2 in
Eccentricity to first bolt column, e	=	81.0 mm	3 3/16 in
Unsupported Length of Plate, c	=	81.0 mm	3 3/16 in

fd equation (Cheng et al. 1984)

*AISC Manual 2011 Part 9

$$F_{cr} = 0.62\pi E\frac{(t_p)^2}{ch_o}f_d$$

Modulus of Elasticity, E	=	200000 MPa	29000 ksi
Thickness of Plate, t_p	=	9.5 mm	3/8 in
Reduced Beam Depth, h_o	=	228.6 mm	9 in
Adjustment Factor, $f_d = 3.5 - 7.5\left(\frac{d_c}{d}\right)$	=	2.5 MPa	2.5 ksi
Critical Stress, F_{cr}	=	4801 MPa	696.5 ksi

Moment Buckling Resistance at Cope, $M_{FB} = \phi_s F_{cr} S_x'$

Factored Moment Buckling Resistance at Cope, M_{FB}	=	358.6 kN-m	3173.3 kips-in
Probable Moment Buckling Resistance at Cope, M_{FB}	=	398.4 kN-m	3525.9 kips-in
Factored Flexural Buckling at Cope, V_{FB}	=	4420 kN	996 kips
Probable Flexural Buckling at Cope, V_{FB}	=	4911 kN	1106 kips

Q equation (classical plate buckling)

*AISC Manual 2011 Part 9

$$F_{cr} = F_y Q$$

Resistance Factor, $Ø_s$	=	0.9	0.9
Thickness of Plate, t_p	=	9.525 mm	3/8 in
Reduced Beam Height, h_o	=	228.6 mm	9 in
Unsupported Length of Plate, c	=	81.0 mm	3 3/16 in
Eccentricity to Cope, e	=	80.96 mm	3 3/16 in
Elastic Section Modulus of Gross Reduced Area, S_x'	=	82959.5 mm^3	5.06 in^3
Yield Strength of Beam, F_y	=	345 MPa	50 ksi
Probable Yield Strength of Beam, R_yF_y	=	380 MPa	55 ksi

$$Q = \begin{cases} 1 \; for \; \lambda \le 0.7 \\ (1.34 - 0.486\lambda) \; for \; 0.7 < \lambda \le 1.41 \\ (1.30 / \lambda^2) \; for \; \lambda > 1.41 \end{cases}$$

Factored Q	=	1	1
Probable Q	=	1	1

where

$$\lambda = \frac{h_o\sqrt{F_y}}{10t_p\sqrt{475 + 280\left(\frac{h_o}{c}\right)^2}}$$

Factored λ	=	0.33	0.33
Probable λ	=	0.34	0.34

Factored Critical Buckling Stress, F_{cr}	=	349.0 MPa	50.0 ksi
Probable Critical Buckling Stress, F_{cr}	=	383.9 MPa	55.0 ksi
Moment Buckling Resistance at Cope, $M_{FB} = \phi_s F_{cr} S_x'$			
Factored Moment Buckling Resistance at Cope, M_{FB}	=	25.7 kN-m	227.8 kips-in
Probable Moment Buckling Resistance at Cope, M_{FB}	=	31.5 kN-m	278.4 kips-in
Factored Flexural Buckling at Cope, V_{FB}	=	317.3 kN	71.5 kips
Probable Flexural Buckling at Cope, V_{FB}	=	387.8 kN	87.4 kips

6) Weld to Supporting Element

*AISC Manual 2011 Extended Config Design Check 5 (10-6)
*S16-09 Cl. 13.13.2.2

$V_W = 0.67\phi_w n_w X_u A_w$

Resistance Factor, $Ø_w$	=	0.67	0.67
Number of Welds, n_w	=	2	2
Ultimate Strength of Electrode, X_u	=	490 MPa	70 ksi
Welded Area, A_w	=	962.3 mm^2	1.49 in^2
Length of Weld, L_w	=	214.3 mm	8 7/16 in
Weld Size, t_w	=	6.4 mm	1/4 in
Factored Weld Resistance, V_w	=	416.2 kN	93.7 kips
Probable Weld Resistance, V_w	=	621.2 kN	139.9 kips

Specimen 1 - Single Cope Unreinforced

Configuration Parameters

Girder		W760x257	(W30x173)	
Beam		W310x60	(W12x40)	
Supporting Stiffener Thickness, t_{sp}	=	19.1 mm	3/4 in	
Cope Length, c	=	177.8 mm	7 in	
Cope Depth, d_c	=	39.7 mm	1 9/16 in	
Bolt Size, d_b	=	19.1 mm	3/4 in	
Number of Bolt Lines, m	=	2	2	
Number of Bolt Rows, n	=	3	3	
Bolt Gauge Distance, D	=	76.2 mm	3 in	
Bolt Pitch Distance, b	=	76.2 mm	3 in	
Bolt Edge Distance	=	38.1 mm	1 1/2 in	
Gap from Beam End to Girder	=	30.2 mm	1 3/16 in	

Computing ICR Coefficient, C *CISC Handbook 2009 Table 3-15

Moment Arm, L	=	114.7 mm	4.52 in	
Number of Bolt Lines, m	=	2	2	
Gauge, D	=	76.2 mm	3 in	
Number of Bolt Rows, n	=	3	3	
Pitch, b	=	76.2 mm	3 in	
L_1	=	100 mm		
C_1	=	3.25		Linear Interpolation
L_2	=	125 mm		
C_2	=	2.77		
Eccentric Loading Coefficient, C	=	2.968	2.968	

Bolts

Bolt Shear

$V_{Bolt} = 0.6\phi_b nmA_b F_u C$ *S16-09 Cl. 13.12.1.2c

Resistance Factor, $Ø_b$	=	0.8	0.8	
Number of Bolts, n	=	1	1	
Number of Shear Planes, m	=	1	1	
Bolt Area, A_b	=	285 mm^2	0.442 in^2	
Tensile Strength of Bolts, F_u	=	825 MPa	120 ksi	
Factored Bolt Shear Resistance, V_{Bolt}	=	335.5 kN	75.6 kips	
Probable Bolt Shear Resistance, V_{Bolt}	=	419.4 kN	94.5 kips	

Supporting Stiffener

Shear Yielding

$V_{SY} = 0.66\phi_s F_y A_w$ *S16-09 Cl. 13.4.1.1

Resistance Factor, $Ø_s$	=	0.9	0.9	
Gross Shear Area, $A_w = t_{sp}d_{sp}$	=	4354.8 mm^2	6.75 in^2	
Supporting Stiffener Thickness, t_{sp}	=	19.1 mm	3/4 in	
Supporting Stiffener Depth, d_{sp}	=	228.6 mm	9 in	
Yield Strength of Plate, F_y	=	345 MPa	50 ksi	
Factored Shear Yielding Resistance in Supporting Stiffener, V_{SY}	=	890.1 kN	200.5 kips	
Probable Yielding Strength of Plate, R_yF_y	=	380 MPa	55 ksi	
Probable Shear Yielding Resistance in Supporting Stiffener, V_{SY}	=	1087.9 kN	245.0 kips	

Bearing

$B_r = min\begin{cases} 3\phi_b d_b t_{sp} F_u C \\ 1.5\phi_u L_c t_{sp} F_u C \end{cases}$ *S16-09 Cl. 13.12.1.2a *AISC Specification 2010 Eq. J3-6b

Resistance Factor, $Ø_b$	=	0.8	0.8	
Resistance Factor, $Ø_u$	=	0.75	0.75	
Tear-out Length, L_c	=	27.0 mm	1 1/16 in	
Bolt Size, d_b	=	19.1 mm	3/4 in	
Supporting Stiffener Thickness, t_{sp}	=	19.1 mm	3/4 in	
Ultimate Strength of Plate, F_u	=	450 MPa	65 ksi	
Factored Bearing Resistance in Supporting Stiffener, B_r	=	767.9 kN	173.0 kips	
Probable Ultimate Strength of Plate, R_yF_u	=	495 MPa	71.5 ksi	
Probable Bearing Resistance in Supporting Stiffener, B_r	=	1126.3 kN	253.7 kips	

Stability

$$\frac{b_{el}}{t} \leq \frac{200}{\sqrt{F_y}}$$

*S16-09 Table 1

Effective Width of Supporting Stiffener, b_{el}	=	182.2 mm	7.17 in
Supporting Stiffener Thickness, t_{sp}	=	19.1 mm	3/4 in
Yield Strength of Plate, F_y	=	345 MPa	50 ksi
Stability Check		Stable	

Beam

Shear Yielding

$$V_{SY} = 0.66\phi_s F_y A_w$$

*S16-09 Cl. 13.4.1.1

Resistance Factor, $Ø_s$	=	0.9	0.9
Gross Shear Area, $A_w = t_w h_o$	=	1967.5 mm^2	3.05 in^2
Beam Web Thickness, t_w	=	7.5 mm	0.295 in
Reduced Beam Height, h_o	=	262.6 mm	10.34 in
Yield Strength of Beam, F_y	=	345 MPa	50 ksi
Factored Shear Yielding Resistance in Beam, V_{SY}	=	402.1 kN	90.6 kips
Probable Yielding Strength of Beam, R_yF_y	=	380 MPa	55 ksi
Probable Shear Yielding Resistance in Beam, V_{SY}	=	491.5 kN	110.7 kips

Bearing

$$B_r = min \begin{cases} 3\phi_b d_b t_w F_u C \\ 1.5\phi_u L_c t_w F_u C \end{cases}$$

*S16-09 Cl. 13.12.1.2a
*AISC Specification 2010 Eq. J3-6b

Resistance Factor, $Ø_b$	=	0.8	0.8
Resistance Factor, $Ø_u$	=	0.75	0.75
Tear-out Length, L_c	=	27.0 mm	1 1/16 in
Bolt Size, d_b	=	19.1 mm	3/4 in
Beam Web Thickness, t_w	=	7.5 mm	0.295 in
Ultimate Strength of Beam, F_u	=	450 MPa	65 ksi
Factored Bearing Resistance in Beam, B_r	=	302.1 kN	68.0 kips
Probable Ultimate Strength of Beam, R_yF_u	=	495 MPa	71.5 ksi
Probable Bearing Resistance in Beam, B_r	=	443.0 kN	99.8 kips

Block Shear

$$V_{BS} = \phi_u \left[U_t A_n F_u + 0.6 A_{gv} \frac{F_y + F_u}{2} \right]$$

*S16-09 Cl. 13.11

Resistance Factor, $Ø_u$	=	0.75	0.75
Efficiency Factor, U_t	=	0.3	0.3
Net Area, A_n	=	606.7 mm^2	0.94 in^2
Gross Area in Shear for Block Shear, A_{gv}	=	1427.4 mm^2	2.21 in^2
Yield Strength of Beam, F_y	=	345 MPa	50 ksi
Ultimate Strength of Beam, F_u	=	450 MPa	65 ksi
Factored Block Shear Failure in Beam, V_{BS}	=	315.2 kN	71.0 kips
Probable Yield Strength of Beam, R_yF_y	=	380 MPa	55 ksi
Probable Ultimate Strength of Beam, R_yF_u	=	495 MPa	71.5 ksi
Probable Block Shear Failure in Beam, V_{BS}	=	462.4 kN	104.1 kips

Flexural Yielding at Cope

$$V_{FY} = \frac{M_{FY}}{e}$$

*S16-09 Cl. 13.5

Resistance Factor, $Ø_s$	=	0.9	0.9
Elastic Section Modulus of Gross Reduced Area, S_x'	=	129667.0 mm^3	7.91 in^3
Reduced Beam Height, h_o	=	262.6 mm	10.34 in
Centroid of Reduced Area, $\bar{y}$	=	82.0 mm	3.23 in
Moment of Inertia of Gross Reduced Area, I_x'	=	23408855.4 mm^4	56.24 in^4
Eccentricity to Cope, e	=	216.3 mm	8 1/2 in
Yield Strength of Beam, F_y	=	345 MPa	50 ksi
Moment Yielding Resistance at Cope, $M_{FY} = \phi_s F_y S_x'$			
Factored Moment Yielding Resistance at Cope, M_{FY}	=	40.2 kN-m	356.1 kips-in
Probable Yield Strength of Beam, R_yF_y	=	380 MPa	55 ksi
Probable Moment Yielding Resistance at Cope, M_{FY}	=	49.2 kN-m	435.2 kips-in
Factored Flexural Yielding at Cope, V_{FY}	=	185.7 kN	41.8 kips
Probable Flexural Yielding at Cope, V_{FY}	=	226.9 kN	51.1 kips

Flexural Buckling at Cope

$$V_{FB} = \frac{M_{FB}}{e}$$

Resistance Factor, $Ø_s$	=	0.9	0.9	
Modulus of Elasticity, E	=	200000 MPa	29000 ksi	
Poisson's Ratio, ν	=	0.3	0.3	
Beam Web Thickness, t_w	=	7.5 mm	0.295 in	
Beam Depth, d	=	302.3 mm	11.9 in	
Effective Reduced Beam Depth, h_1	=	180.5 mm	7.11 in	
Reduced Beam Height, h_o	=	262.6 mm	10.34 in	
Centroid of Reduced Area, $\bar{y}$	=	82.0 mm	3.23 in	
Cope Length, c	=	177.8 mm	7.0 in	

$$F_{cr} = \frac{\pi^2 E}{12(1-\nu^2)}\left(\frac{t_w}{h_1}\right)^2 fk$$ *AISC Manual 2011 Part 9

Plate Buckling Model Adjustment Factor, f

$$f = \begin{cases} \frac{2c}{d} \text{ when } \frac{c}{d} \le 1.0 \\ 1 + \frac{c}{d} \text{ when } \frac{c}{d} > 1.0 \end{cases}$$ = 1.18 1.18

Plate Buckling Coefficient, k

$$k = \begin{cases} 2.2\left(\frac{h_1}{c}\right)^{1.65} \text{ when } \frac{c}{h_1} \le 1.0 \\ \frac{2.2h_1}{c} \text{ when } \frac{c}{h_1} > 1.0 \end{cases}$$ = 2.26 2.26

Critical Buckling Stress, F_{cr}		836.5 MPa	119.8 ksi	
Elastic Section Modulus of Gross Reduced Area, S_x'	=	129667.0 mm^3	7.91 in^3	
Eccentricity to Cope, e	=	216.3 mm	8 1/2 in	

Moment Buckling Resistance at Cope, $M_{FB} = \phi_s F_{cr} S_x'$

Factored Moment Buckling Resistance at Cope, M_{FB}	=	96.4 kN-m	853.5 kips-in	
Probable Moment Buckling Resistance at Cope, M_{FB}	=	107.2 kN-m	948.3 kips-in	
Factored Flexural Buckling at Cope, V_{FB}	=	445.0 kN	100.2 kips	
Probable Flexural Buckling at Cope, V_{FB}	=	494.5 kN	111.4 kips	

Net Shear Rupture

$$V_{SR} = 0.66\phi_u F_u A_{nv}$$ *S16-09 Cl. 13.4.1.1

Resistance Factor, $Ø_u$	=	0.75	0.75	
Net Shear Area, $A_{nv} = t_w h_o$ - bolt holts	=	1467.9 mm^2	2.28 in^2	
Beam Web Thickness, t_w	=	7.5 mm	0.295 in	
Reduced Beam Height, h_o	=	262.6 mm	10.34 in	
Ultimate Yield Strength of Beam, F_u	=	450 MPa	65 ksi	
Factored Shear Rupture Resistance in Beam, V_{SR}	=	325.0 kN	73.2 kips	
Probable Ultimate Strength of Beam, R_yF_u	=	495 MPa	72 ksi	
Probable Shear Rupture Resistance in Beam, V_{SR}	=	476.7 kN	107.4 kips	

Flexural Rupture at Last Line of Bolts

$$V_{FR} = \frac{M_{FR}}{e}$$ *S16-09 Cl. 13.5

Resistance Factor, $Ø_u$	=	0.75	0.75	
Elastic Section Modulus of Net Reduced Area, S_{xn}'	=	98030.4 mm^3	5.98 in^3	
Reduced Beam Height, h_o	=	262.6 mm	10.34 in	
Centroid of Net Reduced Area, $\bar{y}_n$	=	70.1 mm	2.76 in	
Moment of Inertia of Gross Reduced Area, I_{xn}'	=	18867770.5 mm^4	45.33 in^4	
Eccentricity to Last Line of Bolts, e	=	147.4 mm	6.02 in	
Ultimate Yield Strength of Beam, F_u	=	450 MPa	65 ksi	

Moment Rupture Resistance at Last Line of Bolts, $M_{FR} = \phi_u F_u S_{xn}'$

Factored Moment Rupture Resistance at Last Line of Bolts, M_{FB}	=	33.0 kN-m	291.6 kips-in	
Probable Ultimate Strength of Beam, R_yF_u	=	495 MPa	72 ksi	
Probable Moment Rupture Resistance at Last Line of Bolts, M_{FB}	=	48.3 kN-m	427.7 kips-in	
Factored Flexural Rupture Resistance at Last Line of Bolts, V_{FR}	=	215.3 kN	48.5 kips	
Probable Flexural Rupture Resistance at Last Line of Bolts, V_{FR}	=	315.7 kN	71.1 kips	

Von Mises Interaction

$$\left(\frac{V_{SY}}{V_{VM}}\right)^2 + \left(\frac{M_{FY}}{M_{VM}}\right)^2 \leq 1.0$$

therefore

$$V_{VM} = \frac{\phi_s F_y S_x'}{\sqrt{\left(\frac{S_x'}{0.66A_w}\right)^2 + e^2}}$$

Resistance Factor, $Ø_s$	=	0.9	0.9
Elastic Section Modulus of Gross Reduced Area, S_x'	=	129667.0 mm^3	7.91 in^3
Gross Shear Area, A_w	=	1967.5 mm^2	3.05 in^2
Eccentricity to Cope, e	=	216.3 mm	8 1/2 in
Yield Strength of Beam, F_y	=	345 MPa	50 ksi
Factored Von Mises Resistance, V_{VM}	=	168.6	38.0 kips
Probable Yield Strength of Beam, R_yF_y	=	380 MPa	55 ksi
Probable Von Mises Resistance, V_{VM}	=	206.0 kips	46.4 kips

Welds

Weld Strength

$$V_W = 0.67\phi_w n_w X_u A_w$$ *S16-09 Cl. 13.13.2.2

Resistance Factor, $Ø_w$	=	0.67	0.67
Number of Welds, n_w	=	2	2
Ultimate Strength of Electrode, X_u	=	490 MPa	70 ksi
Welded Area, A_w	=	3777.9 mm^2	5.86 in^2
Length of Weld (T distance of Girder), L_w	=	673.1 mm	26 1/2 in
Weld Size, t_w	=	7.9 mm	5/16 in
Factored Weld Resistance, V_w	=	1634.0 kN	368.0 kips
Probable Weld Resistance, V_w	=	2438.7 kN	549.3 kips

Specimen 2 - Single Cope Horizontal Stiffener

Configuration Parameters

Girder		W760x257	(W30x173)	
Beam		W310x60	(W12x40)	
Supporting Stiffener Thickness, t_{sp}	=	19.1 mm	3/4 in	
Cope Length, c	=	177.8 mm	7 in	
Cope Depth, d_c	=	39.7 mm	1 9/16 in	
Bolt Size, d_b	=	19.1 mm	3/4 in	
Number of Bolt Lines, m	=	2	2	
Number of Bolt Rows, n	=	3	3	
Bolt Gauge Distance, D	=	76.2 mm	3 in	
Bolt Pitch Distance, b	=	76.2 mm	3 in	
Bolt Edge Distance - Horizontal	=	38.1 mm	1 1/2 in	
Bolt Edge Distance - Vertical	=	50.8 mm	2 in	
Gap from Beam End to Girder	=	30.2 mm	1 3/16 in	
Horizontal Stiffener Thickness, t_s	=	7.9 mm	5/16 in	
Width of Horizontal Stiffener, b_s	=	50.8 mm	2 in	
Length of Horizontal Stiffener, L_s	=	266.7 mm	10 1/2 in	

Computing ICR Coefficient, C *CISC Handbook 2009 Table 3-15

Moment Arm, L	=	114.7 mm	4.52 in	
Number of Bolt Lines, m	=	2	2	
Gauge, D	=	76.2 mm	3 in	
Number of Bolt Rows, n	=	3	3	
Pitch, b	=	76.2 mm	3 in	
L_1	=	100 mm		
C_1	=	3.25		Linear Interpolation
L_2	=	125 mm		
C_2	=	2.77		
Eccentric Loading Coefficient, C	=	2.968	2.968	

Bolts

Bolt Shear

$$V_{Bolt} = 0.6\phi_b n m A_b F_u C$$ *S16-09 Cl. 13.12.1.2c

Resistance Factor, $Ø_b$	=	0.8	0.8	
Number of Bolts, n	=	1	1	
Number of Shear Planes, m	=	1	1	
Bolt Area, A_b	=	285 mm^2	0.442 in^2	
Tensile Strength of Bolts, F_u	=	825 MPa	120 ksi	
Factored Bolt Shear Resistance, V_{Bolt}	=	335.5 kN	75.6 kips	
Probable Bolt Shear Resistance, V_{Bolt}	=	419.4 kN	94.5 kips	

Supporting Stiffener

Shear Yielding

$$V_{SY} = 0.66\phi_s F_y A_w$$ *S16-09 Cl. 13.4.1.1

Resistance Factor, $Ø_s$	=	0.9	0.9	
Gross Shear Area, $A_w = t_{sp}d_{sp}$	=	4354.8 mm^2	6.75 in^2	
Supporting Stiffener Thickness, t_{sp}	=	19.1 mm	3/4 in	
Supporting Stiffener Depth, d_{sp}	=	228.6 mm	9 in	
Yield Strength of Plate, F_y	=	345 MPa	50 ksi	
Factored Shear Yielding Resistance in Supporting Stiffener, V_{SY}	=	890.1 kN	200.5 kips	
Probable Yielding Strength of Plate, R_yF_y	=	380 MPa	55 ksi	
Probable Shear Yielding Resistance in Supporting Stiffener, V_{SY}	=	1087.9 kN	245.0 kips	

Bearing

$$B_r = min\begin{cases} 3\phi_b d_b t_{sp} F_u C \\ 1.5\phi_u L_c t_{sp} F_u C \end{cases}$$ *S16-09 Cl. 13.12.1.2a *AISC Specification 2010 Eq. J3-6b

Resistance Factor, $Ø_b$	=	0.8	0.8	
Resistance Factor, $Ø_u$	=	0.75	0.75	
Tear-out Length, L_c	=	27.0 mm	1 1/16 in	
Bolt Size, d_b	=	19.1 mm	3/4 in	
Supporting Stiffener Thickness, t_{sp}	=	19.1 mm	3/4 in	

Ultimate Strength of Plate, F_u	=	450 MPa	65 ksi	
Factored Bearing Resistance in Supporting Stiffener, B_r	=	767.9 kN	173.0 kips	
Probable Ultimate Strength of Plate, R_yF_u	=	495 MPa	71.5 ksi	
Probable Bearing Resistance in Supporting Stiffener, B_r	=	1126.3 kN	253.7 kips	

Stability

$$\frac{b_{el}}{t} \leq \frac{200}{\sqrt{F_y}}$$

*S16-09 Table 1

Effective Width of Supporting Stiffener, b_{el}	=	182.2 mm	7.17 in	
Supporting Stiffener Thickness, t_{sp}	=	19.1 mm	3/4 in	
Yield Strength of Plate, F_y	=	345 MPa	50 ksi	
Stability Check		Stable		

Beam

Shear Yielding

$$V_{SY} = 0.66\phi_s F_y A_w$$

*S16-09 Cl. 13.4.1.1

Resistance Factor, $Ø_s$	=	0.9	0.9	
Gross Shear Area, $A_w = t_w h_o$	=	1967.5 mm^2	3.05 in^2	
Beam Web Thickness, t_w	=	7.5 mm	0.295 in	
Reduced Beam Height, h_o	=	262.6 mm	10.34 in	
Yield Strength of Beam, F_y	=	345 MPa	50 ksi	
Factored Shear Yielding Resistance in Beam, V_{SY}	=	402.1 kN	90.6 kips	
Probable Yielding Strength of Beam, R_yF_y	=	380 MPa	55 ksi	
Probable Shear Yielding Resistance in Beam, V_{SY}	=	491.5 kN	110.7 kips	

Bearing

$$B_r = min \begin{cases} 3\phi_b d_b t_w F_u C \\ 1.5\phi_u L_c t_w F_u C \end{cases}$$

*S16-09 Cl. 13.12.1.2a
*AISC Specification 2010 Eq. J3-6b

Resistance Factor, $Ø_b$	=	0.8	0.8	
Resistance Factor, $Ø_u$	=	0.75	0.75	
Tear-out Length, L_c	=	27.0 mm	1 1/16 in	
Bolt Size, d_b	=	19.1 mm	3/4 in	
Beam Web Thickness, t_w	=	7.5 mm	0.295 in	
Ultimate Strength of Beam, F_u	=	450 MPa	65 ksi	
Factored Bearing Resistance in Beam, B_r	=	302.1 kN	68.0 kips	
Probable Ultimate Strength of Beam, R_yF_u	=	495 MPa	71.5 ksi	
Probable Bearing Resistance in Beam, B_r	=	443.0 kN	99.8 kips	

Block Shear

$$V_{BS} = \phi_u \left[U_t A_n F_u + 0.6 A_{gv} \frac{F_y + F_u}{2} \right]$$

*S16-09 Cl. 13.11

Resistance Factor, $Ø_u$	=	0.75	0.75	
Efficiency Factor, U_t	=	0.3	0.3	
Net Area, A_n	=	606.7 mm^2	0.94 in^2	
Gross Area in Shear for Block Shear, A_{gv}	=	1522.6 mm^2	2.36 in^2	
Yield Strength of Beam, F_y	=	345 MPa	50 ksi	
Ultimate Strength of Beam, F_u	=	450 MPa	65 ksi	
Factored Block Shear Failure in Beam, V_{BS}	=	332.2 kN	74.8 kips	
Probable Yield Strength of Beam, R_yF_y	=	380 MPa	55 ksi	
Probable Ultimate Strength of Beam, R_yF_u	=	495 MPa	71.5 ksi	
Probable Block Shear Failure in Beam, V_{BS}	=	487.2 kN	109.7 kips	

Flexural Yielding at Cope

$$V_{FY} = \frac{M_{FY}}{e}$$

*S16-09 Cl. 13.5

Resistance Factor, $Ø_s$	=	0.9	0.9	
Elastic Section Modulus of Gross Reduced Area, S_x'	=	203674.2 mm^3	12.43 in^3	
Reduced Beam Height, h_o	=	262.6 mm	10.34 in	
Centroid of Reduced Area, $\bar{y}$	=	100.3 mm	3.95 in	
Moment of Inertia of Gross Reduced Area, I_x'	=	33044612.9 mm^4	79.39 in^4	
Eccentricity to Cope, e	=	216.3 mm	8 1/2 in	
Yield Strength of Beam, F_y	=	345 MPa	50 ksi	
Moment Yielding Resistance at Cope, $M_{FY} = \phi_s F_y S_x'$				

Factored Moment Yielding Resistance at Cope, M_{FY}	=	63.2 kN-m	559.3 kips-in	
Probable Yield Strength of Beam, R_yF_y	=	380 MPa	55 ksi	
Probable Moment Yielding Resistance at Cope, M_{FY}	=	77.2 kN-m	683.6 kips-in	
Factored Flexural Yielding at Cope, V_{FY}	=	291.6 kN	65.7 kips	
Probable Flexural Yielding at Cope, V_{FY}	=	356.4 kN	80.3 kips	

Net Shear Rupture

$V_{SR} = 0.66\phi_u F_u A_{nv}$ *S16-09 Cl. 13.4.1.1

Resistance Factor, $Ø_u$	=	0.75	0.75	
Net Shear Area, $A_{nv} = t_w h_o$ - bolt holts	=	1467.9 mm^2	2.28 in^2	
Beam Web Thickness, t_w	=	7.5 mm	0.295 in	
Reduced Beam Height, h_o	=	262.6 mm	10.34 in	
Ultimate Yield Strength of Beam, F_u	=	450 MPa	65 ksi	
Factored Shear Rupture Resistance in Beam, V_{SR}	=	325.0 kN	73.2 kips	
Probable Ultimate Strength of Beam, R_yF_u	=	495 MPa	72 ksi	
Probable Shear Rupture Resistance in Beam, V_{SR}	=	476.7 kN	107.4 kips	

Flexural Rupture at Last Line of Bolts

$V_{FR} = \frac{M_{FR}}{e}$ *S16-09 Cl. 13.5

Resistance Factor, $Ø_u$	=	0.75	0.75	
Elastic Section Modulus of Net Reduced Area, S_{xn}'	=	180623.0 mm^3	11.02 in^3	
Reduced Beam Height, h_o	=	262.6 mm	10.34 in	
Centroid of Net Reduced Area, $\bar{y}_n$	=	94.5 mm	3.72 in	
Moment of Inertia of Gross Reduced Area, I_{xn}'	=	30359920.2 mm^4	72.94 in^4	
Eccentricity to Last Line of Bolts, e	=	147.4 mm	6.02 in	
Ultimate Yield Strength of Beam, F_u	=	450 MPa	65 ksi	
Moment Rupture Resistance at Last Line of Bolts, $M_{FR} = \phi_u F_u S_{xn}'$				
Factored Moment Rupture Resistance at Last Line of Bolts, M_{FB}	=	60.7 kN-m	537.3 kips-in	
Probable Ultimate Strength of Beam, R_yF_u	=	495 MPa	72 ksi	
Probable Moment Rupture Resistance at Last Line of Bolts, M_{FB}	=	89.1 kN-m	788.1 kips-in	
Factored Flexural Rupture Resistance at Last Line of Bolts, V_{FR}	=	396.6 kN	89.3 kips	
Probable Flexural Rupture Resistance at Last Line of Bolts, V_{FR}	=	581.7 kN	131.0 kips	

Von Mises Interaction

$$\left(\frac{V_{SY}}{V_{VM}}\right)^2 + \left(\frac{M_{FY}}{M_{VM}}\right)^2 \leq 1.0$$

therefore

$$V_{VM} = \frac{\phi_s F_y S_x'}{\sqrt{\left(\frac{S_x'}{0.66A_w}\right)^2 + e^2}}$$

Resistance Factor, $Ø_s$	=	0.9	0.9	
Elastic Section Modulus of Gross Reduced Area, S_x'	=	203674.2 mm^3	12.43 in^3	
Gross Shear Area, A_w	=	1967.5 mm^2	3.05 in^2	
Eccentricity to Cope, e	=	216.3 mm	8 1/2 in	
Yield Strength of Beam, F_y	=	345 MPa	50 ksi	
Factored Von Mises Resistance, V_{VM}	=	236.1	53.2 kips	
Probable Yield Strength of Beam, R_yF_y	=	380 MPa	55 ksi	
Probable Von Mises Resistance, V_{VM}	=	288.6 kips	65.0 kips	

Welds

Weld Strength

$V_W = 0.67\phi_w n_w X_u A_w$ *S16-09 Cl. 13.13.2.2

Resistance Factor, $Ø_w$	=	0.67	0.67	
Number of Welds, n_w	=	2	2	
Ultimate Strength of Electrode, X_u	=	490 MPa	70 ksi	
Welded Area, A_w	=	3777.9 mm^2	5.86 in^2	
Length of Weld (T distance of Girder), L_w	=	673.1 mm	26 1/2 in	
Weld Size, t_w	=	7.9 mm	5/16 in	
Factored Weld Resistance, V_w	=	1634.0 kN	368.0 kips	
Probable Weld Resistance, V_w	=	2438.7 kN	549.3 kips	

Stiffener

Check if Stiffener is Required

$\frac{h_s}{t_w} \leq 60$ *AISC Manual 2011 Part 9

Effective Beam Depth, h_s	=	250.444 mm	9.86 in	
Beam Web Thickness, t_w	=	7.5 mm	0.295 in	
Stiffener Requirement		OK		

Longitudinal Stiffener Extension

$L_{ext} \geq \frac{c}{3}$ *AISC Manual 2011 Part 9

Stiffener Extension Past Cope, L_{ext}	=	88.9 mm	3 1/2 in	
Cope Length, c	=	177.8 mm	7 in	
Extension Length Requirement - AISC Manual 2010 Part 9		OK		

$L_{ext} \geq 2d_c$ *Yam et al. (2011)

Cope Depth, d_c	=	39.7 mm	1 9/16 in	
Extension Length Requirement - Yam et al. (2011)		OK		

Slenderness Check

$\frac{b_s}{t_s} \leq \frac{200}{\sqrt{F_y}}$ *S16-09 Table 1

Width of Horizontal Stiffener, b_s	=	50.8 mm	2 in	
Thickness of Horizontal Stiffener, t_s	=	7.9 mm	5/16 in	
Yield Strength of Stiffener, F_y	=	345 MPa	50 ksi	
Slenderness Check - S16-09 Table 1		OK		Note: Critical Check

$\frac{b_s}{t_s} \leq \frac{95}{\sqrt{F_y}}$ *AISC Specification 2010 Table B4.

Slenderness Check - AISC Specification (2010), Compression		OK		

$\frac{b_s}{t_s} \leq 0.95\sqrt{\frac{k_c E}{F_L}}$ *AISC Specification 2010 Table B4.

Modulus of Elasticity, E	=	200000 MPa	29000 ksi	
$k_c = \frac{4}{\sqrt{\frac{h_s'}{t_w}}}$	=	0.746	0.746	
Effective Beam Depth Below Horizontal Stiffener, h_s'	=	215.4 mm	8.48 in	
Distance from Stiffener to Bottom Flange, h_s'+k	=	241.3	9 1/2	
k distance of Beam	=	25.9	1.02	
Beam Web Thickness, t_w	=	7.5 mm	0.295 in	
$F_L = 0.7F_y$	=	241.5 MPa	35 ksi	
Yield Strength of Beam, F_y	=	345 MPa	50 ksi	
Slenderness Check - AISC Specification (2010), Welded Flexure		OK		

Welds Along Stiffener

$V_W = 0.67\phi_w n_w X_u A_w$ *S16-09 Cl. 13.13.2.2

Resistance Factor, $Ø_w$	=	0.67	0.67	
Number of Welds, n_w	=	2	2	
Ultimate Strength of Electrode, X_u	=	490 MPa	70 ksi	
Welded Area, A_w	=	399.2 mm^2	0.62 in^2	
Length of Weld (Only Considering Extension Past Cope), L_w	=	88.9 mm	3 1/2 in	
Weld Size, t_w	=	6.4 mm	1/4 in	
Factored Weld Resistance, V_w	=	172.6 kN	38.9 kips	
Probable Weld Resistance, V_w	=	257.7 kN	58.0 kips	

Check if Shear Resistance is Greater than Axial Capacity

$T_{st} = \phi_s F_y A_{st}$

Resistance Factor, $Ø_s$	=	0.9	0.9	
Yield Strength of Stiffener, F_y	=	345 MPa	50 ksi	
Area of Stiffener, A_{st}	=	403.2 mm^2	5/8 in^2	
Effective Width of Horizontal Stiffener, b_s	=	50.8 mm	2 in	
Thickness of Horizontal Stiffener, t_s	=	7.9 mm	5/16 in	
Factored Axial Capacity, T_{st}	=	714.4 kN	28.1 kips	
Probable Yield Strength of Stiffener, R_yF_y	=	380 MPa	55 ksi	
Probable Axial Capacity, T_{st}	=	873.1 kN	34.4 kips	
Factored Weld Resistance Greater than Factored Tensile Strength		OK		
Probable Weld Resistance Greater than Factored Tensile Strength		OK		

Beam Web Shear Yielding Along Weld

$V_{BYW} = 0.66\phi_s m F_y t_w L_{ext}$

Resistance Factor, $Ø_s$	=	0.9	0.9
Shear Planes, m	=	1	1
Yield Strength of Beam, F_y	=	345 MPa	50 ksi
Beam Web Thickness, t_w	=	7.5 mm	0.295 in
Stiffener Extension Past Cope, L_{ext}	=	88.9 mm	3 1/2 in
Factored Beam Web Shear Yielding Along Weld, V_{BYW}	=	136.2 kN	30.7 kips
Factored Shear Resistance Greater than Factored Tensile Strength		OK	
Probable Yield Strength of Beam, R_yF_y	=	380 MPa	55 ksi
Probable Beam Web Shear Yielding Along Weld, V_{BYW}	=	166.4 kN	37.5 kips
Probable Weld Resistance Greater than Factored Tensile Strength		Not OK	

Specimen 3 - Single Cope Doubler Plate

Configuration Parameters

Girder		W760x257	(W30x173)	
Beam		W310x60	(W12x40)	
Supporting Stiffener Thickness, t_{sp}	=	19.1 mm	3/4 in	
Cope Length, c	=	177.8 mm	7 in	
Cope Depth, d_c	=	39.7 mm	1 9/16 in	
Bolt Size, d_b	=	19.1 mm	3/4 in	
Number of Bolt Lines, m	=	2	2	
Number of Bolt Rows, n	=	3	3	
Bolt Gauge Distance, D	=	76.2 mm	3 in	
Bolt Pitch Distance, b	=	76.2 mm	3 in	
Bolt Edge Distance - Horizontal	=	38.1 mm	1 1/2 in	
Bolt Edge Distance - Vertical	=	44.45 mm	1 3/4 in	
Gap from Beam End to Girder	=	30.2 mm	1 3/16 in	
Thickness of Doubler Plate, t_{dp}	=	6.4 mm	1/4 in	
Depth of Doubler Plate, d_{dp}	=	215.9 mm	8 1/2 in	
Length of Doubler Plate, L_{dp}	=	244.5 mm	9 5/8 in	

Computing ICR Coefficient, C *CISC Handbook 2009 Table 3-15

Moment Arm, L	=	114.7 mm	4.52 in	
Number of Bolt Lines, m	=	2	2	
Gauge, D	=	76.2 mm	3 in	
Number of Bolt Rows, n	=	3	3	
Pitch, b	=	76.2 mm	3 in	
L_1	=	100 mm		
C_1	=	3.25		Linear Interpolation
L_2	=	125 mm		
C_2	=	2.77		
Eccentric Loading Coefficient, C	=	2.968	2.968	

Bolts

Bolt Shear

$$V_{Bolt} = 0.6\phi_b n m A_b F_u C$$ *S16-09 Cl. 13.12.1.2c

Resistance Factor, $Ø_b$	=	0.8	0.8	
Number of Bolts, n	=	1	1	
Number of Shear Planes, m	=	1	1	
Bolt Area, A_b	=	285 mm^2	0.442 in^2	
Tensile Strength of Bolts, F_u	=	825 MPa	120 ksi	
Factored Bolt Shear Resistance, V_{Bolt}	=	335.5 kN	75.6 kips	
Probable Bolt Shear Resistance, V_{Bolt}	=	419.4 kN	94.5 kips	

Supporting Stiffener

Shear Yielding

$$V_{SY} = 0.66\phi_s F_y A_w$$ *S16-09 Cl. 13.4.1.1

Resistance Factor, $Ø_s$	=	0.9	0.9	
Gross Shear Area, $A_w = t_{sp}d_{sp}$	=	4354.8 mm^2	6.75 in^2	
Supporting Stiffener Thickness, t_{sp}	=	19.1 mm	3/4 in	
Supporting Stiffener Depth, d_{sp}	=	228.6 mm	9 in	
Yield Strength of Plate, F_y	=	345 MPa	50 ksi	
Factored Shear Yielding Resistance in Supporting Stiffener, V_{SY}	=	890.1 kN	200.5 kips	
Probable Yielding Strength of Plate, R_yF_y	=	380 MPa	55 ksi	
Probable Shear Yielding Resistance in Supporting Stiffener, V_{SY}	=	1087.9 kN	245.0 kips	

Bearing

$$B_r = min\begin{cases} 3\phi_b d_b t_{sp} F_u C \\ 1.5\phi_u L_c t_{sp} F_u C \end{cases}$$ *S16-09 Cl. 13.12.1.2a *AISC Specification 2010 Eq. J3-6b

Resistance Factor, $Ø_b$	=	0.8	0.8	
Resistance Factor, $Ø_u$	=	0.75	0.75	
Tear-out Length, L_c	=	27.0 mm	1 1/16 in	
Bolt Size, d_b	=	19.1 mm	3/4 in	
Supporting Stiffener Thickness, t_{sp}	=	19.1 mm	3/4 in	

Ultimate Strength of Plate, F_u	=	450 MPa	65 ksi	
Factored Bearing Resistance in Supporting Stiffener, B_r	=	767.9 kN	173.0 kips	
Probable Ultimate Strength of Plate, R_yF_u	=	495 MPa	71.5 ksi	
Probable Bearing Resistance in Supporting Stiffener, B_r	=	1126.3 kN	253.7 kips	

Stability

$$\frac{b_{el}}{t} \leq \frac{200}{\sqrt{F_y}}$$

*S16-09 Table 1

Effective Width of Supporting Stiffener, b_{el}	=	182.2 mm	7.17 in	
Supporting Stiffener Thickness, t_{sp}	=	19.1 mm	3/4 in	
Yield Strength of Plate, F_y	=	345 MPa	50 ksi	
Stability Check		Stable		

Beam

Shear Yielding

$$V_{SY} = 0.66\phi_s F_y A_w$$

*S16-09 Cl. 13.4.1.1

Resistance Factor, $Ø_s$	=	0.9	0.9	
Gross Shear Area, $A_w = (t_w*h_o)+(t_{dp}*d_{dp})$	=	3338.42 mm^2	5.17 in^2	
Beam Web Thickness, t_w	=	7.5 mm	0.295 in	
Reduced Beam Height, h_o	=	262.6 mm	10.34 in	
Doubler Plate Thickness, t_{dp}	=	6.35 mm	1/4 in	
Depth of Doubler Plate, d_{dp}	=	215.90 mm	8 1/2 in	
Yield Strength of Beam and Plate, F_y	=	345 MPa	50 ksi	
Factored Shear Yielding Resistance in Beam, V_{SY}	=	682.4 kN	153.7 kips	
Probable Yielding Strength of Beam and Plate, R_yF_y	=	380 MPa	55 ksi	
Probable Shear Yielding Resistance in Beam, V_{SY}	=	834.0 kN	187.8 kips	

Bearing

$$B_r = min\begin{cases} 3\phi_b d_b (t_w + t_{dp}) F_u C \\ 1.5\phi_u L_c (t_w + t_{dp}) F_u C \end{cases}$$

*S16-09 Cl. 13.12.1.2a
*AISC Specification 2010 Eq. J3-6b

Resistance Factor, $Ø_b$	=	0.8	0.8	
Resistance Factor, $Ø_u$	=	0.75	0.75	
Tear-out Length, L_c	=	27.0 mm	1 1/16 in	
Bolt Size, d_b	=	19.1 mm	3/4 in	
Beam Web Thickness, t_w	=	7.5 mm	0.295 in	
Doubler Plate Thickness, t_{dp}	=	6.4 mm	1/4 in	
Ultimate Strength of Beam and Plate, F_u	=	450 MPa	65 ksi	
Factored Bearing Resistance in Beam, B_r	=	558.0 kN	125.7 kips	
Probable Ultimate Strength of Beam and Plate, R_yF_u	=	495 MPa	71.5 ksi	
Probable Bearing Resistance in Beam, B_r	=	818.4 kN	184.3 kips	

Block Shear

$$V_{BS} = \phi_u \left[U_t A_n F_u + 0.6 A_{gv} \frac{F_y + F_u}{2} \right]$$

*S16-09 Cl. 13.11

Resistance Factor, $Ø_u$	=	0.75	0.75	
Efficiency Factor, U_t	=	0.3	0.3	
Net Area, A_n	=	1120.8 mm^2	1.74 in^2	
Gross Area in Shear for Block Shear, A_{gv}	=	2725.0 mm^2	4.22 in^2	
Yield Strength of Beam and Plate, F_y	=	345 MPa	50 ksi	
Ultimate Strength of Beam and Plate, F_u	=	450 MPa	65 ksi	
Factored Block Shear Failure in Beam, V_{BS}	=	598.0 kN	134.7 kips	
Probable Yield Strength of Beam and Plate, R_yF_y	=	380 MPa	55 ksi	
Probable Ultimate Strength of Beam and Plate, R_yF_u	=	495 MPa	71.5 ksi	
Probable Block Shear Failure in Beam, V_{BS}	=	877.1 kN	197.6 kips	

Flexural Yielding at Cope

$$V_{FY} = \frac{M_{FY}}{e}$$

*S16-09 Cl. 13.5

Resistance Factor, $Ø_s$	=	0.9	0.9	
Elastic Section Modulus of Gross Reduced Area, S_x'	=	197693.3 mm^3	12.06 in^3	
Reduced Beam Height, h_o	=	262.6 mm	10.34 in	
Centroid of Reduced Area, $\bar{y}$	=	99.8 mm	3.93 in	
Moment of Inertia of Gross Reduced Area, I_x'	=	32174689.2 mm^4	77.3 in^4	

Eccentricity to Cope, e	=	216.3 mm	8 1/2 in	
Yield Strength of Beam and Plate, F_y	=	345 MPa	50 ksi	
Moment Yielding Resistance at Cope, $M_{FY} = \phi_s F_y S_x'$				
Factored Moment Yielding Resistance at Cope, M_{FY}	=	61.3 kN-m	542.9 kips-in	
Probable Yield Strength of Beam and Plate, $R_y F_y$	=	380 MPa	55 ksi	
Probable Moment Yielding Resistance at Cope, M_{FY}	=	75.0 kN-m	663.5 kips-in	
Factored Flexural Yielding at Cope, V_{FY}	=	283.1 kN	63.8 kips	
Probable Flexural Yielding at Cope, V_{FY}	=	346.0 kN	77.9 kips	

Flexural Buckling at Cope

$$V_{FB} = \frac{M_{FB}}{e}$$

Resistance Factor, $Ø_s$	=	0.9	0.9	
Modulus of Elasticity, E	=	200000 MPa	29000 ksi	
Poisson's Ratio, ν	=	0.3	0.3	
Beam Web Thickness, t_w	=	7.5 mm	0.295 in	
Doubler Plate Thickness, t_{dp}	=	6.4 mm	1/4 in	
Beam Depth, d	=	302.3 mm	11.9 in	
Effective Reduced Beam Depth, h_1	=	162.8 mm	6.41 in	
Reduced Beam Height, h_o	=	262.6 mm	10.34 in	
Centroid of Reduced Area, $\bar{y}$	=	99.8 mm	3.93 in	
Cope Length, c	=	177.8 mm	7.0 in	

$$F_{cr} = \frac{\pi^2 E}{12(1-\nu^2)}\left(\frac{t_w + t_{dp}}{h_1}\right)^2 fk$$ *AISC Manual 2011 Part 9

Plate Buckling Model Adjustment Factor, f

$$f = \begin{cases} \frac{2c}{d} \text{ when } \frac{c}{d} \le 1.0 \\ 1 + \frac{c}{d} \text{ when } \frac{c}{d} > 1.0 \end{cases}$$ = 1.18 1.18

Plate Buckling Coefficient, k

$$k = \begin{cases} 2.2\left(\frac{h_1}{c}\right)^{1.65} \text{ when } \frac{c}{h_1} \le 1.0 \\ \frac{2.2h_1}{c} \text{ when } \frac{c}{h_1} > 1.0 \end{cases}$$ = 2.01 2.01

Critical Buckling Stress, F_{cr}	=	3135.7 MPa	449.2 ksi	
Elastic Section Modulus of Gross Reduced Area, S_x'	=	197693.3 mm^3	12.06 in^3	
Eccentricity to Cope, e	=	216.3 mm	8 1/2 in	
Moment Buckling Resistance at Cope, $M_{FB} = \phi_s F_{cr} S_x'$				
Factored Moment Buckling Resistance at Cope, M_{FB}	=	551.2 kN-m	4877.7 kips-in	
Probable Moment Buckling Resistance at Cope, M_{FB}	=	612.4 kN-m	5419.7 kips-in	
Factored Flexural Buckling at Cope, V_{FB}	=	2543.4 kN	572.8 kips	
Probable Flexural Buckling at Cope, V_{FB}	=	2826.0 kN	636.5 kips	

Net Shear Rupture

$$V_{SR} = 0.66\phi_u F_u A_{nv}$$ *S16-09 Cl. 13.4.1.1

Resistance Factor, $Ø_u$	=	0.75	0.75	
Net Shear Area, A_{nv}	=	2415.4 mm^2	3.74 in^2	
Beam Web Thickness, t_w	=	7.5 mm	0.295 in	
Doubler Plate Thickness, t_{dp}	=	6.4 mm	1/4 in	
Reduced Beam Height, h_o	=	262.6 mm	10.34 in	
Depth of Doubler Plate, d_{dp}	=	215.9 mm	8 1/2 in	
Ultimate Yield Strength of Beam and Plate, F_u	=	450 MPa	65 ksi	
Factored Shear Rupture Resistance in Beam, V_{SR}	=	534.8 kN	120.5 kips	
Probable Ultimate Strength of Beam and Plate, $R_y F_u$	=	495 MPa	72 ksi	
Probable Shear Rupture Resistance in Beam, V_{SR}	=	784.4 kN	176.7 kips	

Flexural Rupture at Last Line of Bolts

$$V_{FR} = \frac{M_{FR}}{e}$$ *S16-09 Cl. 13.5

Resistance Factor, $Ø_u$	=	0.75	0.75	
Elastic Section Modulus of Net Reduced Area, S_{xn}'	=	188170.7 mm^3	11.48 in^3	
Reduced Beam Height, h_o	=	262.6 mm	10.34 in	
Centroid of Net Reduced Area, $\bar{y}_n$	=	97.5 mm	3.84 in	
Moment of Inertia of Gross Reduced Area, I_{xn}'	=	31055026.7 mm^4	74.61 in^4	

Eccentricity to Last Line of Bolts, e	=	147.4 mm	6.02 in
Ultimate Yield Strength of Beam and Plate, F_u	=	450 MPa	65 ksi
Moment Rupture Resistance at Last Line of Bolts, $M_{FR} = \phi_u F_u S_{xn}'$			
Factored Moment Rupture Resistance at Last Line of Bolts, M_{FB}	=	63.3 kN-m	559.8 kips-in
Probable Ultimate Strength of Beam and Plate, R_yF_u	=	495 MPa	72 ksi
Probable Moment Rupture Resistance at Last Line of Bolts, M_{FB}	=	92.8 kN-m	821.0 kips-in
Factored Flexural Rupture Resistance at Last Line of Bolts, V_{FR}	=	413.2 kN	93.1 kips
Probable Flexural Rupture Resistance at Last Line of Bolts, V_{FR}	=	606.0 kN	136.5 kips

Von Mises Interaction

$$\left(\frac{V_{SY}}{V_{VM}}\right)^2 + \left(\frac{M_{FY}}{M_{VM}}\right)^2 \leq 1.0$$

therefore

$$V_{VM} = \frac{\phi_s F_y S_x'}{\sqrt{\left(\frac{S_x'}{0.66A_w}\right)^2 + e^2}}$$

Resistance Factor, $Ø_s$	=	0.9	0.9
Elastic Section Modulus of Gross Reduced Area, S_x'	=	197693.3 mm^3	12.06 in^3
Gross Shear Area, A_w	=	3338.4 mm^2	5.17 in^2
Eccentricity to Cope, e	=	216.3 mm	8 1/2 in
Yield Strength of Beam and Plate, F_y	=	345 MPa	50 ksi
Factored Von Mises Resistance, V_{VM}	=	261.5	58.9 kips
Probable Yield Strength of Beam and Plate, R_yF_y	=	380 MPa	55 ksi
Probable Von Mises Resistance, V_{VM}	=	319.6 kips	72.0 kips

Welds

Weld Strength

$V_W = 0.67\phi_w n_w X_u A_w$ *S16-09 Cl. 13.13.2.2

Resistance Factor, $Ø_w$	=	0.67	0.67
Number of Welds, n_w	=	2	2
Ultimate Strength of Electrode, X_u	=	490 MPa	70 ksi
Welded Area, A_w	=	3777.9 mm^2	5.86 in^2
Length of Weld (T distance of Girder), L_w	=	673.1 mm	26 1/2 in
Weld Size, t_w	=	7.9 mm	5/16 in
Factored Weld Resistance, V_w	=	1634.0 kN	368.0 kips
Probable Weld Resistance, V_w	=	2438.7 kN	549.3 kips

Doubler Plate

Sizing of Welds Between Beam and Doubler Plate *Blodgett (1966)

Flexural Strength of Doubler Past Cope, $M_{DP} = \phi_s S_{DP} F_y$

Resistance Factor, $Ø_s$	=	0.9	0.9
Elastic Section Modulus of Doubler Plate, S_{DP}	=	49331.9 mm^3	3.0 in^3
Thickness of Doubler Plate, t_{dp}	=	6.4 mm	1/4 in
Depth of Doubler Plate, d_{dp}	=	215.9 mm	8 1/2 in
Yield Strength of Doubler Plate, F_y	=	345 MPa	50 ksi
Factored Flexural Strength of Doubler Plate, M_{DP}	=	15.3 kN-m	135.5 kips-in
Probable Yield Strength of Doubler Plate, R_yF_y	=	379.5 MPa	55 ksi
Probable Flexural Strength of Doubler Plate, M_{DP}	=	18.7 kN-m	165.6 kips-in
Torsional Constant, $J_w = \frac{(2b+d)^3}{12} - \frac{b^2(b+d)^2}{(2b+d)}$	=	2818015.8 mm^3	172.0 in^3
Length of Weld Group Past Cope, b	=	76.2 mm	3 in
Depth of Weld Group (Depth of Doubler Plate), d	=	215.9 mm	8 1/2 in
Horizontal Eccentricity of Weld Group Past Cope, e_x	=	60.43 mm	2.38 in
Vertical Eccentricity of Weld Group Past Cope, e_y	=	107.95 mm	4.25 in
Factored Horizontal Force per Unit Length, $f_x = \frac{M_{DP}e_x}{J_w}$	=	0.33 kN/mm	1.87 kips/in
Probable Horizontal Force per Unit Length, f_x	=	0.40 kN/mm	2.29 kips/in
Factored Vertical Force per Unit Length, $f_y = \frac{M_{DP}e_y}{J_w}$	=	0.59 kN/mm	3.35 kips/in

Probable Vertical Force per Unit Length, f_y	=	0.72 kN/mm	4.09 kips/in	
Factored Resulting Force per Unit Length, $f_w = \sqrt{f_x^2 + f_y^2}$	=	0.67 kN/mm	3.84 kips/in	
Probable Resulting Force per Unit Length, $f_w = \sqrt{f_x^2 + f_y^2}$	=	0.82 kN/mm	4.69 kips/in	
Factored Weld Strength Per Weld Area, V_w	=	155.5 kN/mm	22.2 kips/in^2	*S16-09 Cl. 13.13.2.2
Probable Weld Strength Per Weld Area, V_w	=	232.1 kN/mm	33.2 kips/in^2	
Weld Size Based on Factored Strength, $D_w \geq \frac{f_w}{V_w}$	=	4.8 mm	3/16 in	Note: Rounding to nearest 16th of an inch
Weld Size Based on Probable Strength, $D_w \geq \frac{f_w}{V_w}$	=	3.2 mm	1/8 in	Note: Rounding to nearest 16th of an inch
Therefore Select Adequate Weld Size	=	4.8 mm	3/16 in	

$V_{W-Weld} = 0.67\phi_w n_w X_u A_w (1.00 + 0.5sin^{1.5}\theta) M_w$ *S16-09 Cl. 13.13.2.2

Resistance Factor, $Ø_w$	=	0.67	0.67	
Number of Welds- End Welds, n_w	=	1	1	
Number of Welds- Side Welds, n_w	=	2	2	
Ultimate Strength of Electrode, X_u	=	490 MPa	70 ksi	
Parallel to Shear Force Welded Area (End Weld), A_w	=	727.1 mm^2	1.13 in^2	
Length of Weld (Depth of Doubler Plate), L_w	=	215.9 mm	8 1/2 in	
Weld Size, t_w	=	4.8 mm	3/16 in	
Perpendicular to Shear Force Welded Area (Side Weld), A_w	=	256.6 mm^2	0.40 in^2	
Length of Weld (Length of Weld Group Past Cope), L_w	=	76.2 mm	3 in	
Weld Size, t_w	=	4.8 mm	3/16 in	
Strength Reduction Factor, $M_w = \frac{0.85 + \theta_1/600}{0.85 + \theta_2/600}$				
Reduction Factor for End Weld	=	0.85		
θ_1	=	0 degree	0 degrees	
θ_2	=	90 degree	90 degrees	
Reduction Factor for Side Weld	=	1		
θ_1	=	90 degree	90 degrees	
θ_2	=	90 degree	90 degrees	
Factored Weld Metal Strength Past Cope, $V_{W\text{-}Weld}$	=	291.5 kN	65.7 kips	
Probable Weld Metal Strength Past Cope, $V_{W\text{-}Weld}$	=	435.1 kN	98.0 kips	

Base Metal Strength Past Cope

$V_{W-Base} = 0.67\phi_w F_u A_w$ *S16-09 Cl. 13.13.2.2

Resistance Factor, $Ø_w$	=	0.67	0.67	
Parallel to Shear Force Welded Area (End Weld), A_w	=	1028.2 mm^2	1.59 in^2	
Length of Weld (Depth of Doubler Plate), L_w	=	215.9 mm	8 1/2 in	
Weld Size, t_w	=	4.8 mm	3/16 in	
Perpendicular to Shear Force Welded Area (Side Weld), A_w	=	362.9 mm^2	0.56 in^2	
Length of Weld (Length of Weld Group Past Cope), L_w	=	76 mm	3 in	
Weld Size, t_w	=	4.8 mm	3/16 in	
Ultimate Yield Strength of Beam, F_u	=	450 MPa	65 ksi	
Factored Base Metal Strength Past Cope, $V_{W\text{-}Base}$	=	352.2 kN	79.3 kips	
Probable Ultimate Strength of Beam, R_yF_u	=	495 MPa	72 ksi	
Probable Base Metal Strength Past Cope, $V_{W\text{-}Base}$	=	578.3 kN	130.2 kips	
Check Base Metal Strength Larger than Weld Metal Strength (Factored)		OK		
Check Base Metal Strength Larger than Weld Metal Strength (Probable)		OK		

Specimen 4 - Double Cope Unreinforced

Configuration Parameters

Girder		W610x155	(W24x104)	
Beam		W610x113	(W24x76)	
Supporting Stiffener Thickness, t_{sp}	=	15.9 mm	5/8 in	
Cope Length, c	=	168.3 mm	6 5/8 in	
Cope Depth, d_c	=	41.3 mm	1 5/8 in	
Bolt Size, d_b	=	22.2 mm	7/8 in	
Number of Bolt Lines, m	=	2	2	
Number of Bolt Rows, n	=	6	6	
Bolt Gauge Distance, D	=	76.2 mm	3 in	
Bolt Pitch Distance, b	=	76.2 mm	3 in	
Bolt Edge Distance - Horizontal	=	38.1 mm	1 1/2 in	
Bolt Edge Distance - Vertical	=	41.3 mm	1 5/8 in	
Supporting Stiffener Edge Distance	=	44.5 mm	1 3/4 in	
Gap from Beam End to Girder	=	12.7 mm	1/2 in	

Computing ICR Coefficient, C *CISC Handbook 2009 Table 3-15

Moment Arm, L	=	95.3 mm	3.75 in	
Number of Bolt Lines, m	=	2	2	
Gauge, D	=	76.2 mm	3 in	
Number of Bolt Rows, n	=	6	6	
Pitch, b	=	76.2 mm	3 in	
L_1	=	75 mm		
C_1	=	10.30		Linear Interpolation
L_2	=	100 mm		
C_2	=	9.33		
Eccentric Loading Coefficient, C	=	9.514	9.514	

Bolts

Bolt Shear

$$V_{Bolt} = 0.6\phi_b n m A_b F_u C$$

*S16-09 Cl. 13.12.1.2c

Resistance Factor, $Ø_b$	=	0.8	0.8	
Number of Bolts, n	=	1	1	
Number of Shear Planes, m	=	1	1	
Bolt Area, A_b	=	388 mm2	0.601 in2	
Tensile Strength of Bolts, F_u	=	825 MPa	120 ksi	
Factored Bolt Shear Resistance, V_{Bolt}	=	1462.4 kN	329.4 kips	
Probable Bolt Shear Resistance, V_{Bolt}	=	1828.0 kN	411.7 kips	

Supporting Stiffener

Shear Yielding

$$V_{SY} = 0.66\phi_s F_y A_w$$

*S16-09 Cl. 13.4.1.1

Resistance Factor, $Ø_s$	=	0.9	0.9	
Gross Shear Area, $A_w = t_{sp} d_{sp}$	=	3629.0 mm^2	12.9 in^2	
Supporting Stiffener Thickness, t_{sp}	=	15.9 mm	5/8 in	
Supporting Stiffener Depth, $d_{sp} = \min(d_{beam} - d_c, T_{girder})$	=	228.6 mm	20.7 in	
Yield Strength of Plate, F_y	=	345 MPa	50 ksi	
Factored Shear Yielding Resistance in Supporting Stiffener, V_{SY}	=	1701.9 kN	383.3 kips	
Probable Yielding Strength of Plate, $R_y F_y$	=	380 MPa	55 ksi	
Probable Shear Yielding Resistance in Supporting Stiffener, V_{SY}	=	2080.1 kN	468.5 kips	

Bearing

$$B_r = \min \begin{cases} 3\phi_b d_b t_{sp} F_u C \\ 1.5\phi_u L_c t_{sp} F_u C \end{cases}$$

*S16-09 Cl. 13.12.1.2a
*AISC Specification 2010 Eq. J3-6b

Resistance Factor, $Ø_b$	=	0.8	0.8	
Resistance Factor, $Ø_u$	=	0.75	0.75	
Tear-out Length, L_c	=	31.8 mm	1 1/4 in	
Bolt Size, d_b	=	22.2 mm	7/8 in	

Supporting Stiffener Thickness, t_{sp}	=	15.9 mm	5/8 in	
Ultimate Strength of Plate, F_u	=	450 MPa	65 ksi	
Factored Bearing Resistance in Supporting Stiffener, B_r	=	2413.3 kN	543.5 kips	
Probable Ultimate Strength of Plate, R_yF_u	=	495 MPa	71.5 ksi	
Probable Bearing Resistance in Supporting Stiffener, B_r	=	3539.5 kN	797.2 kips	

Stability

$$\frac{b_{el}}{t} \leq \frac{200}{\sqrt{F_y}}$$ *S16-09 Table 1

Effective Width of Supporting Stiffener, b_{el}	=	168.9 mm	6.65 in	
Supporting Stiffener Thickness, t_{sp}	=	15.9 mm	5/8 in	
Yield Strength of Plate, F_y	=	345 MPa	50 ksi	
Stability Check		Stable		

Beam

Shear Yielding

$$V_{SY} = 0.66\phi_s F_y A_w$$ *S16-09 Cl. 13.4.1.1

Resistance Factor, $Ø_s$	=	0.9	0.9	
Gross Shear Area, $A_w = t_w h_o$	=	5861.9 mm^2	9.09 in^2	
Beam Web Thickness, t_w	=	11.2 mm	0.440 in	
Reduced Beam Height, h_o	=	524.5 mm	20.65 in	
Yield Strength of Beam, F_y	=	345 MPa	50 ksi	
Factored Shear Yielding Resistance in Beam, V_{SY}	=	1198.2 kN	269.9 kips	
Probable Yielding Strength of Beam, R_yF_y	=	380 MPa	55 ksi	
Probable Shear Yielding Resistance in Beam, V_{SY}	=	1464.4 kN	329.8 kips	

Bearing

$$B_r = min \begin{cases} 3\phi_b d_b t_w F_u C \\ 1.5\phi_u L_c t_w F_u C \end{cases}$$ *S16-09 Cl. 13.12.1.2a *AISC Specification 2010 Eq. J3-6b

Resistance Factor, $Ø_b$	=	0.8	0.8	
Resistance Factor, $Ø_u$	=	0.75	0.75	
Tear-out Length, L_c	=	25.4 mm	1 in	
Bolt Size, d_b	=	22.2 mm	7/8 in	
Beam Web Thickness, t_w	=	11.2 mm	0.440 in	
Ultimate Strength of Beam, F_u	=	450 MPa	65 ksi	
Factored Bearing Resistance in Beam, B_r	=	1359.2 kN	306.1 kips	
Probable Ultimate Strength of Beam, R_yF_u	=	495 MPa	71.5 ksi	
Probable Bearing Resistance in Beam, B_r	=	1993.5 kN	449.0 kips	

Block Shear

$$V_{BS} = \phi_u \left[U_t A_n F_u + 0.6 A_{gv} \frac{F_y + F_u}{2} \right]$$ *S16-09 Cl. 13.11

Resistance Factor, $Ø_u$	=	0.75	0.75	
Efficiency Factor, U_t	=	0.3	0.3	
Net Area, A_n	=	851.6 mm^2	1.32 in^2	
Gross Area in Shear for Block Shear, A_{gv}	=	4719.3 mm^2	7.32 in^2	
Yield Strength of Beam, F_y	=	345 MPa	50 ksi	
Ultimate Strength of Beam, F_u	=	450 MPa	65 ksi	
Factored Block Shear Failure in Beam, V_{BS}	=	926.1 kN	208.6 kips	
Probable Yield Strength of Beam, R_yF_y	=	380 MPa	55 ksi	
Probable Ultimate Strength of Beam, R_yF_u	=	495 MPa	71.5 ksi	
Probable Block Shear Failure in Beam, V_{BS}	=	1358.3 kN	305.9 kips	

Flexural Yielding at Cope

$$V_{FY} = \frac{M_{FY}}{e}$$ *S16-09 Cl. 13.5

Resistance Factor, $Ø_s$	=	0.9	0.9	
Elastic Section Modulus of Gross Reduced Area, S_x'	=	512439.6 mm^3	31.27 in^3	
Reduced Beam Height, h_o	=	524.5 mm	20.65 in	
Beam Web Thickness, t_w	=	11.2 mm	0.440 in	
Eccentricity to Cope, e	=	187.3 mm	7 3/8 in	

Yield Strength of Beam, F_y	=	345 MPa	50 ksi	
Moment Yielding Resistance at Cope, $M_{FY} = \phi_s F_y S_x'$				
Factored Moment Yielding Resistance at Cope, M_{FY}	=	159.0 kN-m	1407.2 kips-in	
Probable Yield Strength of Beam, R_yF_y	=	380 MPa	55 ksi	
Probable Moment Yielding Resistance at Cope, M_{FY}	=	194.3 kN-m	1719.9 kips-in	
Factored Flexural Yielding at Cope, V_{FY}	=	847.2 kN	190.8 kips	
Probable Flexural Yielding at Cope, V_{FY}	=	1035.4 kN	233.2 kips	

Flexural Buckling at Cope

$$V_{FB} = \frac{M_{FB}}{e}$$

Resistance Factor, $Ø_s$	=	0.9	0.9	
Modulus of Elasticity, E	=	200000 MPa	29000 ksi	
Poisson's Ratio, ν	=	0.3	0.3	
Beam Web Thickness, t_w	=	11.2 mm	0.440 in	
Beam Depth, d	=	607.1 mm	23.9 in	
Reduced Beam Height, h_o	=	524.5 mm	20.65 in	
Cope Length, c	=	168.3 mm	6 5/8 in	
Cope Depth, d_c	=	41.3 mm	1 5/8 in	

$$F_{cr} = 0.62\pi E \frac{t_w^2}{ch_o} f_d$$ *AISC Manual 2011 Part 9

Adjustment Factor, $f_d = 3.5 - 7.5\left(\frac{d_c}{d}\right)$	=	2.99	2.99	
Critical Buckling Stress, F_{cr}	=	1668.3 MPa	239.0 ksi	
Elastic Section Modulus of Gross Reduced Area, S_x'	=	512439.6 mm^3	31.27 in^3	
Eccentricity to Cope, e	=	187.3 mm	7 3/8 in	
Moment Buckling Resistance at Cope, $M_{FB} = \phi_s F_{cr} S_x'$				
Factored Moment Buckling Resistance at Cope, M_{FB}	=	760.1 kN-m	6726.7 kips-in	
Probable Moment Buckling Resistance at Cope, M_{FB}	=	844.6 kN-m	7474.1 kips-in	
Factored Flexural Buckling at Cope, V_{FB}	=	4049.7 kN	912.1 kips	
Probable Flexural Buckling at Cope, V_{FB}	=	4499.7 kN	1013.4 kips	

Net Shear Rupture

$$V_{SR} = 0.66\phi_u F_u A_{nv}$$ *S16-09 Cl. 13.4.1.1

Resistance Factor, $Ø_u$	=	0.75	0.75	
Net Shear Area, $A_{nv} = t_w h_o$ - bolt holts	=	4158.7 mm^2	6.45 in^2	
Beam Web Thickness, t_w	=	11.2 mm	0.440 in	
Reduced Beam Height, h_o	=	524.5 mm	20.65 in	
Ultimate Yield Strength of Beam, F_u	=	450 MPa	65 ksi	
Factored Shear Rupture Resistance in Beam, V_{SR}	=	920.9 kN	207.4 kips	
Probable Ultimate Strength of Beam, R_yF_u	=	495 MPa	72 ksi	
Probable Shear Rupture Resistance in Beam, V_{SR}	=	1350.6 kN	304.2 kips	

Flexural Rupture at Last Line of Bolts

$$V_{FR} = \frac{M_{FR}}{e}$$ *S16-09 Cl. 13.5

Resistance Factor, $Ø_u$	=	0.75	0.75	
Elastic Section Modulus of Net Reduced Area, S_{xn}'	=	373479.7 mm^3	22.79 in^3	
Reduced Beam Height, h_o	=	524.5 mm	20.65 in	
Centroid of Net Reduced Area, $\bar{y}_n$	=	249.7 mm	9.83 in	
Moment of Inertia of Gross Reduced Area, I_{xn}'	=	102642669.6 mm^4	246.6 in^4	
Eccentricity to Last Line of Bolts, e	=	128.6 mm	5.25 in	
Ultimate Yield Strength of Beam, F_u	=	450 MPa	65 ksi	
Moment Rupture Resistance at Last Line of Bolts, $M_{FR} = \phi_u F_u S_{xn}'$				
Factored Moment Rupture Resistance at Last Line of Bolts, M_{FB}	=	125.6 kN-m	1111.1 kips-in	
Probable Ultimate Strength of Beam, R_yF_u	=	495 MPa	72 ksi	
Probable Moment Rupture Resistance at Last Line of Bolts, M_{FB}	=	184.1 kN-m	1629.6 kips-in	
Factored Flexural Rupture Resistance at Last Line of Bolts, V_{FR}	=	939.6 kN	211.6 kips	
Probable Flexural Rupture Resistance at Last Line of Bolts, V_{FR}	=	1378.1 kN	310.4 kips	

Von Mises Interaction

$$\left(\frac{V_{SY}}{V_{VM}}\right)^2 + \left(\frac{M_{FY}}{M_{VM}}\right)^2 \leq 1.0$$

therefore

$$V_{VM} = \frac{\phi_s F_y S_x'}{\sqrt{\left(\frac{S_x'}{0.66A_w}\right)^2 + e^2}}$$

Resistance Factor, $Ø_s$	=	0.9	0.9
Elastic Section Modulus of Gross Reduced Area, S_x'	=	512439.6 mm^3	31.27 in^3
Gross Shear Area, A_w	=	5861.9 mm^2	9.09 in^2
Eccentricity to Cope, e	=	187.3 mm	7 3/8 in
Yield Strength of Beam, F_y	=	345 MPa	50 ksi
Factored Von Mises Resistance, V_{VM}	=	691.7 kN	155.8 kips
Probable Yield Strength of Beam, R_yF_y	=	380 MPa	55 ksi
Probable Von Mises Resistance, V_{VM}	=	845.4 kN	190.4 kips

Welds

Weld Strength

$$V_W = 0.67\phi_w n_w X_u A_w$$

*S16-09 Cl. 13.13.2.2

Resistance Factor, $Ø_w$	=	0.67	0.67
Number of Welds, n_w	=	2	2
Ultimate Strength of Electrode, X_u	=	490 MPa	70 ksi
Welded Area, A_w	=	2958.2 mm^2	4.59 in^2
Length of Weld (T distance of Girder), L_w	=	527.1 mm	20 3/4 in
Weld Size, t_w	=	7.9 mm	5/16 in
Factored Weld Resistance, V_w	=	1279.4 kN	288.2 kips
Probable Weld Resistance, V_w	=	1909.6 kN	430.1 kips

Specimen 5 - Double Cope Horizontal Stiffeners

Configuration Parameters

Girder		W610x155	(W24x104)	
Beam		W610x113	(W24x76)	
Supporting Stiffener Thickness, t_{sp}	=	15.9 mm	5/8 in	
Cope Length, c	=	168.3 mm	6 5/8 in	
Cope Depth, d_c	=	41.3 mm	1 5/8 in	
Bolt Size, d_b	=	22.2 mm	7/8 in	
Number of Bolt Lines, m	=	2	2	
Number of Bolt Rows, n	=	6	6	
Bolt Gauge Distance, D	=	76.2 mm	3 in	
Bolt Pitch Distance, b	=	76.2 mm	3 in	
Bolt Edge Distance - Horizontal	=	38.1 mm	1 1/2 in	
Bolt Edge Distance - Vertical	=	71.4 mm	2 13/16 in	
Supporting Stiffener Edge Distance	=	44.5 mm	1 3/4 in	
Gap from Beam End to Girder	=	12.7 mm	1/2 in	
Horizontal Stiffener Thickness, t_s	=	9.5 mm	3/8 in	
Width of Horizontal Stiffener, b_s	=	76.2 mm	3 in	
Length of Horizontal Stiffener, L_s	=	282.6 mm	11 1/8 in	

Computing ICR Coefficient, C *CISC Handbook 2009 Table 3-15

Moment Arm, L	=	95.3 mm	3.75 in	
Number of Bolt Lines, m	=	2	2	
Gauge, D	=	76.2 mm	3 in	
Number of Bolt Rows, n	=	6	6	
Pitch, b	=	76.2 mm	3 in	
L_1	=	75 mm		
C_1	=	10.30		Linear Interpolation
L_2	=	100 mm		
C_2	=	9.33		
Eccentric Loading Coefficient, C	=	9.514	9.514	

Bolts

Bolt Shear

$$V_{Bolt} = 0.6\phi_b nmA_b F_u C$$ *S16-09 Cl. 13.12.1.2c

Resistance Factor, $Ø_b$	=	0.8	0.8	
Number of Bolts, n	=	1	1	
Number of Shear Planes, m	=	1	1	
Bolt Area, A_b	=	388 mm2	0.601 in2	
Tensile Strength of Bolts, F_u	=	825 MPa	120 ksi	
Factored Bolt Shear Resistance, V_{Bolt}	=	1462.4 kN	329.4 kips	
Probable Bolt Shear Resistance, V_{Bolt}	=	1828.0 kN	411.7 kips	

Supporting Stiffener

Shear Yielding

$$V_{SY} = 0.66\phi_s F_y A_w$$ *S16-09 Cl. 13.4.1.1

Resistance Factor, $Ø_s$	=	0.9	0.9	
Gross Shear Area, $A_w = t_{sp}d_{sp}$	=	3629.0 mm^2	12.9 in^2	
Supporting Stiffener Thickness, t_{sp}	=	15.9 mm	5/8 in	
Supporting Stiffener Depth, $d_{sp} = \min(d_{beam} - d_c, T_{girder})$	=	228.6 mm	20.7 in	
Yield Strength of Plate, F_y	=	345 MPa	50 ksi	
Factored Shear Yielding Resistance in Supporting Stiffener, V_{SY}	=	1701.9 kN	383.3 kips	
Probable Yielding Strength of Plate, R_yF_y	=	380 MPa	55 ksi	
Probable Shear Yielding Resistance in Supporting Stiffener, V_{SY}	=	2080.1 kN	468.5 kips	

Bearing

$$B_r = min\begin{cases} 3\phi_b d_b t_{sp} F_u C \\ 1.5\phi_u L_c t_{sp} F_u C \end{cases}$$ *S16-09 Cl. 13.12.1.2a *AISC Specification 2010 Eq. J3-6b

Resistance Factor, $Ø_b$	=	0.8	0.8	
Resistance Factor, $Ø_u$	=	0.75	0.75	

Tear-out Length, L_c	=	31.8 mm	1 1/4 in	
Bolt Size, d_b	=	22.2 mm	7/8 in	
Supporting Stiffener Thickness, t_{sp}	=	15.9 mm	5/8 in	
Ultimate Strength of Plate, F_u	=	450 MPa	65 ksi	
Factored Bearing Resistance in Supporting Stiffener, B_r	=	2413.3 kN	543.5 kips	
Probable Ultimate Strength of Plate, R_yF_u	=	495 MPa	71.5 ksi	
Probable Bearing Resistance in Supporting Stiffener, B_r	=	3539.5 kN	797.2 kips	

Stability

$$\frac{b_{el}}{t} \leq \frac{200}{\sqrt{F_y}}$$

*S16-09 Table 1

Effective Width of Supporting Stiffener, b_{el}	=	168.9 mm	6.65 in	
Supporting Stiffener Thickness, t_{sp}	=	15.9 mm	5/8 in	
Yield Strength of Plate, F_y	=	345 MPa	50 ksi	
Stability Check		Stable		

Beam

Shear Yielding

$$V_{SY} = 0.66\phi_s F_y A_w$$

*S16-09 Cl. 13.4.1.1

Resistance Factor, $Ø_s$	=	0.9	0.9	
Gross Shear Area, $A_w = t_w h_o$	=	5861.9 mm^2	9.09 in^2	
Beam Web Thickness, t_w	=	11.2 mm	0.440 in	
Reduced Beam Height, h_o	=	524.5 mm	20.65 in	
Yield Strength of Beam, F_y	=	345 MPa	50 ksi	
Factored Shear Yielding Resistance in Beam, V_{SY}	=	1198.2 kN	269.9 kips	
Probable Yielding Strength of Beam, R_yF_y	=	380 MPa	55 ksi	
Probable Shear Yielding Resistance in Beam, V_{SY}	=	1464.4 kN	329.8 kips	

Bearing

$$B_r = min \begin{cases} 3\phi_b d_b t_w F_u C \\ 1.5\phi_u L_c t_w F_u C \end{cases}$$

*S16-09 Cl. 13.12.1.2a
*AISC Specification 2010 Eq. J3-6b

Resistance Factor, $Ø_b$	=	0.8	0.8	
Resistance Factor, $Ø_u$	=	0.75	0.75	
Tear-out Length, L_c	=	25.4 mm	1 in	
Bolt Size, d_b	=	22.2 mm	7/8 in	
Beam Web Thickness, t_w	=	11.2 mm	0.440 in	
Ultimate Strength of Beam, F_u	=	450 MPa	65 ksi	
Factored Bearing Resistance in Beam, B_r	=	1359.2 kN	306.1 kips	
Probable Ultimate Strength of Beam, R_yF_u	=	495 MPa	71.5 ksi	
Probable Bearing Resistance in Beam, B_r	=	1993.5 kN	449.0 kips	

Block Shear

$$V_{BS} = \phi_u \left[U_t A_n F_u + 0.6 A_{gv} \frac{F_y + F_u}{2} \right]$$

*S16-09 Cl. 13.11

Resistance Factor, $Ø_u$	=	0.75	0.75	
Efficiency Factor, U_t	=	0.3	0.3	
Net Area, A_n	=	851.6 mm^2	1.32 in^2	
Gross Area in Shear for Block Shear, A_{gv}	=	5056.4 mm^2	7.84 in^2	
Yield Strength of Beam, F_y	=	345 MPa	50 ksi	
Ultimate Strength of Beam, F_u	=	450 MPa	65 ksi	
Factored Block Shear Failure in Beam, V_{BS}	=	986.1 kN	222.1 kips	
Probable Yield Strength of Beam, R_yF_y	=	380 MPa	55 ksi	
Probable Ultimate Strength of Beam, R_yF_u	=	495 MPa	71.5 ksi	
Probable Block Shear Failure in Beam, V_{BS}	=	1446.3 kN	325.7 kips	

Flexural Yielding at Cope

$$V_{FY} = \frac{M_{FY}}{e}$$

*S16-09 Cl. 13.5

Resistance Factor, $Ø_s$	=	0.9	0.9	

Elastic Section Modulus of Gross Reduced Area, S_x'	=	853001.5 mm^3	52.05 in^3
Reduced Beam Height, h_o	=	524.5 mm	20.65 in
Centroid of Reduced Area, $\bar{y}$	=	262.6 mm	10.34 in
Moment of Inertia of Gross Reduced Area, I_x'	=	223378919.2 mm^4	536.67 in^4
Eccentricity to Cope, e	=	187.3 mm	7 3/8 in
Yield Strength of Beam, F_y	=	345 MPa	50 ksi
Moment Yielding Resistance at Cope, $M_{FY} = \phi_s F_y S_x'$			
Factored Moment Yielding Resistance at Cope, M_{FY}	=	264.7 kN-m	2342.4 kips-in
Probable Yield Strength of Beam, R_yF_y	=	380 MPa	55 ksi
Probable Moment Yielding Resistance at Cope, M_{FY}	=	323.5 kN-m	2862.9 kips-in
Factored Flexural Yielding at Cope, V_{FY}	=	1410.2 kN	317.6 kips
Probable Flexural Yielding at Cope, V_{FY}	=	1723.6 kN	388.2 kips

Net Shear Rupture

$V_{SR} = 0.66\phi_u F_u A_{nv}$ *S16-09 Cl. 13.4.1.1

Resistance Factor, $Ø_u$	=	0.75	0.75
Net Shear Area, $A_{nv} = t_w h_o$ - bolt holts	=	4158.7 mm^2	6.45 in^2
Beam Web Thickness, t_w	=	11.2 mm	0.440 in
Reduced Beam Height, h_o	=	524.5 mm	20.65 in
Ultimate Yield Strength of Beam, F_u	=	450 MPa	65 ksi
Factored Shear Rupture Resistance in Beam, V_{SR}	=	920.9 kN	207.4 kips
Probable Ultimate Strength of Beam, R_yF_u	=	495 MPa	72 ksi
Probable Shear Rupture Resistance in Beam, V_{SR}	=	1350.6 kN	304.2 kips

Flexural Rupture at Last Line of Bolts

$V_{FR} = \frac{M_{FR}}{e}$ *S16-09 Cl. 13.5

Resistance Factor, $Ø_u$	=	0.75	0.75
Elastic Section Modulus of Net Reduced Area, S_{xn}'	=	730444.7 mm^3	44.57 in^3
Reduced Beam Height, h_o	=	524.5 mm	20.65 in
Centroid of Net Reduced Area, $\bar{y}_n$	=	261.9 mm	10.31 in
Moment of Inertia of Gross Reduced Area, I_{xn}'	=	191841064.1 mm^4	460.9 in^4
Eccentricity to Last Line of Bolts, e	=	128.6 mm	5.25 in
Ultimate Yield Strength of Beam, F_u	=	450 MPa	65 ksi
Moment Rupture Resistance at Last Line of Bolts, $M_{FR} = \phi_u F_u S_{xn}'$			
Factored Moment Rupture Resistance at Last Line of Bolts, M_{FB}	=	245.5 kN-m	2173.0 kips-in
Probable Ultimate Strength of Beam, R_yF_u	=	495 MPa	72 ksi
Probable Moment Rupture Resistance at Last Line of Bolts, M_{FB}	=	360.1 kN-m	3187.1 kips-in
Factored Flexural Rupture Resistance at Last Line of Bolts, V_{FR}	=	1837.7 kN	413.9 kips
Probable Flexural Rupture Resistance at Last Line of Bolts, V_{FR}	=	2695.4 kN	607.1 kips

Von Mises Interaction

$$\left(\frac{V_{SY}}{V_{VM}}\right)^2 + \left(\frac{M_{FY}}{M_{VM}}\right)^2 \leq 1.0$$

therefore

$$V_{VM} = \frac{\phi_s F_y S_x'}{\sqrt{\left(\frac{S_x'}{0.66A_w}\right)^2 + e^2}}$$

Resistance Factor, $Ø_s$	=	0.9	0.9
Elastic Section Modulus of Gross Reduced Area, S_x'	=	853001.5 mm^3	52.05 in^3
Gross Shear Area, A_w	=	5861.9 mm^2	9.09 in^2
Eccentricity to Cope, e	=	187.3 mm	7 3/8 in
Yield Strength of Beam, F_y	=	345 MPa	50 ksi
Factored Von Mises Resistance, V_{VM}	=	913.1 kN	205.7 kips
Probable Yield Strength of Beam, R_yF_y	=	380 MPa	55 ksi
Probable Von Mises Resistance, V_{VM}	=	1116.0 kips	251.4 kips

Welds

Weld Strength

$V_W = 0.67\phi_w n_w X_u A_w$ *S16-09 Cl. 13.13.2.2

Resistance Factor, $Ø_w$	=	0.67	0.67

Number of Welds, n_w	=	2	2	
Ultimate Strength of Electrode, X_u	=	490 MPa	70 ksi	
Welded Area, A_w	=	2958.2 mm^2	4.59 in^2	
Length of Weld (T distance of Girder), L_w	=	527.1 mm	20 3/4 in	
Weld Size, t_w	=	7.9 mm	5/16 in	
Factored Weld Resistance, V_w	=	1279.4 kN	288.2 kips	
Probable Weld Resistance, V_w	=	1909.6 kN	430.1 kips	

Stiffeners

Check if Stiffener is Required

$$\frac{h_s}{t_w} \leq 60$$ *AISC Manual 2011 Part 9

Effective Beam Depth, h_s	=	547.116 mm	21.54 in	
Beam Web Thickness, t_w	=	11.2 mm	0.440 in	
Stiffener Requirement		OK		

Longitudinal Stiffener Extension

$$L_{ext} \geq \frac{c}{3}$$ *AISC Manual 2011 Part 9

Stiffener Extension Past Cope, L_{ext}	=	114.3 mm	4 1/2 in	
Cope Length, c	=	168.3 mm	6 5/8 in	
Extension Length Requirement - AISC Manual 2011 Part 9		OK		

$$L_{ext} \geq 2d_c$$ *Yam et al. (2011)

Cope Depth, d_c	=	41.3 mm	1 5/8 in	
Extension Length Requirement - Yam et al. (2011)		OK		

Slenderness Check

$$\frac{b_s}{t_s} \leq \frac{200}{\sqrt{F_y}}$$ *S16-09 Table 1

Width of Horizontal Stiffener, b_s	=	76 mm	3 in	
Thickness of Horizontal Stiffener, t_s	=	9.5 mm	3/8 in	
Yield Strength of Stiffener, F_y	=	345 MPa	50 ksi	
Slenderness Check - S16-09 Table 1		OK		

$$\frac{b_s}{t_s} \leq \frac{95}{\sqrt{F_y}}$$ *AISC Specification 2010 Table B4.

Slenderness Check - AISC Specification (2010), Compression		OK		

$$\frac{b_s}{t_s} \leq 0.95\sqrt{\frac{k_c E}{F_L}}$$ *AISC Specification 2010 Table B4.

Modulus of Elasticity, E	=	200000 MPa	29000 ksi	
$k_c = \frac{4}{\sqrt{\frac{h_s'}{t_w}}}$	=	0.625	0.625	
Effective Beam Depth Between Horizontal Stiffener, h_s'	=	457.2 mm	18.00 in	
Beam Web Thickness, t_w	=	11.2 mm	0.440 in	
$F_L = 0.7F_y$	=	241.5 MPa	35 ksi	
Yield Strength of Beam, F_y	=	345 MPa	50 ksi	
Slenderness Check - AISC Specification (2010), Welded Flexure		OK		

Welds Along Stiffener

$$V_W = 0.67\phi_w n_w X_u A_w$$ *S16-09 Cl. 13.13.2.2

Resistance Factor, $Ø_w$	=	0.67	0.67	
Number of Welds, n_w	=	4	4	
Ultimate Strength of Electrode, X_u	=	490 MPa	70 ksi	
Welded Area, A_w	=	641.5 mm^2	0.99 in^2	
Length of Weld (Only Considering Extension Past Cope), L_w	=	114 2/7 mm	4 1/2 in	
Weld Size, t_w	=	7.9 mm	5/16 in	
Factored Weld Resistance, V_w	=	554.9 kN	125.0 kips	
Probable Weld Resistance, V_w	=	828.3 kN	186.5 kips	

Check if Shear Resistance is Greater than Axial Capacity

$$T_{st} = \phi_s F_y A_{st}$$

Resistance Factor, $Ø_s$	=	0.9	0.9	
Yield Strength of Stiffener, F_y	=	345 MPa	50 ksi	
Area of Stiffener, A_{st}	=	725.8 mm^2	1 1/8 in^2	
Effective Width of Horizontal Stiffener, b_s	=	76.2 mm	3 in	

Thickness of Horizontal Stiffener, t_s	=	9.5 mm	3/8 in
Factored Axial Capacity, T_{st}	=	1285.9 kN	50.6 kips
Probable Yield Strength of Stiffener, R_yF_y	=	380 MPa	55 ksi
Probable Axial Capacity, T_{st}	=	1571.6 kN	61.9 kips
Factored Weld Resistance Greater than Factored Tensile Strength		OK	
Probable Weld Resistance Greater than Factored Tensile Strength		OK	

Beam Web Shear Yielding Along Weld

$V_{BYW} = 0.66\phi_s m F_y t_w L_{ext}$

Resistance Factor, $Ø_s$	=	0.9	0.9
Shear Planes, m	=	1	1
Yield Strength of Beam, F_y	=	345 MPa	50 ksi
Beam Web Thickness, t_w	=	11.2 mm	0.440 in
Stiffener Extension Past Cope, L_{ext}	=	114.3 mm	4 1/2 in
Factored Beam Web Shear Yielding Along Weld, V_{BYW}	=	261.1 kN	58.8 kips
Factored Shear Resistance Greater than Factored Tensile Strength		OK	
Probable Yield Strength of Beam, R_yF_y	=	380 MPa	55 ksi
Probable Beam Web Shear Yielding Along Weld, V_{BYW}		319.1 kN	71.9 kips
Probable Weld Resistance Greater than Factored Tensile Strength		Not OK	

Specimen 6 - Double Cope Doubler Plate

Configuration Parameters

Girder		W610x155	(W24x104)	
Beam		W610x113	(W24x76)	
Supporting Stiffener Thickness, t_{sp}	=	15.9 mm	5/8 in	
Cope Length, c	=	168.3 mm	6 5/8 in	
Cope Depth, d_c	=	41.3 mm	1 5/8 in	
Bolt Size, d_b	=	22.2 mm	7/8 in	
Number of Bolt Lines, m	=	2	2	
Number of Bolt Rows, n	=	6	6	
Bolt Gauge Distance, D	=	76.2 mm	3 in	
Bolt Pitch Distance, b	=	76.2 mm	3 in	
Bolt Edge Distance - Horizontal	=	47.625 mm	1 7/8 in	
Bolt Edge Distance - Vertical	=	69.9 mm	2 3/4 in	
Supporting Stiffener Edge Distance	=	38.1 mm	1 1/2 in	
Gap from Beam End to Girder	=	12.7 mm	1/2 in	
Thickness of Doubler Plate, t_{dp}	=	7.9 mm	5/16 in	
Depth of Doubler Plate, d_{dp}	=	493.7 mm	19 7/16 in	
Length of Doubler Plate, L_{dp}	=	285.8 mm	11 1/4 in	

Computing ICR Coefficient, C

Moment Arm, L	=	104.8 mm	4.13 in	*CISC Handbook 2009 Table 3-15
Number of Bolt Lines, m	=	2	2	
Gauge, D	=	76.2 mm	3 in	
Number of Bolt Rows, n	=	6	6	
Pitch, b	=	76.2 mm	3 in	
L_1	=	100 mm		
C_1	=	9.33		Linear Interpolation
L_2	=	125 mm		
C_2	=	8.42		
Eccentric Loading Coefficient, C	=	9.156	9.156	

Bolts

Bolt Shear

$$V_{Bolt} = 0.6\phi_b nmA_b F_u C$$ *S16-09 Cl. 13.12.1.2c

Resistance Factor, $Ø_b$	=	0.8	0.8	
Number of Bolts, n	=	1	1	
Number of Shear Planes, m	=	1	1	
Bolt Area, A_b	=	388 mm2	0.601 in2	
Tensile Strength of Bolts, F_u	=	825 MPa	120 ksi	
Factored Bolt Shear Resistance, V_{Bolt}	=	1407.3 kN	317.0 kips	
Probable Bolt Shear Resistance, V_{Bolt}	=	1759.2 kN	396.2 kips	

Supporting Stiffener

Shear Yielding

$$V_{SY} = 0.66\phi_s F_y A_w$$ *S16-09 Cl. 13.4.1.1

Resistance Factor, $Ø_s$	=	0.9	0.9	
Gross Shear Area, $A_w = t_{sp}d_{sp}$	=	3931.4 mm^2	12.9 in^2	
Supporting Stiffener Thickness, t_{sp}	=	15.9 mm	5/8 in	
Supporting Stiffener Depth, $d_{sp} = \min(d_{beam} - d_c, T_{girder})$	=	247.7 mm	20.7 in	
Yield Strength of Plate, F_y	=	345 MPa	50 ksi	
Factored Shear Yielding Resistance in Supporting Stiffener, V_{SY}	=	1701.9 kN	383.3 kips	
Probable Yielding Strength of Plate, R_yF_y	=	380 MPa	55 ksi	
Probable Shear Yielding Resistance in Supporting Stiffener, V_{SY}	=	2080.1 kN	468.5 kips	

Bearing

$$B_r = min\begin{cases} 3\phi_b d_b t_{sp} F_u C \\ 1.5\phi_u L_c t_{sp} F_u C \end{cases}$$ *S16-09 Cl. 13.12.1.2a *AISC Specification 2010 Eq. J3-6b

Resistance Factor, $Ø_b$	=	0.8	0.8	
Resistance Factor, $Ø_u$	=	0.75	0.75	

Tear-out Length, L_c	=	25.4 mm	1 in	
Bolt Size, d_b	=	22.2 mm	7/8 in	
Supporting Stiffener Thickness, t_{sp}	=	15.9 mm	5/8 in	
Ultimate Strength of Plate, F_u	=	450 MPa	65 ksi	
Factored Bearing Resistance in Supporting Stiffener, B_r	=	1858.0 kN	418.5 kips	
Probable Ultimate Strength of Plate, R_yF_u	=	495 MPa	71.5 ksi	
Probable Bearing Resistance in Supporting Stiffener, B_r	=	2725.1 kN	613.8 kips	

Stability

$$\frac{b_{el}}{t} \leq \frac{200}{\sqrt{F_y}}$$

*S16-09 Table 1

Effective Width of Supporting Stiffener, b_{el}	=	168.9 mm	6.65 in	
Supporting Stiffener Thickness, t_{sp}	=	15.9 mm	5/8 in	
Yield Strength of Plate, F_y	=	345 MPa	50 ksi	
Stability Check		Stable		

Beam

Shear Yielding

$$V_{SY} = 0.66\phi_s F_y A_w$$

*S16-09 Cl. 13.4.1.1

Resistance Factor, $Ø_s$	=	0.9	0.9	
Gross Shear Area, $A_w = (t_w*h_o)+(t_{dp}*d_{dp})$	=	5861.9 mm^2	15.16 in^2	
Beam Web Thickness, t_w	=	11.2 mm	0.440 in	
Reduced Beam Height, h_o	=	524.5 mm	20.65 in	
Thickness of Doubler Plate, t_{dp}	=	7.9 mm	5/16 in	
Depth of Doubler Plate, d_{dp}	=	493.7 mm	19 7/16 in	
Yield Strength of Beam and Plate, F_y	=	345 MPa	50 ksi	
Factored Shear Yielding Resistance in Beam, V_{SY}	=	1999.1 kN	450.3 kips	
Probable Yielding Strength of Beam and Plate, R_yF_y	=	380 MPa	55 ksi	
Probable Shear Yielding Resistance in Beam, V_{SY}	=	2443.4 kN	550.3 kips	

Bearing

$$B_r = min \begin{cases} 3\phi_b d_b (t_w + t_{dp}) F_u C \\ 1.5\phi_u L_c (t_w + t_{dp}) F_u C \end{cases}$$

*S16-09 Cl. 13.12.1.2a
*AISC Specification 2010 Eq. J3-6b

Resistance Factor, $Ø_b$	=	0.8	0.8	
Resistance Factor, $Ø_u$	=	0.75	0.75	
Tear-out Length, L_c	=	34.9 mm	1 3/8 in	
Bolt Size, d_b	=	22.2 mm	7/8 in	
Beam Web Thickness, t_w	=	11.2 mm	0.440 in	
Thickness of Doubler Plate, t_{dp}	=	7.9 mm	5/16 in	
Ultimate Strength of Beam and Plate, F_u	=	450 MPa	65 ksi	
Factored Bearing Resistance in Beam, B_r	=	3075.9 kN	692.8 kips	
Probable Ultimate Strength of Beam and Plate, R_yF_u	=	495 MPa	71.5 ksi	
Probable Bearing Resistance in Beam, B_r	=	4511.3 kN	1016.1 kips	

Block Shear

$$V_{BS} = \phi_u \left[U_t A_n F_u + 0.6 A_{gv} \frac{F_y + F_u}{2} \right]$$

*S16-09 Cl. 13.11

Resistance Factor, $Ø_u$	=	0.75	0.75	
Efficiency Factor, U_t	=	0.3	0.3	
Net Area, A_n	=	1638.5 mm^2	2.54 in^2	
Gross Area in Shear for Block Shear, A_{gv}	=	8617.3 mm^2	13.36 in^2	
Yield Strength of Beam and Plate, F_y	=	345 MPa	50 ksi	
Ultimate Strength of Beam and Plate, F_u	=	450 MPa	65 ksi	
Factored Block Shear Failure in Beam, V_{BS}	=	1699.4 kN	382.8 kips	
Probable Yield Strength of Beam and Plate, R_yF_y	=	380 MPa	55 ksi	
Probable Ultimate Strength of Beam and Plate, R_yF_u	=	495 MPa	71.5 ksi	
Probable Block Shear Failure in Beam, V_{BS}	=	2492.5 kN	561.4 kips	

Flexural Yielding at Cope

$$V_{FY} = \frac{M_{FY}}{e}$$ *S16-09 Cl. 13.5

Resistance Factor, $Ø_s$	=	0.9	0.9
Elastic Section Modulus of Gross Reduced Area, S_x'	=	804770.8 mm^3	49.11 in^3
Reduced Beam Height, h_o	=	524.5 mm	20.65 in
Centroid of Reduced Area, $\bar{y}$	=	259.6 mm	10.22 in
Moment of Inertia of Gross Reduced Area, I_x'	=	213227034.7 mm^4	512.28 in^4
Eccentricity to Cope, e	=	187.3 mm	7 3/8 in
Yield Strength of Beam and Plate, F_y	=	345 MPa	50 ksi
Moment Yielding Resistance at Cope, $M_{FY} = \phi_s F_y S_x'$			
Factored Moment Yielding Resistance at Cope, M_{FY}	=	249.7 kN-m	2210.0 kips-in
Probable Yield Strength of Beam and Plate, R_yF_y	=	380 MPa	55 ksi
Probable Moment Yielding Resistance at Cope, M_{FY}	=	305.2 kN-m	2701.1 kips-in
Factored Flexural Yielding at Cope, V_{FY}	=	1330.5 kN	299.7 kips
Probable Flexural Yielding at Cope, V_{FY}	=	1626.1 kN	366.2 kips

Flexural Buckling at Cope

$$V_{FB} = \frac{M_{FB}}{e}$$

Resistance Factor, $Ø_s$	=	0.9	0.9
Modulus of Elasticity, E	=	200000 MPa	29000 ksi
Poisson's Ratio, ν	=	0.3	0.3
Beam Web Thickness, t_w	=	11.2 mm	0.440 in
Thickness of Doubler Plate, t_{dp}	=	7.9 mm	5/16 in
Beam Depth, d	=	607.1 mm	23.9 in
Reduced Beam Height, h_o	=	524.5 mm	20.65 in
Cope Length, c	=	168.3 mm	6 5/8 in
Cope Depth, d_c	=	41.3 mm	1 5/8 in

$$F_{cr} = 0.62\pi E \frac{(t_w + t_{dp})^2}{ch_o} f_d$$ *AISC Manual 2011 Part 9

Adjustment Factor, $f_d = 3.5 - 7.5\left(\frac{d_c}{d}\right)$	=	2.99	2.99	*AISC Manual 2011 Part 9
Critical Buckling Stress, F_{cr}	=	4879.6 MPa	699.1 ksi	
Elastic Section Modulus of Gross Reduced Area, S_x'	=	804770.8 mm^3	49.11 in^3	
Eccentricity to Cope, e	=	187.3 mm	7 3/8 in	
Moment Buckling Resistance at Cope, $M_{FB} = \phi_s F_{cr} S_x'$				
Factored Moment Buckling Resistance at Cope, M_{FB}	=	3491.6 kN-m	30898.7 kips-in	
Probable Moment Buckling Resistance at Cope, M_{FB}	=	3879.5 kN-m	34331.9 kips-in	
Factored Flexural Buckling at Cope, V_{FB}	=	18602.1 kN	4189.7 kips	
Probable Flexural Buckling at Cope, V_{FB}	=	20669.0 kN	4655.2 kips	

Net Shear Rupture

$$V_{SR} = 0.66\phi_u F_u A_{nv}$$ *S16-09 Cl. 13.4.1.1

Resistance Factor, $Ø_u$	=	0.75	0.75
Net Shear Area, A_{nv}	=	8034.0 mm^2	12.45 in^2
Beam Web Thickness, t_w	=	11.2 mm	0.440 in
Doubler Plate Thickness, t_{dp}	=	7.9 mm	5/16 in
Reduced Beam Height, h_o	=	524.5 mm	20.65 in
Depth of Doubler Plate, d_{dp}	=	493.7 mm	19 7/16 in
Ultimate Yield Strength of Beam and Plate, F_u	=	450 MPa	65 ksi
Factored Shear Rupture Resistance in Beam, V_{SR}	=	1779.0 kN	400.7 kips
Probable Ultimate Strength of Beam and Plate, R_yF_u	=	495 MPa	72 ksi
Probable Shear Rupture Resistance in Beam, V_{SR}	=	2609.1 kN	587.6 kips

Flexural Rupture at Last Line of Bolts

$$V_{FR} = \frac{M_{FR}}{e}$$ *S16-09 Cl. 13.5

Resistance Factor, $Ø_u$	=	0.75	0.75
Elastic Section Modulus of Net Reduced Area, S_{xn}'	=	625312.6 mm^3	38.16 in^3

Reduced Beam Height, h_o	=	524.5 mm	20.65 in	
Centroid of Net Reduced Area, $\bar{y}_n$	=	262.4 mm	10.33 in	
Moment of Inertia of Gross Reduced Area, I_{xn}'	=	163911935.4 mm^4	393.8 in^4	
Eccentricity to Last Line of Bolts, e	=	137.8 mm	5.63 in	
Ultimate Yield Strength of Beam and Plate, F_u	=	450 MPa	65 ksi	
Moment Rupture Resistance at Last Line of Bolts, $M_{FR} = \phi_u F_u S_{xn}'$				
Factored Moment Rupture Resistance at Last Line of Bolts, M_{FB}	=	210.2 kN-m	1860.2 kips-in	
Probable Ultimate Strength of Beam and Plate, R_yF_u	=	495 MPa	72 ksi	
Probable Moment Rupture Resistance at Last Line of Bolts, M_{FB}	=	308.3 kN-m	2728.4 kips-in	
Factored Flexural Rupture Resistance at Last Line of Bolts, V_{FR}	=	1468.4 kN	330.7 kips	
Probable Flexural Rupture Resistance at Last Line of Bolts, V_{FR}	=	2153.6 kN	485.0 kips	

Von Mises Interaction

$$\left(\frac{V_{SY}}{V_{VM}}\right)^2 + \left(\frac{M_{FY}}{M_{VM}}\right)^2 \leq 1.0$$

therefore

$$V_{VM} = \frac{\phi_s F_y S_x'}{\sqrt{\left(\frac{S_x'}{0.66A_w}\right)^2 + e^2}}$$

Resistance Factor, $Ø_s$	=	0.9	0.9	
Elastic Section Modulus of Gross Reduced Area, S_x'	=	804770.8 mm^3	49.11 in^3	
Gross Shear Area, A_w	=	5861.9 mm^2	15.16 in^2	
Eccentricity to Cope, e	=	187.3 mm	7 3/8 in	
Yield Strength of Beam and Plate, F_y	=	345 MPa	50 ksi	
Factored Von Mises Resistance, V_{VM}	=	1107.6 kN	249.5 kips	
Probable Yield Strength of Beam and Plate, R_yF_y	=	380 MPa	55 ksi	
Probable Von Mises Resistance, V_{VM}	=	1353.7 kips	304.9 kips	

Welds

Weld Strength

$$V_W = 0.67\phi_w n_w X_u A_w$$ *S16-09 Cl. 13.13.2.2

Resistance Factor, $Ø_w$	=	0.67	0.67	
Number of Welds, n_w	=	2	2	
Ultimate Strength of Electrode, X_u	=	490 MPa	70 ksi	
Welded Area, A_w	=	2958.2 mm^2	4.59 in^2	
Length of Weld (T distance of Girder), L_w	=	527.1 mm	20 3/4 in	
Weld Size, t_w	=	7.9 mm	5/16 in	
Factored Weld Resistance, V_w	=	1279.4 kN	288.2 kips	
Probable Weld Resistance, V_w	=	1909.6 kN	430.1 kips	

Doubler Plate

Sizing of Welds Between Beam and Doubler Plate *Blodgett (1966)

Flexural Strength of Doubler Past Cope, $M_{DP} = \phi_s S_{DP} F_y$

Resistance Factor, $Ø_s$	=	0.9	0.9	
Elastic Section Modulus of Doubler Plate, S_{DP}	=	322463.6 mm^3	19.7 in^3	
Thickness of Doubler Plate, t_{dp}	=	7.9 mm	5/16 in	
Depth of Doubler Plate, d_{dp}	=	493.7 mm	19 7/16 in	
Yield Strength of Doubler Plate, F_y	=	345 MPa	50 ksi	
Factored Flexural Strength of Doubler Plate, M_{DP}	=	100.1 kN-m	885.5 kips-in	
Probable Yield Strength of Doubler Plate, R_yF_y	=	380 MPa	55 ksi	
Probable Flexural Strength of Doubler Plate, M_{DP}	=	122.3 kN-m	1082.3 kips-in	
Torsional Constant, $J_w = \frac{(2b+d)^3}{12} - \frac{b^2(b+d)^2}{(2b+d)}$	=	26524540.8 mm^3	1618.6 in^3	
Length of Weld Group Past Cope, b	=	127 mm	5 in	
Depth of Weld Group (Depth of Doubler Plate), d	=	493.7 mm	19 4/9 in	
Horizontal Eccentricity of Weld Group Past Cope, e_x	=	105.44 mm	4.15 in	
Vertical Eccentricity of Weld Group Past Cope, e_y	=	246.86 mm	9.72 in	
Factored Horizontal Force per Unit Length, $f_x = \frac{M_{DP}e_x}{J_w}$	=	0.40 kN/mm	2.27 kips/in	

Probable Horizontal Force per Unit Length, f_x	=	0.49 kN/mm	2.78 kips/in	
Factored Vertical Force per Unit Length, $f_y = \frac{M_{DP} e_y}{J_w}$	=	0.93 kN/mm	5.32 kips/in	
Probable Vertical Force per Unit Length, f_y	=	1.14 kN/mm	6.50 kips/in	
Factored Resulting Force per Unit Length, $f_w = \sqrt{f_x^2 + f_y^2}$	=	1.01 kN/mm	5.78 kips/in	
Probable Resulting Force per Unit Length, $f_w = \sqrt{f_x^2 + f_y^2}$	=	1.24 kN/mm	7.07 kips/in	
Factored Weld Strength Per Weld Area, V_w	=	155.5 kN/mm	22.2 kips/in^2	*S16-09 Cl. 13.13.2.2
Probable Weld Strength Per Weld Area, V_w	=	232.1 kN/mm	33.2 kips/in^2	
Weld Size Based on Factored Strength, $D_w \geq \frac{f_w}{V_w}$	=	6.4 mm	1/4 in	Note: Rounding to nearest 16th of an inch
Weld Size Based on Probable Strength, $D_w \geq \frac{f_w}{V_w}$	=	4.8 mm	3/16 in	Note: Rounding to nearest 16th of an inch
Therefore Select Adequate Weld Size	=	6.4 mm	1/4 in	

$V_{W-Weld} = 0.67\phi_w n_w X_u A_w (1.00 + 0.5 sin^{1.5}\theta) M_w$ *S16-09 Cl. 13.13.2.2

Resistance Factor, $Ø_w$	=	0.67	0.67	
Number of Welds- End Welds, n_w	=	1	1	
Number of Welds- Side Welds, n_w	=	2	2	
Ultimate Strength of Electrode, X_u	=	490 MPa	70 ksi	
Parallel to Shear Force Welded Area (End Weld), A_w	=	2216.8 mm^2	3.44 in^2	
Length of Weld (Depth of Doubler Plate)	=	493.7 mm	19 7/16 in	
Weld Size, t_w	=	6.4 mm	1/4 in	
Perpendicular to Shear Force Welded Area (Side Weld), A_w	=	570.2 mm^2	0.88 in^2	
Length of Weld (Length of Weld Group Past Cope)	=	127.0 mm	5 in	
Weld Size, t_w	=	6.4 mm	1/4 in	
Strength Reduction Factor, $M_w = \frac{0.85 + \theta_1/600}{0.85 + \theta_2/600}$				
Reduction Factor for End Weld	=	0.85		
θ_1	=	0 degree	0 degrees	
θ_2	=	90 degree	90 degrees	
Reduction Factor for Side Weld	=	1		
θ_1	=	90 degree	90 degrees	
θ_2	=	90 degree	90 degrees	
Factored Weld Metal Strength Past Cope, $V_{W\text{-}Weld}$	=	758.4 kN	170.8 kips	
Probable Weld Metal Strength Past Cope, $V_{W\text{-}Weld}$	=	1131.9 kN	254.9 kips	

Base Metal Strength Past Cope

$V_{W-Base} = 0.67\phi_w F_u A_w$ *S16-09 Cl. 13.13.2.2

Resistance Factor, $Ø_w$	=	0.67	0.67	
Parallel to Shear Force Welded Area (End Weld), A_w	=	3135.1 mm^2	4.86 in^2	
Length of Weld (Depth of Doubler Plate)	=	493.7 mm	19 7/16 in	
Weld Size, t_w	=	6.4 mm	1/4 in	
Perpendicular to Shear Force Welded Area (Side Weld), A_w	=	806.5 mm^2	1.25 in^2	
Length of Weld (Length of Weld Group Past Cope)	=	127 mm	5 in	
Weld Size, t_w	=	6.4 mm	1/4 in	
Ultimate Yield Strength of Beam, F_u	=	450 MPa	65 ksi	
Factored Base Metal Strength Past Cope, $V_{W\text{-}Base}$	=	953.4 kN	214.7 kips	
Probable Ultimate Strength of Beam, R_yF_u	=	495 MPa	72 ksi	
Probable Base Metal Strength Past Cope, $V_{W\text{-}Base}$	=	1565.3 kN	352.6 kips	
Check Base Metal Strength Larger than Weld Metal Strength (Factored)		OK		
Check Base Metal Strength Larger than Weld Metal Strength (Probable)		OK		

Specimen 7 - Single Cope Haunched

Configuration Parameters

Girder		W610x155	(W24x104)	
Beam		W310x60	(W12x40)	
Supporting Stiffener Thickness, t_{sp}	=	15.9 mm	5/8 in	
Cope Length, c	=	177.8 mm	7 in	
Cope Depth, d_c	=	133.4 mm	5 1/4 in	
Bolt Size, d_b	=	19.1 mm	3/4 in	
Number of Bolt Lines, m	=	2	2	
Number of Bolt Rows, n	=	3	3	
Bolt Gauge Distance, D	=	76.2 mm	3 in	
Bolt Pitch Distance (top two rows), b_1	=	76.2 mm	3 in	
Bolt Pitch Distance (bottom two rows), b_2	=	95.3 mm	3 3/4 in	
Bolt Edge Distance	=	38.1 mm	1 1/2 in	
Gap from Beam End to Girder	=	12.7 mm	1/2 in	
Length of Haunch Plate, L_H	=	335.0 mm	13 3/16 in	
Thickness of Haunch Plate, t_H	=	7.9 mm	5/16 in	
Depth of Haunch Plate, d_H	=	92.1 mm	3 5/8 in	

Computing ICR Coefficient, C *CISC Handbook 2009 Table 3-15

Moment Arm, L	=	95.3 mm	3.75 in	
Coefficient for Top Two Rows				
Number of Bolt Lines, m	=	2	2	
Gauge, D	=	76 mm	3 in	
Number of Bolt Rows, n	=	3	3	
Pitch, b_1	=	76.2 mm	3 in	
L_1	=	75 mm		
C_1	=	3.88		Linear Interpolation
L_2	=	100 mm		
C_2	=	3.25		
Eccentric Loading Coefficient, C_{Top}	=	3.370	3.370	
Coefficient for Bottom Two Rows				
Number of Bolt Lines, m	=	2	2	
Gauge, D	=	76.2 mm	3 in	
Number of Bolt Rows, n	=	3	3	
Pitch, b_2	=	95.3 mm	3 3/4 in	
L_1	=	75 mm		
C_1	=	4.30		Linear Interpolation
L_2	=	100 mm		
C_2	=	3.68		
Eccentric Loading Coefficient, C_{Bot}	=	3.798	3.798	
Eccentric Loading Coefficient, C	=	3.584	3.584	Average of C_{Top} and C_{Bot}

Bolts

Bolt Shear

$$V_{Bolt} = 0.6\phi_b n m A_b F_u C$$ *S16-09 Cl. 13.12.1.2c

Resistance Factor, $Ø_b$	=	0.8	0.8	
Number of Bolts, n	=	1	1	
Number of Shear Planes, m	=	1	1	
Bolt Area, A_b	=	285 mm^2	0.442 in^2	
Tensile Strength of Bolts, F_u	=	825 MPa	120 ksi	
Factored Bolt Shear Resistance, V_{Bolt}	=	405.1 kN	91.2 kips	
Probable Bolt Shear Resistance, V_{Bolt}	=	506.4 kN	114.0 kips	

Supporting Stiffener

Shear Yielding

$$V_{SY} = 0.66\phi_s F_y A_w$$ *S16-09 Cl. 13.4.1.1

Resistance Factor, $Ø_s$	=	0.9	0.9	
Gross Shear Area, $A_w = t_{sp}d_{sp}$	=	4133.1 mm^2	6.41 in^2	
Supporting Stiffener Thickness, t_{sp}	=	15.9 mm	5/8 in	

Supporting Stiffener Depth, d_{sp}	=	260.4 mm	10 1/4 in	
Yield Strength of Plate, F_y	=	345 MPa	50 ksi	
Factored Shear Yielding Resistance in Supporting Stiffener, V_{SY}	=	844.8 kN	190.3 kips	
Probable Yielding Strength of Plate, R_yF_y	=	380 MPa	55 ksi	
Probable Shear Yielding Resistance in Supporting Stiffener, V_{SY}	=	1032.5 kN	232.5 kips	

Bearing

$$B_r = min \begin{cases} 3\phi_b d_b t_{sp} F_u C \\ 1.5\phi_u L_c t_{sp} F_u C \end{cases}$$

*S16-09 Cl. 13.12.1.2a
*AISC Specification 2010 Eq. J3-6b

Resistance Factor, $Ø_b$	=	0.8	0.8	
Resistance Factor, $Ø_u$	=	0.75	0.75	
Tear-out Length, L_c	=	27.0 mm	1 1/16 in	
Bolt Size, d_b	=	19.1 mm	3/4 in	
Supporting Stiffener Thickness, t_{sp}	=	15.9 mm	5/8 in	
Ultimate Strength of Plate, F_u	=	450 MPa	65 ksi	
Factored Bearing Resistance in Supporting Stiffener, B_r	=	772.7 kN	174.0 kips	
Probable Ultimate Strength of Plate, R_yF_u	=	495 MPa	71.5 ksi	
Probable Bearing Resistance in Supporting Stiffener, B_r	=	1133.3 kN	255.2 kips	

Stability

$$\frac{b_{el}}{t} \leq \frac{200}{\sqrt{F_y}}$$

*S16-09 Table 1

Effective Width of Supporting Stiffener, b_{el}	=	165.1 mm	6 1/2 in	
Supporting Stiffener Thickness, t_{sp}	=	15.9 mm	5/8 in	
Yield Strength of Plate, F_y	=	345 MPa	50 ksi	
Stability Check		Stable		

Beam

Shear Yielding

$$V_{SY} = 0.66\phi_s F_y A_w$$

*S16-09 Cl. 13.4.1.1

Resistance Factor, $Ø_s$	=	0.9	0.9	
Gross Shear Area, A_w	=	1996.5 mm^2	3.09 in^2	
Beam Web Thickness, t_w	=	7.5 mm	0.295 in	
Reduced Beam Height, h_o	=	168.9 mm	6.65 in	
Thickness of Haunch Plate, t_H	=	7.9 mm	5/16 in	
Depth of Haunch Plate, d_H	=	92.1 mm	3 5/8 in	
Yield Strength of Beam, F_y	=	345 MPa	50 ksi	
Factored Shear Yielding Resistance in Beam, V_{SY}	=	408.1 kN	91.9 kips	
Probable Yielding Strength of Beam, R_yF_y	=	380 MPa	55 ksi	
Probable Shear Yielding Resistance in Beam, V_{SY}	=	498.8 kN	112.3 kips	

Bearing

$$B_r = min \begin{cases} 3\phi_b d_b t_w F_u C \\ 1.5\phi_u L_c t_w F_u C \end{cases}$$

*S16-09 Cl. 13.12.1.2a
*AISC Specification 2010 Eq. J3-6b

Resistance Factor, $Ø_b$	=	0.8	0.8	
Resistance Factor, $Ø_u$	=	0.75	0.75	
Tear-out Length, L_c	=	27.0 mm	1 1/16 in	
Bolt Size, d_b	=	19.1 mm	3/4 in	
Beam Web Thickness, t_w	=	7.5 mm	0.295 in	
Ultimate Strength of Beam, F_u	=	450 MPa	65 ksi	
Factored Bearing Resistance in Beam, B_r	=	364.7 kN	82.1 kips	
Probable Ultimate Strength of Beam, R_yF_u	=	495 MPa	71.5 ksi	
Probable Bearing Resistance in Beam, B_r	=	534.9 kN	120.5 kips	

Flexural Yielding at Cope

$$V_{FY} = \frac{M_{FY}}{e}$$

*S16-09 Cl. 13.5

Resistance Factor, $Ø_s$	=	0.9	0.9	
Elastic Section Modulus of Gross Reduced Area, S_x'	=	83740.1 mm^3	5.11 in^3	
Effective Reduced Beam Depth, h_1	=	144.1 mm	5.68 in	

Reduced Beam Height, h_o	=	168.9 mm	6.65 in	
Depth of Haunch Plate, d_H	=	92.1 mm	3 5/8 in	
Centroid of Reduced Area, $\bar{y}$	=	116.8 mm	4.6 in	
Moment of Inertia of Gross Reduced Area, I_x'	=	12070711.3 mm^4	29 in^4	
Eccentricity to Cope, e	=	198.8 mm	7 5/6 in	
Yield Strength of Beam, F_y	=	345 MPa	50 ksi	
Moment Yielding Resistance at Cope, $M_{FY} = \phi_s F_y S_x'$				
Factored Moment Yielding Resistance at Cope, M_{FY}	=	26.0 kN-m	230.0 kips-in	
Probable Yield Strength of Beam, R_yF_y	=	380 MPa	55 ksi	
Probable Moment Yielding Resistance at Cope, M_{FY}	=	31.8 kN-m	281.1 kips-in	
Factored Flexural Yielding at Cope, V_{FY}	=	130.4 kN	29.4 kips	
Probable Flexural Yielding at Cope, V_{FY}	=	159.4 kN	35.9 kips	

Flexural Buckling at Cope

$$V_{FB} = \frac{M_{FB}}{e}$$

Resistance Factor, $Ø_s$	=	0.9	0.9	
Beam Web Thickness, t_w	=	7.5 mm	0.295 in	
Reduced Beam Height, h_o	=	168.9 mm	6.65 in	
Depth of Haunch Plate, d_H	=	92.1 mm	3 5/8 in	
Thickness of Haunch Plate, t_H	=	7.9 mm	5/16 in	
Cope Length, c	=	177.8 mm	7 in	
Eccentricity to Cope, e	=	198.82 mm	7.83 in	
Elastic Section Modulus of Gross Reduced Area, S_x'	=	83740.1 mm^3	5.11 in^3	
Yield Strength of Beam, F_y	=	345 MPa	50 ksi	
Probable Yield Strength of Beam, R_yF_y	=	380 MPa	55 ksi	

$F_{cr} = F_yQ$ *AISC Manual 2011 Part 9

$$Q = \begin{cases} 1 \; for \; \lambda \leq 0.7 \\ (1.34 - 0.486\lambda) \; for \; 0.7 < \lambda \leq 1.41 \\ (1.30 / \lambda^2) \; for \; \lambda > 1.41 \end{cases}$$

Factored Q	=	0.986	0.986
Probable Q	=	0.969	0.969

where

$$\lambda = \frac{(h_o + d_H)\sqrt{F_y}}{10\left(\frac{t_w + t_H}{2}\right)\sqrt{475 + 280\left(\frac{h_o + d_H}{c}\right)^2}}$$

Factored λ	=	0.73	0.73
Probable λ	=	0.76	0.76
Factored Critical Buckling Stress, F_{cr}	=	344.1 MPa	49.3 ksi
Probable Critical Buckling Stress, F_{cr}	=	371.9 MPa	53.3 ksi
Moment Buckling Resistance at Cope, $M_{FB} = \phi_s F_{cr} S_x'$			
Factored Moment Buckling Resistance at Cope, M_{FB}	=	25.6 kN-m	226.7 kips-in
Probable Moment Buckling Resistance at Cope, M_{FB}	=	30.8 kN-m	272.3 kips-in
Factored Flexural Buckling at Cope, V_{FB}	=	128.6 kN	29.0 kips
Probable Flexural Buckling at Cope, V_{FB}	=	154.4 kN	34.8 kips

Net Shear Rupture

$V_{SR} = 0.66\phi_u F_u A_{nv}$ *S16-09 Cl. 13.4.1.1

Resistance Factor, $Ø_u$	=	0.75	0.75
Net Shear Area, $A_{nv} = A_w$ - bolt holts	=	1487.0 mm^2	2.30 in^2
Beam Web Thickness, t_w	=	7.5 mm	0.295 in
Reduced Beam Height, h_o	=	168.9 mm	6.65 in
Thickness of Haunch Plate, t_H	=	7.9 mm	5/16 in
Depth of Haunch Plate, d_H	=	92.1 mm	3 5/8 in
Ultimate Yield Strength of Beam, F_u	=	450 MPa	65 ksi
Factored Shear Rupture Resistance in Beam, V_{SR}	=	329.3 kN	74.2 kips
Probable Ultimate Strength of Beam, R_yF_u	=	495 MPa	72 ksi
Probable Shear Rupture Resistance in Beam, V_{SR}	=	482.9 kN	108.8 kips

Von Mises Interaction

$$\left(\frac{V_{SY}}{V_{VM}}\right)^2 + \left(\frac{M_{FY}}{M_{VM}}\right)^2 \leq 1.0$$

therefore

$$V_{VM} = \frac{\phi_s F_y S_x'}{\sqrt{\left(\frac{S_x'}{0.66A_w}\right)^2 + e^2}}$$

Resistance Factor, $Ø_s$	=	0.9	0.9
Elastic Section Modulus of Gross Reduced Area, S_x'	=	83740.1 mm^3	5.11 in^3
Gross Shear Area, A_w	=	1996.5 mm^2	3.09 in^2
Eccentricity to Cope, e	=	198.8 mm	7 5/6 in
Yield Strength of Beam, F_y	=	345 MPa	50 ksi
Factored Von Mises Resistance, V_{VM}	=	124.2	28.0 kips
Probable Yield Strength of Beam, R_yF_y	=	380 MPa	55 ksi
Probable Von Mises Resistance, V_{VM}	=	151.9 kips	34.2 kips

Welds

Weld Strength

$$V_W = 0.67\phi_w n_w X_u A_w$$

*S16-09 Cl. 13.13.2.2

Resistance Factor, $Ø_w$	=	0.67	0.67
Number of Welds, n_w	=	2	2
Ultimate Strength of Electrode, X_u	=	490 MPa	70 ksi
Welded Area, A_w	=	2958.2 mm^2	4.59 in^2
Length of Weld (T distance of Girder), L_w	=	527.1 mm	20 3/4 in
Weld Size, t_w	=	7.9 mm	5/16 in
Factored Weld Resistance, V_w	=	1279.4 kN	288.2 kips
Probable Weld Resistance, V_w	=	1909.6 kN	430.1 kips

Haunch

Determine Force Haunch Must Resist Based on Number of Bolts

$$V_{BSH} = \frac{V_{Bolt}}{3}$$

*One-third of the bolts in the connection are on the haunch plate

Factored Bolt Resistance, V_{Bolts}	=	405.1 kN	91.2 kips
Probable Bolt Resistance, V_{Bolts}	=	506.4 kN	114.0 kips
Factored Applied Force on Haunch, V_{BSH}	=	135.0 kN	30.4 kips
Probable Applied Force on Haunch, V_{BSH}	=	168.8 kN	38.0 kips

Plate Capacity

Resistance Factor, $Ø_s$	=	0.9	0.9
Thickness of Haunch Plate, t_H	=	7.9 mm	5/16 in
Length of Haunch Plate, L_H	=	335.0 mm	13 3/16 in
Distance from Girder Centroid to Interface Between Beam and Haunch, $L_{H\text{-}CI}$	=	186.1 mm	7.33 in
Yield Strength of Haunch, F_y	=	345 MPa	50 ksi
Factored Applied Force on Haunch, V_{BSH}	=	135.0 kN	30.4 kips
Probable Applied Force on Haunch, V_{BSH}	=	168.8 kN	38.0 kips

Total Applied Stress on Haunch, $F_{TOT} = F_T + F_b$

Tensile Stress, $F_T = \frac{V_{BSH}}{t_H L_H}$

Factored Tensile Stress, F_T	=	51.51 MPa	7.38 ksi
Probable Tensile Stress, F_T	=	64.39 MPa	9.22 ksi

Bending Stress, $F_b = \frac{V_{BSH} L_{H-CI}}{\left(\frac{t_H L_H^2}{6}\right)}$

Factored Bending Stress, F_b	=	171.73 MPa	24.60 ksi
Probable Bending Stress, F_b	=	214.66 MPa	30.75 ksi
Factored Total Applied Stress, F_{TOT}	=	223.2 MPa	32.0 ksi
Probable Total Applied Stress, F_{TOT}	=	279.1 MPa	40.0 ksi

Check Applied Stress is Less Than Yielding Stress, $F_{TOT} \leq \phi_s F_y$

Check Factored Total Applied Stress		OK	
Probable Yield Strength of Haunch, R_yF_y	=	380 MPa	55 ksi
Check Probable Total Applied Stress		OK	

Local Capacity of Beam Web to Avoid Web Crippling

Thickness of Haunch Plate, t_H	=	7.9 mm	5/16 in	
Length of Haunch Plate, L_H	=	335.0 mm	13 3/16 in	
Bearing Length, $N = \frac{2}{3}\left(\frac{L_H}{2}\right)$	=	111.7 mm	4.4 in	
Factored Tensile Stress, F_T	=	51.51 MPa	7.38 ksi	
Probable Tensile Stress, F_T	=	64.39 MPa	9.22 ksi	
Factored Bending Stress, F_b	=	171.73 MPa	24.60 ksi	
Probable Bending Stress, F_b	=	214.66 MPa	30.75 ksi	
Total Applied Force on Haunch, $P_{TOT} = P_T + P_b$				
Tensile Force, $P_T = F_T t_H N$				
Factored Tensile Force, P_T	=	45.0 kN	10.1 kips	
Probable Tensile Force, P_T	=	56.3 kN	12.7 kips	
Bending Force, $P_b = \frac{F_b\left(\frac{L_H}{2}\right)}{2} t_H$				
Factored Bending Force, P_b	=	112.5 kN	25.3 kips	
Probable Bending Force, P_b	=	140.7 kN	31.7 kips	
Factored Total Applied Force, P_{TOT}	=	157.6 kN	35.5 kips	
Probable Total Applied Force, P_{TOT}	=	196.9 kN	44.4 kips	
Bearing Resistance, $B_{r-crip} = \phi_{bi} t_w (N + 10t_f) F_y$				*S16-09 Cl. 14.3.2i
Resistance Factor, $Ø_{bi}$	=	0.8	0.8	
Beam Web Thickness, t_w	=	7.5 mm	0.295 in	
Beam Flange Thickness, t_f	=	13.1 mm	0.515 in	
Yield Strength of Haunch, F_y	=	345 MPa	50 ksi	
Factored Bearing Resistance, $B_{r\text{-}crip}$	=	500.1 kN	112.6 kips	
Probable Yield Strength of Haunch, R_yF_y	=	380 MPa	55 ksi	
Probable Bearing Resistance, $B_{r\text{-}crip}$	=	687.7 kN	154.9 kips	
Check Factored Bearing Resistance is Greater than Applied Force		OK		
Check Probable Bearing Resistance is Greater than Applied Force		OK		

Weld Between Beam and Haunch

Thickness of Haunch Plate, t_H	=	7.9 mm	5/16 in	
Factored Tensile Stress, F_T	=	51.51 MPa	7.38 ksi	
Probable Tensile Stress, F_T	=	64.39 MPa	9.22 ksi	
Factored Bending Stress, F_b	=	171.73 MPa	24.60 ksi	
Probable Bending Stress, F_b	=	214.66 MPa	30.75 ksi	
Total Applied Force per Unit Length, $f_{wTOT} = F_{Tw} + F_{bw}$				
Tensile Force per Unit Length of Weld, $f_{Tw} = \frac{F_T t_H}{2}$				
Factored Tensile Force per Unit Length, f_{Tw}	=	0.20 kN/mr	1.15 kips/in	
Probable Tensile Force per Unit Length, f_{Tw}	=	0.25 kN/mr	1.44 kips/in	
Bending Force per Unit Length of Weld, $f_{bw} = \frac{F_b t_H}{2}$				
Factored Bending Force per Unit Length, f_{bw}	=	0.67 kN/mr	3.84 kips/in	
Probable Bending Force per Unit Length, f_{bw}	=	0.84 kN/mr	4.81 kips/in	
Factored Total Applied Force per Unit Length, f_{wTOT}	=	0.87 kN/mr	5.00 kips/in	
Probable Total Applied Force per Unit Length, f_{wTOT}	=	1.09 kN/mr	6.25 kips/in	
Weld Resistance per Weld Area, $V_W = 0.67\phi_w n_w X_u A_w$				*S16-09 Cl. 13.13.2.2
Resistance Factor, $Ø_w$	=	0.67	0.67	
Ultimate Strength of Electrode, X_u	=	490 MPa	70 ksi	
Factored Weld Resistance per Weld Area, V_w	=	155.5 kN/mr	22.2 kips/in^2	
Probable Weld Resistance per Weld Area, V_w	=	232.1 kN/mr	33.2 kips/in^2	
Weld Size Based on Factored Strength, $D_w \geq \frac{f_w}{V_w}$	=	6.4 mm	1/4 in	Note: Rounding to nearest 16th of an inch
Weld Size Based on Probable Strength, $D_w \geq \frac{f_w}{V_w}$	=	4.8 mm	3/16 in	Note: Rounding to nearest 16th of an inch
Therefore Select Adequate Weld Size	=	6.4 mm	1/4 in	

Specimen 8 - Double Cope Welded In Shop

Configuration Parameters

Girder		W310x143	(W12x96)	
Beam		W310x74	(W12x50)	
Cope Length, c	=	160.3 mm	6 5/16 in	
Cope Depth - Top, $d_{c\text{-}Top}$	=	47.6 mm	1 7/8 in	
Cope Depth - Bottom, $d_{c\text{-}Bot}$	=	38.1 mm	1 1/2 in	

Beam

Shear Yielding

$$V_{SY} = 0.66\phi_s F_y A_w$$ *S16-09 Cl. 13.4.1.1

Resistance Factor, $Ø_s$	=	0.9	0.9	
Gross Shear Area, $A_w = t_w h_o$	=	2106.6 mm^2	3.27 in^2	
Beam Web Thickness, t_w	=	9.4 mm	0.370 in	
Reduced Beam Height, h_o	=	224.2 mm	8.83 in	
Yield Strength of Plate, F_y	=	345 MPa	50 ksi	
Factored Shear Yielding Resistance in Beam, V_{SY}	=	430.6 kN	97.0 kips	
Probable Yielding Strength of Beam, R_yF_y	=	380 MPa	55 ksi	
Probable Shear Yielding Resistance in Beam, V_{SY}	=	526.3 kN	118.5 kips	

Flexural Yielding at Cope

$$V_{FY} = \frac{M_{FY}}{e}$$ *S16-09 Cl. 13.5

Resistance Factor, $Ø_s$	=	0.9	0.9	
Elastic Section Modulus of Gross Reduced Area, S_x'	=	78701.1 mm^3	4.80 in^3	
Reduced Beam Height, h_o	=	224.2 mm	8.83 in	
Beam Web Thickness, t_w	=	9.4 mm	0.370 in	
Eccentricity to Cope, e	=	167.3 mm	6.59 in	
Yield Strength of Beam, F_y	=	345 MPa	50 ksi	
Moment Yielding Resistance at Cope, $M_{FY} = \phi_s F_y S_x'$				
Factored Moment Yielding Resistance at Cope, M_{FY}	=	24.4 kN-m	216.1 kips-in	
Probable Yield Strength of Beam, R_yF_y	=	380 MPa	55 ksi	
Probable Moment Yielding Resistance at Cope, M_{FY}	=	29.8 kN-m	264.1 kips-in	
Factored Flexural Yielding at Cope, V_{FY}	=	145.7 kN	32.8 kips	
Probable Flexural Yielding at Cope, V_{FY}	=	178.0 kN	40.1 kips	

Flexural Buckling at Cope

$$V_{FB} = \frac{M_{FB}}{e}$$

Resistance Factor, $Ø_s$	=	0.9	0.9	
Beam Web Thickness, t_w	=	9.4 mm	0.370 in	
Reduced Beam Height, h_o	=	224.2 mm	8.83 in	
Cope Length, c	=	160.3 mm	6 5/16 in	
Eccentricity to Cope, e	=	167.32 mm	6.59 in	
Elastic Section Modulus of Gross Reduced Area, S_x'	=	78701.1 mm^3	4.80 in^3	
Yield Strength of Beam, F_y	=	345 MPa	50 ksi	
Probable Yield Strength of Beam, R_yF_y	=	380 MPa	55 ksi	

$$F_{cr} = F_y Q$$ *AISC Manual 2011 Part 9

$$Q = \begin{cases} 1 \; for \; \lambda \le 0.7 \\ (1.34 - 0.486\lambda) \; for \; 0.7 < \lambda \le 1.41 \\ (1.30 / \lambda^2) \; for \; \lambda > 1.41 \end{cases}$$

Factored Q	=	1	1	
Probable Q	=	1	1	

where

$$\lambda = \frac{h_o\sqrt{F_y}}{10t_w\sqrt{475 + 280\left(\frac{h_o}{c}\right)^2}}$$

Factored λ	=	0.53	0.53	

Probable λ	=	0.55	0.55
Factored Critical Buckling Stress, F_{cr}	=	349.0 MPa	50.0 ksi
Probable Critical Buckling Stress, F_{cr}	=	383.9 MPa	55.0 ksi
Moment Buckling Resistance at Cope, $M_{FB} = \phi_s F_{cr} S_x'$			
Factored Moment Buckling Resistance at Cope, M_{FB}	=	24.4 kN-m	216.1 kips-in
Probable Moment Buckling Resistance at Cope, M_{FB}	=	29.8 kN-m	264.1 kips-in
Factored Flexural Buckling at Cope, V_{FB}	=	145.7 kN	32.8 kips
Probable Flexural Buckling at Cope, V_{FB}	=	178.0 kN	40.1 kips

Von Mises Interaction

$$\left(\frac{V_{SY}}{V_{VM}}\right)^2 + \left(\frac{M_{FY}}{M_{VM}}\right)^2 \leq 1.0$$

therefore

$$V_{VM} = \frac{\phi_s F_y S_x'}{\sqrt{\left(\frac{S_x'}{0.66A_w}\right)^2 + e^2}}$$

Resistance Factor, $Ø_s$	=	0.9	0.9
Elastic Section Modulus of Gross Reduced Area, S_x'	=	78701.1 mm^3	4.80 in^3
Gross Shear Area, A_w	=	2106.6 mm^2	3.27 in^2
Eccentricity to Cope, e	=	167.3 mm	6 3/5 in
Yield Strength of Beam, F_y	=	345 MPa	50 ksi
Factored Von Mises Resistance, V_{VM}	=	138.0	31.1 kips
Probable Yield Strength of Beam, R_yF_y	=	380 MPa	55 ksi
Probable Von Mises Resistance, V_{VM}	=	168.6 kips	38.0 kips

Welds

Weld Strength

$$V_W = 0.67\phi_w n_w X_u A_w$$

*S16-09 Cl. 13.13.2.2

Resistance Factor, $Ø_w$	=	0.67	0.67
Number of Welds, n_w	=	2	2
Ultimate Strength of Electrode, X_u	=	490 MPa	70 ksi
Welded Area, A_w	=	1140.5 mm^2	1.77 in^2
Length of Weld, L_w	=	203.2 mm	8 in
Weld Size, t_w	=	7.9 mm	5/16 in
Factored Weld Resistance, V_w	=	493.3 kN	111.1 kips
Probable Weld Resistance, V_w	=	736.2 kN	165.8 kips

Specimen 10 - Single Cope Welded In Shop

Configuration Parameters

Girder		W760x257	(W30x173)
Beam		W610x140	(W24x94)
Cope Length, c	=	195.3 mm	7 11/16 in
Cope Depth, d_c	=	50.8 mm	2 in

Beam

Shear Yielding

$V_{SY} = 0.66\phi_s F_y A_w$ *S16-09 Cl. 13.4.1.1

Resistance Factor, $Ø_s$	=	0.9	0.9
Gross Shear Area, $A_w = t_w h_o$	=	7409.3 mm^2	11.48 in^2
Beam Web Thickness, t_w	=	13.1 mm	0.515 in
Reduced Beam Height, h_o	=	566.4 mm	22.30 in
Yield Strength of Plate, F_y	=	345 MPa	50 ksi
Factored Shear Yielding Resistance in Beam, V_{SY}	=	1514.4 kN	341.1 kips
Probable Yielding Strength of Beam, $R_y F_y$	=	380 MPa	55 ksi
Probable Shear Yielding Resistance in Beam, V_{SY}	=	1851.0 kN	416.9 kips

Flexural Yielding at Cope

$V_{FY} = \frac{M_{FY}}{e}$ *S16-09 Cl. 13.5

Resistance Factor, $Ø_s$	=	0.9	0.9
Elastic Section Modulus of Gross Reduced Area, S_x'	=	699466.4 mm^3	42.68 in^3
Reduced Beam Height, h_o	=	566.4 mm	22.30 in
Beam Web Thickness, t_w	=	13.1 mm	0.515 in
Eccentricity to Cope, e	=	203.6 mm	8.02 in
Yield Strength of Beam, F_y	=	345 MPa	50 ksi
Moment Yielding Resistance at Cope, $M_{FY} = \phi_s F_y S_x'$			
Factored Moment Yielding Resistance at Cope, M_{FY}	=	217.0 kN-m	1920.8 kips-in
Probable Yield Strength of Beam, $R_y F_y$	=	380 MPa	55 ksi
Probable Moment Yielding Resistance at Cope, M_{FY}	=	265.3 kN-m	2347.6 kips-in
Factored Flexural Yielding at Cope, V_{FY}	=	1064.0 kN	239.6 kips
Probable Flexural Yielding at Cope, V_{FY}	=	1300.5 kN	292.9 kips

Flexural Buckling at Cope

$V_{FB} = \frac{M_{FB}}{e}$

Resistance Factor, $Ø_s$	=	0.9	0.9
Modulus of Elasticity, E	=	200000 MPa	29000 ksi
Poisson's Ratio, ν	=	0.3	0.3
Beam Web Thickness, t_w	=	13.1 mm	0.515 in
Beam Depth, d	=	617.2 mm	24.3 in
Cope Length, c	=	195.3 mm	7.69 in
Reduced Beam Height, h_o	=	566.4 mm	22.30 in

$F_{cr} = \frac{\pi^2 E}{12(1-\nu^2)}\left(\frac{t_w}{h_0}\right)^2 fk$ *AISC Manual 2011 Part 9

Plate Buckling Model Adjustment Factor, f

$$f = \begin{cases} \frac{2c}{d} \text{ when } \frac{c}{d} \le 1.0 \\ 1 + \frac{c}{d} \text{ when } \frac{c}{d} > 1.0 \end{cases}$$

	=	0.63	0.63

Plate Buckling Coefficient, k

$$k = \begin{cases} 2.2\left(\frac{h_0}{c}\right)^{1.65} \text{ when } \frac{c}{h_0} \le 1.0 \\ \frac{2.2h_0}{c} \text{ when } \frac{c}{h_0} > 1.0 \end{cases}$$

		12.75	12.75
Critical Buckling Stress, F_{cr}	=	787.3 MPa	112.8 ksi
Elastic Section Modulus of Gross Reduced Area, S_x'	=	699466.4 mm^3	42.68 in^3
Eccentricity to Cope, e	=	203.6 mm	8.02 in
Moment Buckling Resistance at Cope, $M_{FB} = \phi_s F_{cr} S_x'$			
Factored Moment Buckling Resistance at Cope, M_{FB}	=	489.6 kN-m	4332.9 kips-in

Probable Moment Buckling Resistance at Cope, M_{FB}	=	544.0 kN-m	4814.3 kips-in
Factored Flexural Buckling at Cope, V_{FB}	=	2400.3 kN	540.6 kips
Probable Flexural Buckling at Cope, V_{FB}	=	2666.9 kN	600.7 kips

Von Mises Interaction

$$\left(\frac{V_{SY}}{V_{VM}}\right)^2 + \left(\frac{M_{FY}}{M_{VM}}\right)^2 \leq 1.0$$

therefore

$$V_{VM} = \frac{\phi_s F_y S_x'}{\sqrt{\left(\frac{S_x'}{0.66A_w}\right)^2 + e^2}}$$

Resistance Factor, $Ø_s$	=	0.9	0.9
Elastic Section Modulus of Gross Reduced Area, S_x'	=	699466.4 mm^3	42.68 in^3
Gross Shear Area, A_w	=	7409.3 mm^2	11.48 in^2
Eccentricity to Cope, e	=	203.6 mm	8 in
Yield Strength of Beam, F_y	=	345 MPa	50 ksi
Factored Von Mises Resistance, V_{VM}	=	870.6	196.1 kips
Probable Yield Strength of Beam, R_yF_y	=	380 MPa	55 ksi
Probable Von Mises Resistance, V_{VM}	=	1064.1 kips	239.7 kips

Welds

Weld Strength

$$V_W = 0.67\phi_w n_w X_u A_w$$

*S16-09 Cl. 13.13.2.2

Resistance Factor, $Ø_w$	=	0.67	0.67
Number of Welds, n_w	=	2	2
Ultimate Strength of Electrode, X_u	=	490 MPa	70 ksi
Welded Area, A_w	=	2281.0 mm^2	3.54 in^2
Length of Weld, L_w	=	406.4 mm	16 in
Weld Size, t_w	=	7.9 mm	5/16 in
Factored Weld Resistance, V_w	=	986.5 kN	222.2 kips
Probable Weld Resistance, V_w	=	1472.5 kN	331.6 kips

APPENDIX B

FABRICATION DRAWINGS

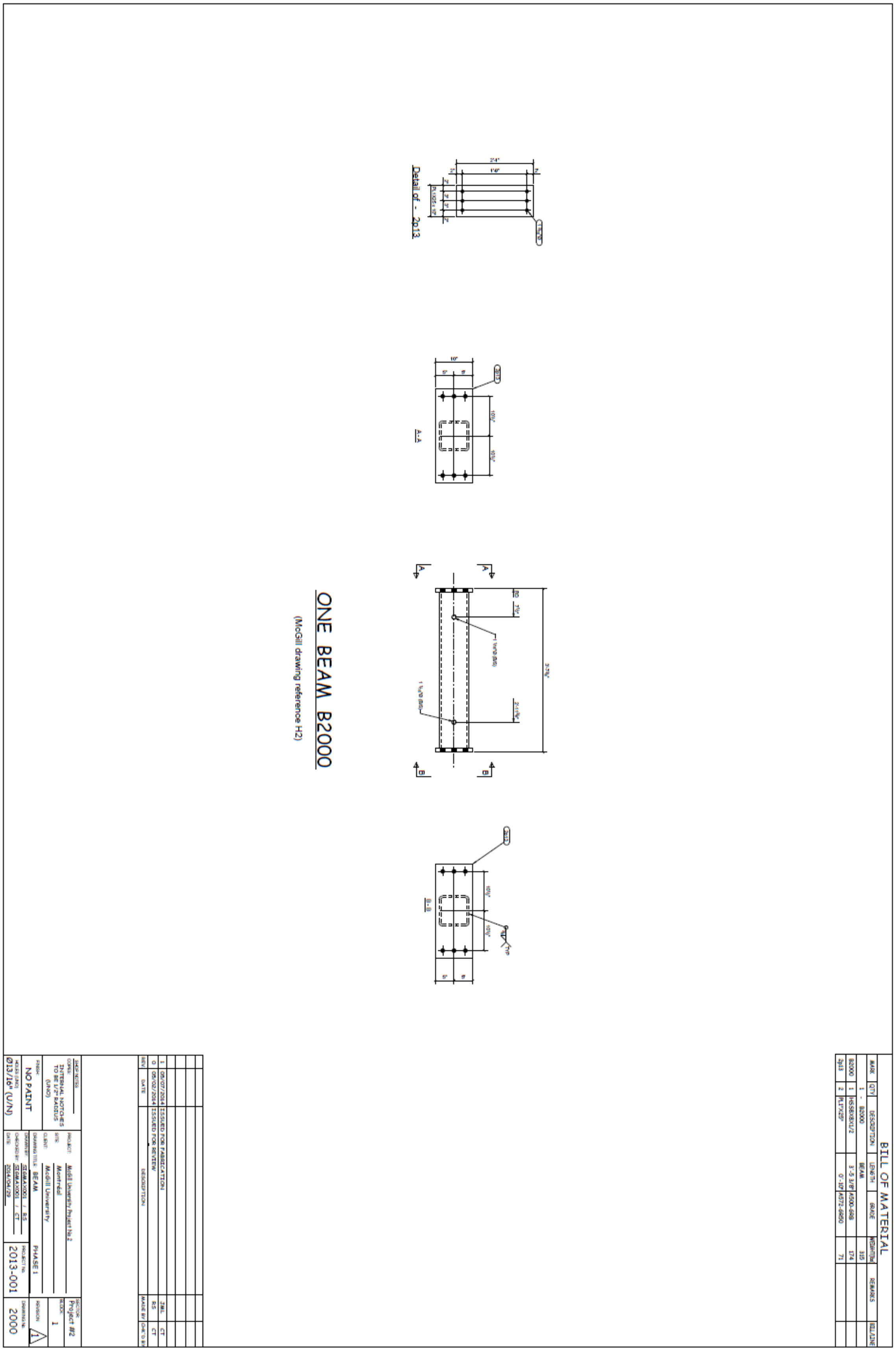
ONE BEAM B2000
(McGill drawing reference H2)
BILL OF MATERIAL

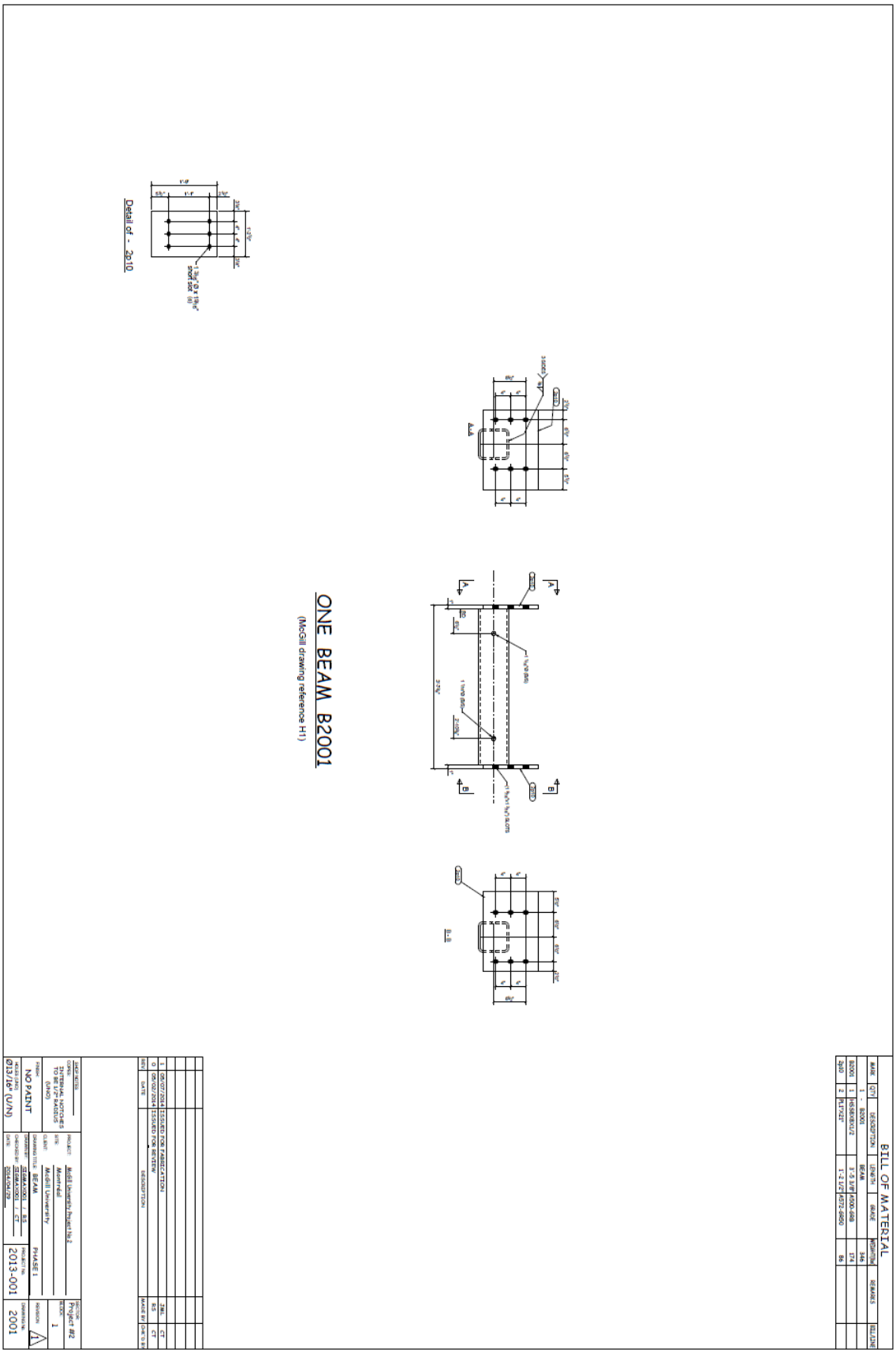
ONE BEAM B2001
(McGill drawing reference H1)
Detail of - 2p10
BILL OF MATERIAL
NO PAINT
Ø13/16" (U/N)
McGill Steel#3 Project No.1
Montreal
McGill University
PHASE 1
BEAM
2013-001
2001
Project #2

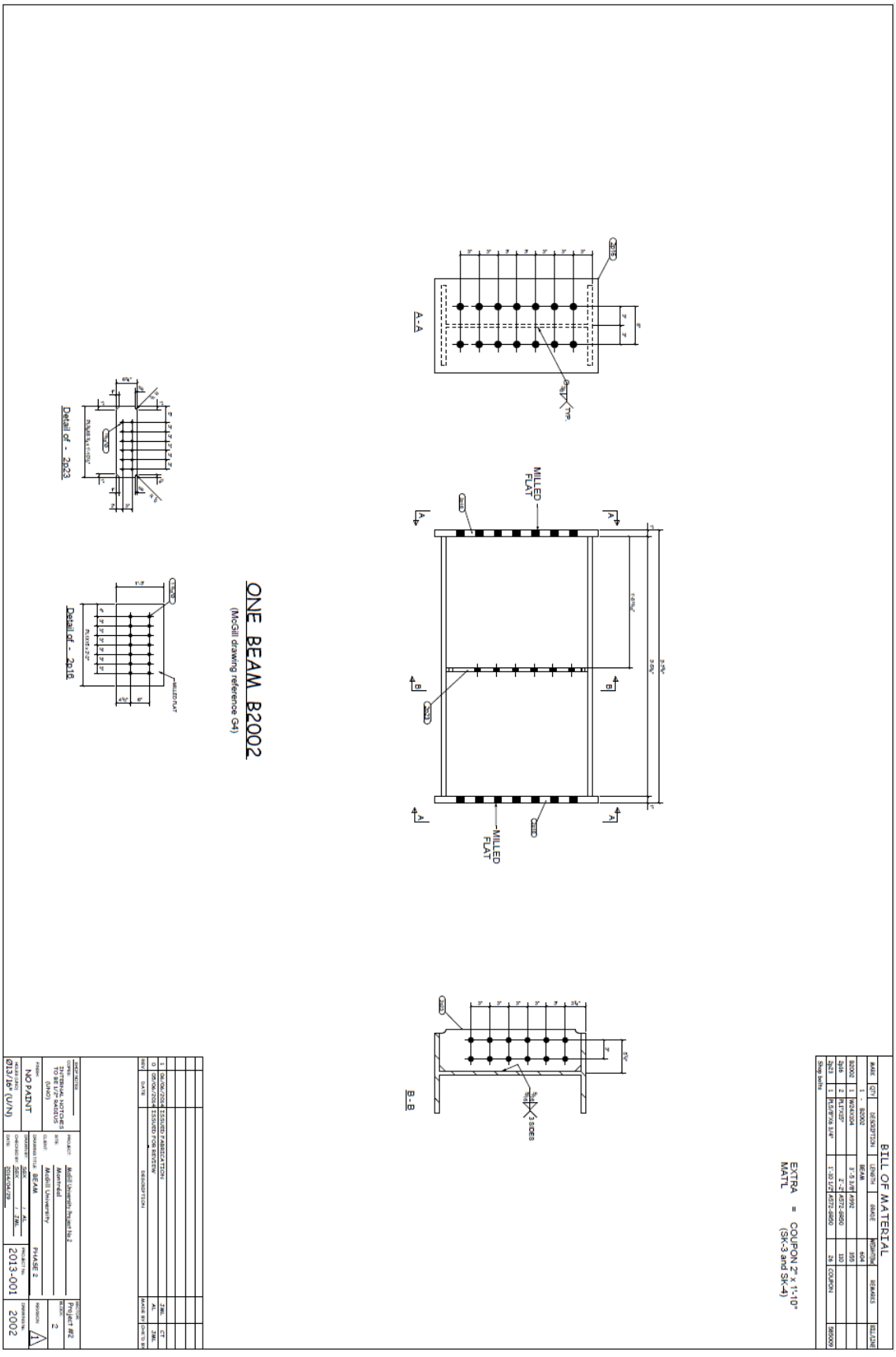
ONE BEAM B2002
(McGill drawing reference G4)
BILL OF MATERIAL
EXTRA MAT'L = COUPON 2" x 1'-10" (SK-3 and SK-4)
A-A
B-B
MILLED FLAT
Detail of - 2p16
Detail of - 2p23
NO PAINT
Ø13/16" (U/N)
2013-001
2002
Project #2
Phase 2
McGill University
Montreal

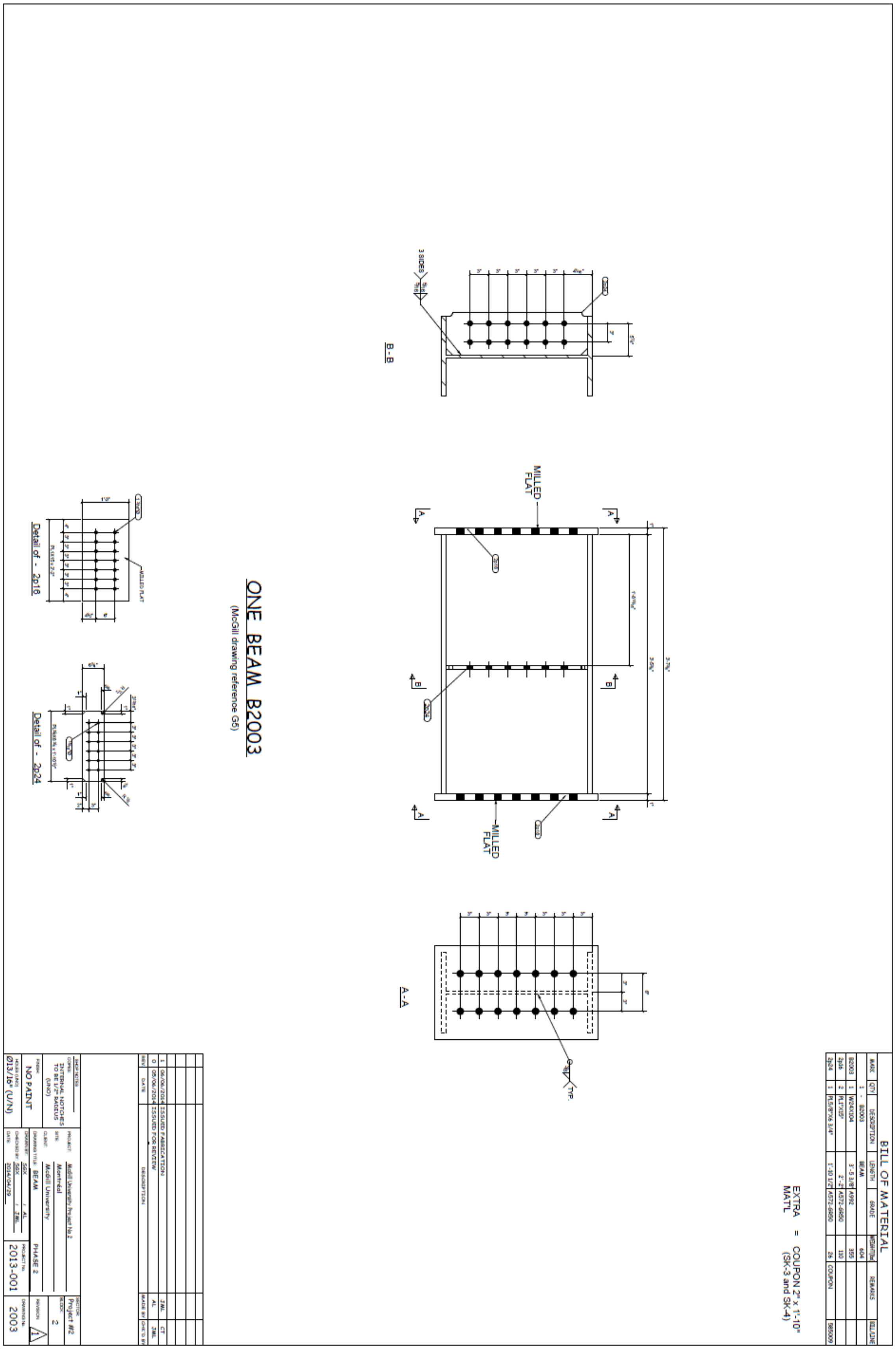
ONE BEAM B2003
(McGill drawing reference G5)
B-B
A-A
MILLED FLAT
MILLED FLAT
Detail of - 2p16
Detail of - 2p24
BILL OF MATERIAL
EXTRA MATL = COUPON 2" x 1'-10" (SK-3 and SK-4)
NO PAINT
BEAM
PHASE 2
2013-001
2003

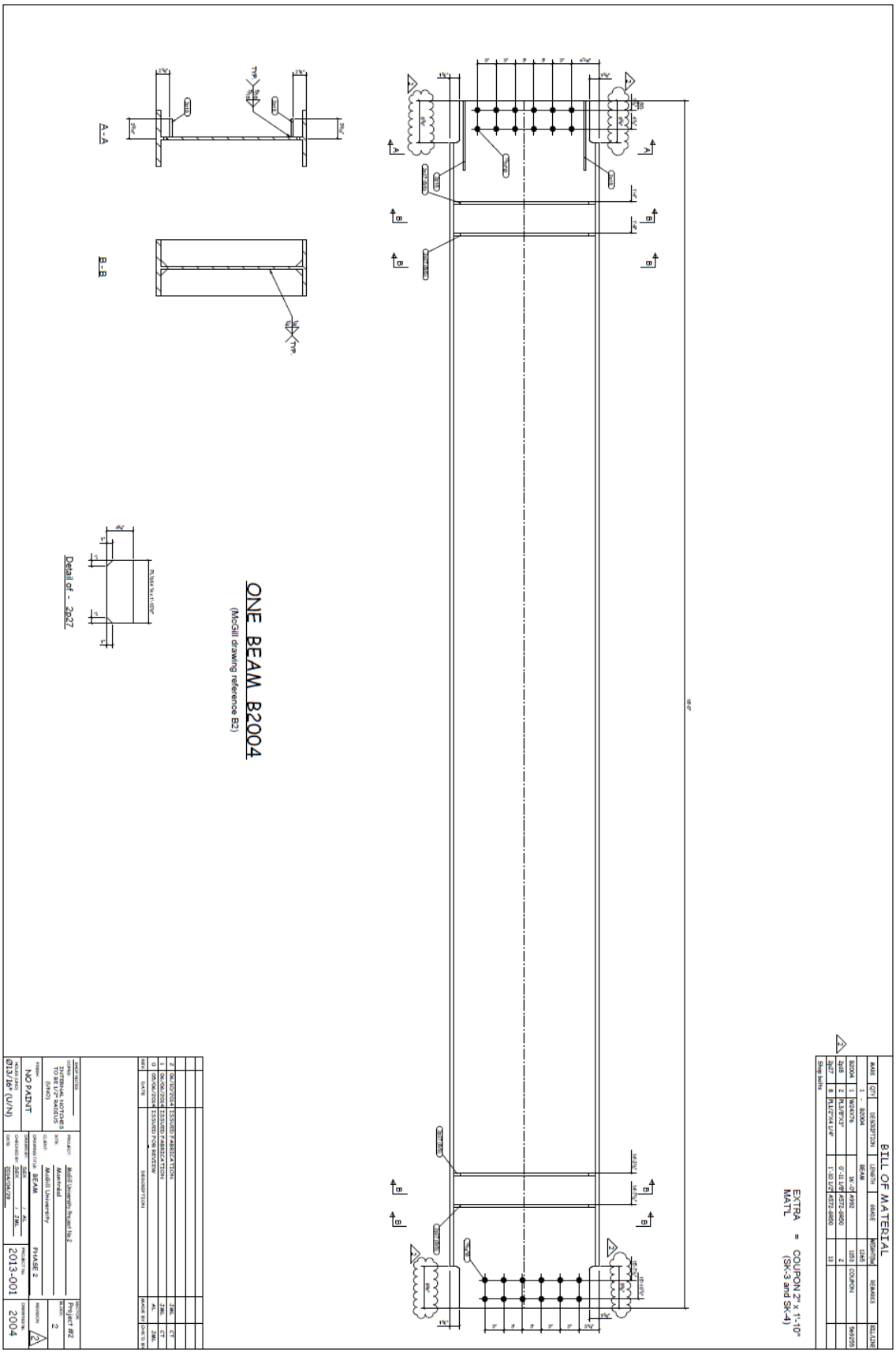
ONE BEAM B2004
(McGill drawing reference B2)
A-A
B-B
Detail of - 2627
BILL OF MATERIAL
EXTRA MATL = COUPON 2" x 1'-10" (SK-3 and SK-4)
NO PAINT
Ø13/16" (U/N)
INTERNAL NOTCHES TO BE 1/2" RADIUS (UNO)
McGill University
PHASE 2
2013-001
2004
Project #2

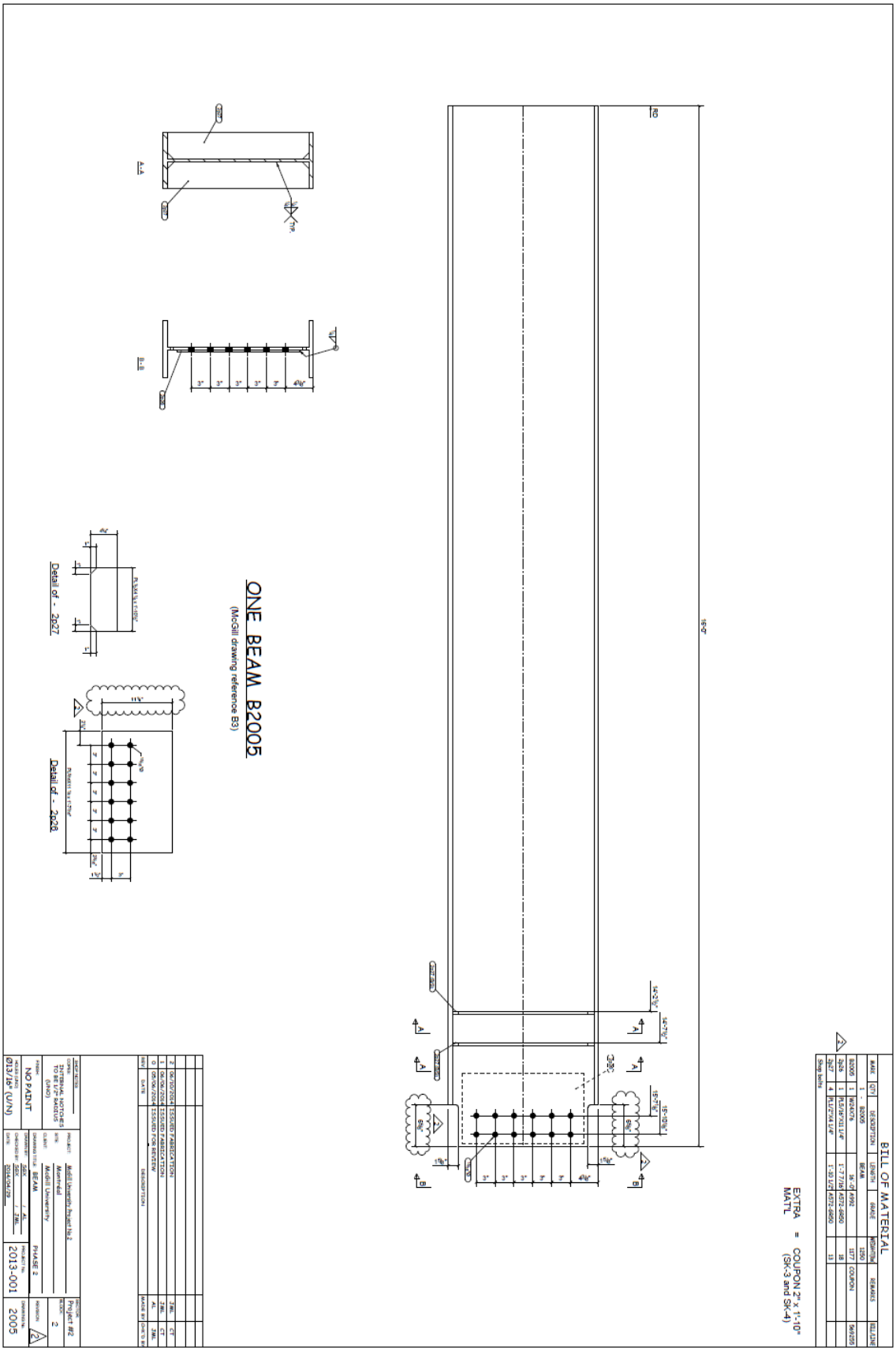
ONE BEAM B2005
(McGill drawing reference B3)
BILL OF MATERIAL
EXTRA MATL = COUPON 2" x 1'-10" (SK-3 and SK-4)
NO PAINT
Ø13/16" (U/N)
2013-001
2005
Project #2
Mcgill University
PHASE 2
BEAM

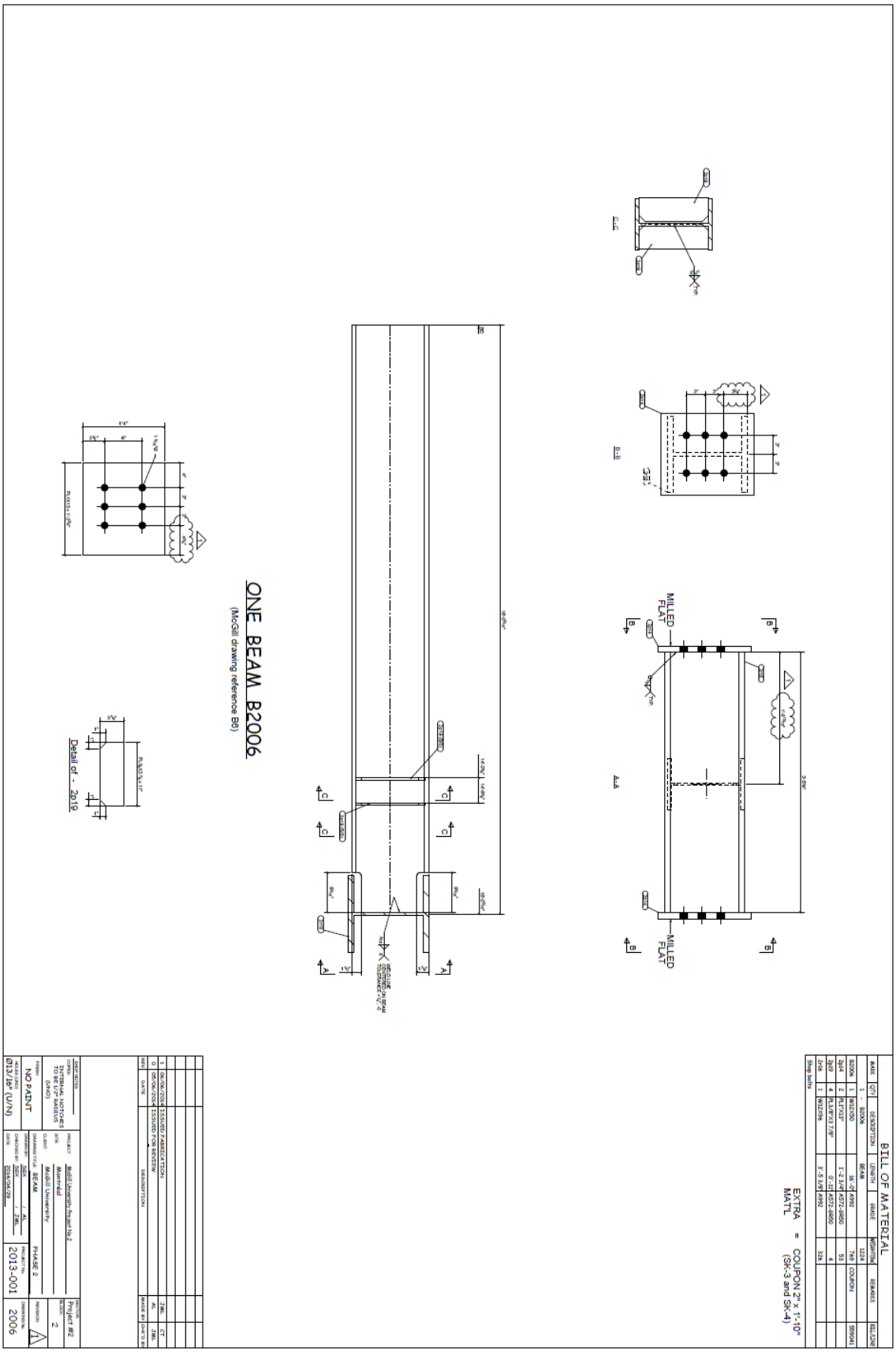
ONE BEAM B2006
(McGill drawing reference B8)
Detail of - 2p19
MILLED FLAT
MILLED FLAT
BILL OF MATERIAL
EXTRA MATL = COUPON 2"x 1'-10" (SK-3 and SK-4)
NO PAINT
PHASE 2
2013-001
Project #2
2006

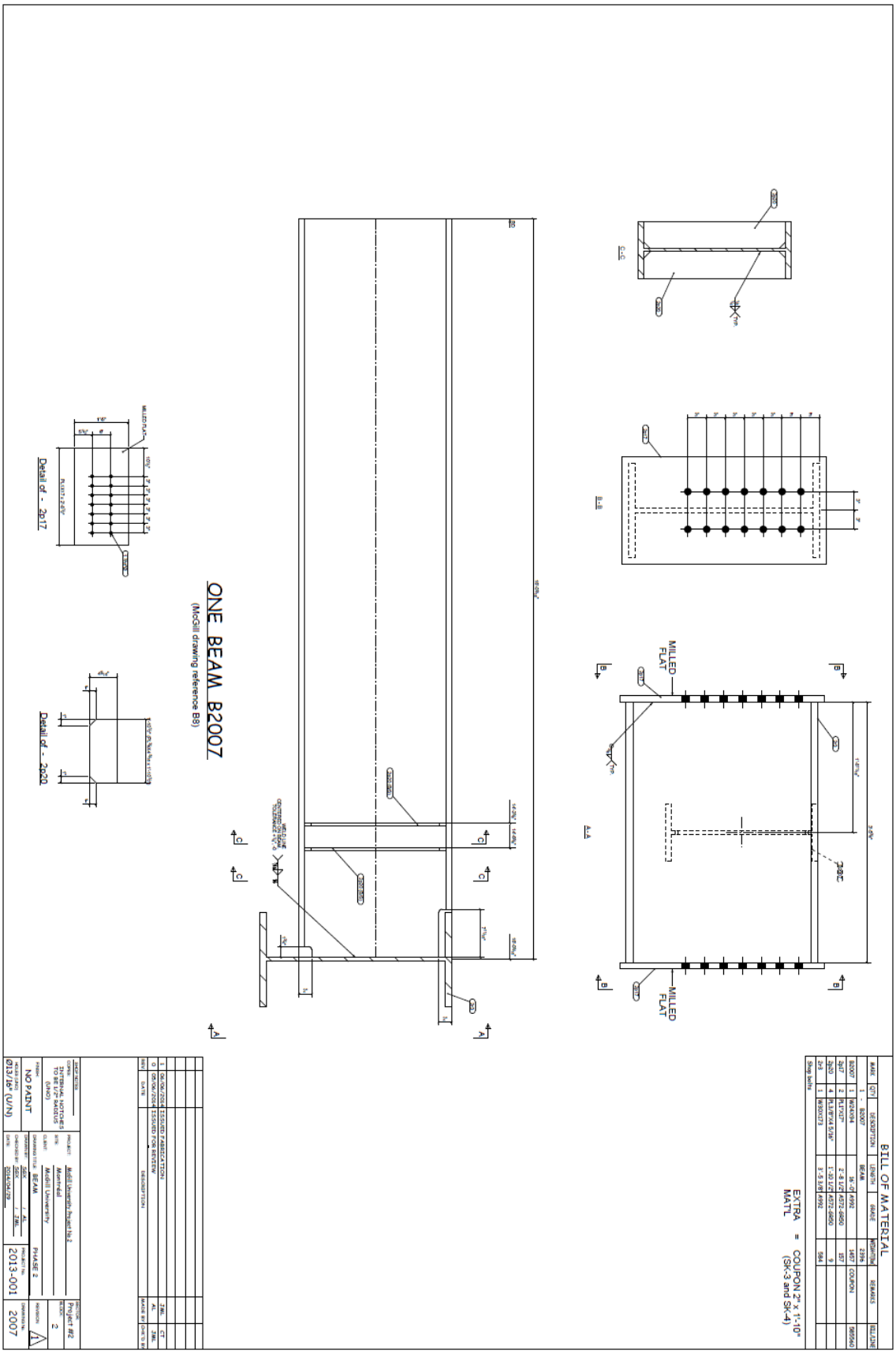
ONE BEAM B2007
(McGill drawing reference B8)
Detail of - 2b17
Detail of - 2b20
MILLED FLAT
MILLED FLAT
BILL OF MATERIAL
EXTRA MATL = COUPON 2" x 1'-10" (SK-3 and SK-4)
NO PAINT
Ø13/16" (U/N)
INTERNAL NOTCHES TO BE 1/2" RADIUS (TYP.)
McGill University
PHASE 2
2013-001
2007
Project #2

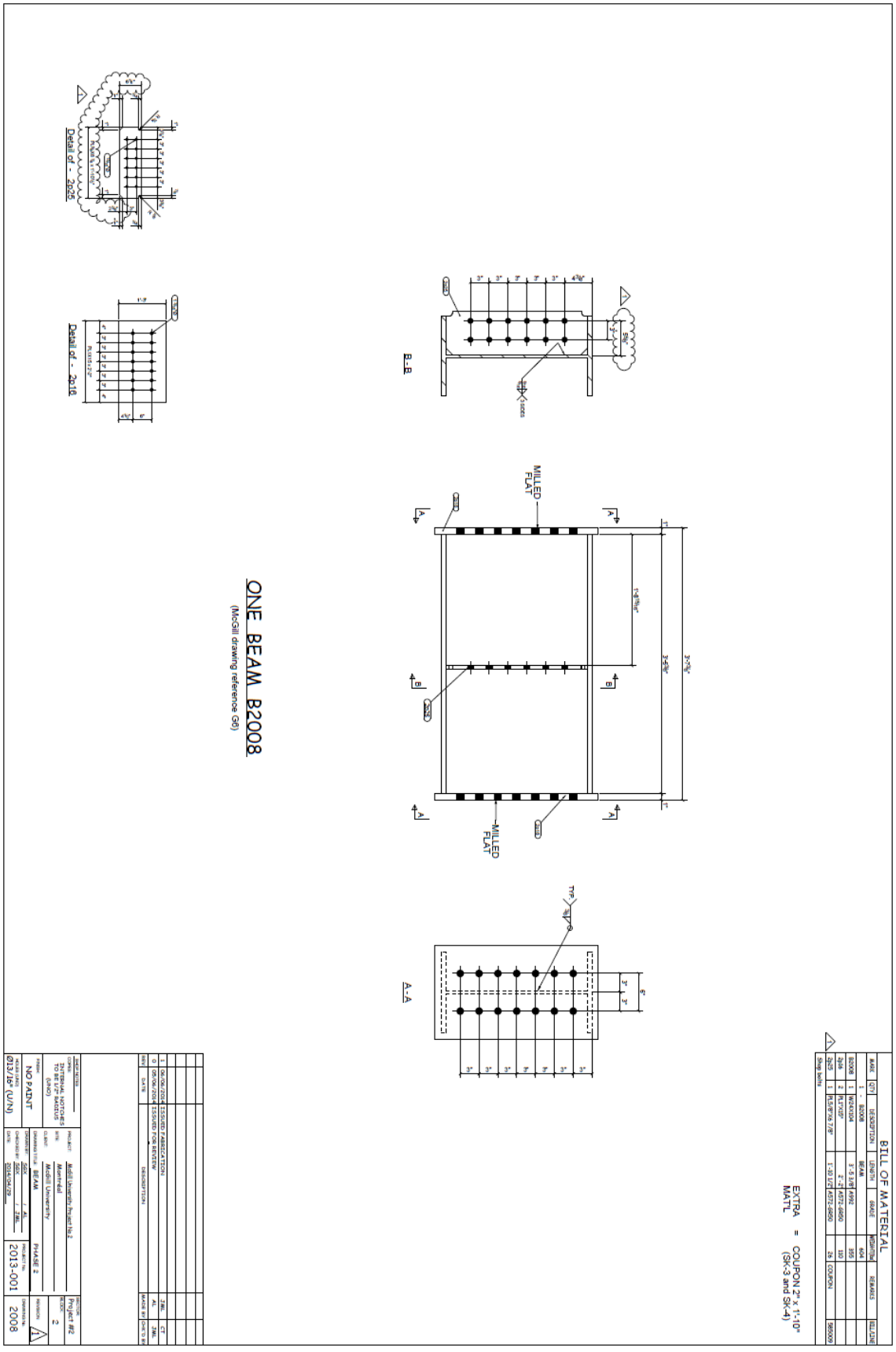
ONE_BEAM_B2008
(McGill drawing reference G6)
BILL OF MATERIAL
EXTRA MATL = COUPON 2" x 1'-10" (SK-3 and SK-4)
MILLED FLAT
MILLED FLAT
A-A
B-B
Detail of - 2p16
Detail of - 2p25
NO PAINT
2013-001
2008

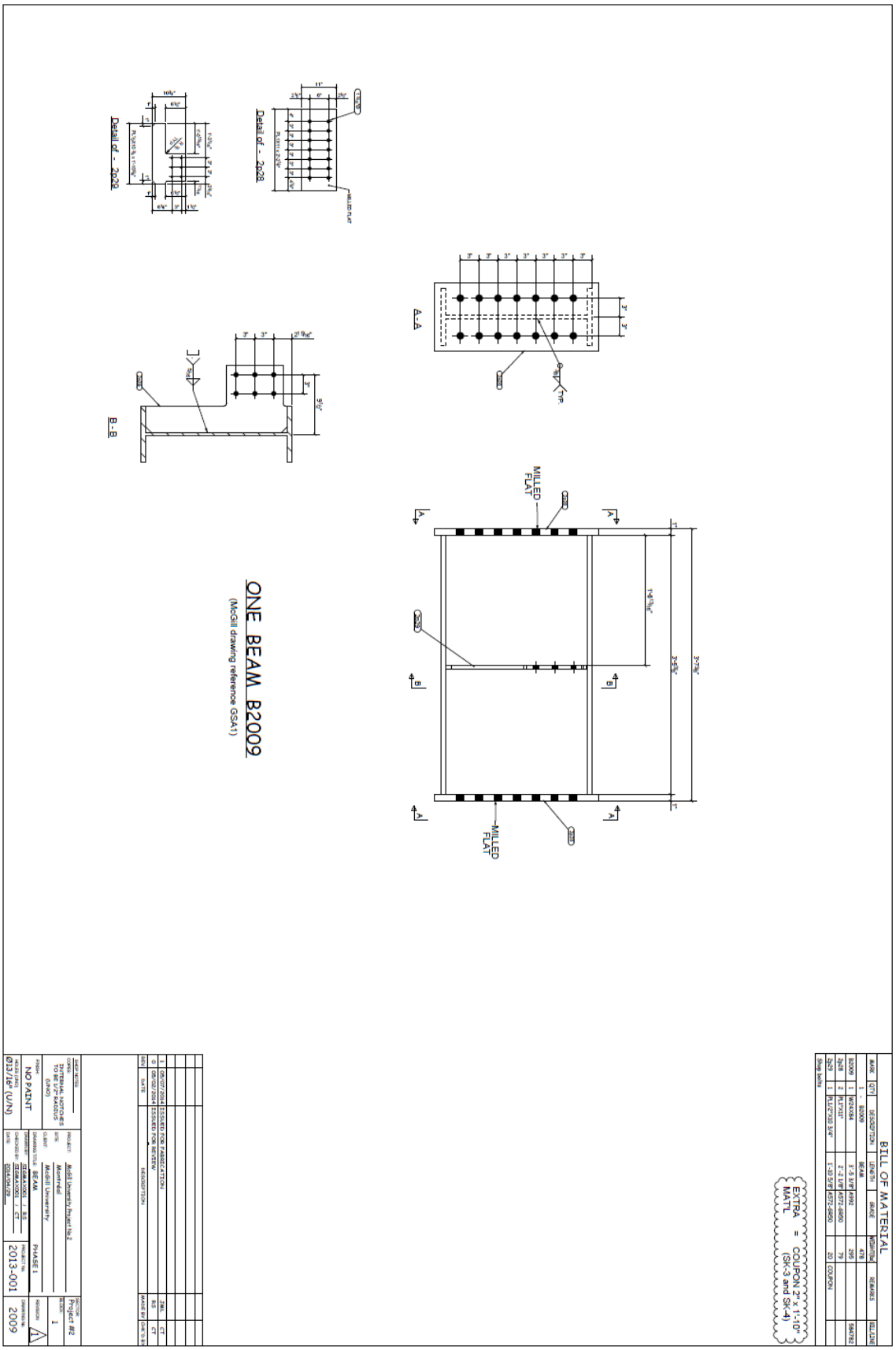
ONE BEAM B2009
(McGill drawing reference GSA1)
Detail of - 2x28
Detail of - 2x28
A - A
B - B
MILLED FLAT
MILLED FLAT
BILL OF MATERIAL
EXTRA = COUPON 22"-110" MATL (SK-3 and SK-4)
NO PAINT
Ø13/16" (U/N)
2013-001
2009
Project #2
PHASE I
McGill University
Montreal

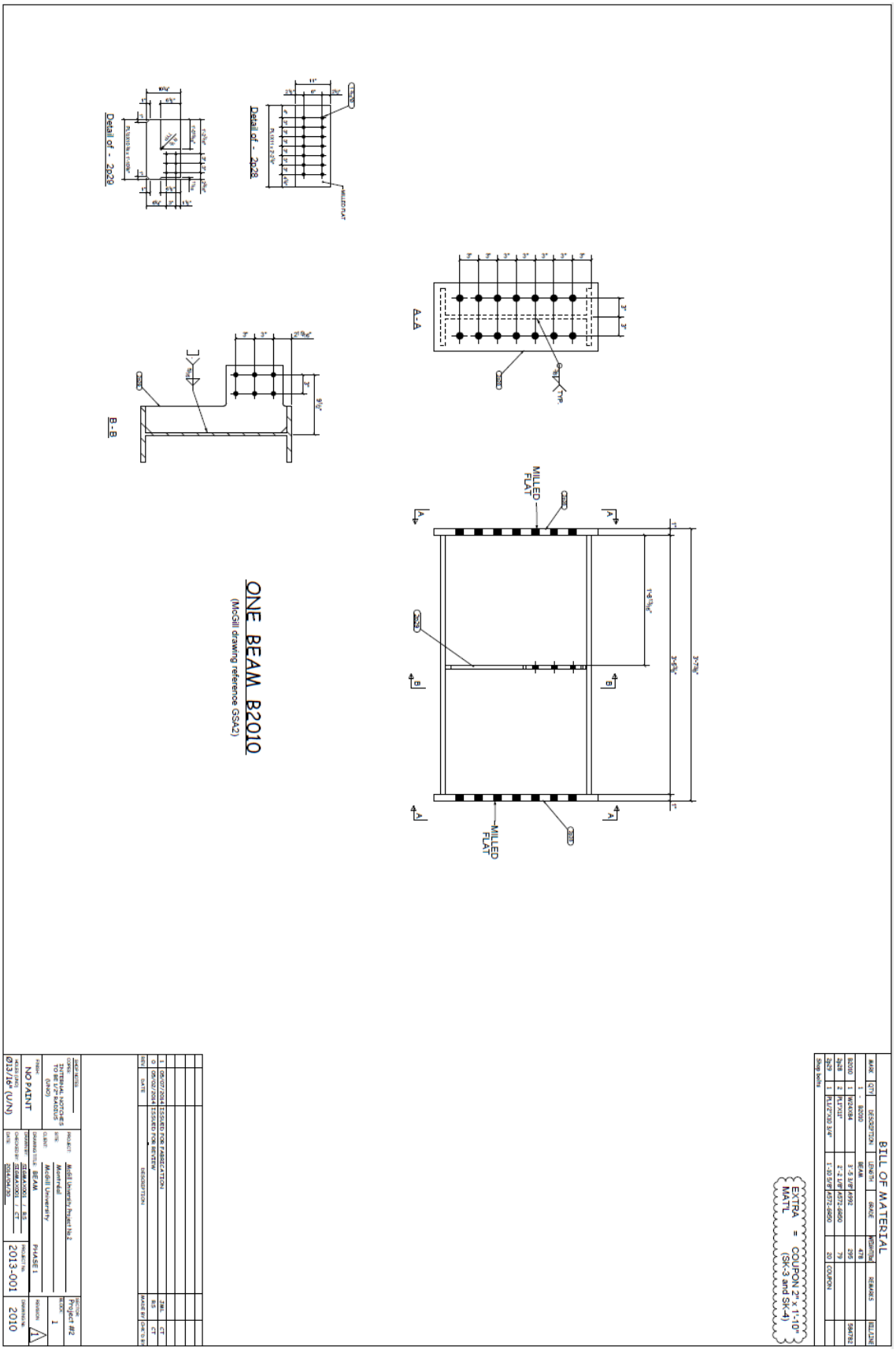
ONE BEAM B2010
(McGill drawing reference GSA2)
Detail of - 2628
Detail of - 2629
A - A
B - B
MILLED FLAT
MILLED FLAT
BILL OF MATERIAL
EXTRA = COUPON 2" x 1'-10"
MATL (SK-3 and SK-4)
NO PAINT
Ø13/16" (U/N)
McGill University
PHASE 1
2013-001
2010
Project #2

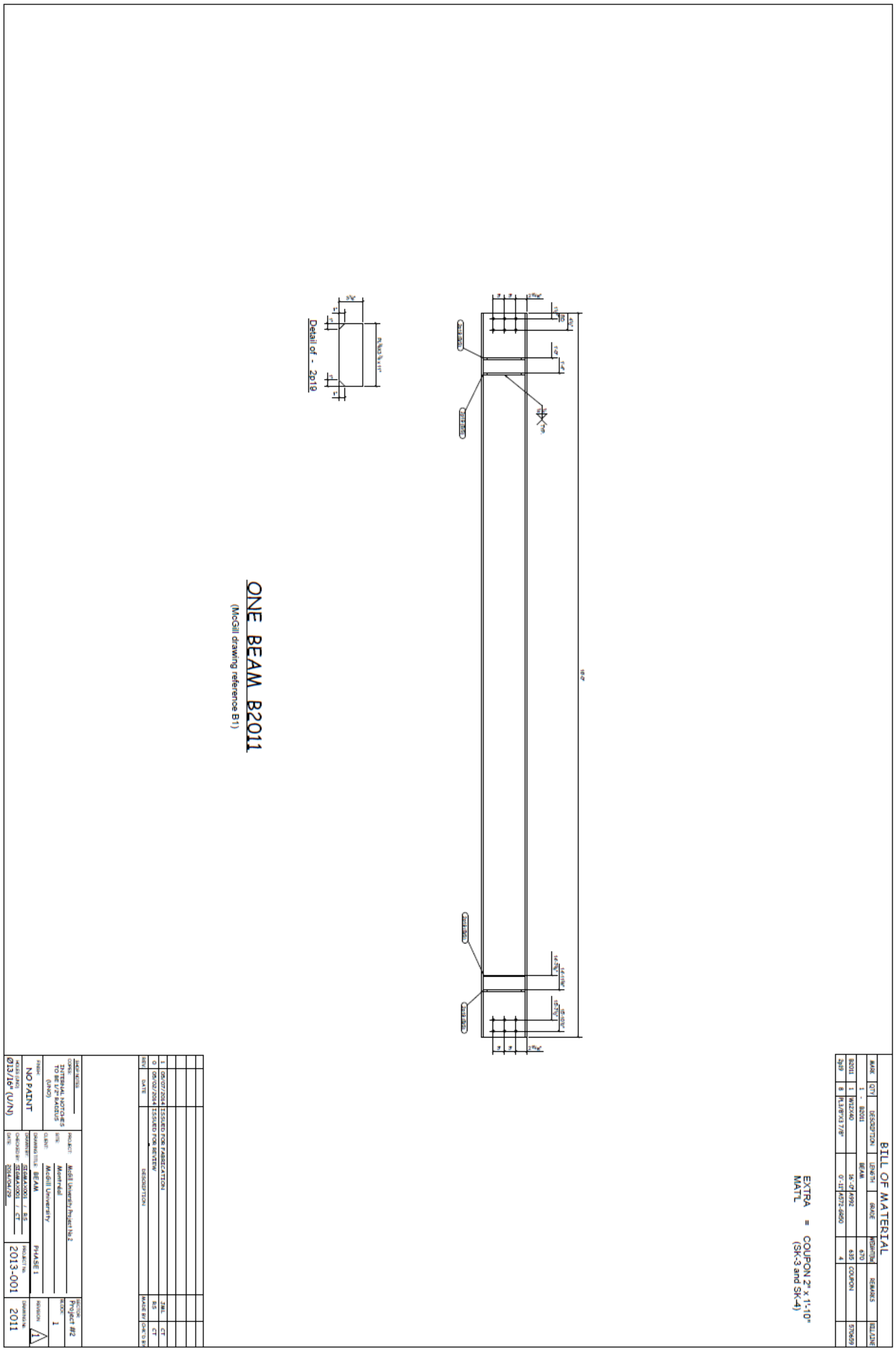
ONE BEAM B2011
(McGill drawing reference B1)
Detail of - 2p19
BILL OF MATERIAL
EXTRA MATL = COUPON 2" x 1'-10" (SK-3 and SK-4)
NO PAINT

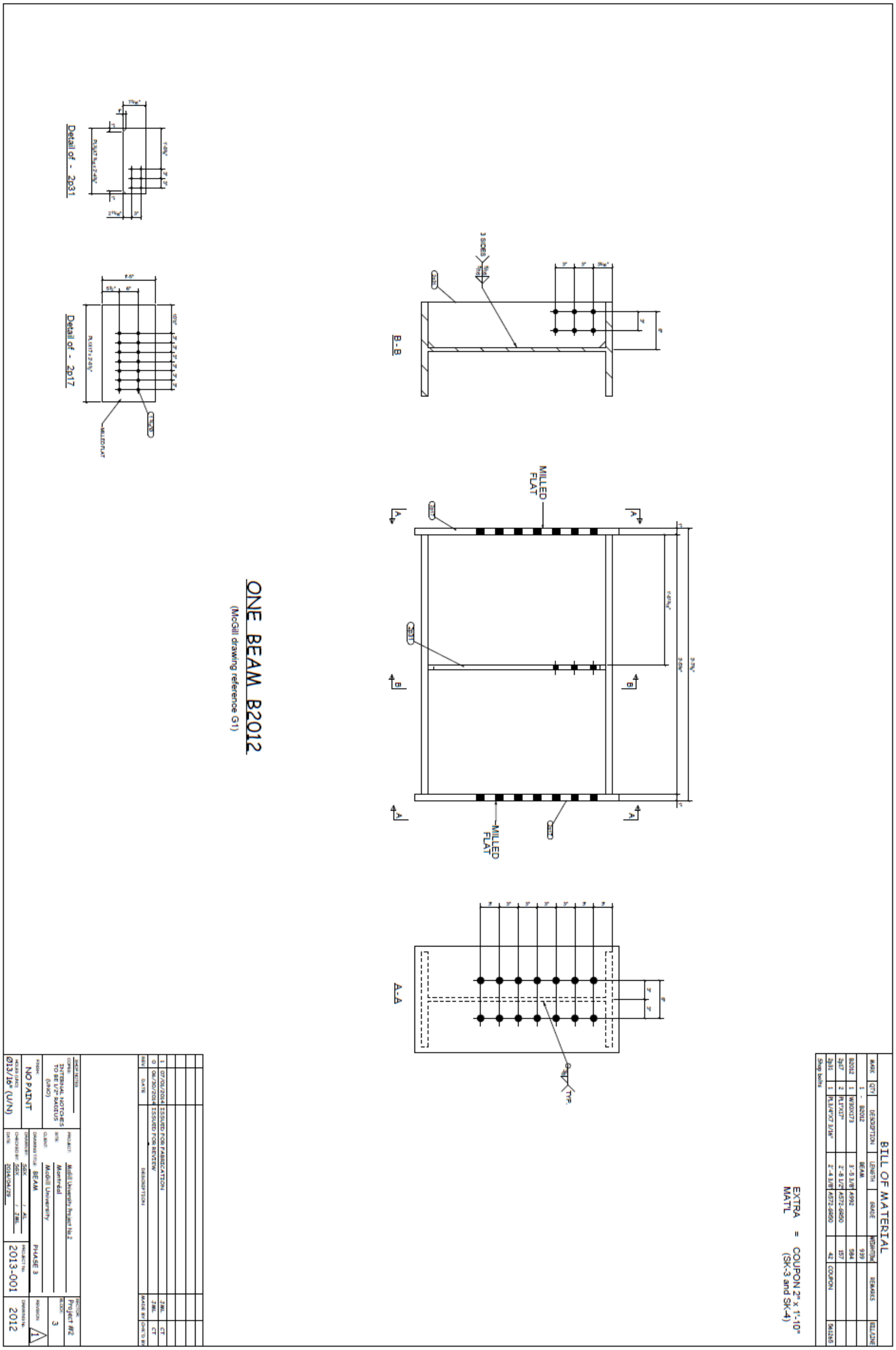
ONE BEAM B2012
(McGill drawing reference G1)
Detail of - 2p31
Detail of - 2p17
B-B
A-A
MILLED FLAT
BILL OF MATERIAL
EXTRA MATL = COUPON 2" x 1'-10" (SK-3 and SK-4)
NO PAINT
2013-001
2012

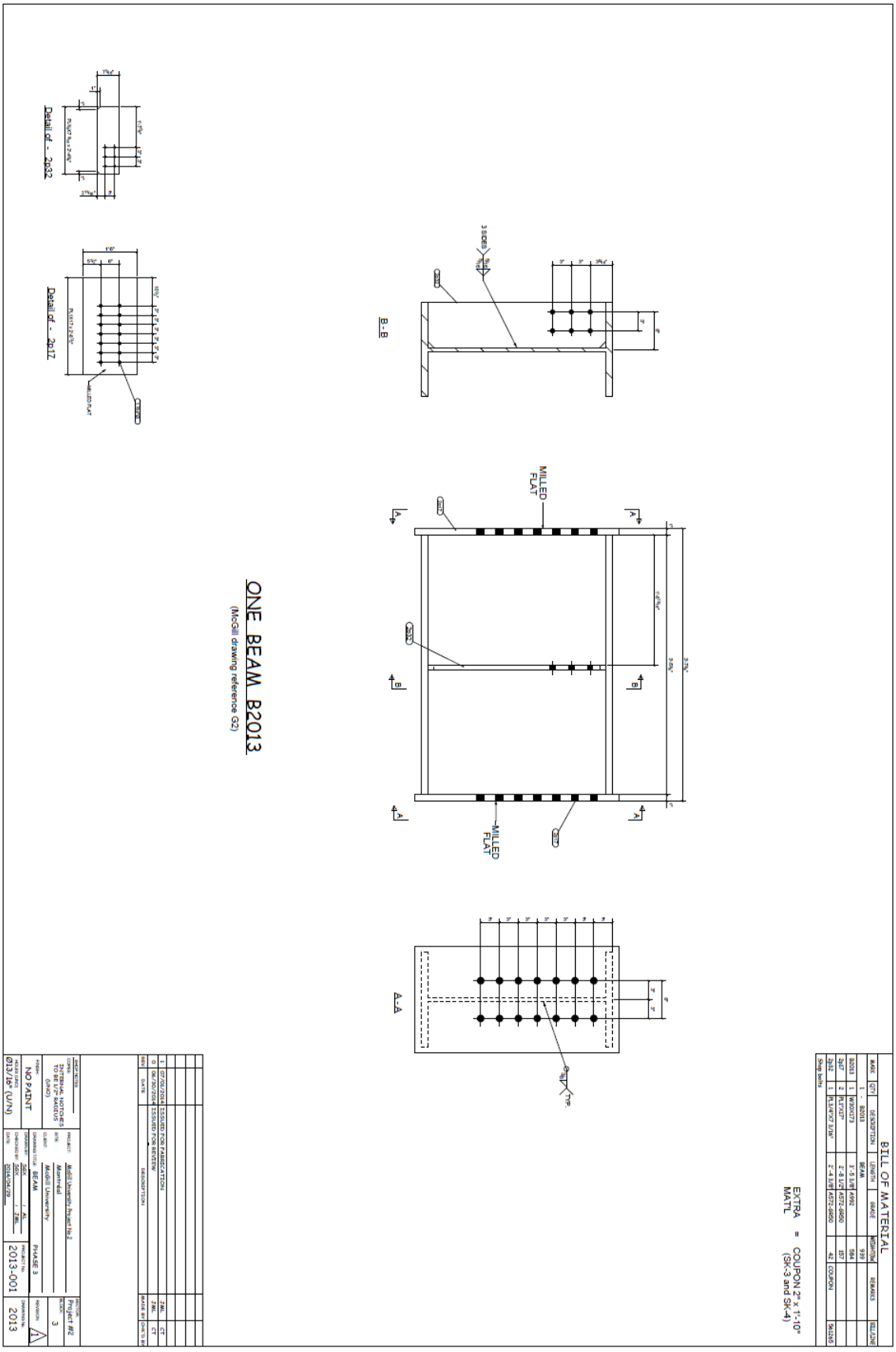
ONE BEAM B2013
(McGill drawing reference G2)
BILL OF MATERIAL
EXTRA MATL = COUPON 2"± x 1'-10" (SK-3 and SK-4)
MILLED FLAT
MILLED FLAT
B-B
A-A
Detail of - 2a32
Detail of - 2a17
NO PAINT
2013/16" (U/N)
McGill Steelfab Project No.2
Montreal
McGill University
BEAM
PHASE 2
2013-001
Project #2
2013

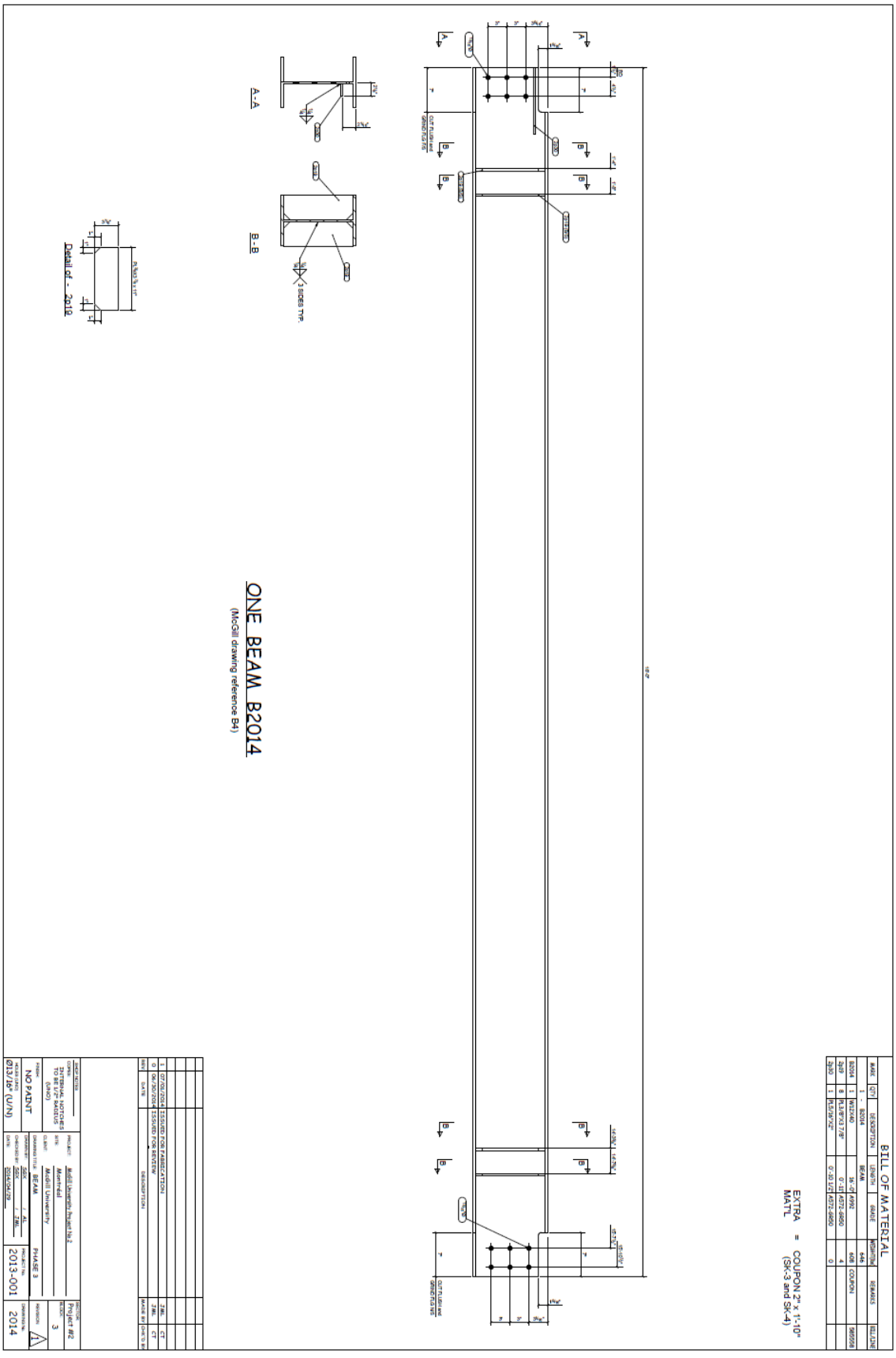
ONE BEAM B2014
(McGill drawing reference B4)
A - A
B - B
Detail of 2pl2
BILL OF MATERIAL
EXTRA MATL = COUPON 2" x 1'-10" (SK-3 and SK-4)
NO PAINT
Ø13/16" (U/N)
Project #2
2013-001
2014

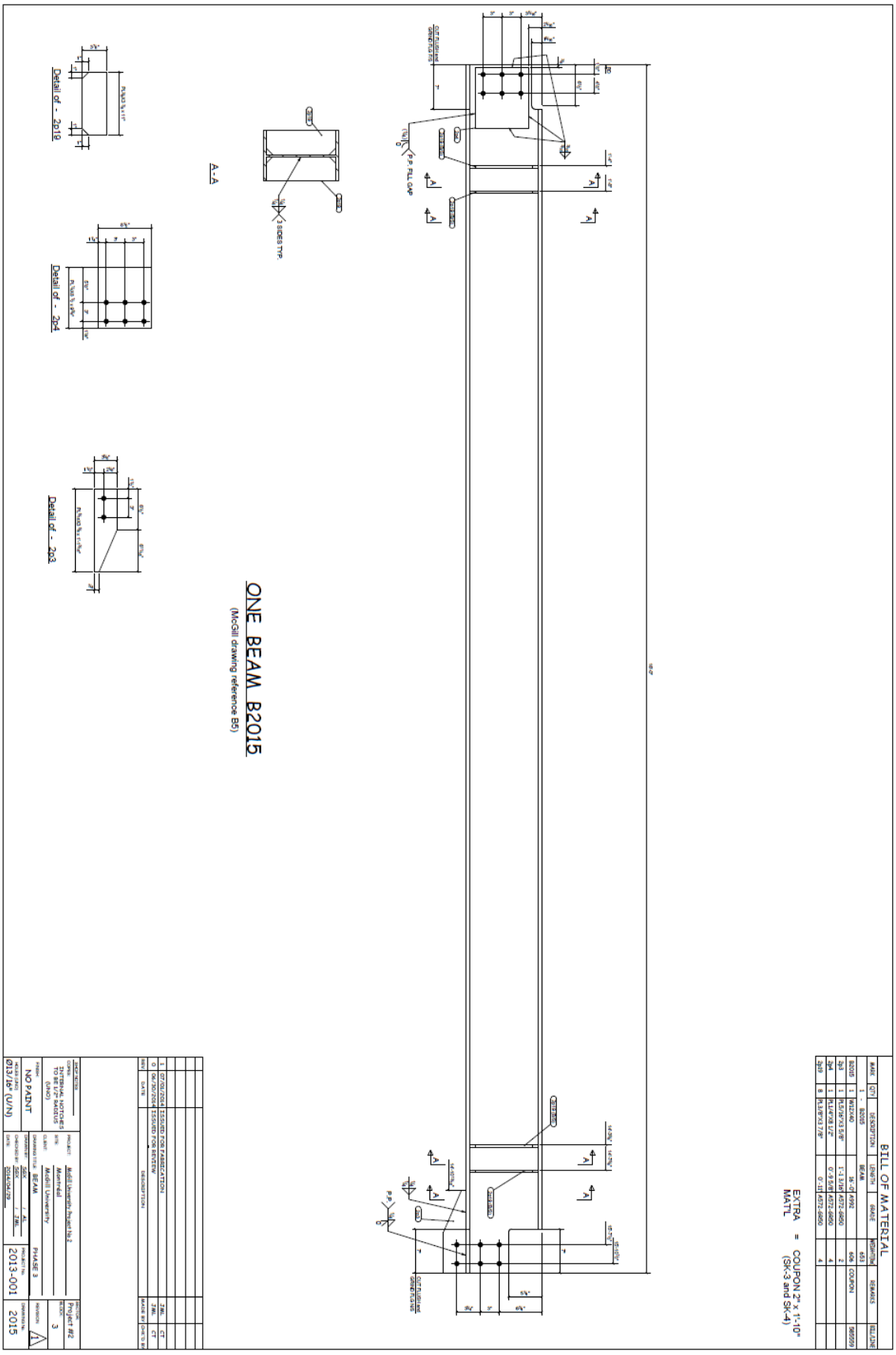
ONE BEAM B2015
(McGill drawing reference B5)
BILL OF MATERIAL
EXTRA MATL = COUPON 2"± x 1'-10" (SK-3 and SK-4)
Detail of - 2pl3
Detail of - 2pl4
Detail of - 2pl9
A - A
3 SIDES TYP.
F.P. FILL GAP
NO PAINT
2013-001
2015
Project #2
PHASE 3
BEAM

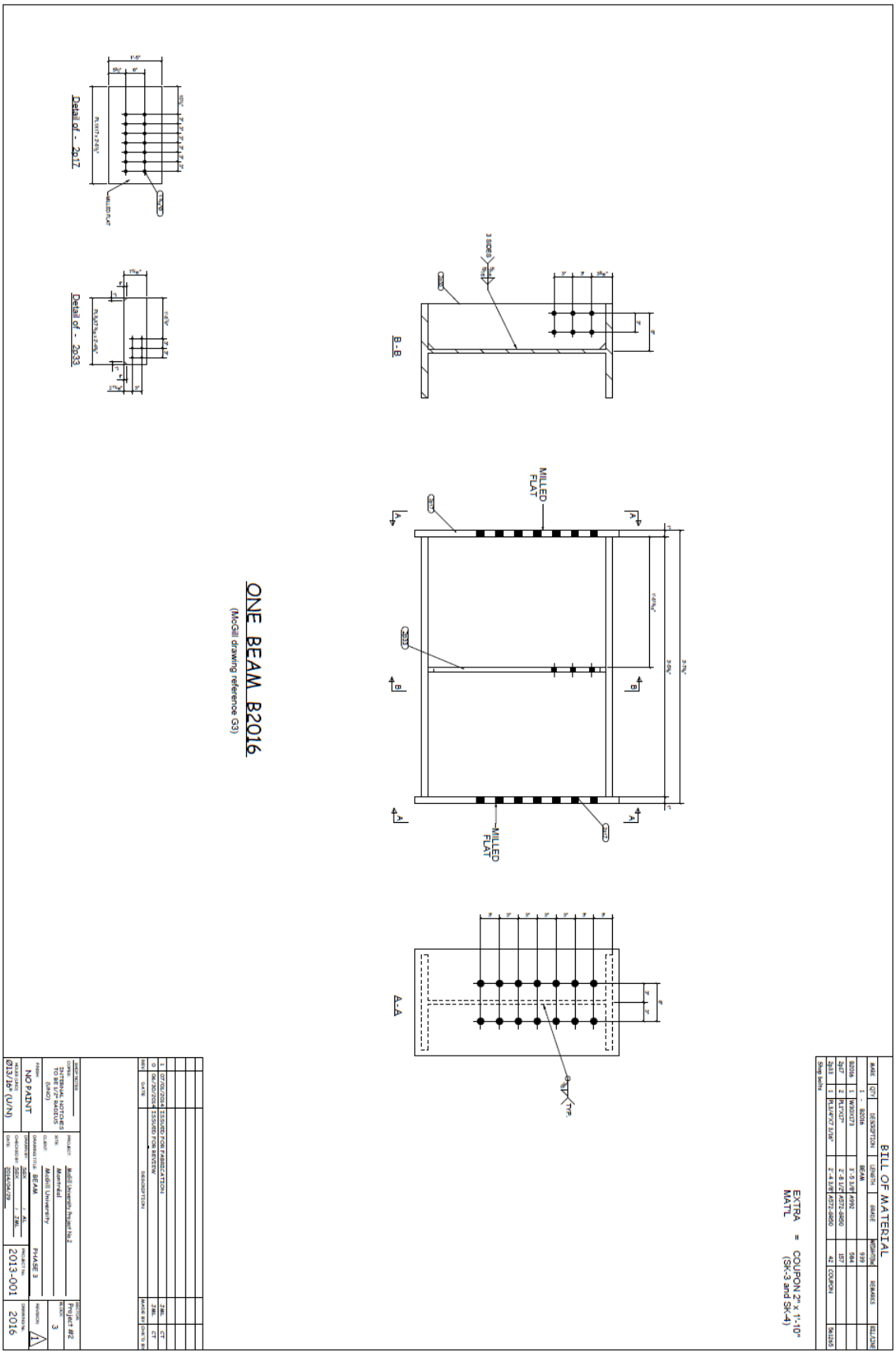
ONE BEAM B2016
(McGill drawing reference G3)
BILL OF MATERIAL
EXTRA MATL = COUPON 2" x 1'-10" (SK-3 and SK-4)
A-A
B-B
MILLED FLAT
Detail of - 2p17
Detail of - 2p33
NO PAINT
Project #2
2013-001
2016
PHASE 3
McGill University
Montreal
BEAM

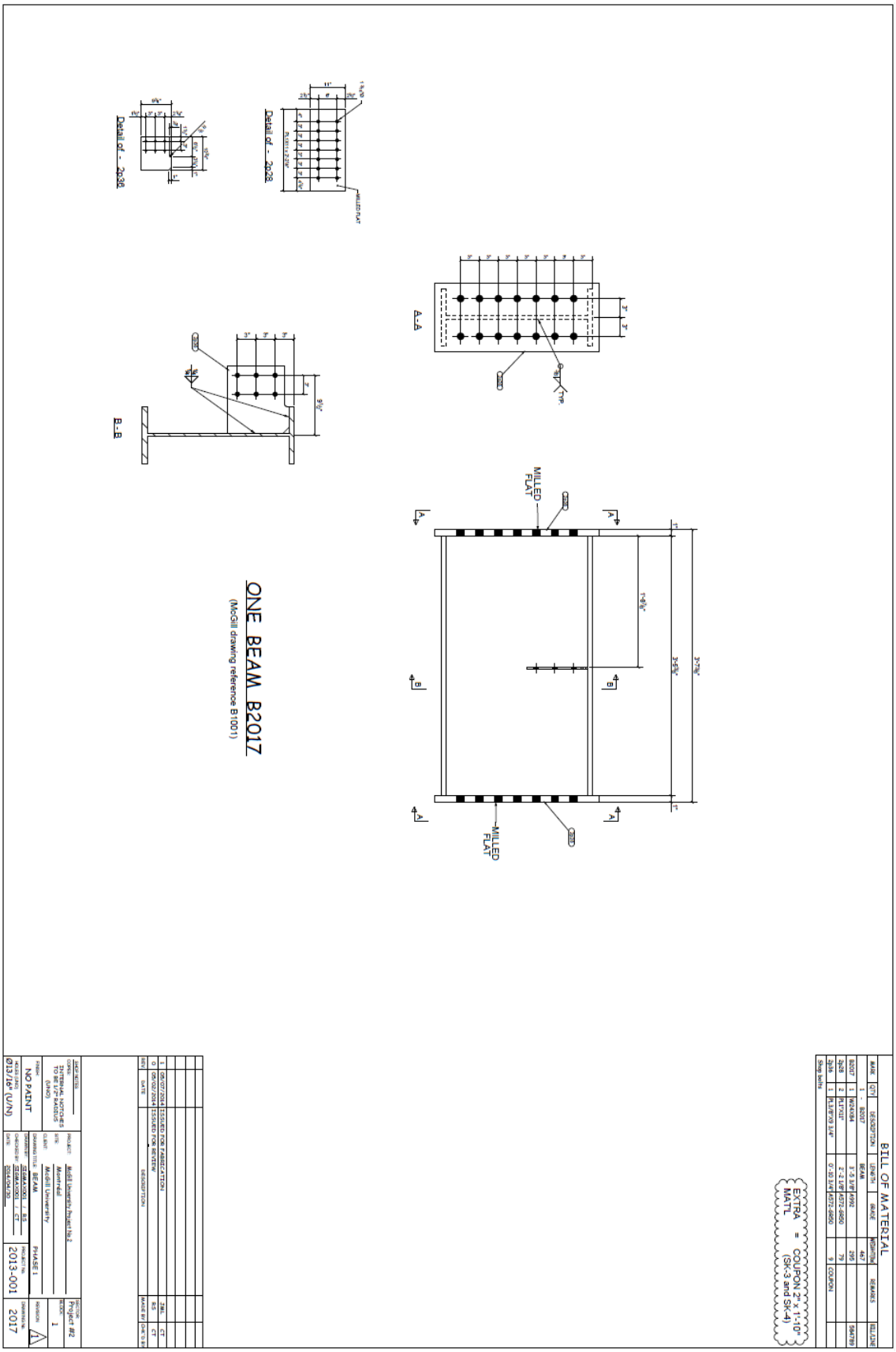
ONE BEAM B2017
(McGill drawing reference B1001)
MILLED FLAT
MILLED FLAT
A–A
B–B
Detail of – 2x28
Detail of – 2x38
BILL OF MATERIAL
EXTRA = COUPON 2" x 1'-10"
MATL (SK-3 and SK-4)
NO PAINT
Ø13/16" (U/N)
INTERNAL NOTCHES
TO BE 1/2" RADIUS
(UNO)
McGill University
PHASE 1
2013-001
2017
Project #2
1

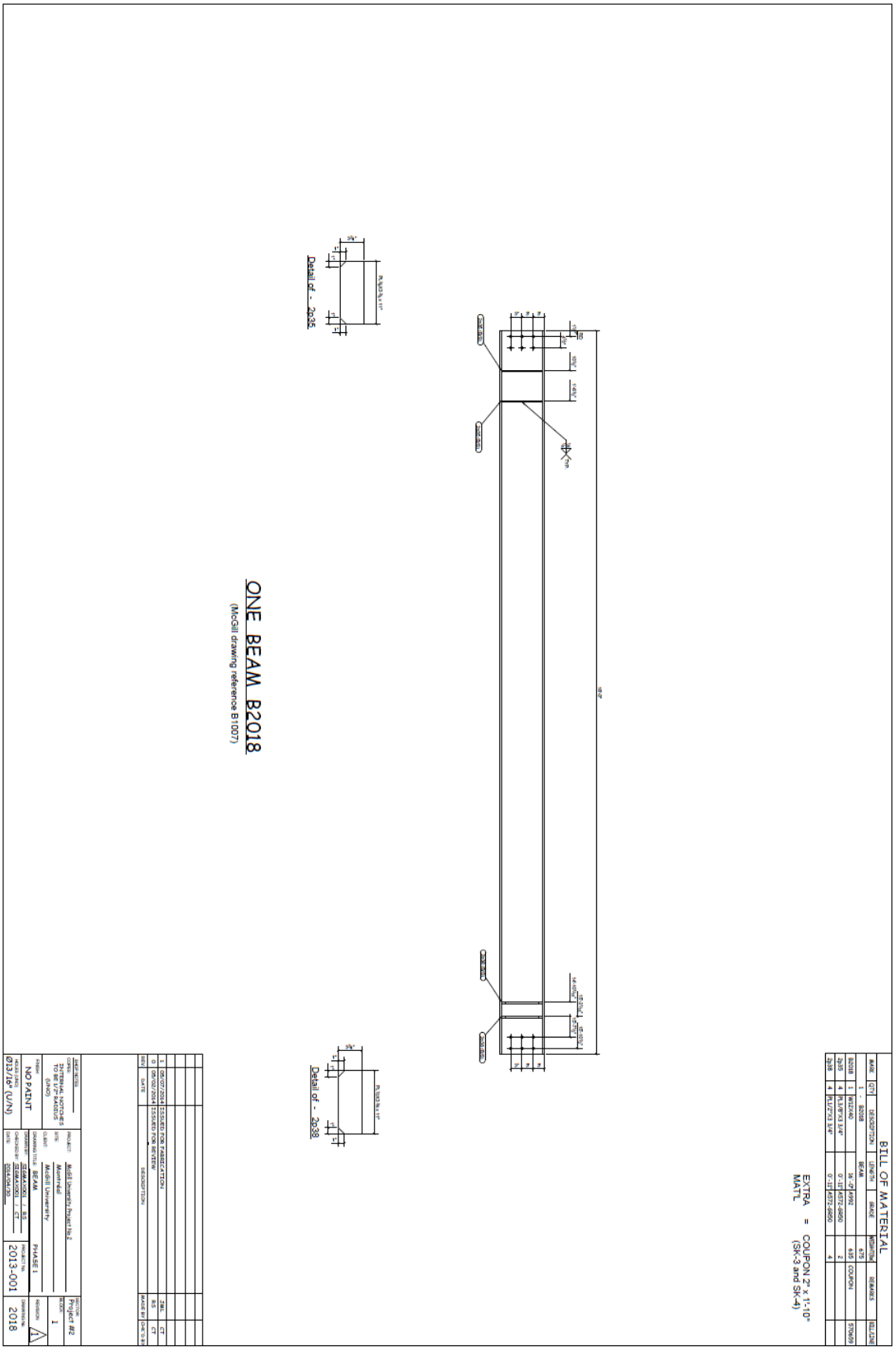
ONE BEAM B2018
(McGill drawing reference B1007)
BILL OF MATERIAL
EXTRA = COUPON 2"x 1'-10"
MAT'L (SK-3 and SK-4)
Detail of - 2p35
Detail of - 2p38
NO PAINT
2013-001
2018
PHASE 1
Project #2
McGill University Project No.2

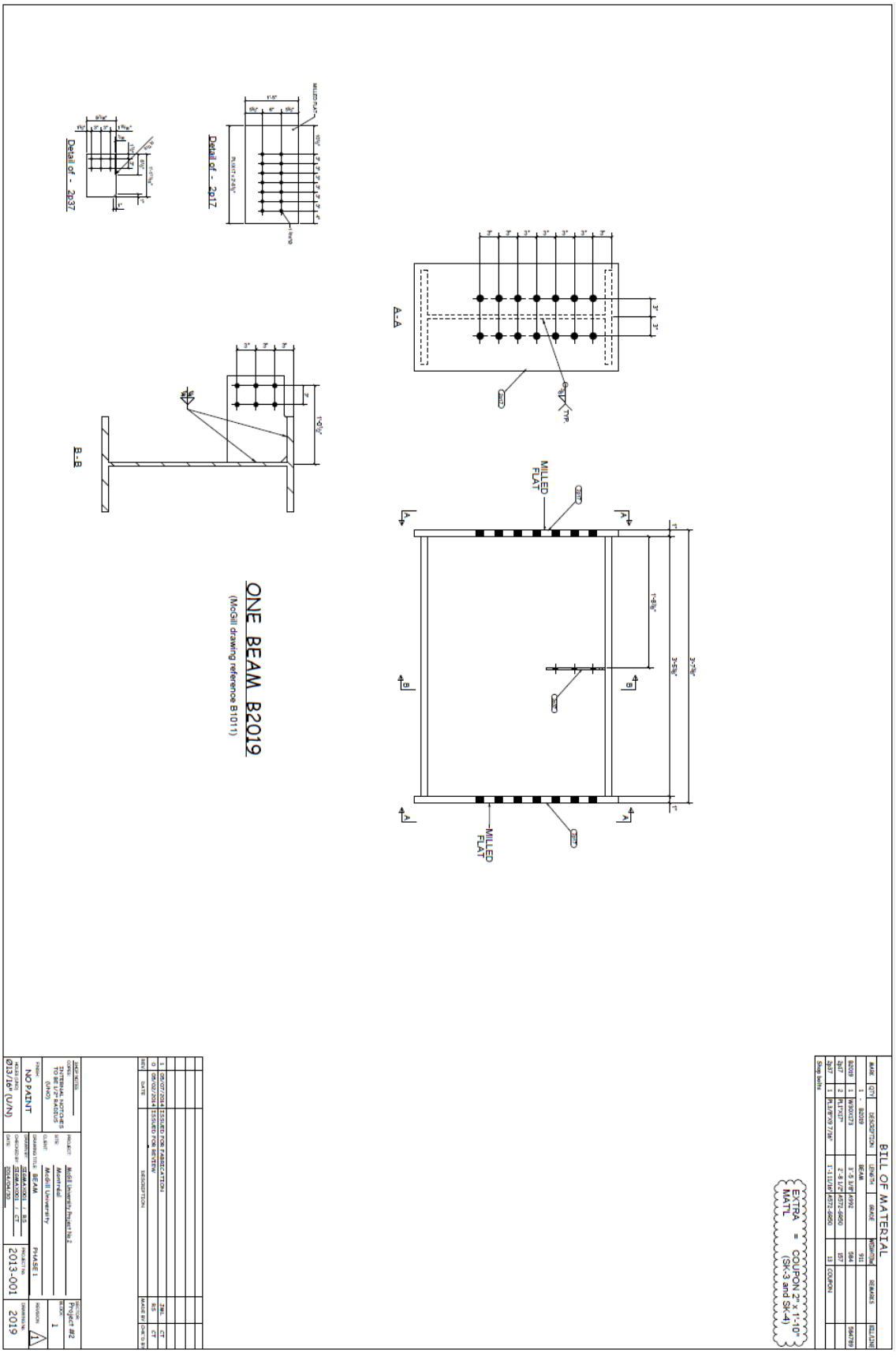
ONE BEAM B2019
(McGill drawing reference B1011)
BILL OF MATERIAL
EXTRA MATL = COUPON 2"x 1-1/2" (SK-3 and SK-4)
MILLED FLAT
MILLED FLAT
A-A
B-B
Detail of - 2a17
Detail of - 2a37
NO PAINT
Ø13/16" (U/N)
McGill University
PHASE 1
2013-001
2019

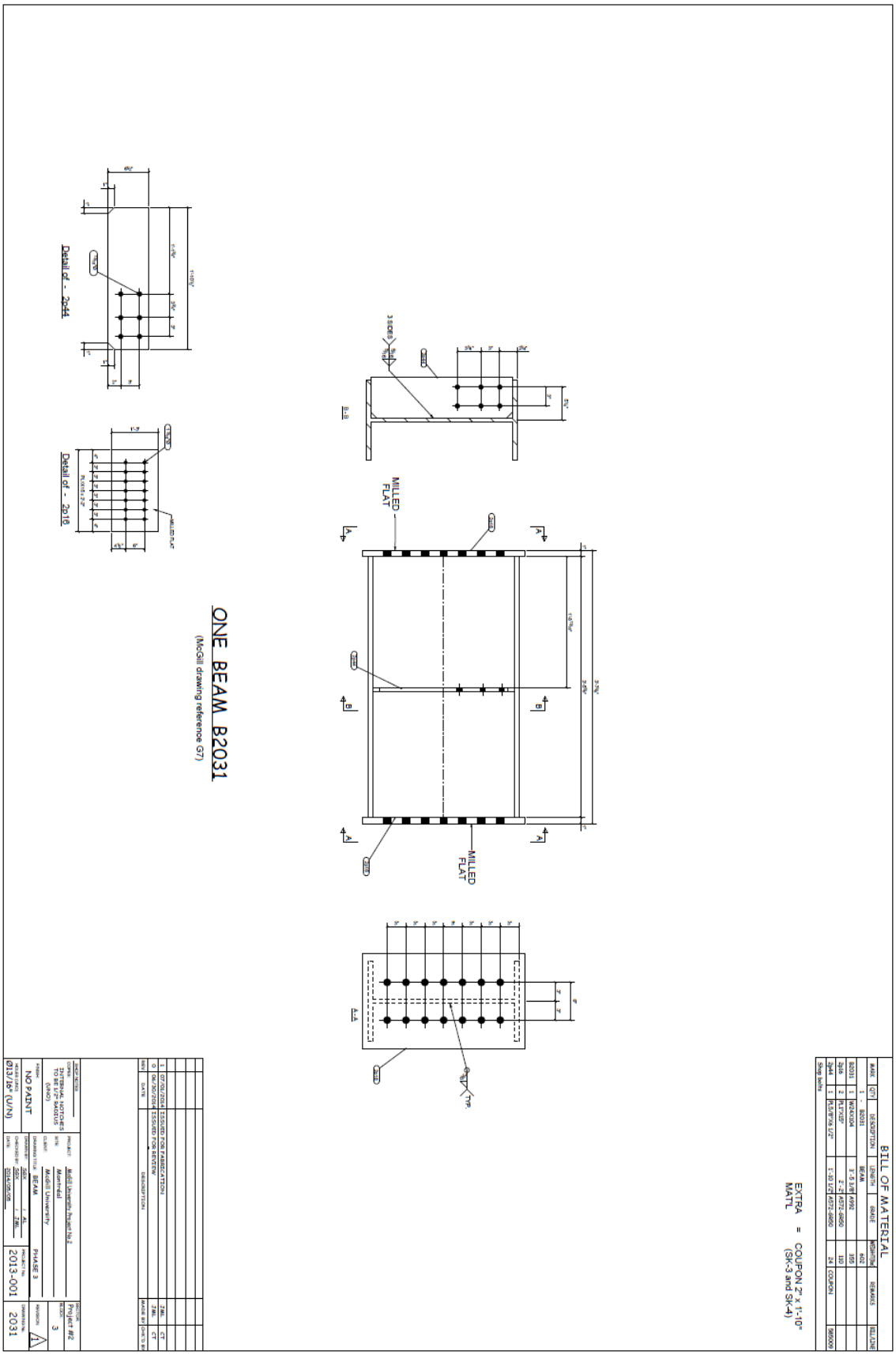
ONE BEAM B2031
(McGill drawing reference G7)
Detail of - 2p44
Detail of - 2p16
MILLED FLAT
MILLED FLAT
TYP.
BILL OF MATERIAL
EXTRA MATL = COUPON 2" x 1'-10" (SK-3 and SK-4)
NO PAINT
Ø13/16" (U/N)
2013-001
2031
Project #2
3

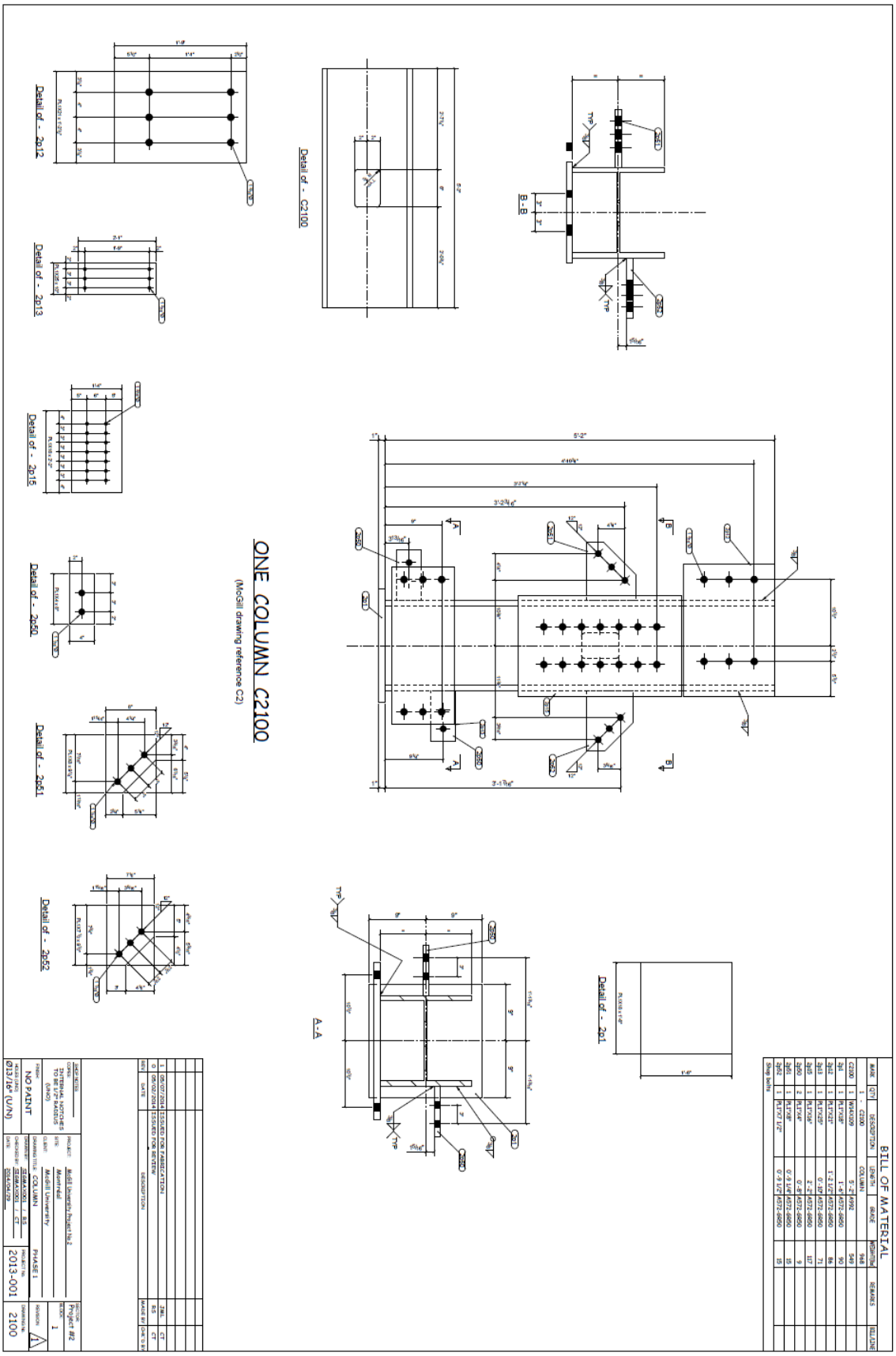
ONE COLUMN C2100
(McGill drawing reference C2)
Detail of - 2p12
Detail of - 2p13
Detail of - 2p15
Detail of - 2p50
Detail of - 2p51
Detail of - 2p52
Detail of - C2100
B - B
A - A
Detail of - 2p1
BILL OF MATERIAL
NO PAINT
Ø13/16" (U/N)
2013-001
2100
Project #2
McGill University
PHASE 1

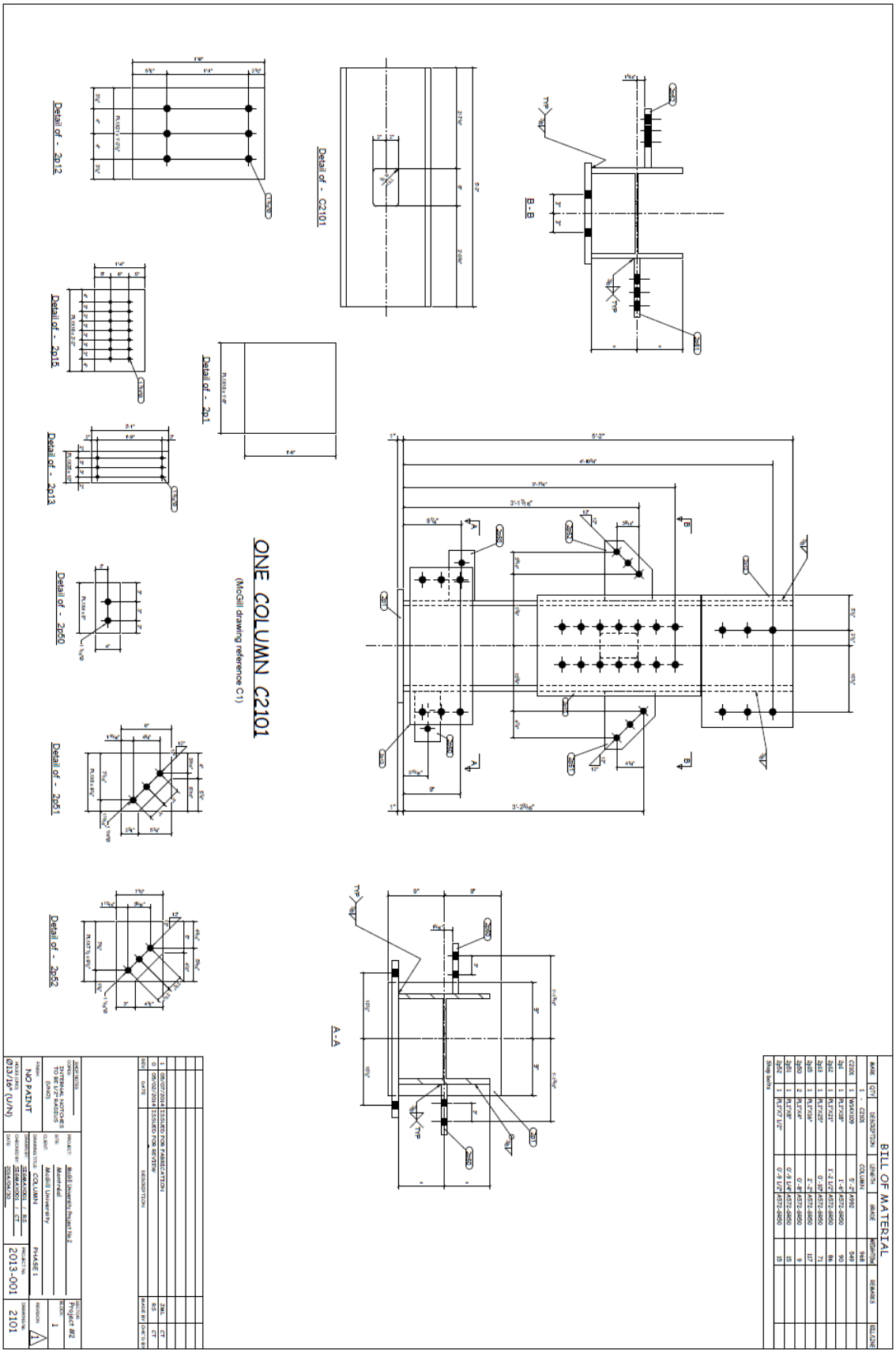
ONE COLUMN C2101
(McGill drawing reference C1)
Detail of - 2p12
Detail of - C2101
B - B
Detail of - 2p15
Detail of - 2p1
Detail of - 2p13
Detail of - 2p50
Detail of - 2p51
Detail of - 2p52
A - A
BILL OF MATERIAL
MARK
QTY
DESCRIPTION
LENGTH
GRADE
WEIGHT(lbs)
REMARKS
BELLOW
C2101
1
COLUMN
5' - 2"
A992
1968
2p1
1
PLATE
1' - 4"
A572-50/50
549
2p2
1
PLATE
1' - 11 1/2"
A572-50/50
96
2p3
1
PLATE
0' - 4"
A572-50/50
75
2p4
1
PLATE
2' - 4"
A572-50/50
177
2p5
1
PLATE
0' - 4"
A572-50/50
37
2p50
2
PLATE
0' - 4"
A572-50/50
8
2p51
1
PLATE
0' - 9 1/4"
A572-50/50
35
2p52
1
PLATE 1/2"
0' - 9 1/2"
A572-50/50
35
Shop bolts
NO PAINT
Ø13/16" (U/N)
INTERNAL NOTCHES TO BE MASKED (TYP)
McGill University Project No.2
McGill University
PHASE 1
COLUMN
2013-001
2101
Project #2
1
REVISIONS
1 05/07/2014 ISSUED FOR FABRICATION
0 05/02/2014 ISSUED FOR REVIEW

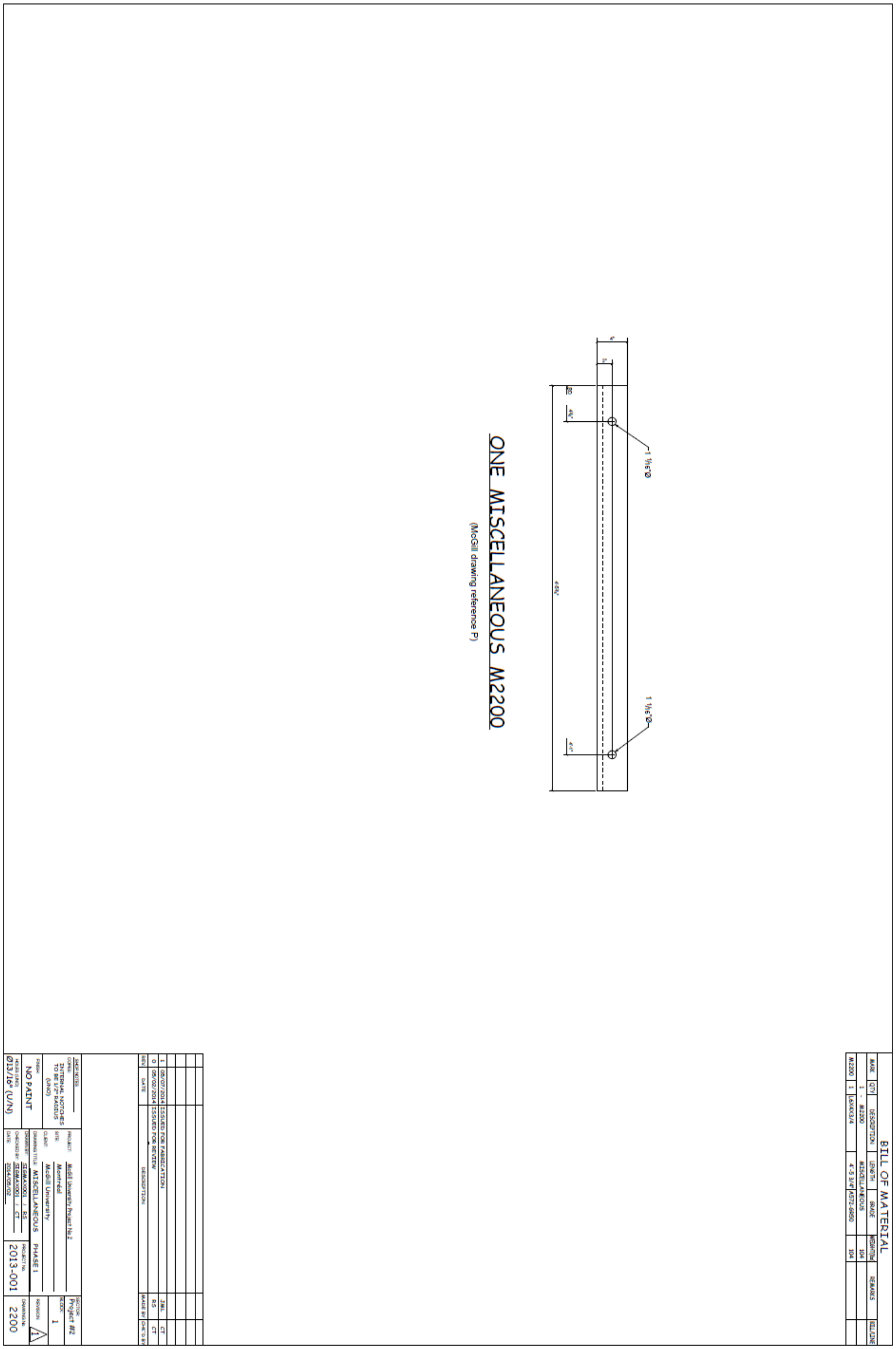
ONE MISCELLANEOUS M2200
(McGill drawing reference P)
BILL OF MATERIAL
NO PAINT
2013-001
2200

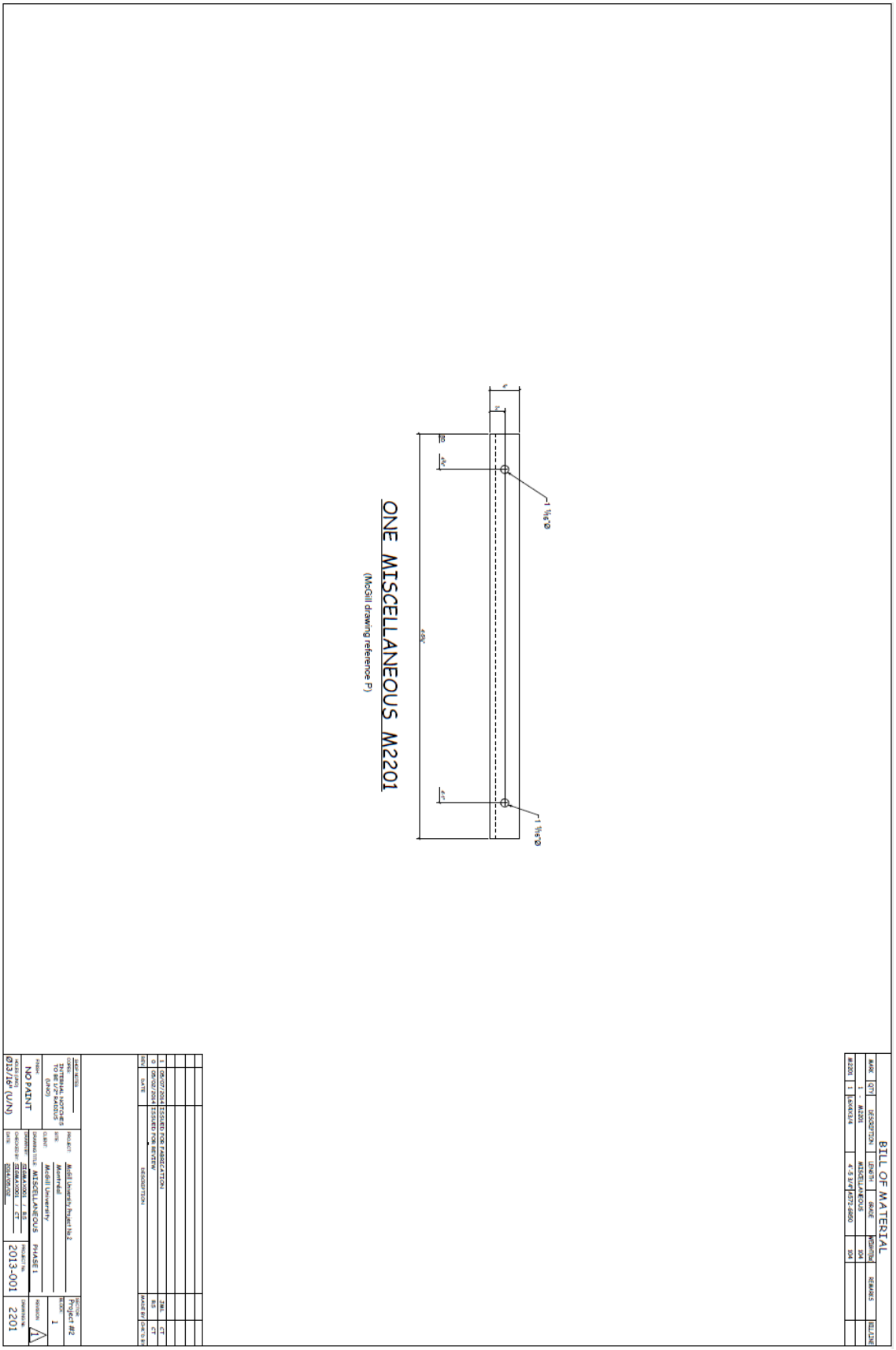
BILL OF MATERIAL
MARK
QTY
DESCRIPTION
LENGTH
GRADE
SPECIFICATION
REMARKS
BELOW
M2201
1
M2201
MISCELLANEOUS
300
M2201
1
BAR/PLATE
4-0 3/4"
ASTM A-36/50
300
ONE MISCELLANEOUS M2201
(McGill drawing reference P)
1 15/16"Ø
1 15/16"Ø
MARK NOTES
INTERNAL NOTCHES TO BE 1/2" RADIUS (MAX)
FINISH
NO PAINT
ROUND TO NEAREST
Ø13/16" (U/N)
DRAWN BY
CHECKED BY
DATE
2014/06/06
PROJECT
McGill Ironpitch Project No.2
SITE
McGill University
CLIENT
MISCELLANEOUS
PHASE 1
DRAWING TITLE
PROJECT NO.
2013-001
DRAWING NO.
2201
REVISION
1
ISSUED FOR
Project #2
0
05/07/2014
ISSUED FOR FABRICATION
PM
CT
1
05/02/2014
ISSUED FOR REVIEW
RS
CT
DATE
DESCRIPTION
MADE BY
CHK'D BY

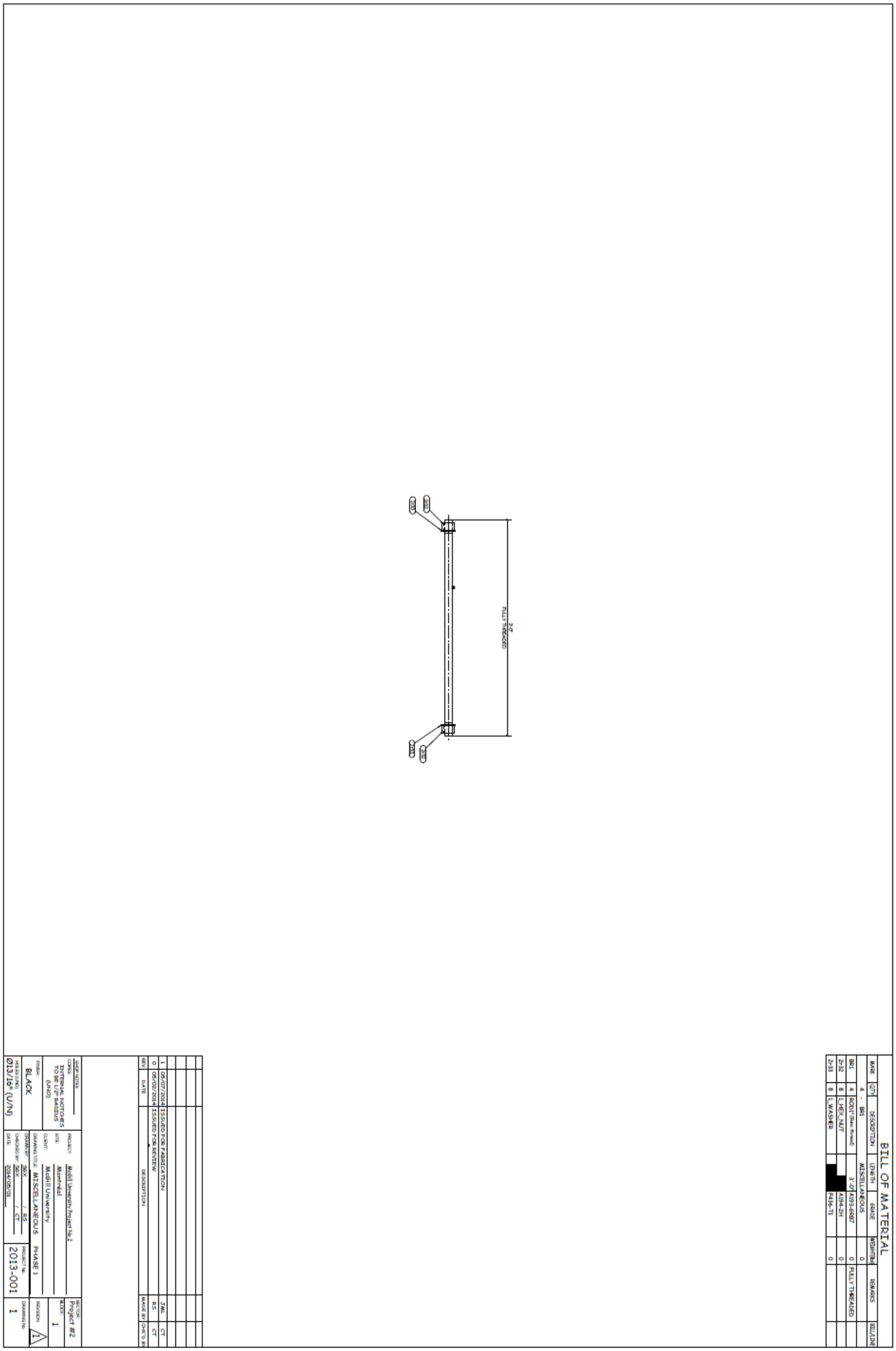
3'-0"
FULLY THREADED
BILL OF MATERIAL
MARK
QTY
DESCRIPTION
LENGTH
GRADE
REMARKS
4 - BR1
MISCELLANEOUS
0
BR1
4
A193-GRB7
FULLY THREADED
2r32
8
L_HEX_NUT
A194-2H
2r33
8
L_WASHER
F436-T1
SHOP NOTES
COPES:
INTERNAL NOTCHES TO BE 1/2" RADIUS (U.N.O)
FINISH:
BLACK
Ø13/16" (U/N)
PROJECT:
McGill University Project No 2
SITE:
Montréal
CLIENT:
McGill University
DRAWING TITLE:
MISCELLANEOUS
PHASE 1
DRAWN BY:
CHECKED BY:
DATE:
2014/08/01
PROJECT No.
2013-001
SECTOR:
Project #2
BLOCK:
1
REVISION
DRAWING No.
REV.
DATE
DESCRIPTION
MADE BY
1
08/07/2014
ISSUED FOR FABRICATION
JML
CT
0
05/02/2014
ISSUED FOR REVIEW
RS

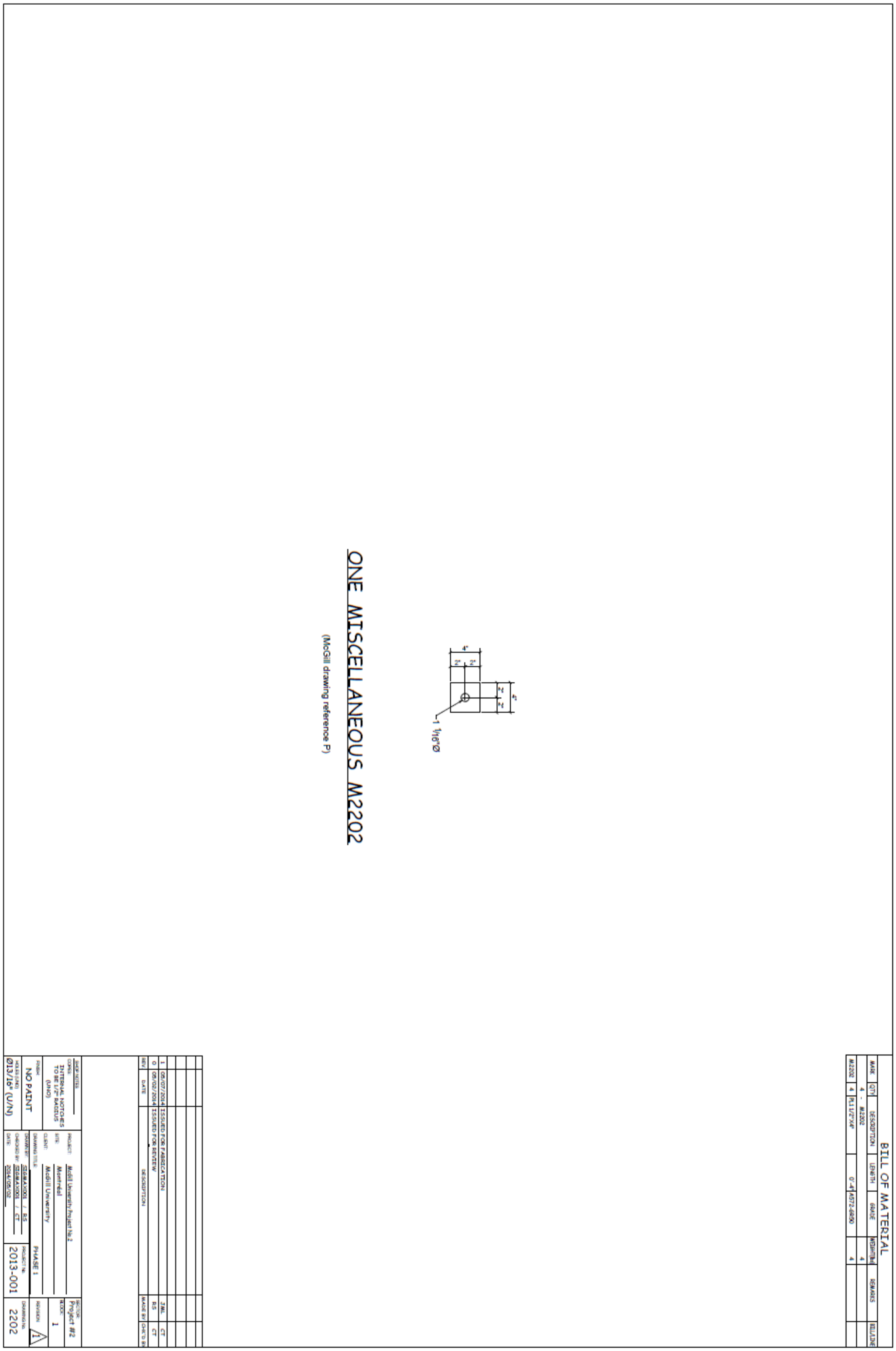
BILL OF MATERIAL
MARK QTY DESCRIPTION LENGTH GRADE WEIGHT(lbs) REMARKS BILL/LINE
4 - M2202 4
M2202 4 PL1 1/2"X4" 0'-4" A572-GR50 4
4"
2" 2"
1 1/16"Ø
ONE MISCELLANEOUS M2202
(McGill drawing reference P)
1 05/07/2014 ISSUED FOR FABRICATION JML CT
0 05/02/2014 ISSUED FOR REVIEW RS CT
REV DATE DESCRIPTION MADE BY CHK'D BY
SHOP NOTES
INTERNAL NOTCHES TO BE 1/2" RADIUS (UNO)
NO PAINT
Ø13/16" (U/N)
PROJECT: McGill University Project No 2
SITE: Montréal
CLIENT: McGill University
PHASE 1
SIGMAX001 / RS
SIGMAX001 / CT
2014/05/02
2013-001
Project #2
1
2202

APPENDIX C

INSTRUMENTATION LAYOUTS

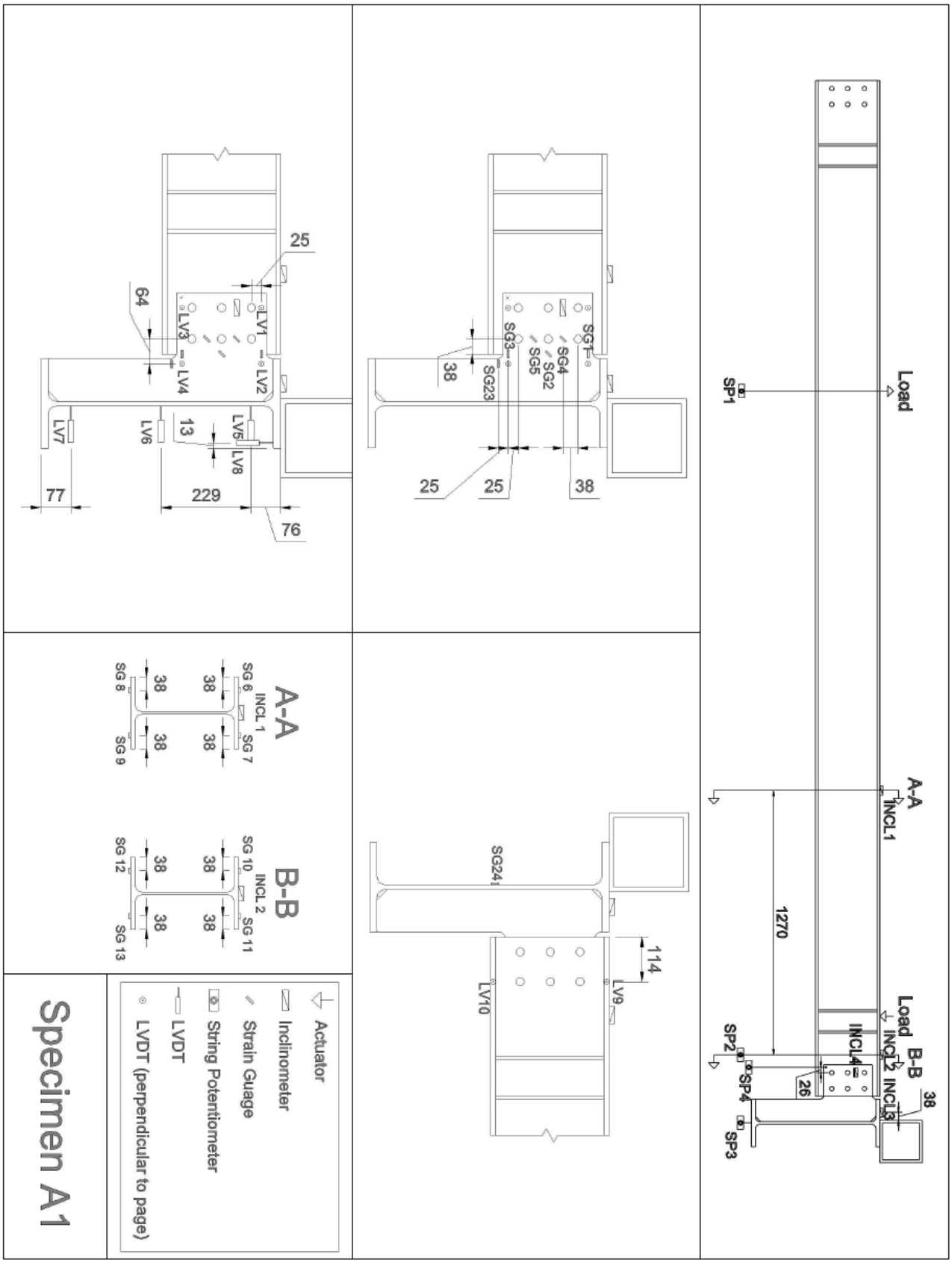
Load
SP1
A-A
INCL1
1270
Load
B-B
INCL2
INCL3
INCL4
SP2
SP4
SP3
26
38
SG24
114
LV9
LV10
SG1
SG2
SG3
SG4
SG5
SG23
38
25
25
38
25
64
LV1
LV2
LV3
LV4
LV5
LV6
LV7
LV8
13
77
229
76
A-A
INCL 1
SG 6
SG 7
SG 8
SG 9
38
B-B
INCL 2
SG 10
SG 11
SG 12
SG 13
Actuator
Inclinometer
Strain Guage
String Potentiometer
LVDT
LVDT (perpendicular to page)
Specimen A1

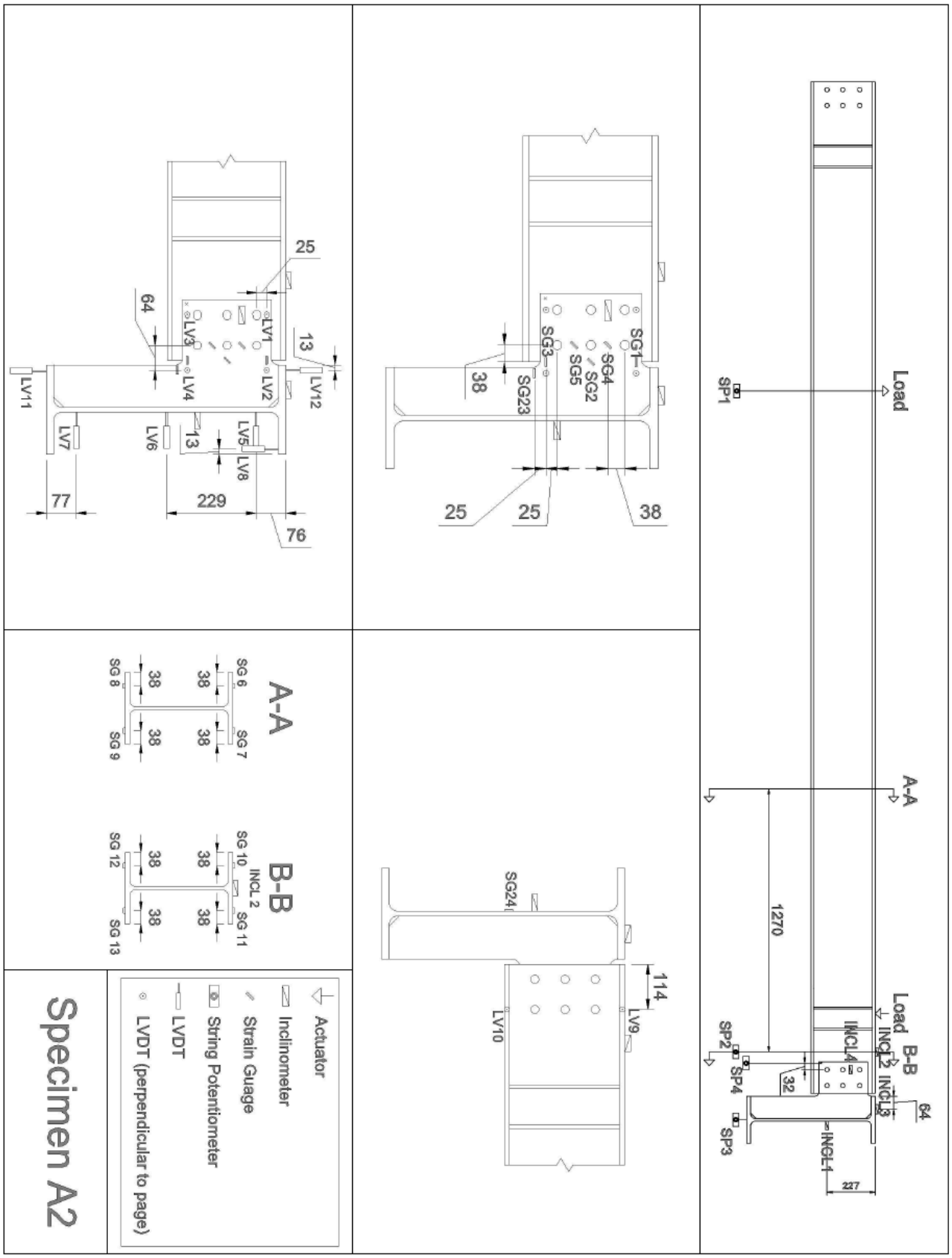
Load
SP1
A-A
1270
Load
B-B
INCL4
INCL2
INCL3
SP2
SP4
SP3
INCL1
32
64
227
SG1
SG4
SG2
SG5
SG3
SG23
38
25
25
38
SG24
114
LV9
LV10
25
64
LV1
LV3
13
LV2
LV12
LV11
LV4
LV7
LV6
13
LV5
LV8
77
229
76
A-A
SG 6
SG 7
SG 8
SG 9
38
B-B
SG 10
INCL 2
SG 11
SG 12
SG 13
Actuator
Inclinometer
Strain Guage
String Potentiometer
LVDT
LVDT (perpendicular to page)
Specimen A2

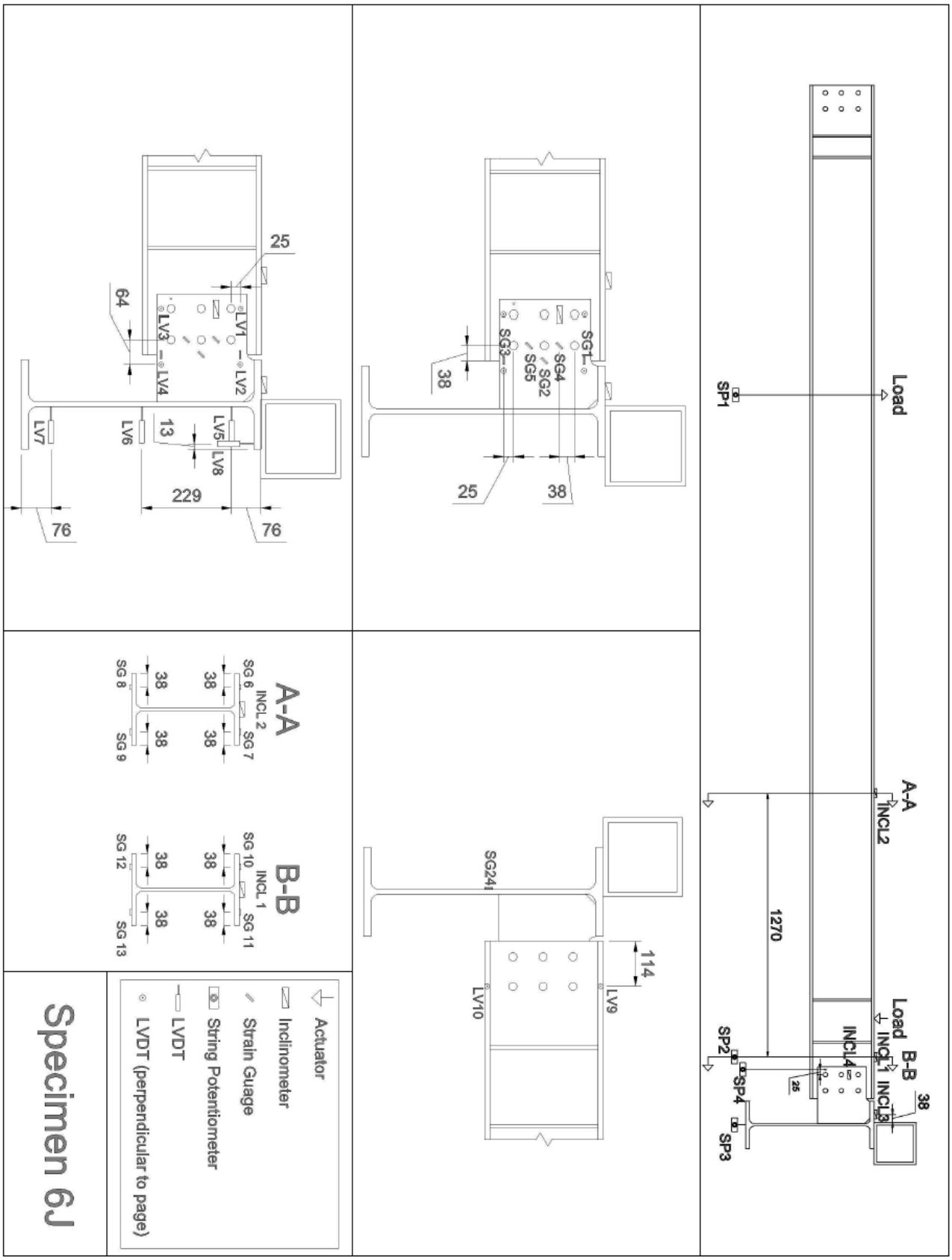
Load
SP1
A-A
INCL2
1270
Load B-B
INCL1
INCL3
INCL4
SP2
SP4
SP3
38
25
SG1
SG3
SG5
SG2
SG4
38
25
38
SG24
LV10
LV9
114
25
64
LV1
LV3
LV2
LV4
LV7
LV6
13
LV5
LV8
229
76
76
A-A
INCL 2
SG 6
SG 7
SG 8
SG 9
38
38
38
38
B-B
INCL 1
SG 10
SG 11
SG 12
SG 13
38
38
38
38
Actuator
Inclinometer
Strain Guage
String Potentiometer
LVDT
LVDT (perpendicular to page)
Specimen 6J

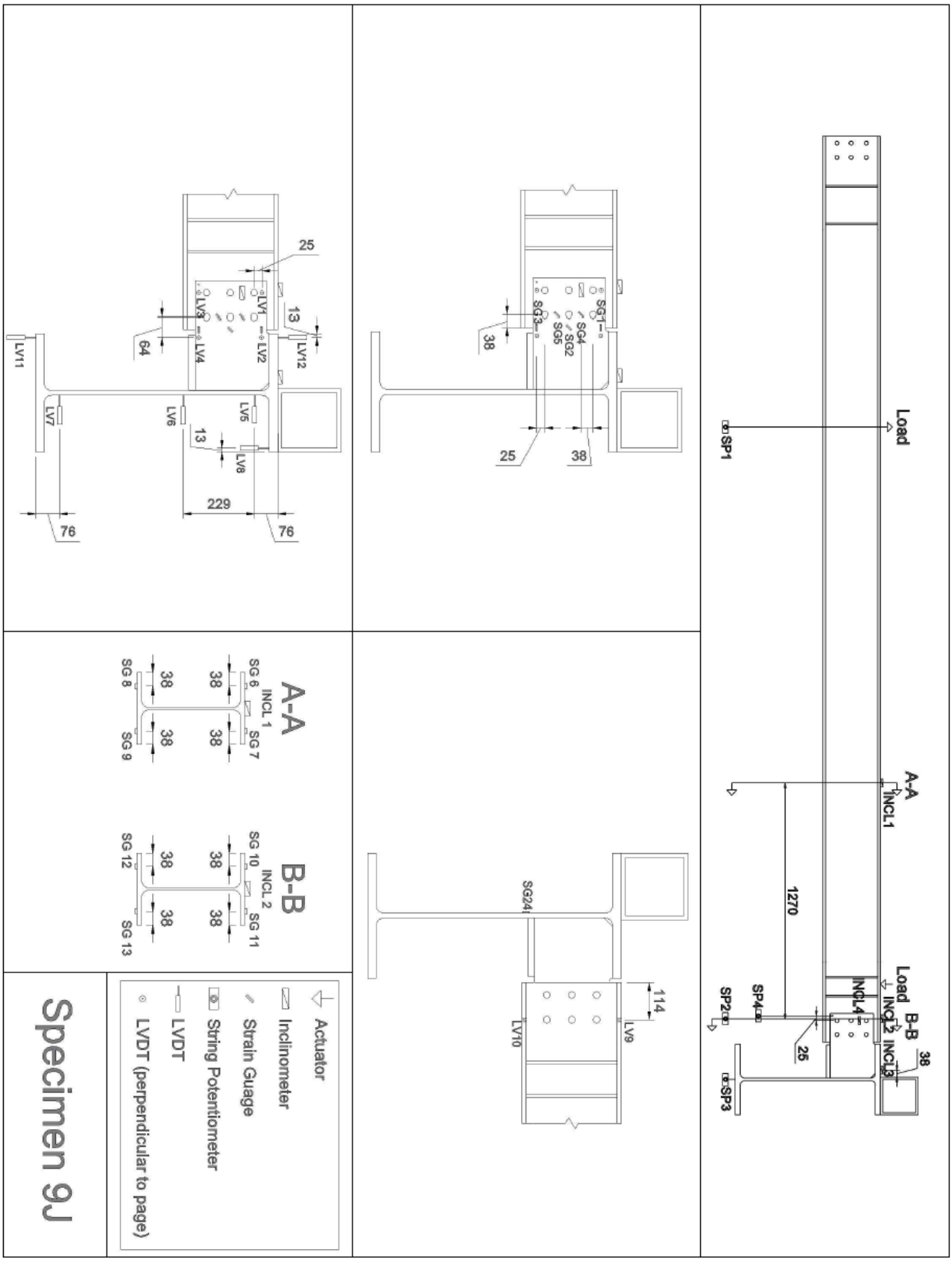
Load
SP1
A-A
INCL1
1270
Load
B-B
INCL4
INCL2
INCL3
38
SP4
SP2
25
SP3
SG1
SG3
SG4
SG5
SG2
38
25
38
SG24
LV10
LV9
114
25
13
LV1
LV3
LV2
LV12
64
LV4
LV11
LV7
LV6
LV5
13
LV8
229
76
76
A-A
INCL 1
SG 6
SG 7
SG 8
SG 9
38
B-B
INCL 2
SG 10
SG 11
SG 12
SG 13
Actuator
Inclinometer
Strain Guage
String Potentiometer
LVDT
LVDT (perpendicular to page)
Specimen 9J

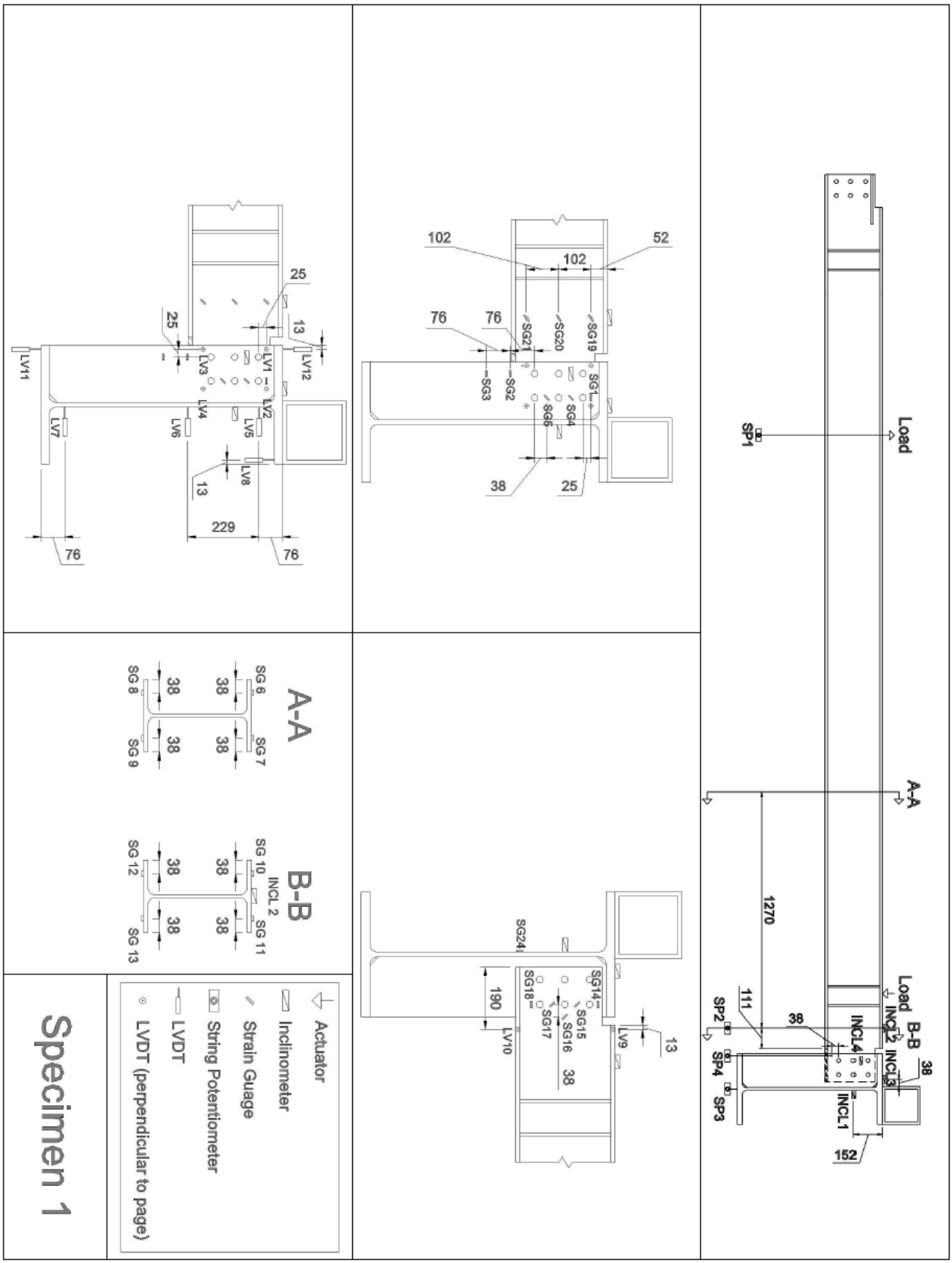
Load
SP1
A-A
1270
Load
B-B
SP2
111
38
INCL4
INCL2
INCL3
38
SP4
SP3
INCL1
152
102
52
102
76
76
SG21
SG20
SG19
SG3
SG2
SG1
SG6
SG4
38
25
25
25
13
LV11
LV12
LV1
LV3
LV2
LV4
LV7
LV6
LV5
LV8
13
229
76
76
SG24
SG14
SG18
SG15
SG17
SG16
38
190
LV10
LV9
13
A-A
SG 6
SG 8
SG 7
SG 9
38
B-B
SG 10
INCL 2
SG 11
SG 12
SG 13
Actuator
Inclinometer
Strain Guage
String Potentiometer
LVDT
LVDT (perpendicular to page)
Specimen 1

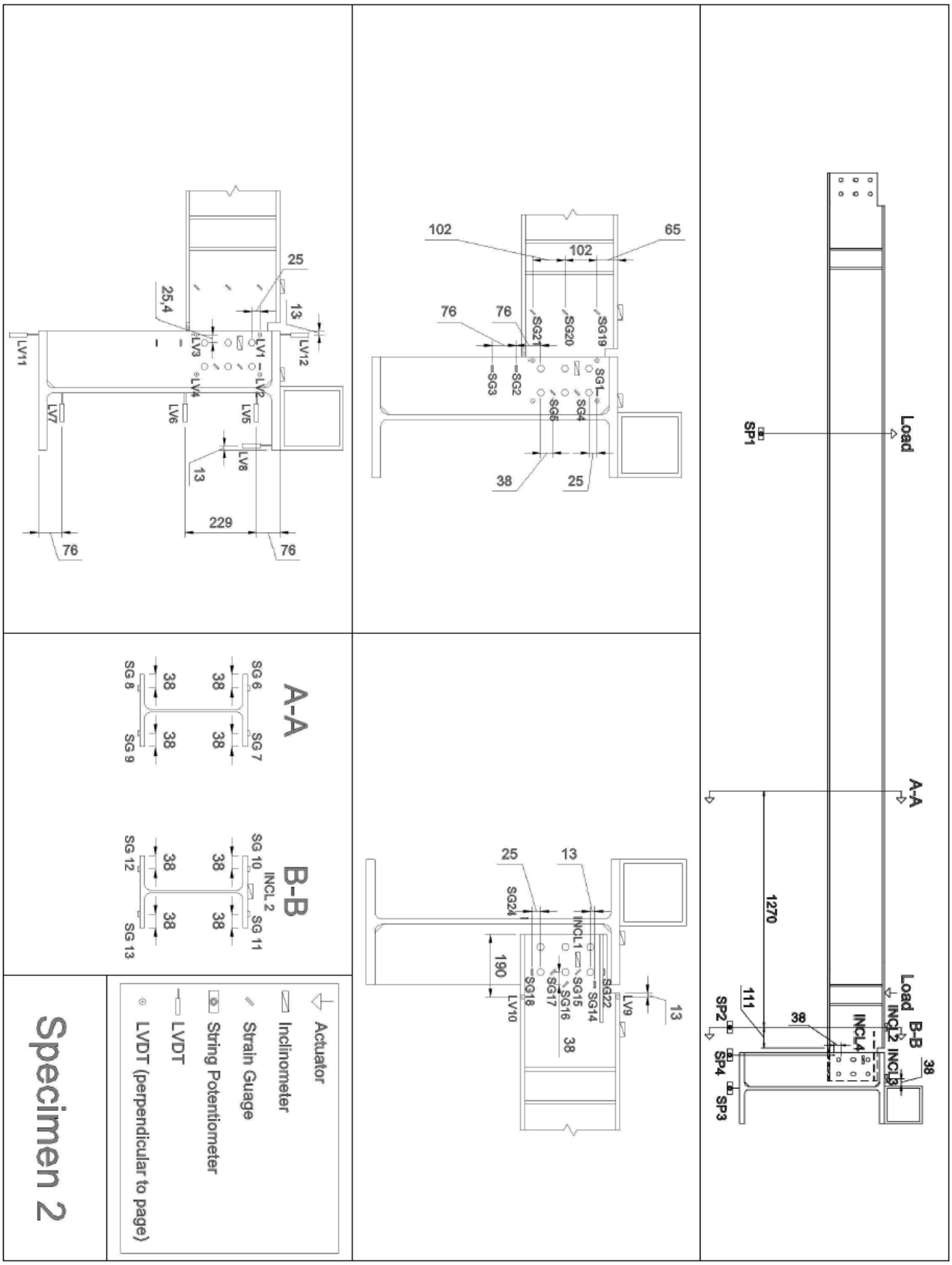
Load
SP1
A-A
1270
Load
B-B
SP2
111
38
INCL4
INCL3
38
SP4
SP3
102
65
102
76
76
SG21
SG20
SG19
SG3
SG2
SG1
SG5
SG4
38
25
25
13
25,4
LV11
LV3
LV1
LV2
LV12
LV4
LV7
LV6
LV5
LV8
13
229
76
76
25
13
SG24
INCL1
SG15
SG14
SG22
190
SG18
SG17
SG16
38
LV10
LV9
13
A-A
SG 6
SG 7
SG 8
SG 9
38
38
38
38
B-B
SG 10
INCL 2
SG 11
SG 12
SG 13
38
38
38
38
Specimen 2
Actuator
Inclinometer
Strain Guage
String Potentiometer
LVDT
LVDT (perpendicular to page)

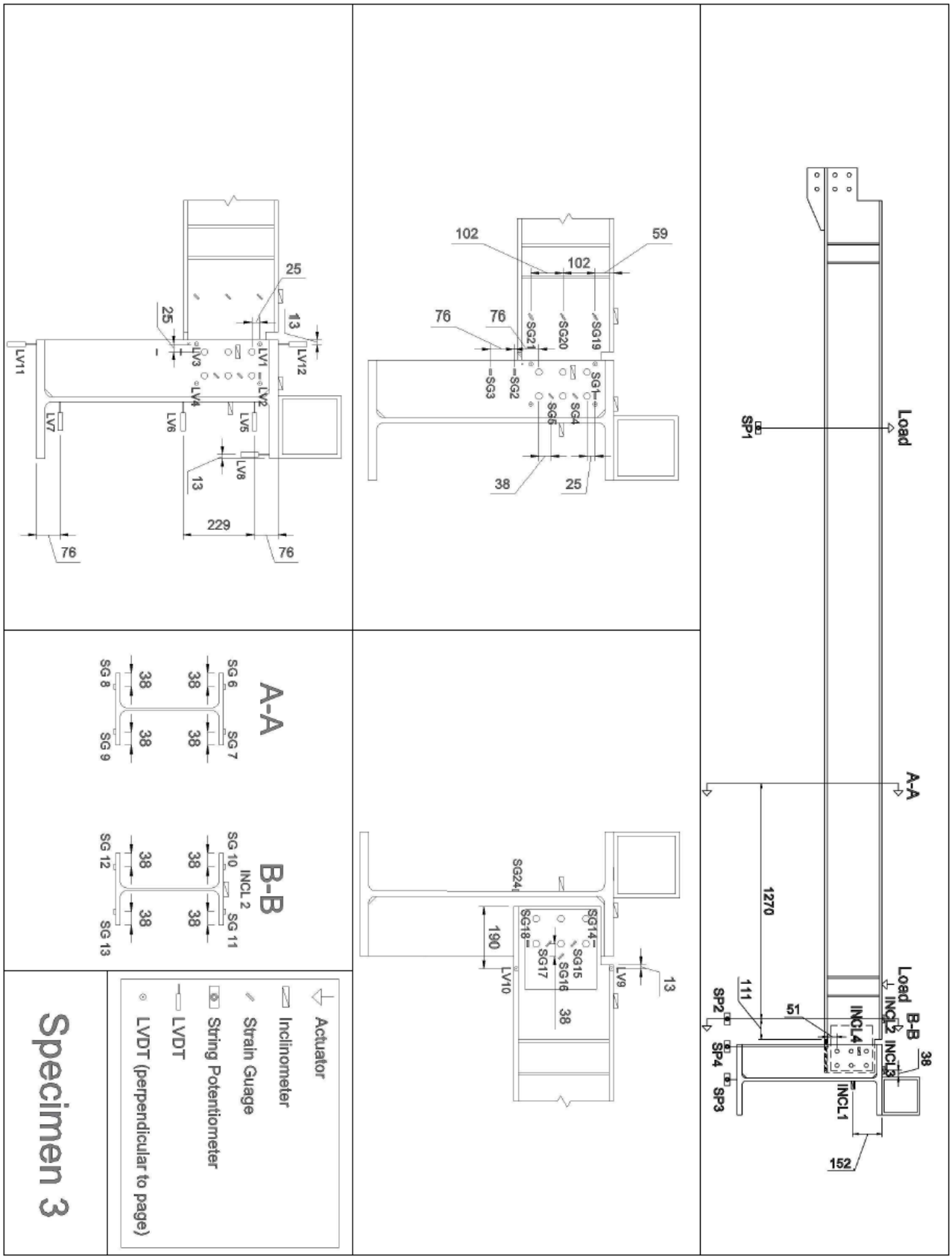
Load
SP1
A-A
1270
Load
B-B
INCL2
INCL3
INCL4
INCL1
SP2
SP4
SP3
111
51
38
152
102
59
102
76
76
SG21
SG20
SG19
SG3
SG2
SG1
SG6
SG4
38
25
25
25
13
LV11
LV3
LV1
LV12
LV4
LV2
LV7
LV6
LV5
LV8
13
229
76
76
SG24
SG14
SG15
SG18
SG17
SG16
190
LV10
LV9
13
38
A-A
SG 6
SG 7
SG 8
SG 9
38
38
38
38
B-B
SG 10
SG 11
INCL 2
SG 12
SG 13
38
38
38
38
Specimen 3
Actuator
Inclinometer
Strain Guage
String Potentiometer
LVDT
LVDT (perpendicular to page)

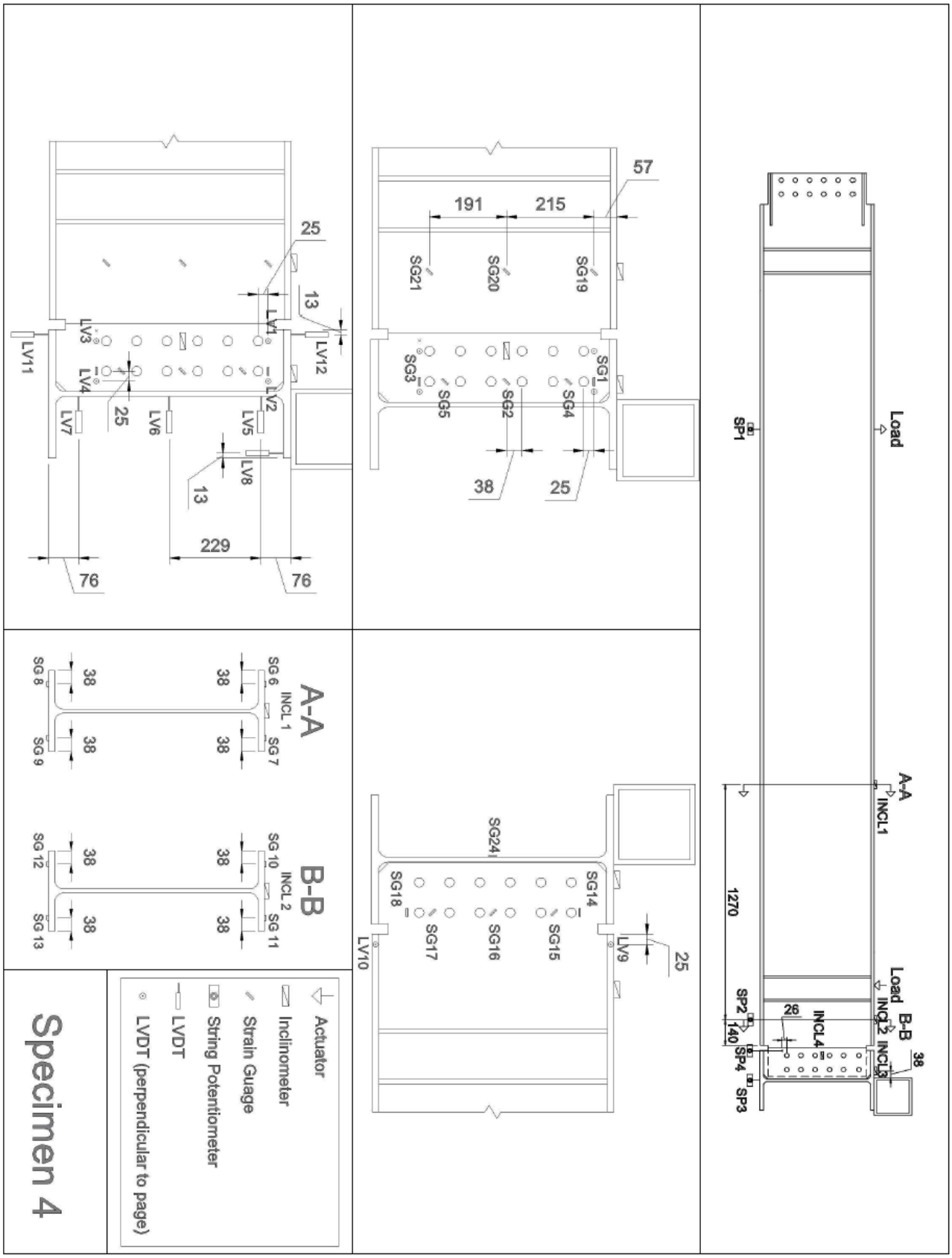
Load
SP1
A-A
INCL1
1270
Load
INCL2
B-B
INCL4
INCL3
SP2
SP4
SP3
26
140
38
57
191
215
SG21
SG20
SG19
SG3
SG5
SG2
SG4
SG1
38
25
SG24
SG18
SG17
SG16
SG15
SG14
LV10
LV9
25
25
13
LV1
LV3
LV11
LV12
LV4
LV2
25
LV7
LV6
LV5
LV8
13
229
76
76
A-A
INCL 1
SG 6
SG 7
SG 8
SG 9
38
B-B
INCL 2
SG 10
SG 11
SG 12
SG 13
Actuator
Inclinometer
Strain Guage
String Potentiometer
LVDT
LVDT (perpendicular to page)
Specimen 4

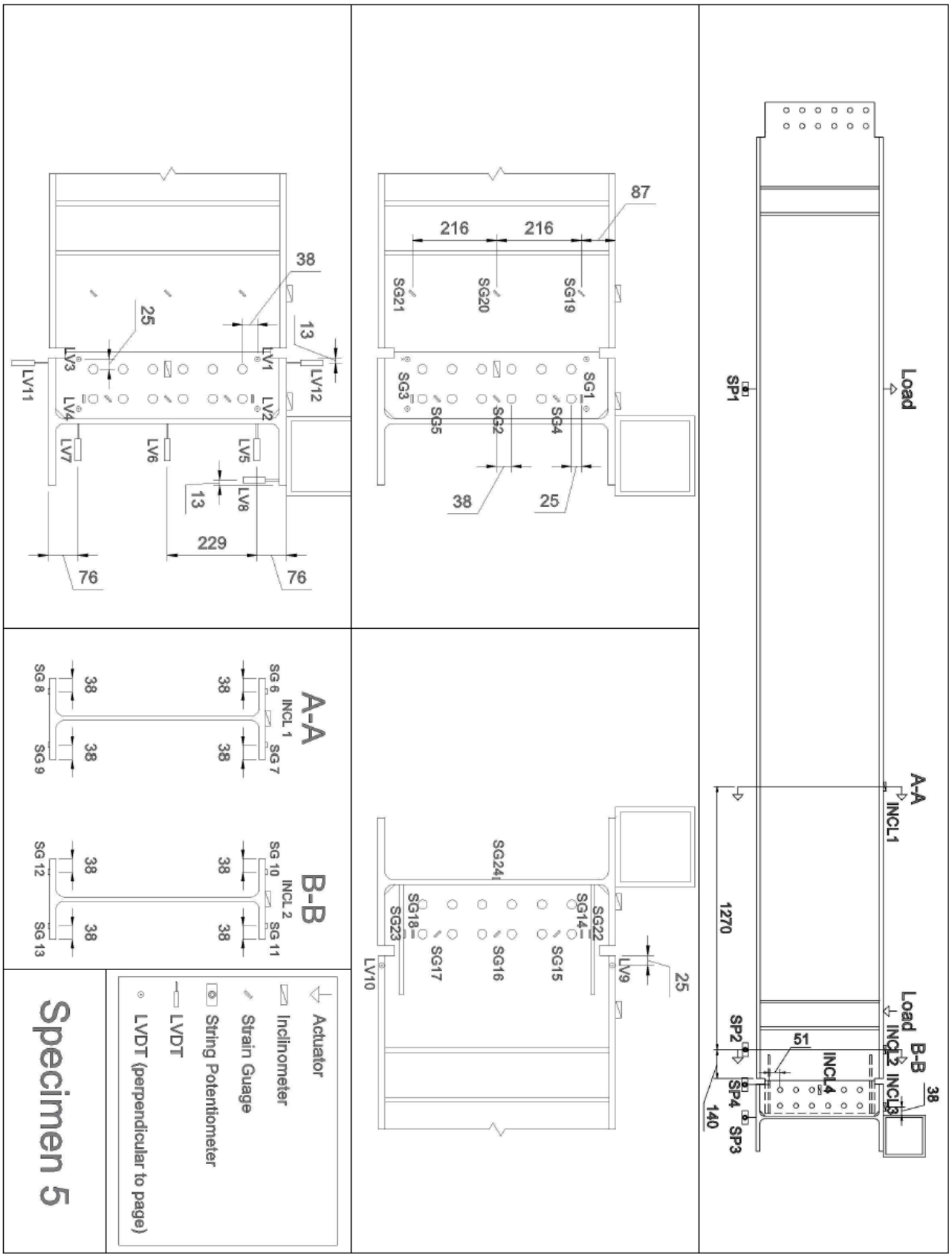
Load
SP1
A-A
INCL1
Load
B-B
INCL2
INCL3
INCL4
SP2
SP4
SP3
51
38
140
1270
87
216
216
SG21
SG20
SG19
SG3
SG5
SG2
SG4
SG1
38
25
SG24
SG22
SG14
SG18
SG23
SG17
SG16
SG15
LV10
LV9
25
38
25
13
LV11
LV3
LV1
LV12
LV4
LV2
LV7
LV6
LV5
LV8
13
229
76
76
A-A
INCL 1
SG 6
SG 7
SG 8
SG 9
B-B
INCL 2
SG 10
SG 11
SG 12
SG 13
Actuator
Inclinometer
Strain Guage
String Potentiometer
LVDT
LVDT (perpendicular to page)
Specimen 5

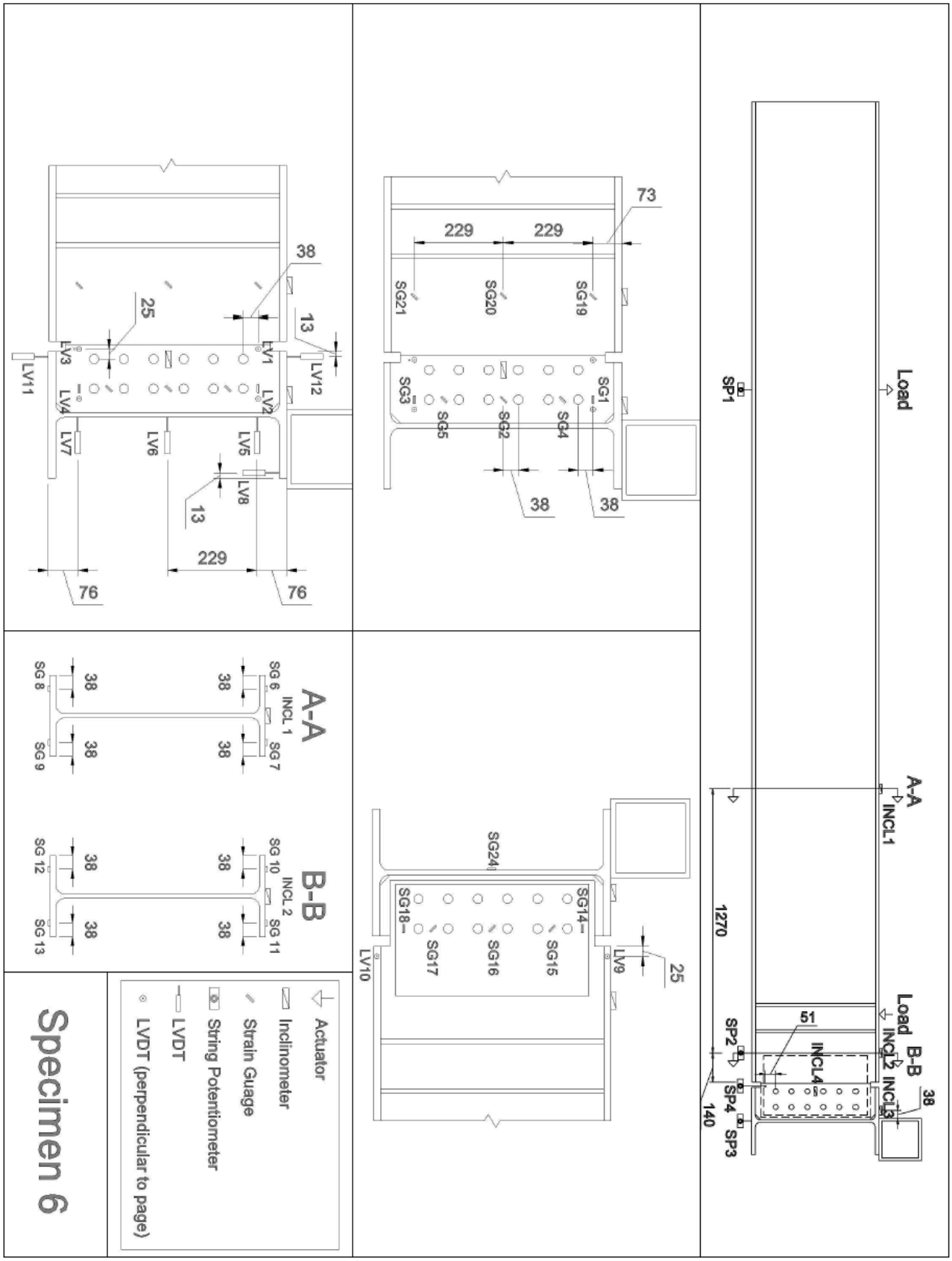
Load
SP1
A-A
INCL1
1270
Load
B-B
INCL2
INCL3
INCL4
51
SP2
SP4
SP3
140
38
73
229
229
SG21
SG20
SG19
SG3
SG5
SG2
SG4
SG1
38
38
SG24
SG14
SG18
SG17
SG16
SG15
LV10
LV9
25
38
25
13
LV11
LV3
LV1
LV12
LV4
LV2
LV7
LV6
LV5
LV8
13
229
76
76
A-A
SG 6
INCL 1
SG 7
SG 8
SG 9
B-B
SG 10
INCL 2
SG 11
SG 12
SG 13
Actuator
Inclinometer
Strain Guage
String Potentiometer
LVDT
LVDT (perpendicular to page)
Specimen 6

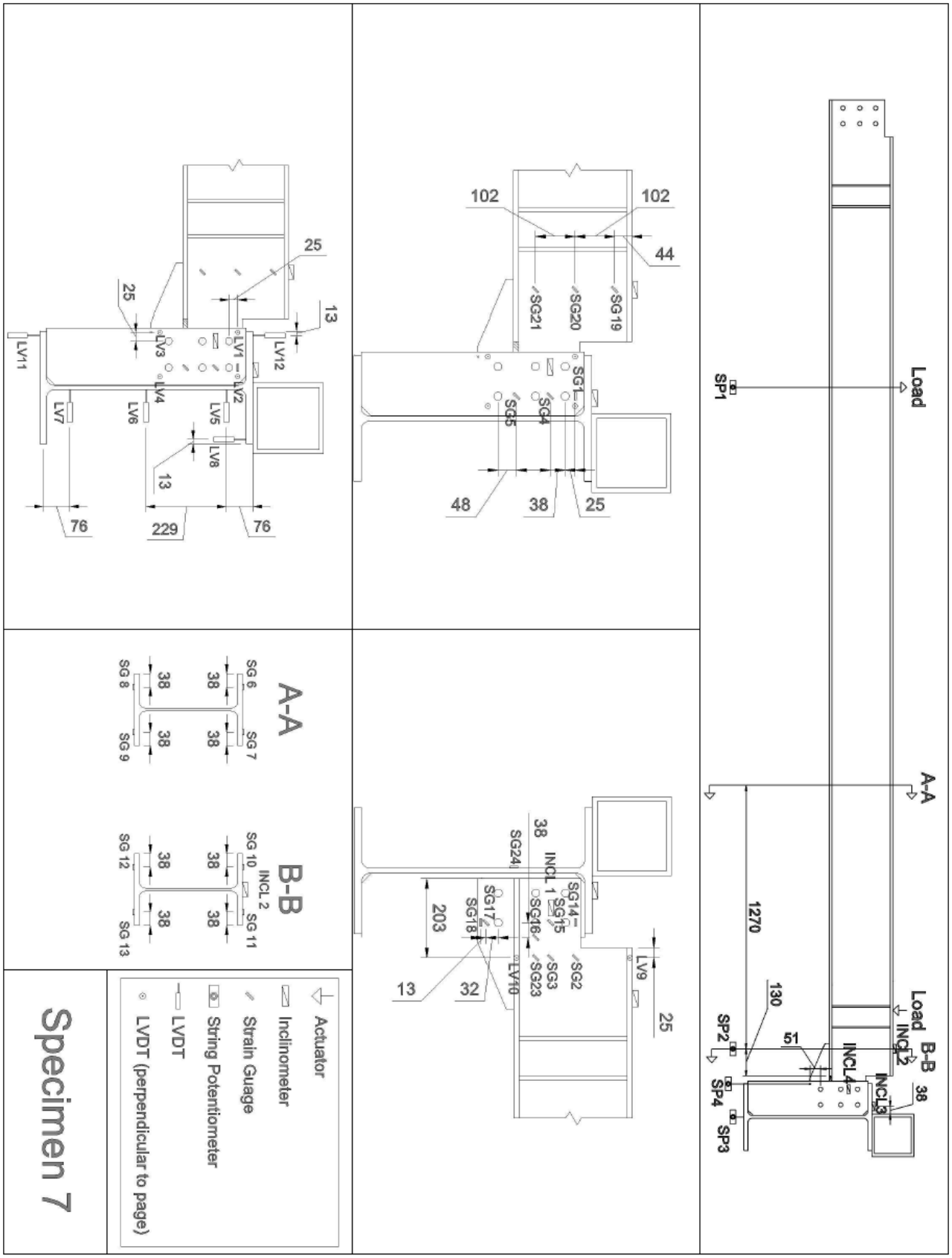
Load
SP1
A-A
B-B
Load
INCL 2
SP2
SP4
SP3
INCL4
INCL3
1270
130
51
38
102
102
44
SG21
SG20
SG19
SG1
SG5
SG4
48
38
25
38
INCL 1
SG24
SG14
SG15
SG16
SG17
SG18
SG3
SG2
SG23
LV10
LV9
203
13
32
25
25
13
LV11
LV3
LV1
LV12
LV2
LV4
LV7
LV6
LV5
LV8
13
76
229
76
A-A
SG 6
SG 7
SG 8
SG 9
38
B-B
SG 10
INCL 2
SG 11
SG 12
SG 13
Actuator
Inclinometer
Strain Guage
String Potentiometer
LVDT
LVDT (perpendicular to page)
Specimen 7

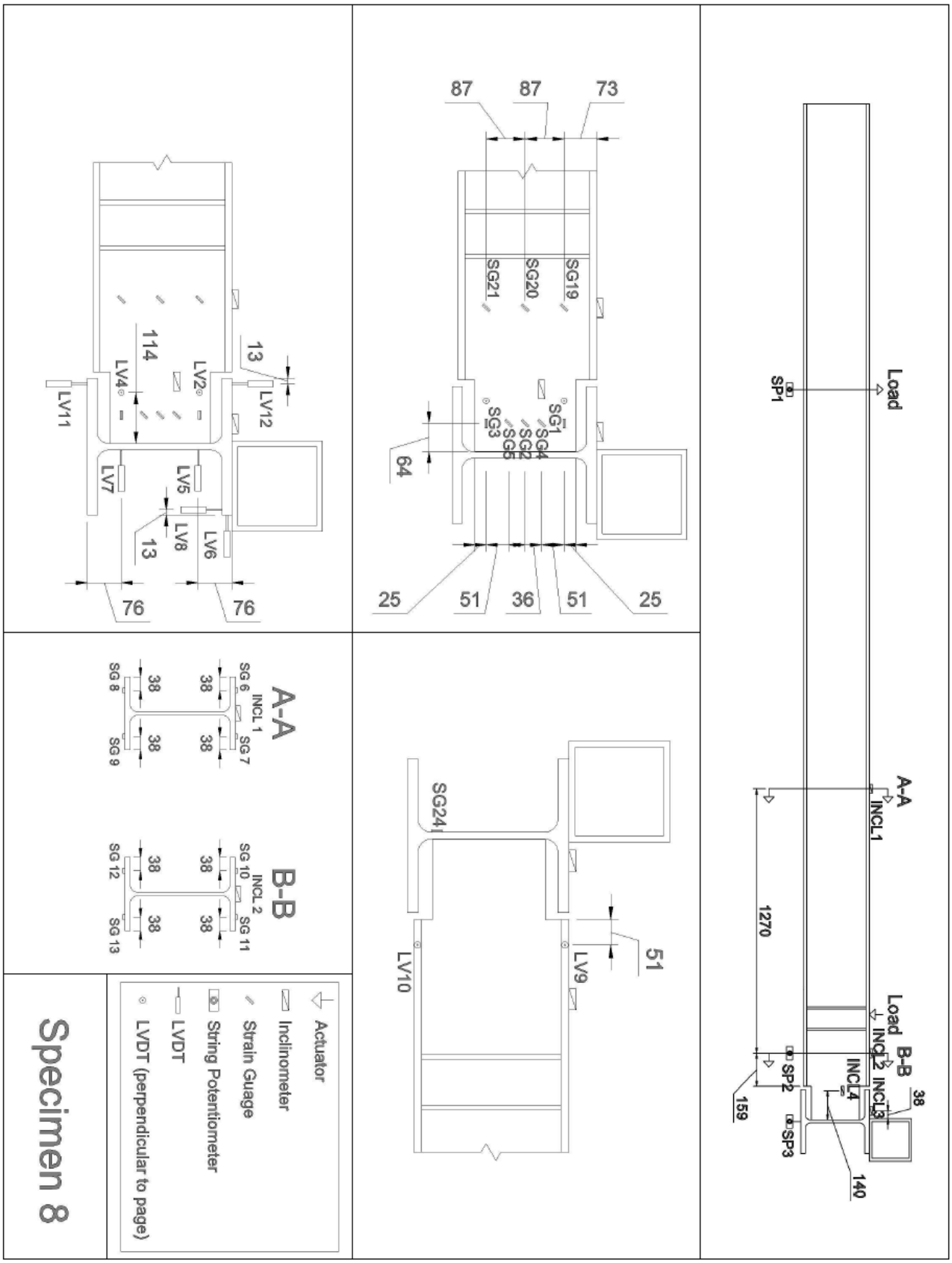
Load
SP1
A-A
INCL1
1270
Load
B-B
INCL2
INCL3
INCL4
SP2
SP3
159
38
140
87
87
73
SG21
SG20
SG19
SG1
SG4
SG2
SG5
SG3
64
25
51
36
51
25
SG24
LV10
LV9
51
LV11
LV12
13
114
LV4
LV2
LV7
LV5
LV8
LV6
13
76
76
A-A
INCL 1
SG 6
SG 7
SG 8
SG 9
38
B-B
INCL 2
SG 10
SG 11
SG 12
SG 13
Actuator
Inclinometer
Strain Guage
String Potentiometer
LVDT
LVDT (perpendicular to page)
Specimen 8

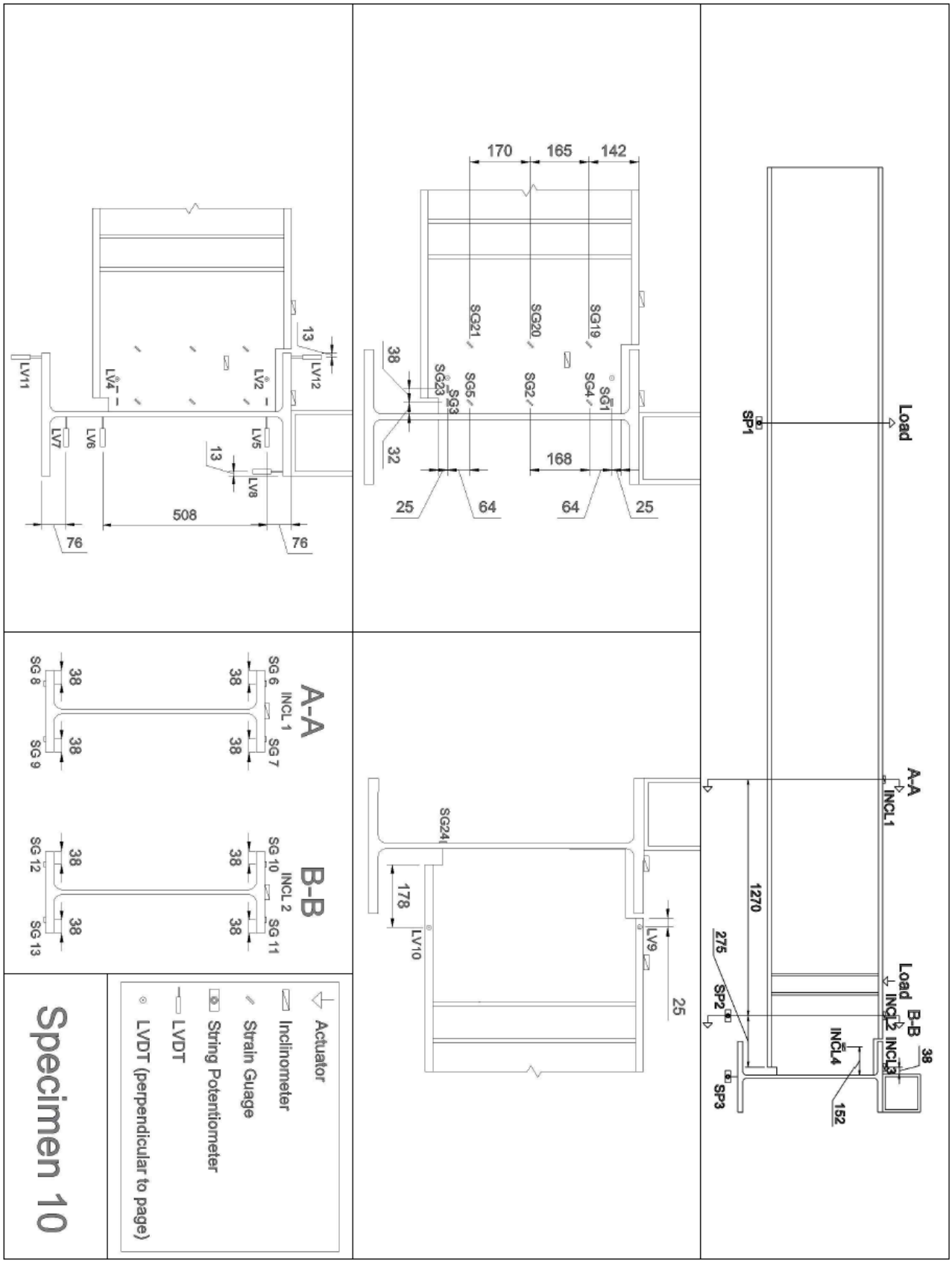
Load
SP1
A-A
INCL1
1270
Load
B-B
INCL2
INCL3
INCL4
SP2
SP3
275
152
38
SG24
178
LV10
LV9
25
170
165
142
SG21
SG20
SG19
SG23
SG5
SG3
SG2
SG4
SG1
38
32
168
25
64
64
25
LV11
LV12
LV4
LV2
LV7
LV6
LV5
LV8
13
13
508
76
76
A-A
INCL 1
SG 6
SG 7
SG 8
SG 9
B-B
INCL 2
SG 10
SG 11
SG 12
SG 13
Specimen 10
Actuator
Inclinometer
Strain Guage
String Potentiometer
LVDT
LVDT (perpendicular to page)

APPENDIX D

MOVEMENT OF INFLECTION POINT

Specimen A1

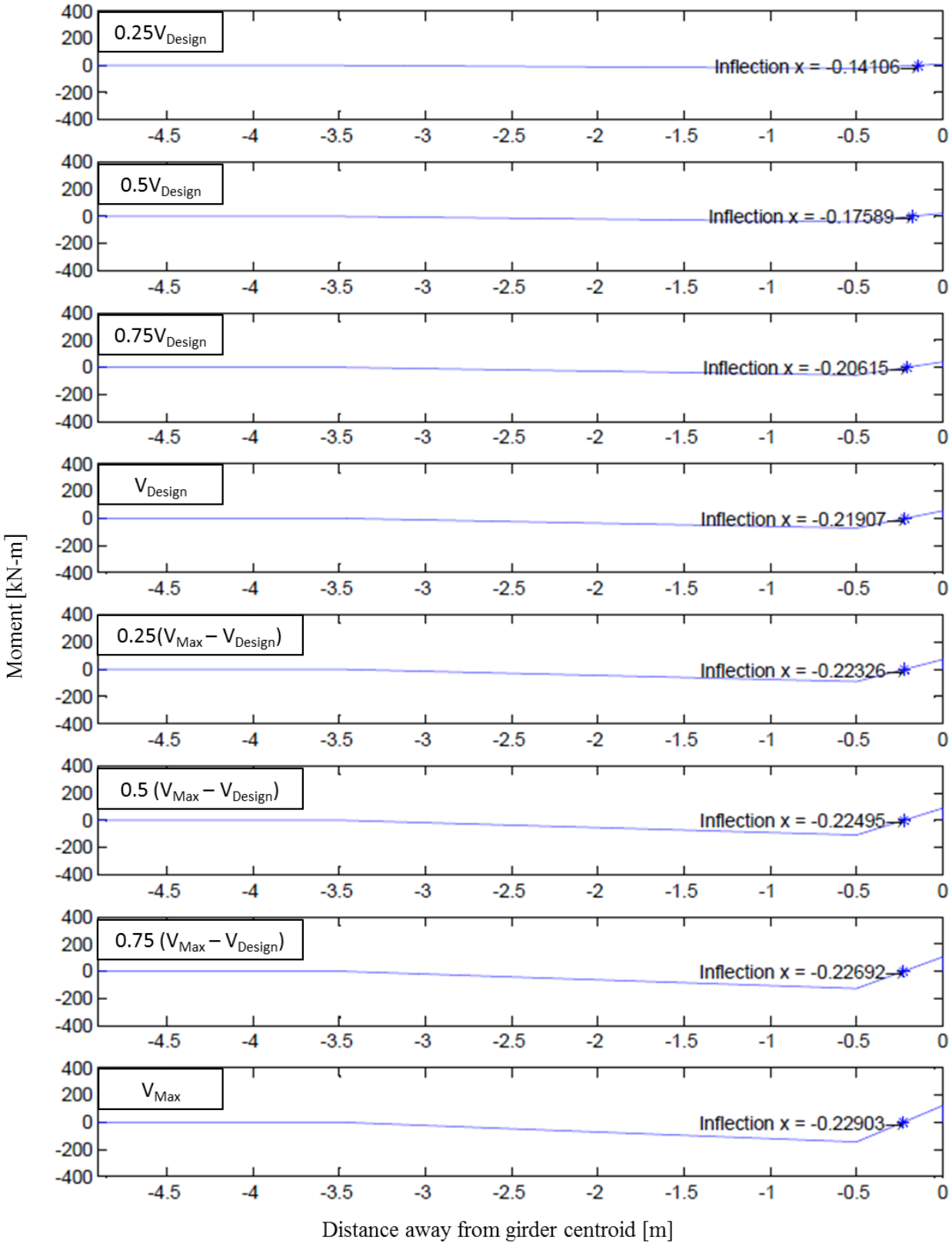
0.25V_Design
Inflection x = -0.14106
0.5V_Design
Inflection x = -0.17589
0.75V_Design
Inflection x = -0.20615
V_Design
Inflection x = -0.21907
0.25(V_Max – V_Design)
Inflection x = -0.22326
0.5 (V_Max – V_Design)
Inflection x = -0.22495
0.75 (V_Max – V_Design)
Inflection x = -0.22692
V_Max
Inflection x = -0.22903
Moment [kN-m]
Distance away from girder centroid [m]

Specimen A2

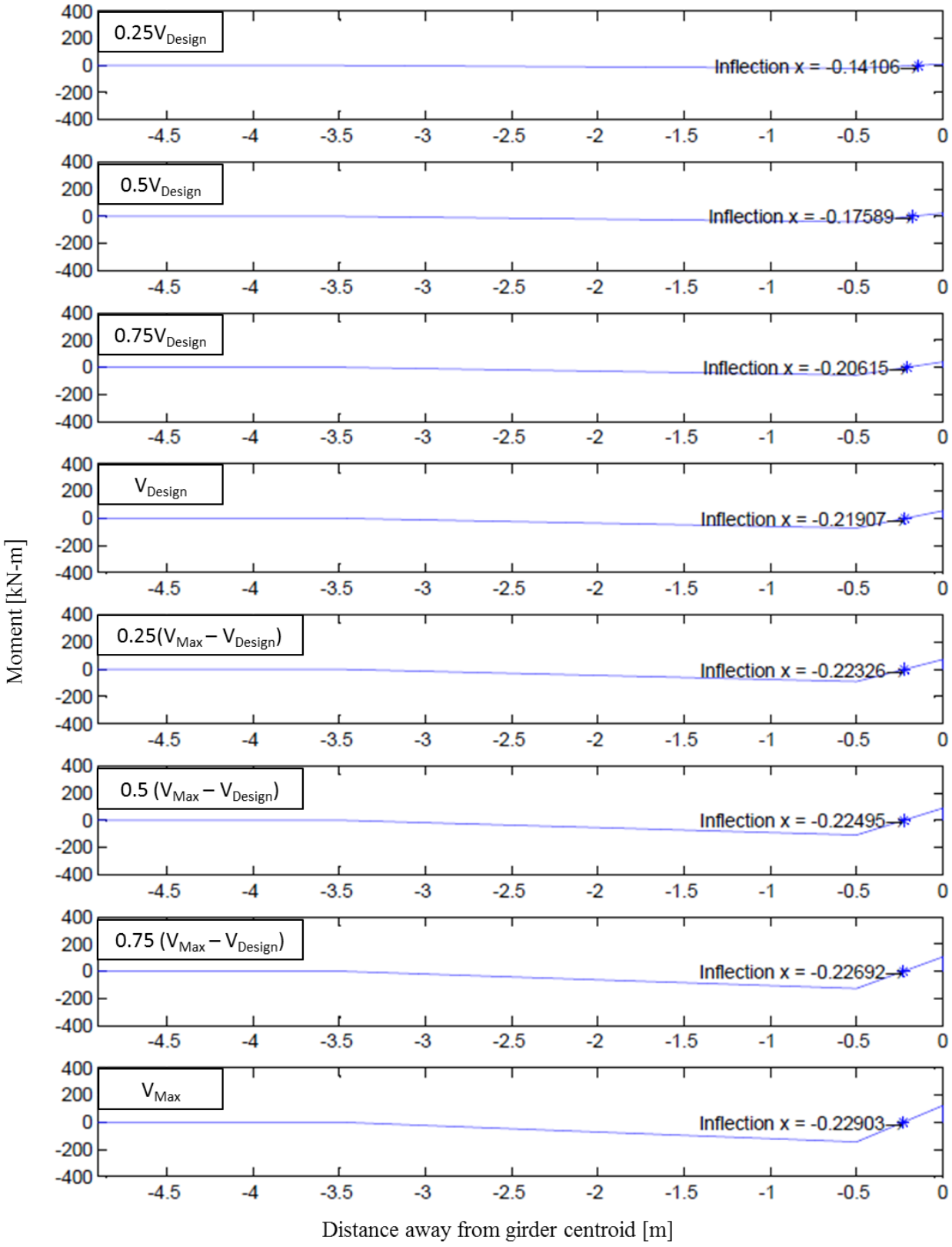
0.25V_Design
Inflection x = -0.14106
0.5V_Design
Inflection x = -0.17589
0.75V_Design
Inflection x = -0.20615
V_Design
Inflection x = -0.21907
0.25(V_Max – V_Design)
Inflection x = -0.22326
0.5 (V_Max – V_Design)
Inflection x = -0.22495
0.75 (V_Max – V_Design)
Inflection x = -0.22692
V_Max
Inflection x = -0.22903
Moment [kN-m]
Distance away from girder centroid [m]

Specimen 6J

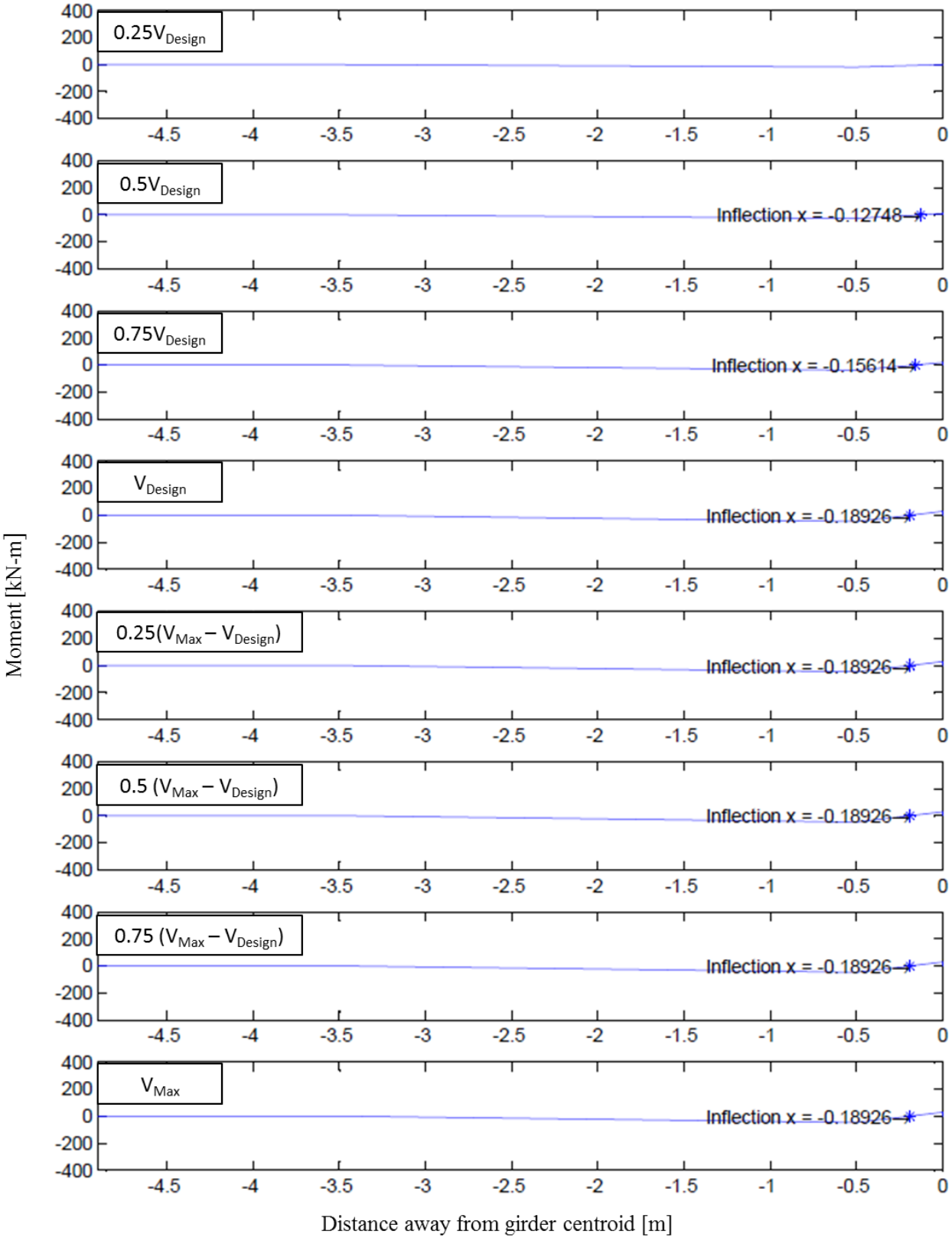
0.25V_Design
0.5V_Design
Inflection x = -0.12748
0.75V_Design
Inflection x = -0.15614
V_Design
Inflection x = -0.18926
0.25(V_Max – V_Design)
Inflection x = -0.18926
0.5 (V_Max – V_Design)
Inflection x = -0.18926
0.75 (V_Max – V_Design)
Inflection x = -0.18926
V_Max
Inflection x = -0.18926
400
200
0
-200
-400
-4.5
-4
-3.5
-3
-2.5
-2
-1.5
-1
-0.5
0
Moment [kN-m]
Distance away from girder centroid [m]

Specimen 9J

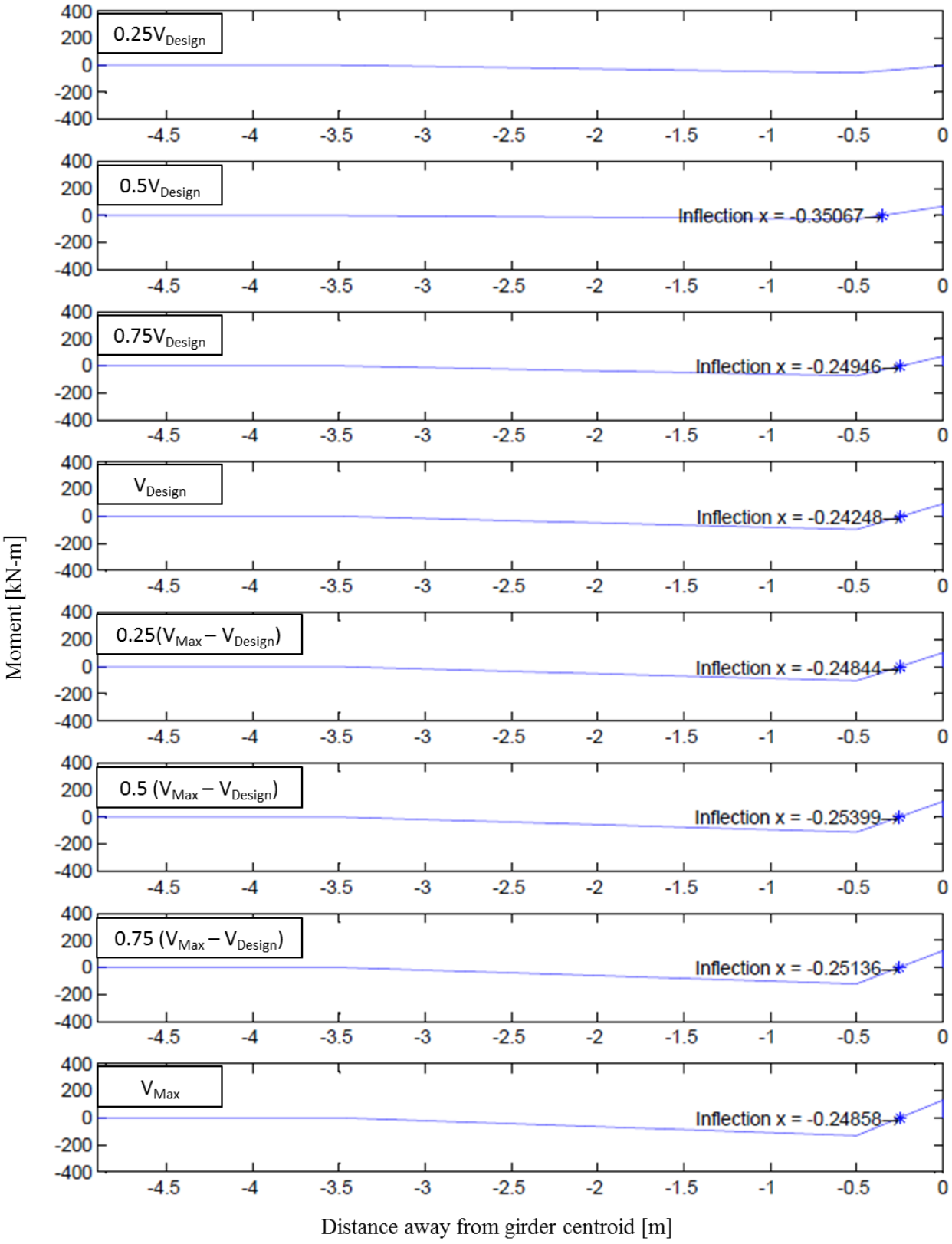
0.25V_Design
0.5V_Design
Inflection x = -0.35067
0.75V_Design
Inflection x = -0.24946
V_Design
Inflection x = -0.24248
0.25(V_Max – V_Design)
Inflection x = -0.24844
0.5 (V_Max – V_Design)
Inflection x = -0.25399
0.75 (V_Max – V_Design)
Inflection x = -0.25136
V_Max
Inflection x = -0.24858
400
200
0
-200
-400
-4.5
-4
-3.5
-3
-2.5
-2
-1.5
-1
-0.5
0
Moment [kN-m]
Distance away from girder centroid [m]

Specimen 1

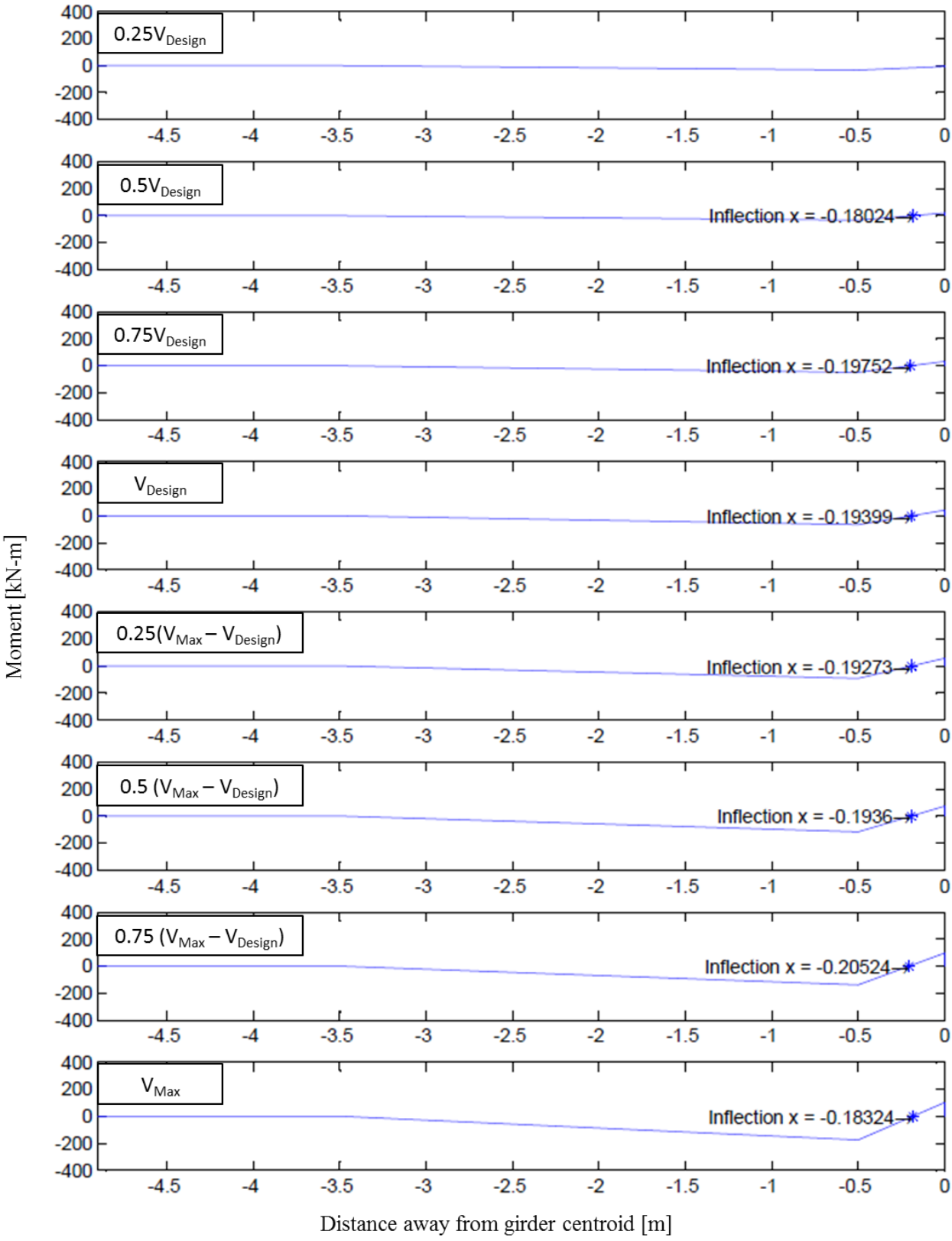
0.25V_Design
0.5V_Design
Inflection x = -0.18024
0.75V_Design
Inflection x = -0.19752
V_Design
Inflection x = -0.19399
0.25(V_Max – V_Design)
Inflection x = -0.19273
0.5 (V_Max – V_Design)
Inflection x = -0.1936
0.75 (V_Max – V_Design)
Inflection x = -0.20524
V_Max
Inflection x = -0.18324
400
200
0
-200
-400
-4.5
-4
-3.5
-3
-2.5
-2
-1.5
-1
-0.5
0
Moment [kN-m]
Distance away from girder centroid [m]

Specimen 2

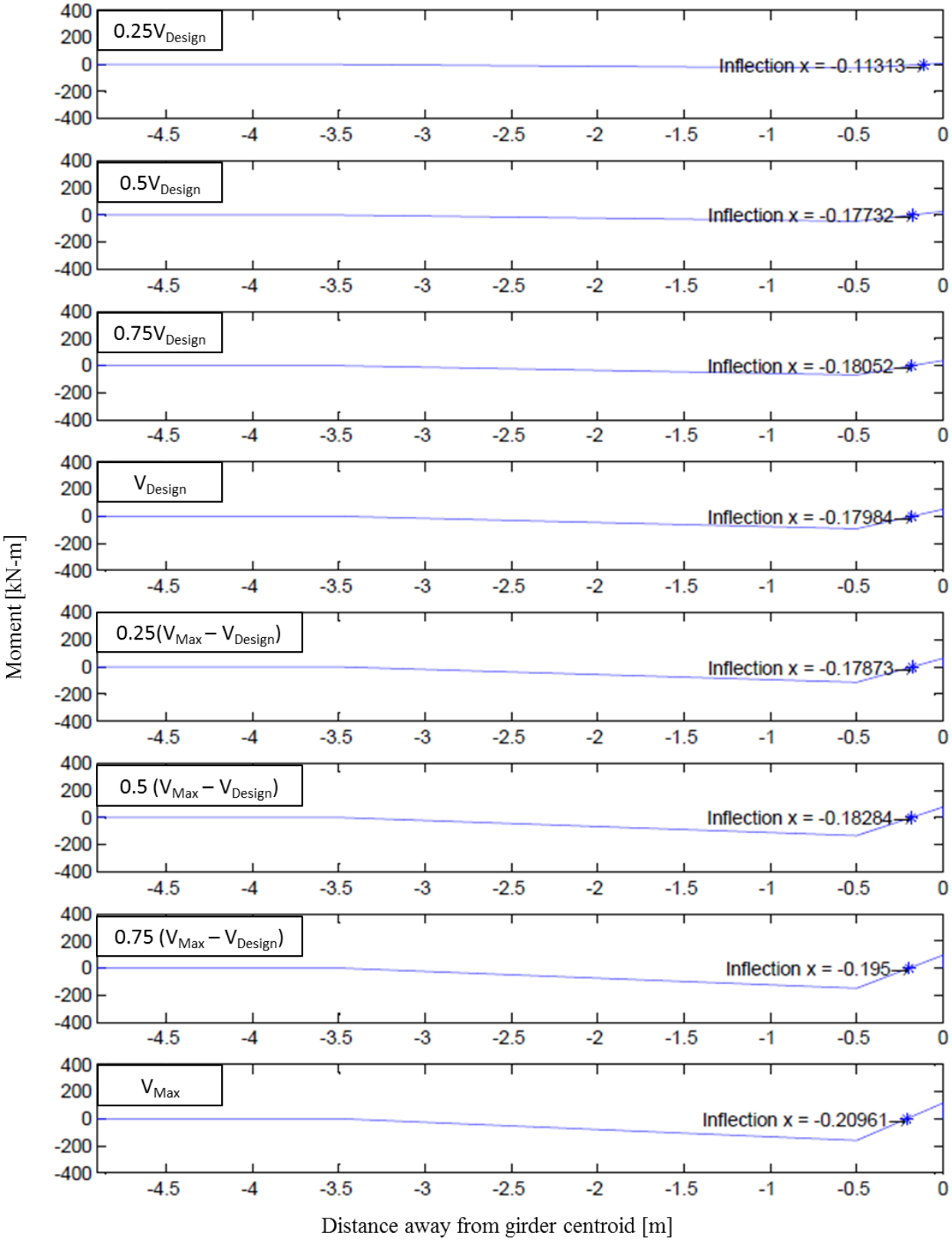
0.25V_Design
Inflection x = -0.11313
0.5V_Design
Inflection x = -0.17732
0.75V_Design
Inflection x = -0.18052
V_Design
Inflection x = -0.17984
0.25(V_Max – V_Design)
Inflection x = -0.17873
0.5 (V_Max – V_Design)
Inflection x = -0.18284
0.75 (V_Max – V_Design)
Inflection x = -0.195
V_Max
Inflection x = -0.20961
400
200
0
-200
-400
-4.5
-4
-3.5
-3
-2.5
-2
-1.5
-1
-0.5
0
Moment [kN-m]
Distance away from girder centroid [m]

Specimen 3

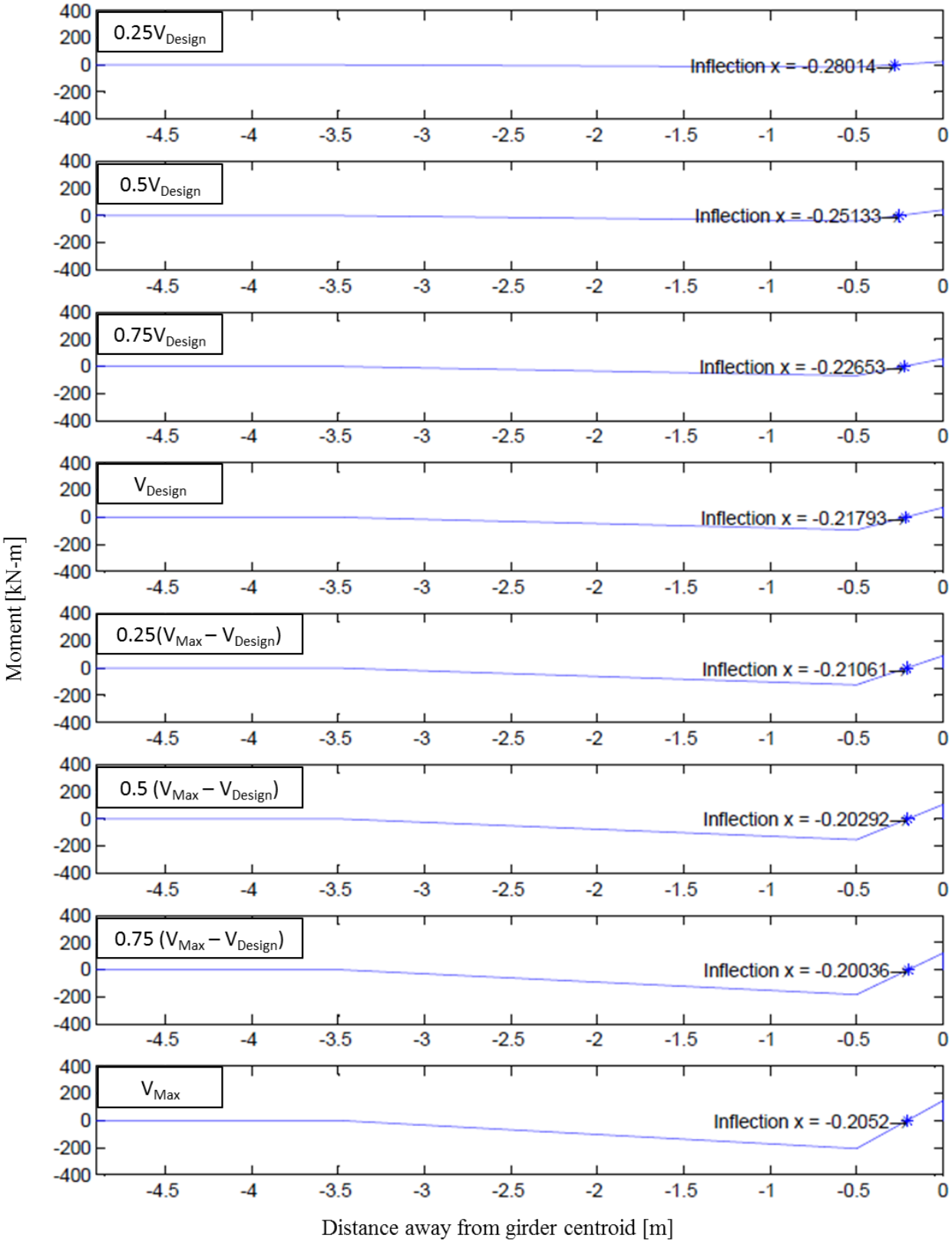
0.25V_Design
Inflection x = -0.28014
0.5V_Design
Inflection x = -0.25133
0.75V_Design
Inflection x = -0.22653
V_Design
Inflection x = -0.21793
0.25(V_Max – V_Design)
Inflection x = -0.21061
0.5 (V_Max – V_Design)
Inflection x = -0.20292
0.75 (V_Max – V_Design)
Inflection x = -0.20036
V_Max
Inflection x = -0.2052
Moment [kN-m]
Distance away from girder centroid [m]

Specimen 4

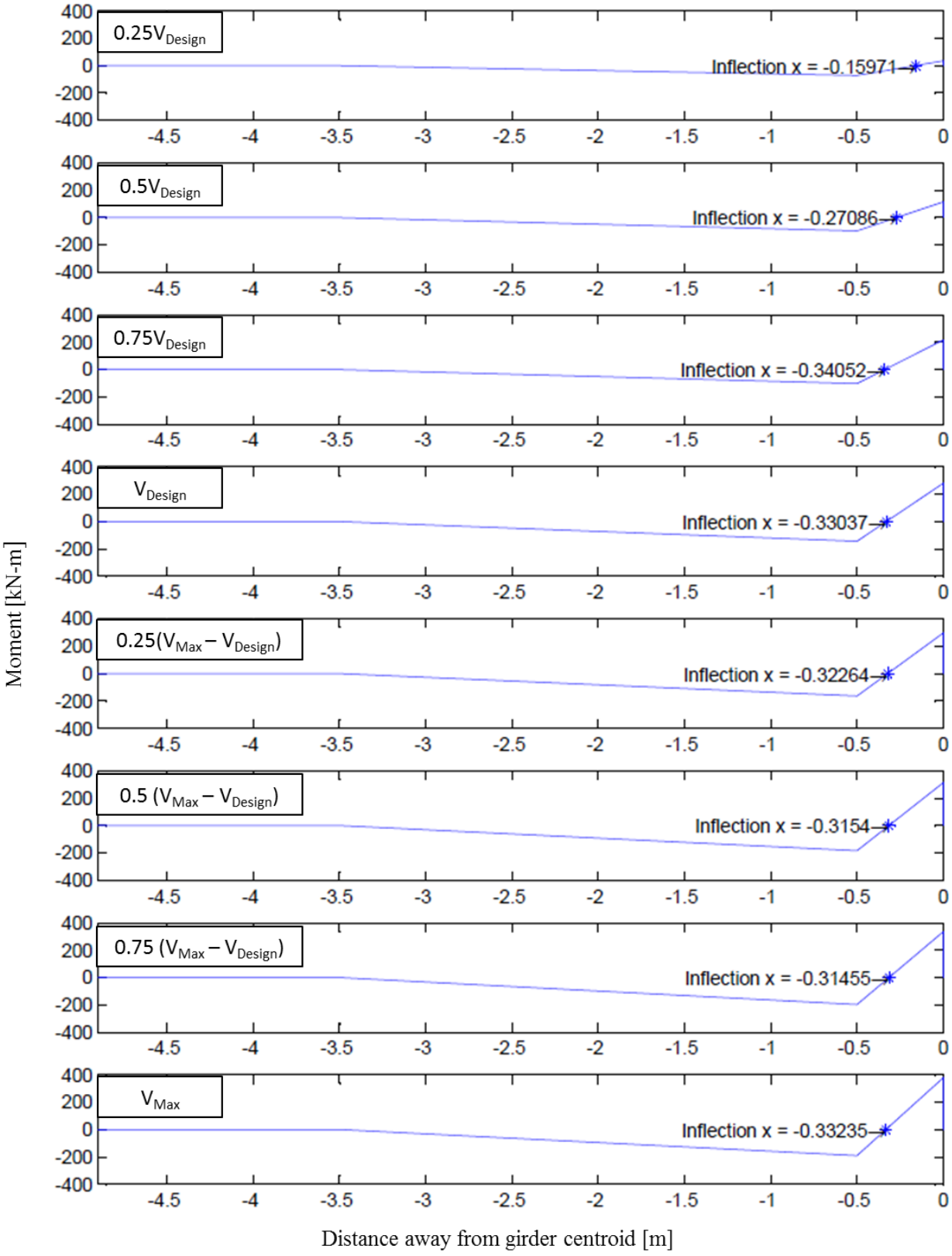
0.25V_Design
Inflection x = -0.15971
0.5V_Design
Inflection x = -0.27086
0.75V_Design
Inflection x = -0.34052
V_Design
Inflection x = -0.33037
0.25(V_Max – V_Design)
Inflection x = -0.32264
0.5 (V_Max – V_Design)
Inflection x = -0.3154
0.75 (V_Max – V_Design)
Inflection x = -0.31455
V_Max
Inflection x = -0.33235
Moment [kN-m]
Distance away from girder centroid [m]

Specimen 5

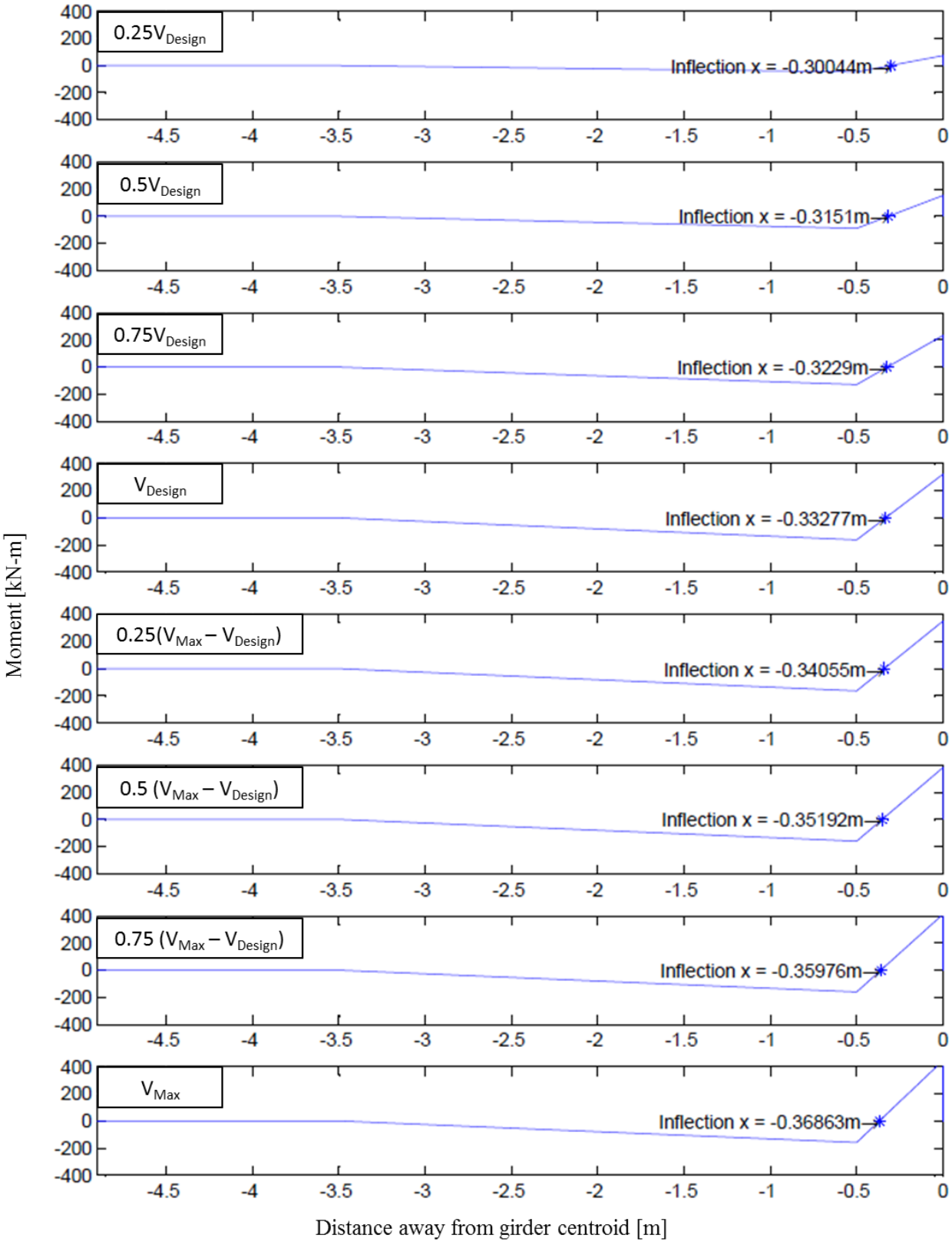
0.25V_Design
Inflection x = -0.30044m
0.5V_Design
Inflection x = -0.3151m
0.75V_Design
Inflection x = -0.3229m
V_Design
Inflection x = -0.33277m
0.25(V_Max – V_Design)
Inflection x = -0.34055m
0.5 (V_Max – V_Design)
Inflection x = -0.35192m
0.75 (V_Max – V_Design)
Inflection x = -0.35976m
V_Max
Inflection x = -0.36863m
Moment [kN-m]
Distance away from girder centroid [m]

Specimen 6

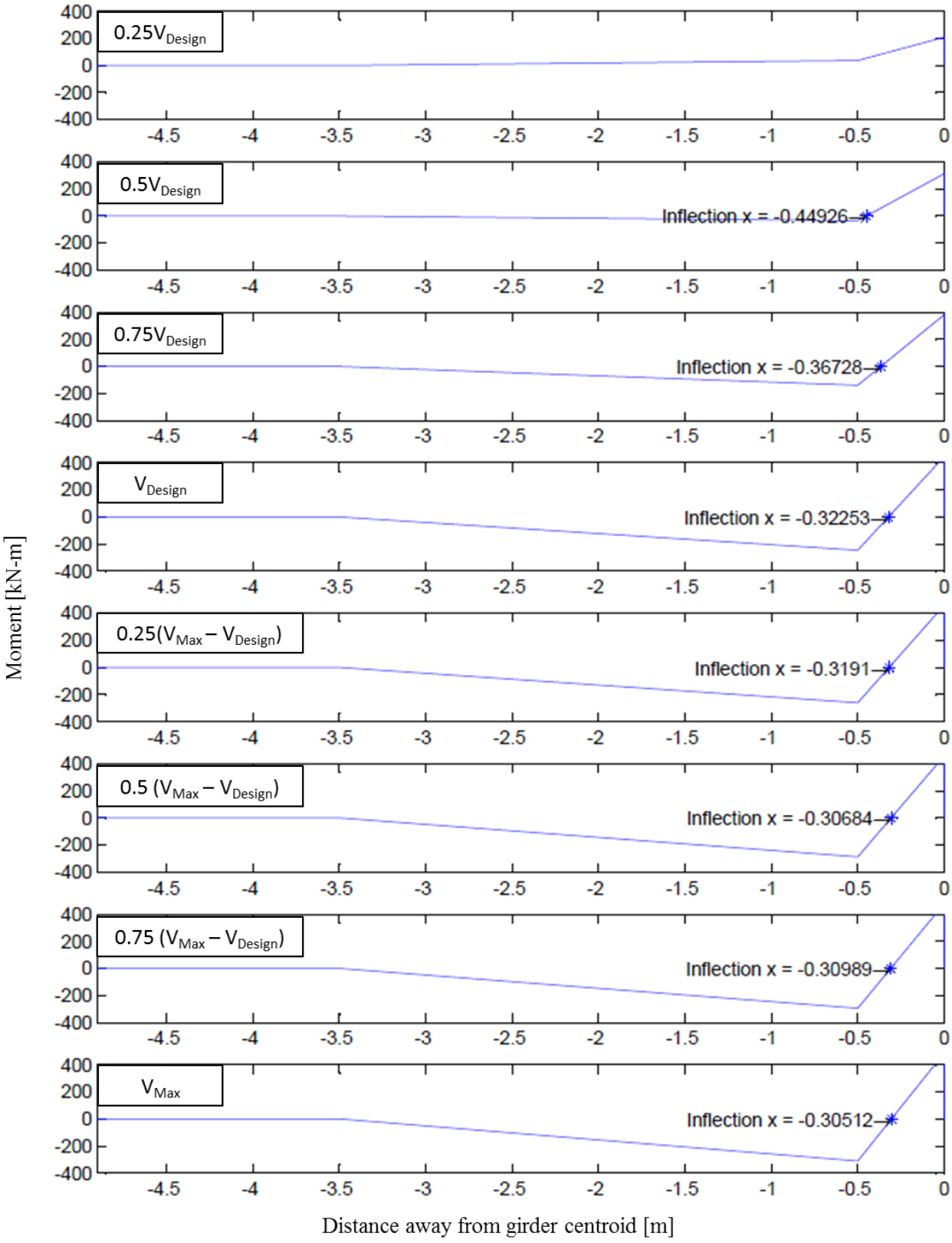
0.25V_Design
0.5V_Design
Inflection x = -0.44926
0.75V_Design
Inflection x = -0.36728
V_Design
Inflection x = -0.32253
0.25(V_Max – V_Design)
Inflection x = -0.3191
0.5 (V_Max – V_Design)
Inflection x = -0.30684
0.75 (V_Max – V_Design)
Inflection x = -0.30989
V_Max
Inflection x = -0.30512
400
200
0
-200
-400
-4.5
-4
-3.5
-3
-2.5
-2
-1.5
-1
-0.5
0
Moment [kN-m]
Distance away from girder centroid [m]

Specimen 7

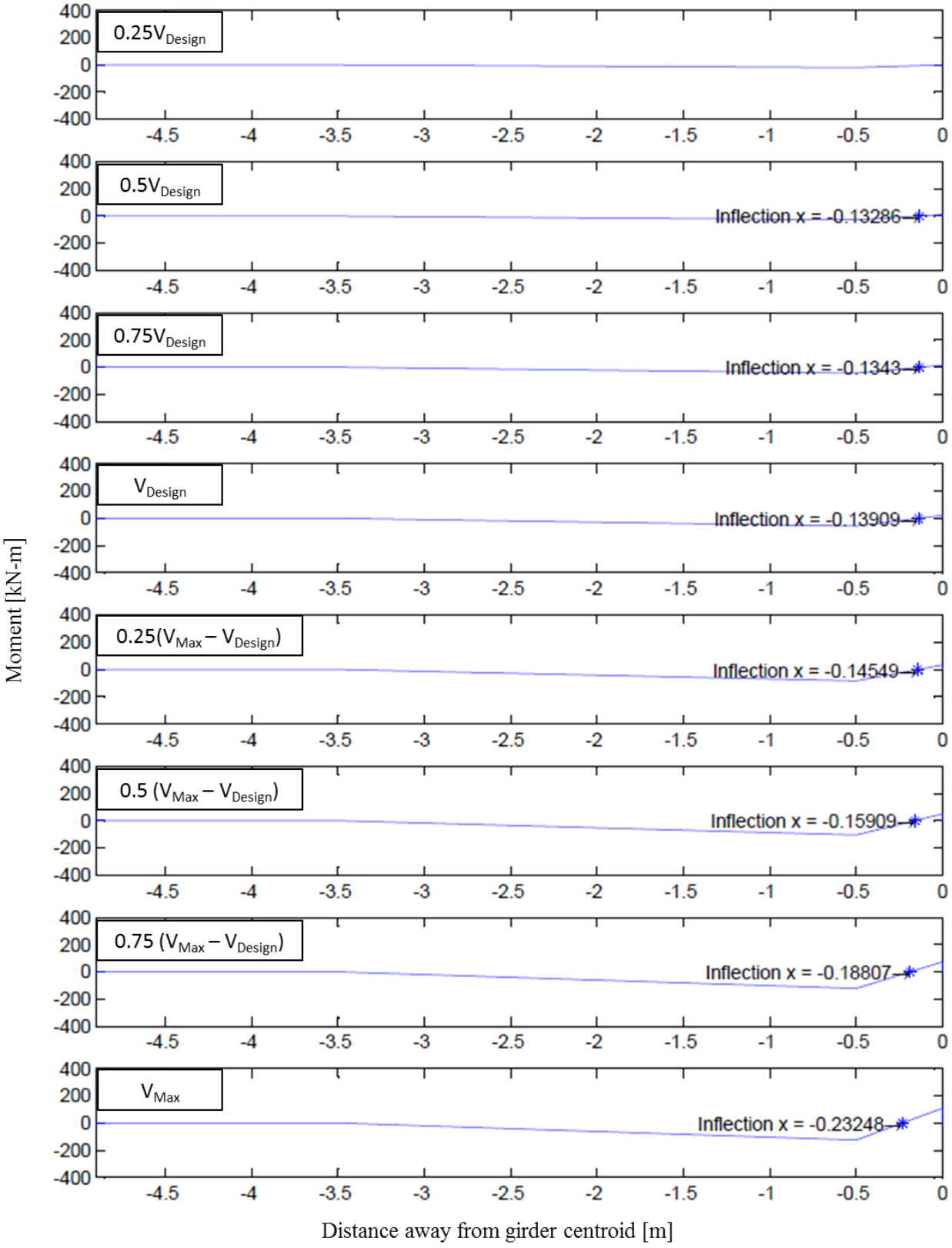
0.25V_Design
0.5V_Design
Inflection x = -0.13286
0.75V_Design
Inflection x = -0.1343
V_Design
Inflection x = -0.13909
0.25(V_Max – V_Design)
Inflection x = -0.14549
0.5 (V_Max – V_Design)
Inflection x = -0.15909
0.75 (V_Max – V_Design)
Inflection x = -0.18807
V_Max
Inflection x = -0.23248
400
200
0
-200
-400
-4.5
-4
-3.5
-3
-2.5
-2
-1.5
-1
-0.5
0
Moment [kN-m]
Distance away from girder centroid [m]

Specimen 8

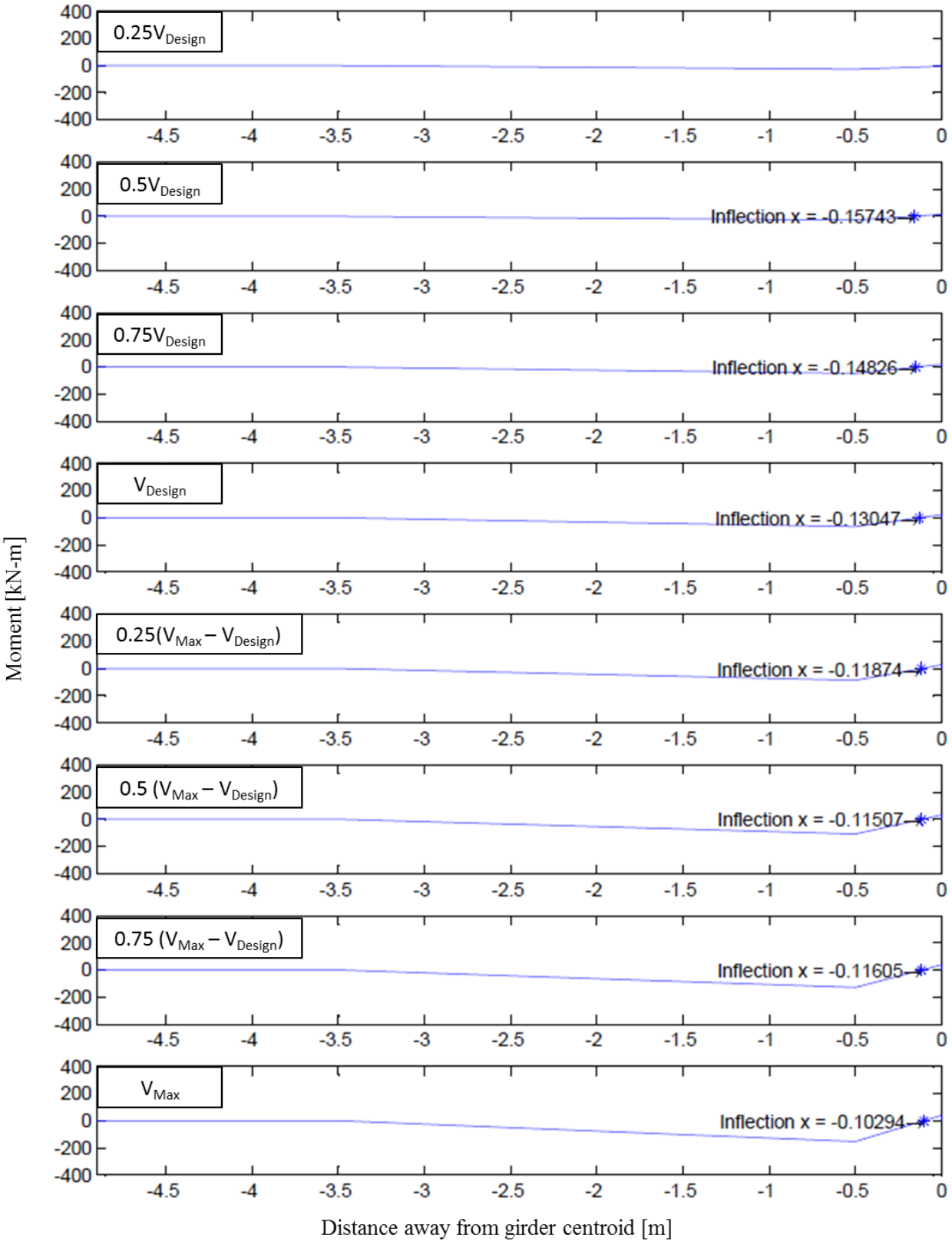
0.25V_Design
0.5V_Design
Inflection x = -0.15743
0.75V_Design
Inflection x = -0.14826
V_Design
Inflection x = -0.13047
0.25(V_Max – V_Design)
Inflection x = -0.11874
0.5 (V_Max – V_Design)
Inflection x = -0.11507
0.75 (V_Max – V_Design)
Inflection x = -0.11605
V_Max
Inflection x = -0.10294
400
200
0
-200
-400
-4.5
-4
-3.5
-3
-2.5
-2
-1.5
-1
-0.5
0
Moment [kN-m]
Distance away from girder centroid [m]

Specimen 10

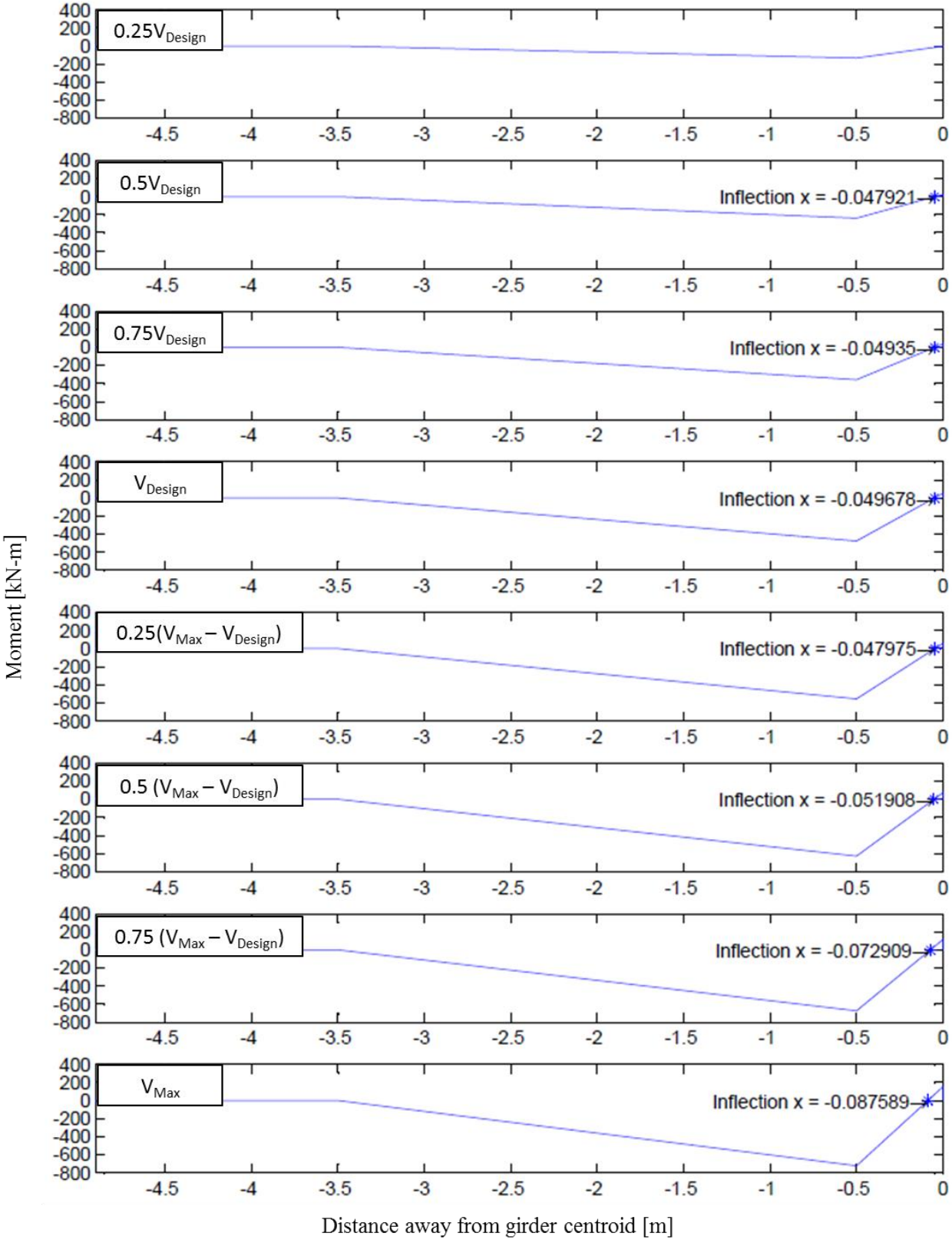
0.25V_Design
0.5V_Design
Inflection x = -0.047921
0.75V_Design
Inflection x = -0.04935
V_Design
Inflection x = -0.049678
0.25(V_Max – V_Design)
Inflection x = -0.047975
0.5 (V_Max – V_Design)
Inflection x = -0.051908
0.75 (V_Max – V_Design)
Inflection x = -0.072909
V_Max
Inflection x = -0.087589
Moment [kN-m]
Distance away from girder centroid [m]